Final Report

Project Title: Research and Development for Off-Road Fuel Cell Applications
U.S. Department of Energy Grant DE-FG36-04GO14303

Project Period: September 1, 2004 – September 30, 2012
Date of Report: April 2013
Recipient: IdaTech, LLC.
Award Number: DE-FG36-04GO14303

Working Partners: IdaTech, LLC, The Toro Company, University of California – Davis, Donaldson, The River's Edge Golf Course, High Desert Museum

Cost-Sharing Partners: IdaTech, LLC, The Toro Company, UC – Davis, Donaldson

Contact: Mike Hicks, (541) 322-1040, mike.hicks@h2powertech.com

U.S. DOE Managers: David Peterson, DOE Golden Field Office

Table of Contents

PROJECT OBJECTIVES

To determine the effects of off-road air quality, shock, and vibration, on an advanced Proton Exchange Membrane (PEM) fuel cell and reformer subsystems and its integration with a Toro Workman™ Lawn Tractor.

BACKGROUND

The program originally consisted of the following four tasks

1. System Study of Lawn Tractor Load Profiles
2. Impulse and Vibration Study
    a. Source Identification of Vibration and Shock on-Off Road Vehicles
    b. Fuel Cell System Vibration and Shock Spectrum Testing
3. Air Quality Study
    a. Fuel Cell Air Contaminants
    b. Air Filter Development
4. Fuel Cell Specification

The program began in September 2004, was suspended in 2005 and was restarted in November 2007. During the suspension, Donaldson and Toro independently completed some of the tasks that were proposed under this program:

- A database of airborne fuel cell contaminants was generated (Task 3a)
- Air filter development was completed (Task 3b)
- Load profiles and power requirements for a Toro Workman™ were generated (Task 4)
- IdaTech under a US Navy program (Subcontract to HoKu, Program ID 06UJ9A00008B) developed a portable liquid fueled fuel cell system (FCS3000) of the size required for this program

After work resumed on this program in 2007 and as a result of the work independently completed during the suspension, Task 4 was modified to the following:

4. Design, Assemble, and Test Two Toro Workman™ Mid Duty Utility Vehicle with an IdaTech FCS 3000 Liquid Fueled Fuel Cell System

Additionally, due to the fact that there was leftover money as a result of some of the tasks being completed during the suspension and that Donaldson decided not to produce the fuel cell air filter designed in Task 3b, Task 3c - Air Filter Testing, was added in 2010 in order to evaluate available filters.

From the original task list, two items will not be included in the final report since they were paid for by their respective companies during the suspension. Those items are Task 3b – Air Filter Development and Task 4 – Fuel Cell Specification.

OVERVIEW

This program has addressed the load profiles for off-road PEM fuel cell utilization, including typical load profiles and drive train and power take off

devices. The program has also gathered information on the air contaminants that may have an effect on fuel cell operation and performance degradation. Toro has developed the Workman Model e2065 mid-duty truck equipped to operate on DC voltages, and had accelerometers installed and evaluated shock and vibration under this grant.

TASK 1: SYSTEM STUDY OF LAWN TRACTOR LOAD PROFILES

Investigation of Load Profiles for Agricultural Tractors
and Fuel Cell Power Train Recommendations

University of California, Davis

Michael Beerman, Graduate Student
Uriel A. Rosa, Assistant Professor
Bryan Jenkins, Professor
Paul Erickson, Assistant Professor

INTRODUCTION

The modern Agricultural tractor has many uses. Each of those uses has a different power demand. The purpose of this investigation is to determine load profiles for different classes of off-road equipment using predominantly existing information from agricultural, military and other equipment testing programs (e.g. Nebraska Tractor Testing Laboratory, Aberdeen Test Center, OECD and OEM data). This effort focuses on agricultural applications where such information is available. Agricultural equipment to be considered includes lighter-duty general-purpose 2-wheel and 4-wheel drive tractors, which are considered to be primary targets for adapting fuel cell power units in the near term.

An investigation has been conducted on tractor requirements for traction, power train, prime mover torque, speed and acceleration, power profiles, typical power take-off (PTO) and hydraulic actuators. Operating requirements and changes in the power train required to facilitate a fuel cell power unit to accommodate functional differences, and differences in the transient response of the fuel cell compared with internal combustion engines are discussed. Finally recommendations are made regarding the power train design of three power classes of tractors <20 kW, 20 to 200 kW, and >200 kW, as well as for the prototype vehicle to be field-tested.

This review indicates that electric motors provide favorable characteristics for agricultural applications and that uncoupling the mechanical power from the load may increase efficiency allowing the power supply to operate at peak efficiency while the electric motor provides the time varying torque.

The data collected are representative of North American agricultural tractors, in that there are different economic and social demands for farm equipment in different countries. Gasoline or diesel internal combustion engines power current tractors on the market in North America. Although there have been electric tractor (Alcock, 1983; Vik et al., 1984; Thoreson et al., 1986) and Fuel cell tractor

(Ihrig, 1960) prototypes made, none of these has made it into widespread use.

LOAD PROFILES

There are different profiles expected for different vehicles. For small vehicles it is expected that the power demand will be much more transient. Whereas for large vehicles used to work large fields it is expected that the load profile will be fairly steady with oscillations occurring only when abnormalities are encountered (such as rocks in plowing or equipment malfunction).

Testings

Tractor testing is performed internationally at several OECD approved testing centers where market ready tractors are tested to find their operational limits and fuel efficiencies at different loads (OECD ; SAE, 1999). First the tractor is allowed a run-in period where a representative from the manufacturer is allowed to run the tractor and make any tuning modifications. During the tractor test the engine power and torque are measured by a dynamometer bench attached to the PTO at several different speeds (the rated engine speed, the standard PTO speed 540 or 1000 rpm, and at various different engine speeds). Torque, engine speed and hourly fuel consumption are recorded on the bench tests, and the tractor is field driven to determine drawbar performance.

Drawbar power is defined as the power actually required to pull, or move, an implement at a uniform speed. Drawbar power is not only a function of engine power, but also of tractive efficiency, which is dependent on weight distribution, field conditions, and the tires.

The Power Take Off (PTO) is a shaft that can be accessible usually either at the front or rear of the tractor (or at both) in which a mounted or pulled implement can receive mechanical power to perform an operation. For example a pick up baler is an implement, which is hitched to the tractor and connected to the PTO drive. As the tractor pass through the field of cut-dry hay the baler uses the power supplied by the PTO to pick up the hay, compress it, bind it with twine and then push the bound bale out of the machine to start a new bale.

If we evaluate the power demand on the engine during an operation such as baling we have the following to consider. The tractive power demand on the engine should be fairly constant (assuming a dry field, and slow speeds), and the PTO power used to bale the hay fluctuates due to the changing operation of the implement as can be seen in Figure 1.

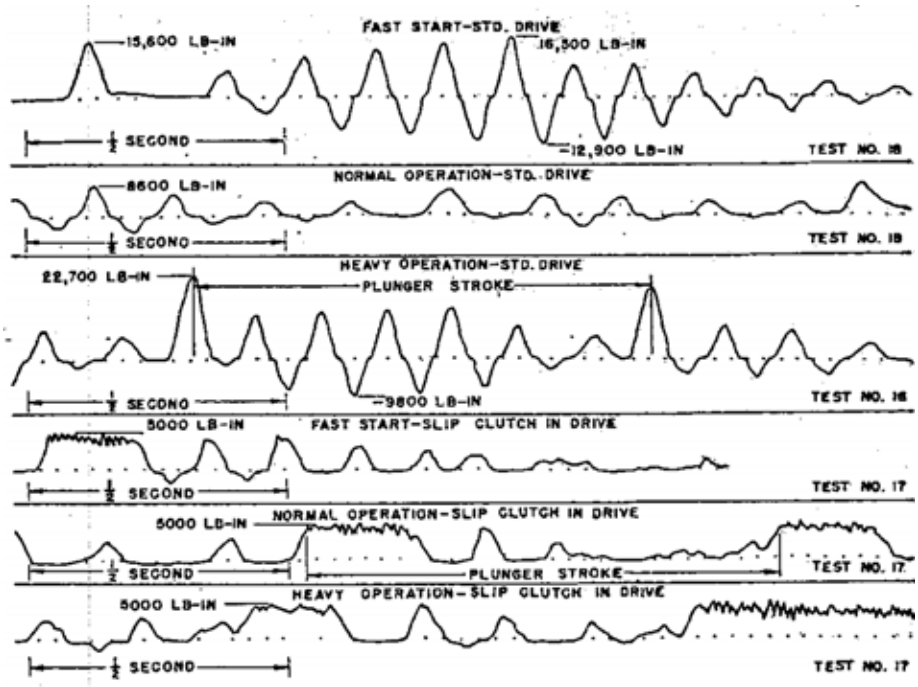

Figure 1: Torque meter charts with a slip clutch (Hansen, M., 1952)

Case Studies

While searching for load profiles a search was performed to find traces similar to those used to evaluate automotive performance (velocity and grade vs. time). Since the use of tractors is fundamentally different from automobiles as a result they are not evaluated in the same manner. In order to determine what kind of loads the engine of a tractor will experience, torque and power traces were then sought after. It is possible to obtain maximum power and torque measurements recorded by the Nebraska Tractor Test facility at their web site TUhttp://tractortestlab.unl.edu/testreports.htmUT. For tractors sold outside the US one can see the test reports posted by the OECD at TUhttp://www2.oecd.org/agr-coddb/index_en.aspUT. One significant addition to the OECD reports are the engine maps of torque and power vs speed. However, neither of these tells us how the load that a tractor might experience varies over time. To obtain these data, research papers have been evaluated and several illustrative studies are mentioned as follows.

In a study of torsional loads on nine separate tractors the loads imposed on the PTO shafts were analyzed during different operations. Table 1 shows the torsional properties of eight of the nine tractors evaluated. Table 2 displays the findings of the variation in the torque during different operations. In this analysis it is found that there are three factors that play a large roll in the magnitude of peak PTO torsional loads. The first is the amount of kinetic energy stored in the rotating parts of the tractor, the second the moment of inertia of the rotating parts in the implement, and third the amount of resilience in the drive between the heavy rotating parts of the tractor and the rotating parts of the driven implement. Figure 2 shows the oscillatory nature of the implement loads on the PTO shaft

due to the misalignment of the universal joint connecting the implement to the PTO shaft.

Table 1: Kinetic energy of rotating parts and torsional properties of PTO drives of current tractor models (Hansen, 1952)

Tractor Make and Model	Approx Max. hp of Tractor	I of Rotating Parts (lb-ft/sec2)	E or Rotating Parts at Rated Speed (ft-lb)	Torsional Deflection of PTO Train at Y.P. (Degrees)	Torsional Yield Strength of PTO Train (lb-in)	Energy PTO Drive Will Absorb at Y.P. (ft-lb)	Ratio E in Rotating Parts to PTO Drive
1	35	2.33	12,120	20	17,600	256	47.3
2	25	1.32	11,300				
3	35	3.23	16,820	37	28,000	753	22.2
4	45	6.17	33,700				
5	35	1.034	11,900	20	28,000	407	29.2
6	25			14.5	20,200	213	
7	30			12.5	17,670	161	
8	30			17.5	25,000	318	

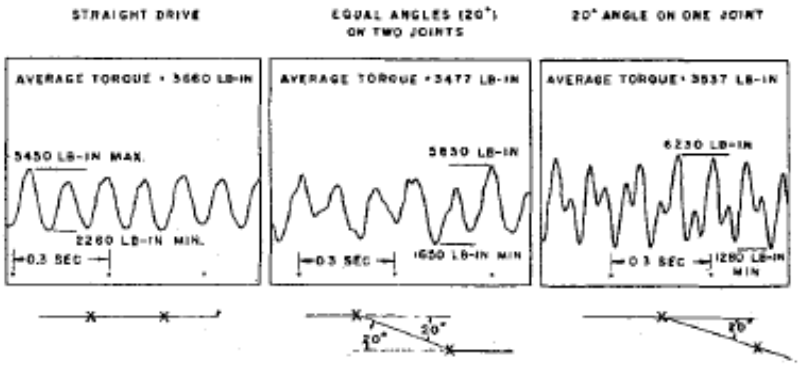

Figure 2: Torque meter charts showing the effect of universal joint misalignment while transmitting an average load of approximately 30 (Hansen, 1952)

Table 2: Power take-off torsional loads (Hansen, 1952)

Test No.	Tractor Model	Approx. Max. Tractor bhp	Implement Make and Model	Coupling in PTO Drive	Max Starting Torque w/ Normal Clutch Engagement (lb-in)	Max Starting Torque w/ Rapid Clutch Engagement (lb-in)	Max. Operational Torque Average Conditions (lb-in)	Max. Operational Torque Near Plugged Conditions (lb-in)	Ave. Torque Norm. Op. Conditions (lb-in)	Work Being Performed
					4900 - 6400	10800 - 15370	4680 - 6390	5450 - 7140		
2	1	35	Ensilage Harvester A	Spec. Slip		8660	5112 - 5723	6025 - 6865	3200	Chopping Heavy Drilled Corn
3	9	40	Ensilage Harvester A	Standard		11600	4700 - 4925	6200 - 8025	3261	Chopping Heavy Drilled Corn
4	1	35	Ensilage Harvester B	Standard	2600 - 4000*		3520 - 3820	3960 - 7630*	2390	Chopping Heavy Drilled Corn
5	1	35	Forage Harvester C	Standard		14600	3730 - 7200	6370 - 7200	2870	Chopping Green Alfalfa
6	1	35	Forage Harvester C			9800 - 7530*	5230 - 6700	6100 - 8700	3270	Chopping Green Alfalfa
7	1	35	Forage Harvester C	Standard		12500 - 10900	6060 - 7460	9500	3600	Chopping Green Alfalfa
8	1	35	Forage Harvester C	Standard		21400				Attempting to Start a Plugged Machine
9	1	35	Corn Picker D	Standard	1570 - 1740	3990	622 - 1031		727	Picking Corn
10	1	35	Baler E	Standard		18300 - 20600	5860 - 7470	12100	1140	Baling Alfalfa
11	1	35	Baler E	Standard	13100		6550 - 8140	11600 -	1545	Recheck of

Test No.	Tractor Model	Approx. Max. Tractor bhp	Implement Make and Model	Coupling in PTO Drive	Max Starting Torque w/ Normal Clutch Engagement (lb-in)	Max Starting Torque w/ Rapid Clutch Engagement (lb-in)	Max. Operational Torque Average Conditions (lb-in)	Max. Operational Torque Near Plugged Conditions (lb-in)	Ave. Torque Norm. Op. Conditions (lb-in)	Work Being Performed
								15000		Test 10
12	1	35	Baler E	Spec. Slip	10700 - 12100*	10700 - 12100*	7250 - 8920	11500 - 13300*	2250	Baling Alfalfa
13	1	35	Baler E	Spec. Slip	10100*		5600 - 11100	10350 - 12600	1580	Baling Straw
14	9	40	Baler E	Standard	12250		7749 - 10945	10960 - 12095	1938	Baling Alfalfa
15	1	35	Baler E	Standard And Universal Joints Aligned			4501 - 5867		1383	Baling Alfalfa
16	1	35	Baler F	Standard	16500		8600	22700		Baling Alfalfa
17	1	35	Combine G	Spec. Slip	5000*	5000*	5000*	5000*		Baling Alfalfa
18	1	35	Combine G	Standard		10100 - 16600*	3760	9380	1890	Combining Windrows
19	1	35	Combine G	Spec. Slip			7150	7760 - 9130	1700	Combining Windrows
20	1	35	Combine G	Spec. Slip		7350 - 8650	4160 - 4200	7470	1600	Straight Combining
21	2	25	Hammer Mill H	Standard	9030	17500 - 20150	4145	7270	2700	Grinding Ear Corn
22	1	35	Hammer Mill H	Standard	6130		3740	14900	2140	Grinding Ear Corn
23	1	35	Hammer Mill H	Spec. Slip	8230*	8230*		6920	4210	Grinding Ear Corn
24	4	45	Hammer Mill J	Standard	10150	25800	7800	13000	5450	Grinding Ear Corn
* Safety Clutch in PTO Line Slipped Limiting Torsional Load to This Value										

In a study on engine loading, an AC D-17 tractor was instrumented and used for several different tasks (Ricketts and Weber, 1961). The test tractor was used on twelve different farms and the recorded data (figures 3 through 6) show the range of engine power and speed in which each task was performed. Figure 7 shows a breakdown of the number of hours that a typical farm tractor is used over a varying number of tasks. The data were compiled from the yearly log of 25 different farmers near the University of Illinois, Urbana.

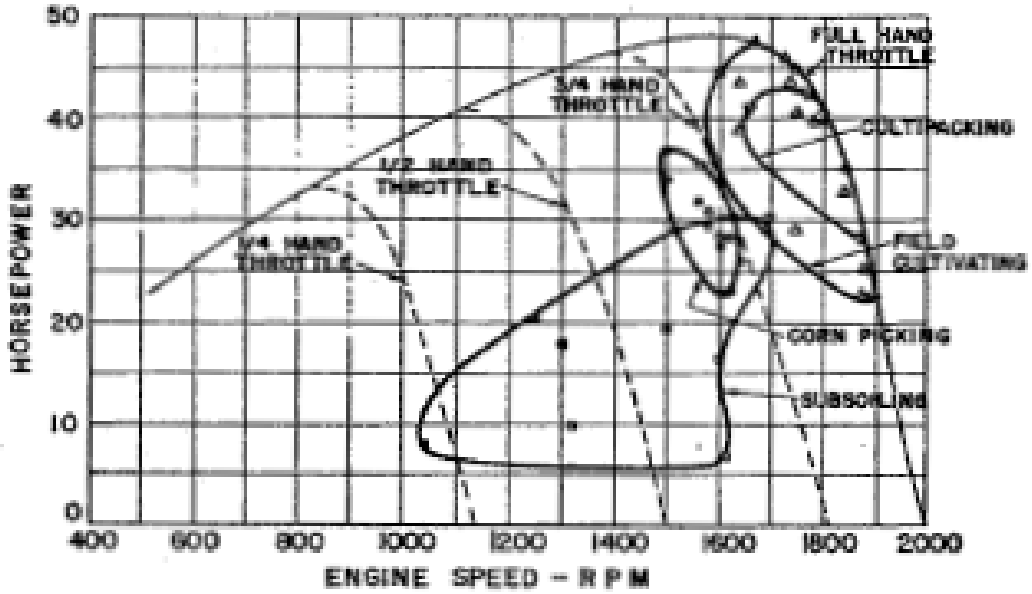

Figure 3: Range of engine horsepower and speed requirements for corn picking, subsoiling, field cultivating and soil packing (Ricketts, 1961)

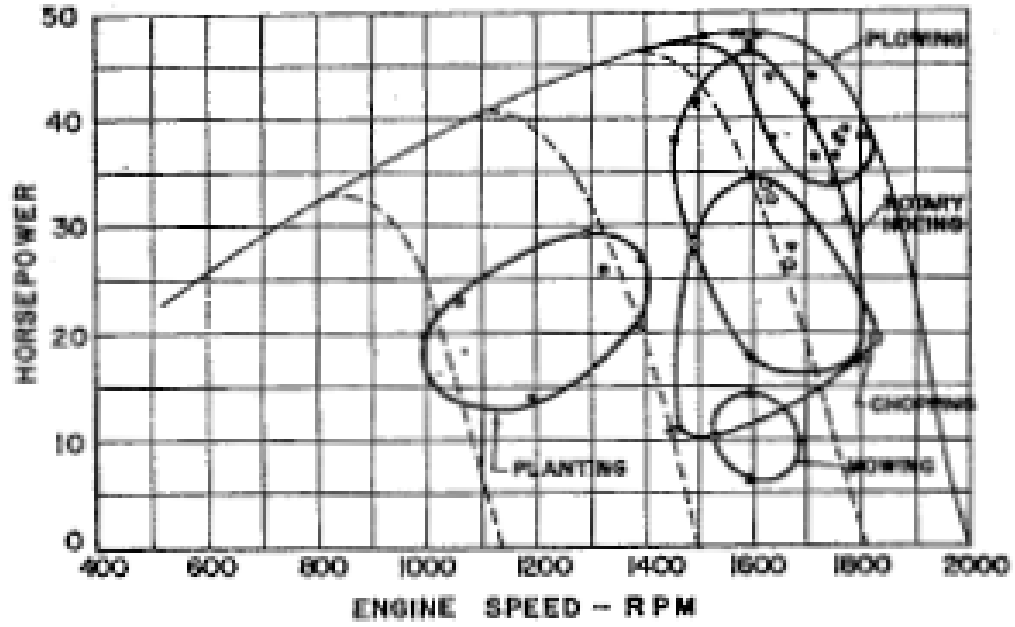

Figure 4: Range of engine horsepower and speed requirements for planting, mowing, chopping, rotary hoeing and plowing (Ricketts, 1961)

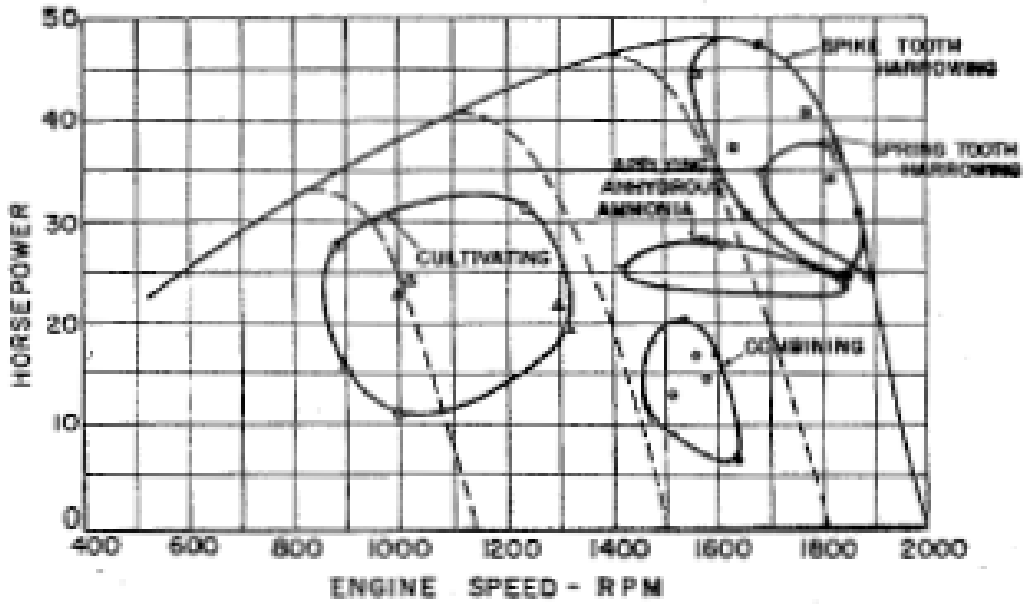

Figure 5: Range of engine horsepower and speed requirements for cultivating, combining, applying anhydrous ammonia, and spike- and springtooth harrowing (Ricketts, 1961)

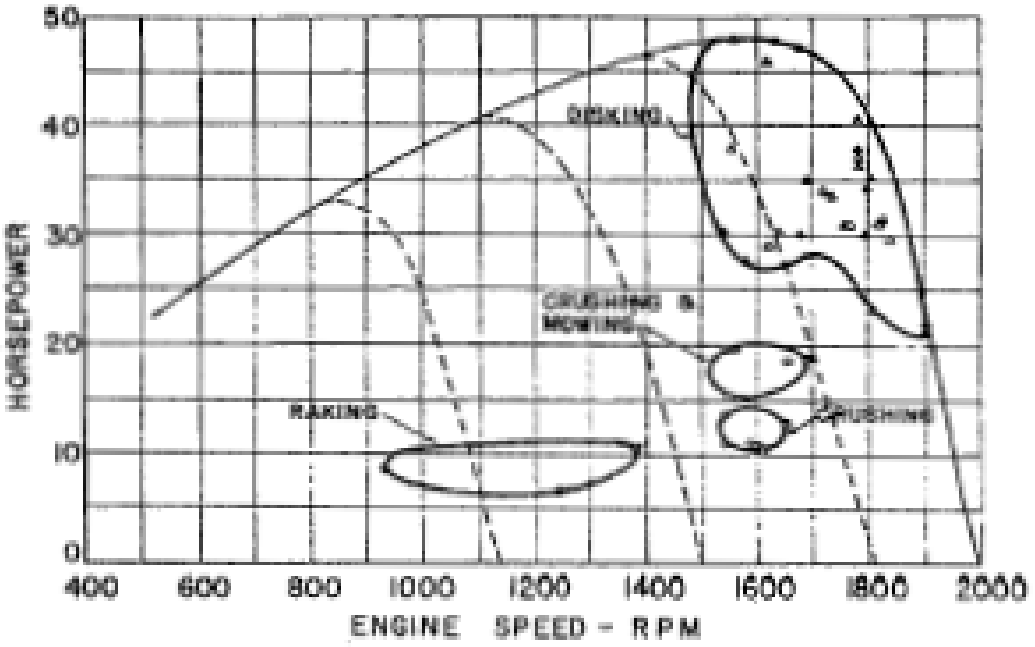

Figure 6: Range of engine horsepower and speed requirements for raking, crushing, crushing and mowing, and disking (Ricketts, 1961)

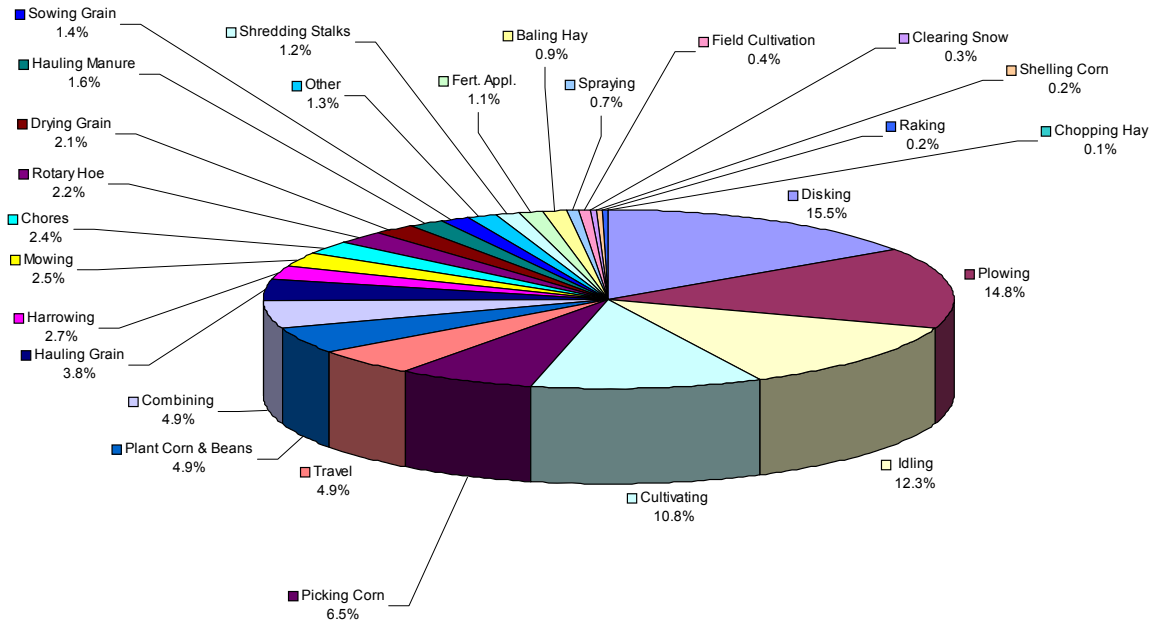

Figure 7: Distribution of hours of tractor use by operation – average of 340 hours for 25 tractors (Ricketts, 1961)

A paper presenting the functionality of a portable instrumentation package that was designed for tractors can give us an idea of load variation. Figure 8 shows both the vehicle speed and the draft power required for chisel plowing with a John Deere 3020 tractor.

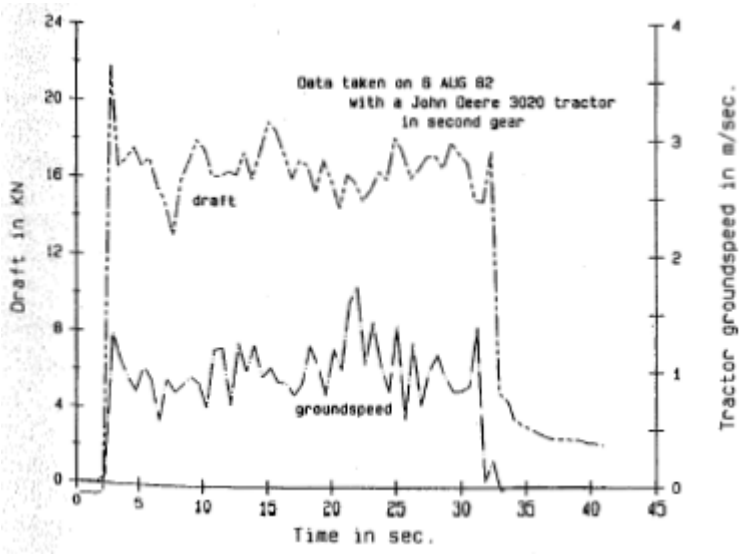

Figure 8: Data from chisel plowing in dewey oats stubble (Strange et al., 1984)

In a different case a Cockshutt 30 hp (22kW) tractor was fitted with a torque meter on the shaft connecting the clutch to the transmission. Figure 9 shows the variable load of an implement (Gerlach, 1966).

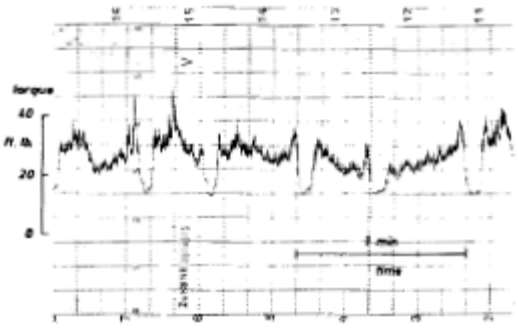

Figure 9: PTO torque characteristics when operating a grain binder (Gerlach, 1966)

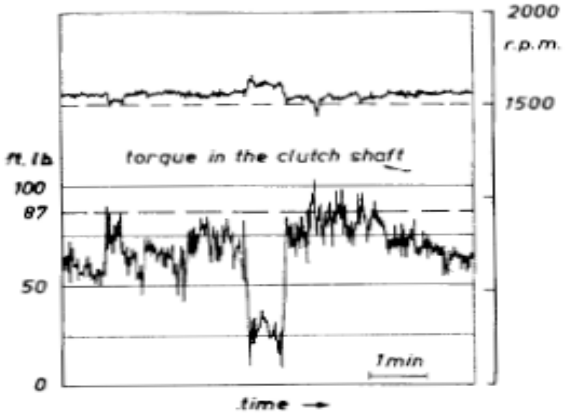

Figure 10: Engine speed and torque when plowing heavy ground (Gerlach, 1966)

In the interest of directly mapping the power demand on a tractor a study was performed to observe which regions of the engine map were most commonly used during various operations. A turbo-charged Ford 6610 AC (50 hp, 37kW) was fitted with data acquisition equipment, and was used by different operators and different tasks to show the change in engine usage. The change in engine usage then translates into a change in fuel consumption (Hansen et al., 1986). The Z-axis in figures 11 through 16 shows a percent time spent at that point. A number is specified at the origin to represent the amount of time at idle. The idle time was not plotted because it would have made the rest of the data difficult to be visualized.

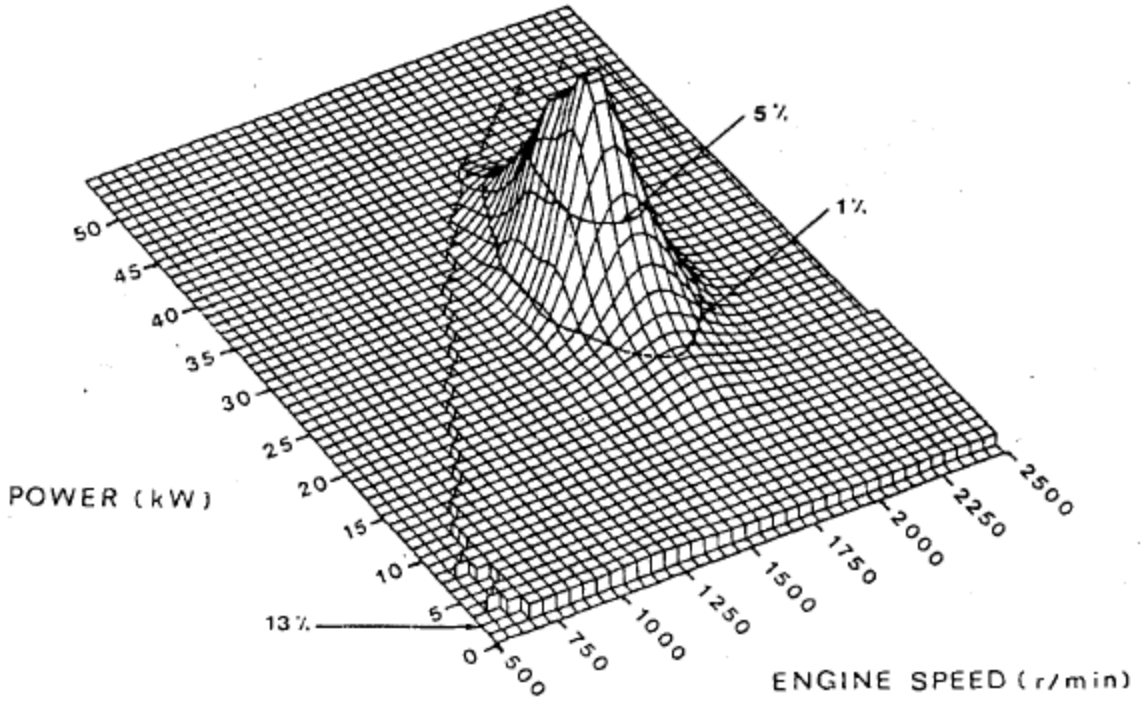

Figure 11: Surface of field time data for operator 1 using a moldboard plow (Hansen et al., 1986)

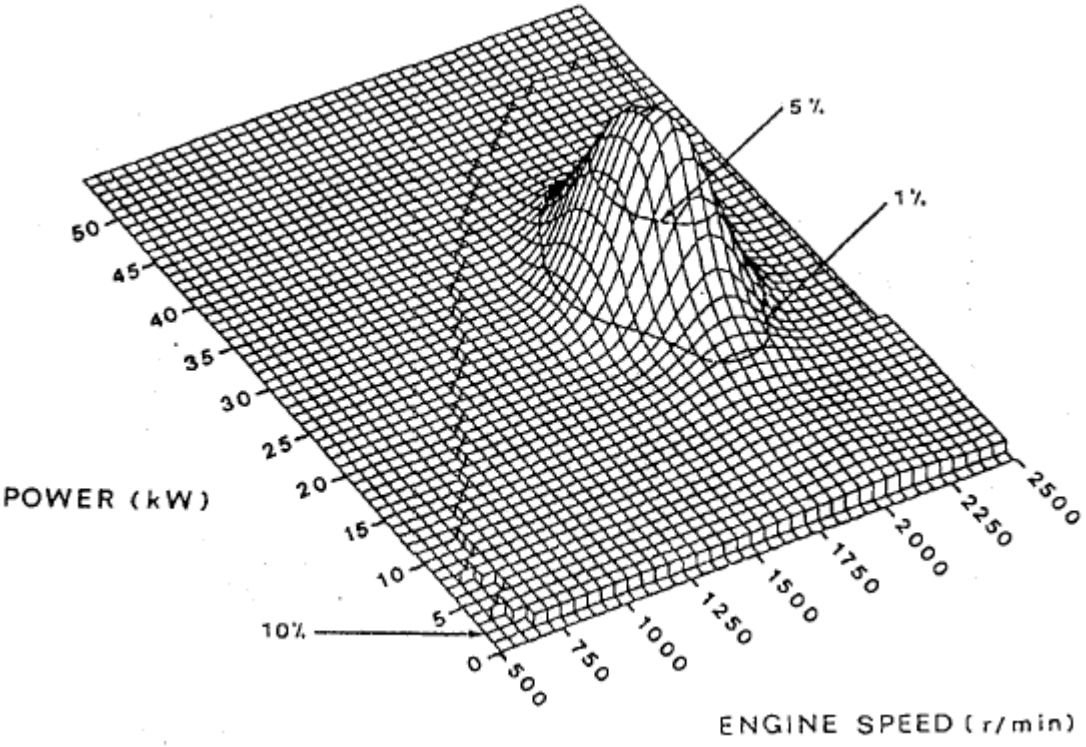

Figure 12: Surface of field time data for operator 2 using a moldboard plow (Hansen et al., 1986)

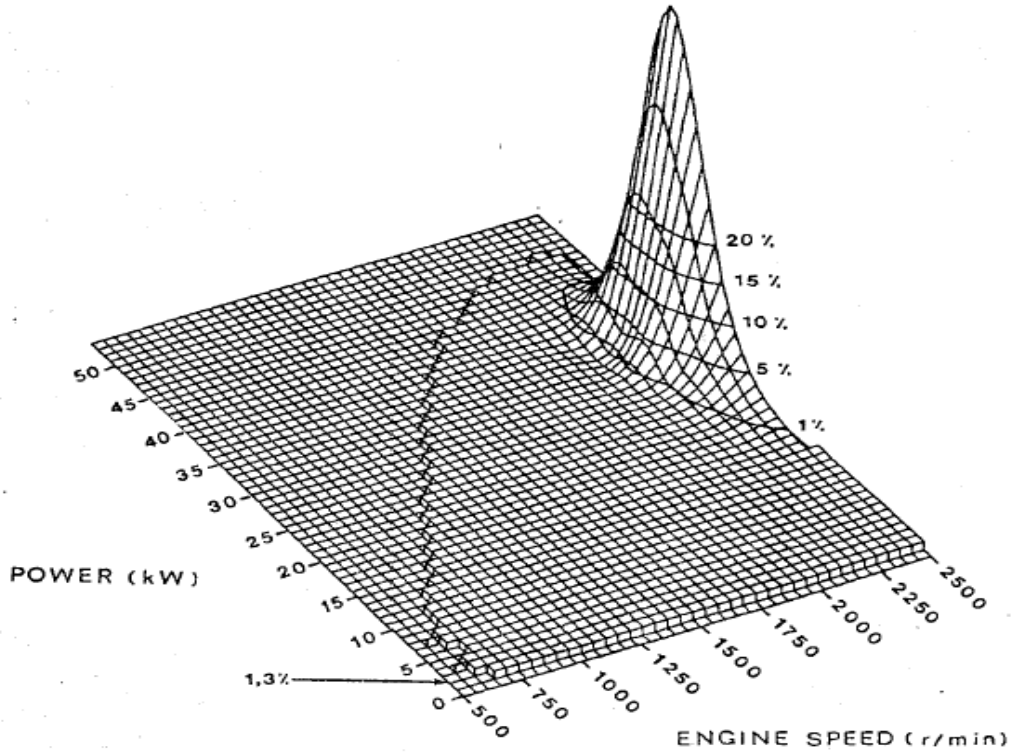

Figure 13: Surface of field time data for operator 3 using a moldboard plow (Hansen et al., 1986)

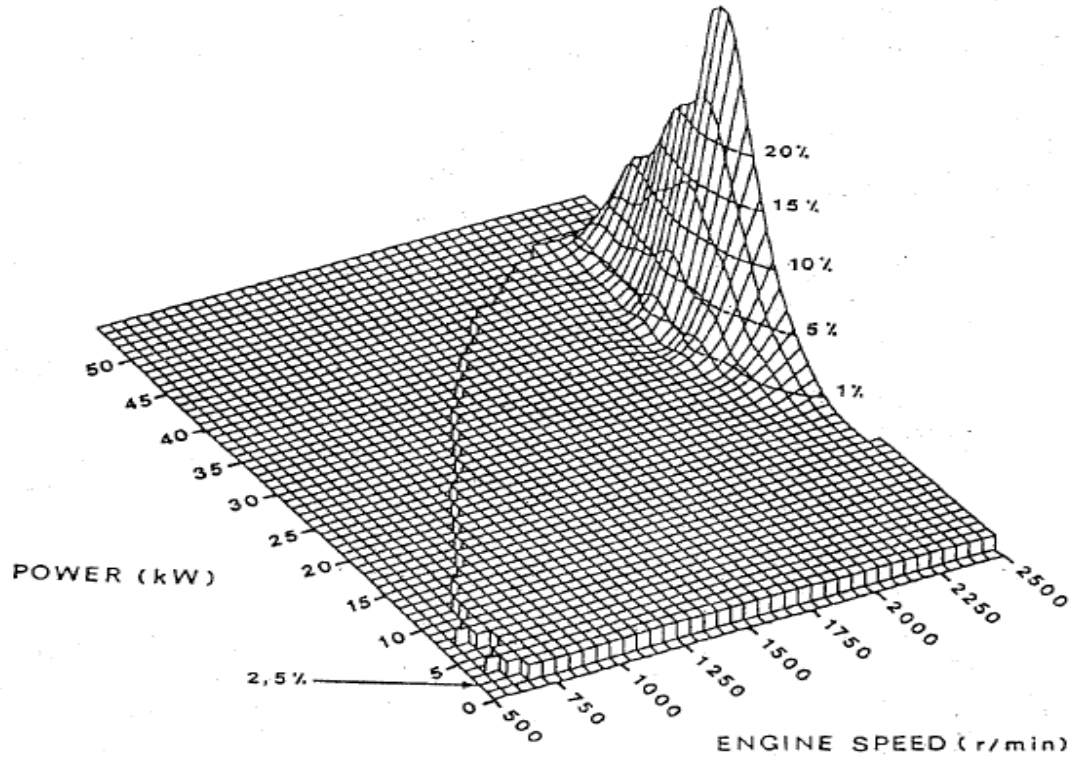

Figure 14: Surface of field time data for a disk harrowing operation (Hansen et al., 1986)

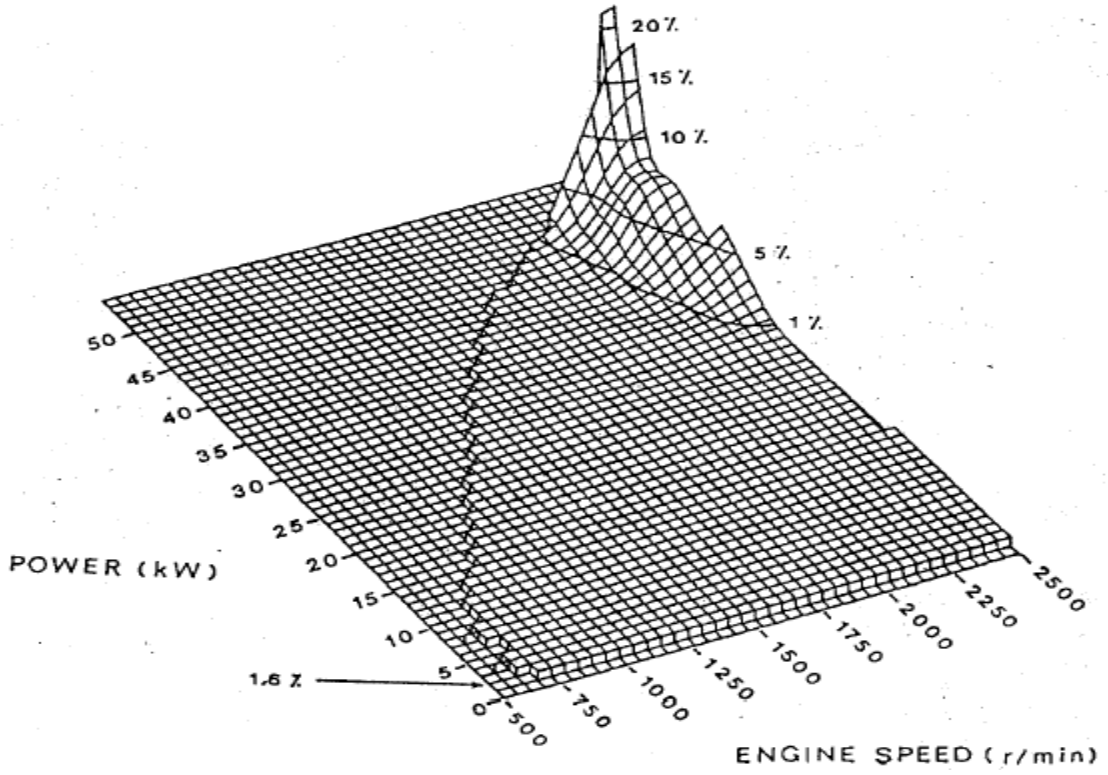

Figure 15: Surface of field time data for a ripping operation (Hansen et al., 1986)

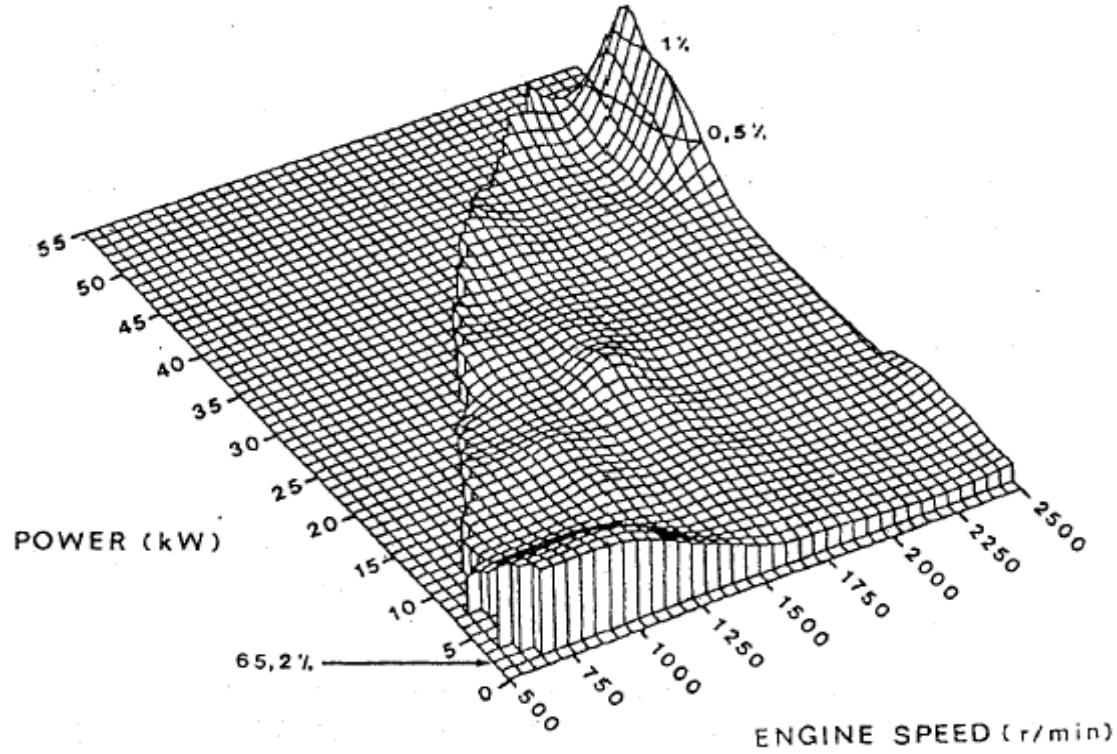

Figure 16: Surface of field time data for a haulage operation (Hansen et al., 1986)

Figures 17 and 18 show plotted torque vs. time for a tilling operation. The only differences between these two conditions were the tiller blade shapes and rotation direction. The operation was performed in Bangkok clay soil. The PTO speed was 540 rpm (Salokhe and Ramalingam, 2002).

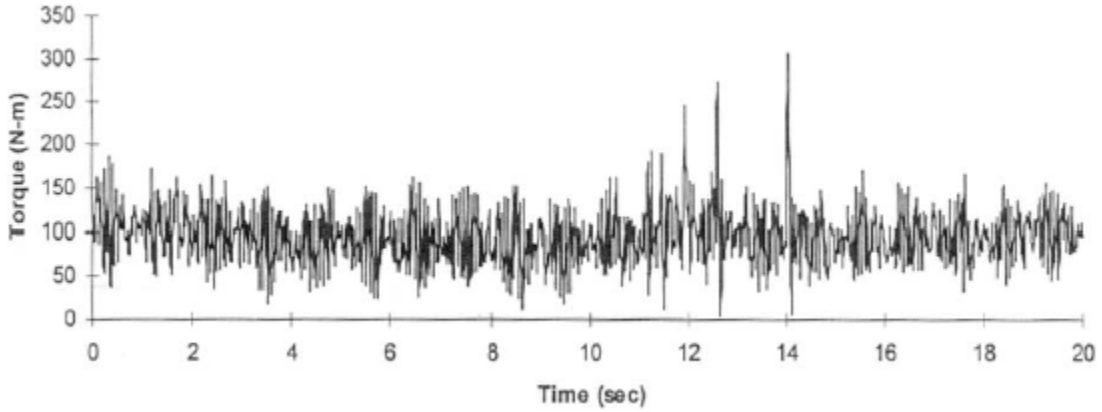

Figure 17: Torque signals measured for the scoop blades on reverse-rotary tiller (Salokhe and Ramalingam, 2002)

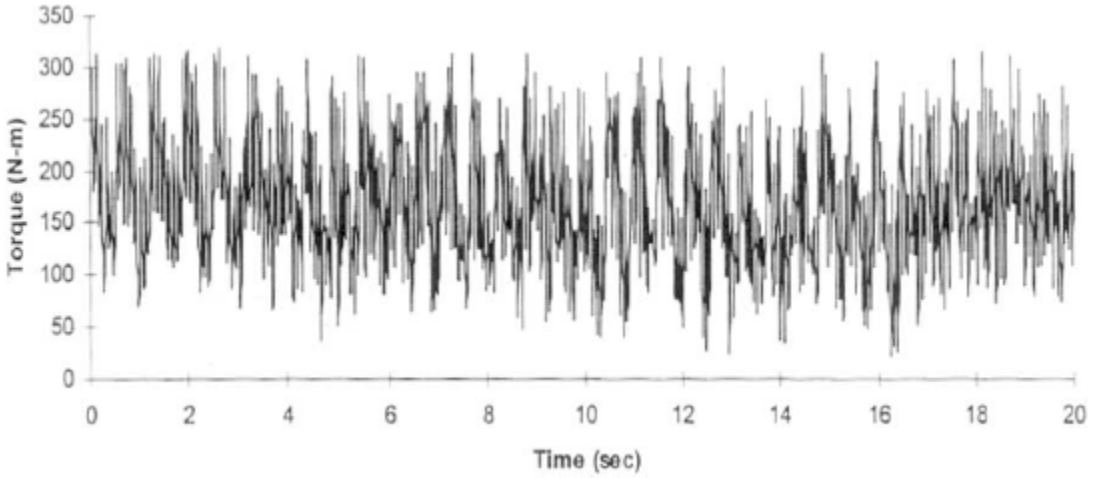

Figure 18: Torque signals recorded for C-blade rotary tiller with forward rotation (conventional)(Salokhe and Ramalingam, 2002)

Implement Power Draw

Because agricultural tractors are designed to perform a myriad of tasks, the American Society of Agricultural Engineers has developed equations for calculating the draft and rotary power for agricultural implements (ASAE, 2003). These equations and tables of coefficients yield an average value of the power required for each operation taking into account the dimensions of the implement and the conditions of the soil. As has been shown these power draws do vary significantly with time depending on the operation. However, the variations are periodic and can be predicted.

VEHICLE REQUIREMENTS

For fuel cell powered tractors to be considered viable competitors to diesel powered tractors they need to show similar performance. The information that follows discusses performance ranges for three groups of agricultural tractors in order to obtain performance set points for a fuel cell tractor. In each case three groups of tractors were evaluated based on their PTO power. The first group consisted of tractors with PTO power of up to 20 kW, the next group with PTO power between 20 and 200 kW, and finally tractors with a PTO power greater than 200 kW.

Traction Requirements

Tractors were originally designed around the basis of creating greater traction for vehicles used in off road work. Thus this topic has been studied in great depth. Presented below is only a slight mention of the overall subject. Traction has been defined as "the force derived from the interaction between a device and a medium that can be used to facilitate a desired motion over the medium" (Gill, 1986). The net traction for a tractor drive wheel is determined by Equations 1 and 2 below (ASAE, 2003).P

$$NT = W\left(0.88\left(1-e^{-0.1B_n}\right)\left(1-e^{-7.5s}\right)-\frac{1}{B_n}-\frac{0.5s}{\sqrt{B_n}}\right) \quad \text{EQ. 1}$$

$$B_n = \left(\frac{CIbd}{W}\right)\left(\frac{1+5\frac{\delta}{h}}{1+3\frac{b}{d}}\right) \quad \text{EQ. 2}$$

Where:

S = Slip
W = Dynamic wheel load in force units normal to the soil surface
CI = Cone index for the soil
b = Unloaded tire section width
d = Unloaded tire diameter
h = Tire section height
δ = Tire deflection

As can be seen by the equations above, traction is directly related to weight. Larger tractors can develop greater traction resulting in larger drawbar power. It is also important to realize in agricultural applications that traction improvements should not be accomplished at the detriment of the soil structure. Larger tractors might develop greater traction, but may also compact the soil, reducing aeration and causing erosion. Even before the engine power is available to the wheels, limited transmission efficiencies, which range between 82% and 87%, cut into the available power (ASAE, 2003). Wheel slip also plays a large roll in the overall efficiency of the tractor accounting for an additional 7% to 12% (Ryu et al., 2003). The design for maximum efficiency requires sizing the available drawbar power to meet the net traction of the tractor.

Power Train Configurations
There are several variations of tractor drive train configurations especially when evaluating the differences between wheeled, tracked and articulated tractors. Figure 19 shows a block diagram of a standard tractor drive train.

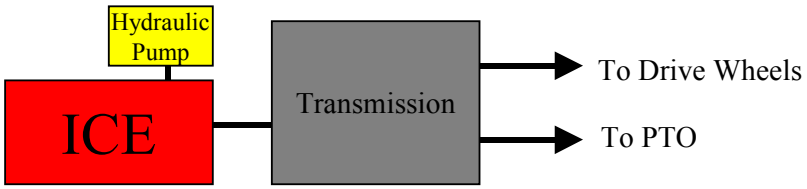

Figure 19: Block diagram of tractor power train

Depending upon the vehicle a tractor transmission can transmit power to the rear drive wheels, the front drive wheels, as well as the front and rear PTOs. The transmission is vital to the effectiveness of the tractor since torque requirements can demand large variations during operation, and most often the maximum amount of engine power is required as has been shown. The transmissions are generally very costly due to the number of gears, and the high stress present under low RPM and high torque work.

Prime Mover Torque
The measure of prime mover torque is the moment that a vehicle can continuously exert trough the drive wheels. The torque at the wheels is increased by the use of gear reduction, but the amount of torque available to the transmission is dependent on the engine characteristics. If the maximum torque the vehicle can supply is insufficient to meet the load the engine will stall. Thus with current tractor design it is important to have a sufficient torque reserve (or torque back-up) (Culpin, 1992). When an engine has a higher torque at an engine speed slower than that corresponding to the maximum power it is said to have a torque reserve. When operating at maximum power if a higher torque is required the engine speed drops and the torque increases to meet the demand

From the data collected from the Nebraska tractor tests and OEM data it is seen that there is a large range of vehicles with different available torques. For tractors in between 20 to 200 kW the maximum torque output varied from 96 to 953 Ft Lb. For tractors with PTO power greater than 200 kW the maximum torque ranged from 901 to 1757 Ft Lb. In every case the tractors evaluated had a torque reserve. (There was no torque available for the tractors with less than 20 kW of PTO power).

Vehicle Speed and Acceleration
Generally speaking tractors are not evaluated on the time it takes to accelerate from 0 to 60 mph. That is because most tractors are not designed to work at 60 mph. Although acceleration is not a key factor in agricultural vehicles for a

comparison of a fuel cell tractor to a traditional tractor acceleration should be similar. It would be useful to have a simulation to predict the acceleration of a tractor with changes made to the drive train. However, for an evaluation we can look at the laws of physics starting with Equation 3.

$$F = ma \qquad \text{EQ. 3}$$

If the mass of the tractor stays the same and the forces on the tractor are equivalent in the case of the fuel cell tractor and the internal combustion engine tractor than the acceleration should be the same. By making the torque equivalent the acceleration should also be equivalent.

The vehicle speed V is equal to the angular velocity of the wheels times the effective rolling radius of the wheels running on a particular soil. The angular velocity of the wheels depends on the torque supplied to the wheel and the tractive efficiency of the wheel (Zoz et al., 2002).

Power Profiles

A more detailed analysis of power profiles is given in the beginning of this report with data focusing mostly on field operations. It is believed that the power requirements, although transient in nature and dependent on the operation, are less variable for medium to large-scale tractors. For smaller tractors it is expected that the average use of the tractor will be chore work implying vast transient operations.

Typical PTO by Class

Max PTO power recorded at 540 RPM and 1000RPM was collected from the Nebraska tractor test reports, and when not available from the manufacturers. The data collected were divided into three tables: one for tractors with up to 20 kW of PTO power, next for tractors with PTO power between 20 kW and 200 kW and finally for tractors with PTO power greater than 200 kW, all of which can be seen in Appendix A. For each of the three groups examined there is a broad range of PTO powers available enabling a tractor choice for almost any power level, which is very different from the automobile market where distinct classes exist. It is the authors recommendation that if the goal is to build a prototype to compare with the 20 kW group of compact tractors that the highest power rating of 20 kW be chosen. However, with the broad ranges of available tractors it is dificult to give a general PTO requirement for each of these three groups.

Typical Hydraulic Actuator Requirements by Class

For the 20 kW tractor group the hydraulic power ranged from 4.1 to 9.4 kW. For the 20 to 200 kW group the hydraulic power ranged from 7.8 to 50.6 kW, and for the 200 kW and up group the hydraulic power varied from 26 to 51 kW (can be seen in Appendix A). It is also worthy to note that several tractors came with the option of an upgraded hydraulic pump yielding higher hydraulic power. In general it is difficult to choose a general hydraulic power requirement for each of these groups since the spread of possibilities is so vast just as in the case of PTO

power. For the traditional tractors it was found that the hydraulic pump was powered by a mechanical connection to the engine. Although hydraulic power was recorded, the performance of the hydraulic systems can be very different in nature despite similar power. This is due to different uses, flow rates and pressures. Once again if a comparison was to be made it would be advisable to use a hydraulic system with similar specifications to the control tractor.

Combine Harvesters

Limited amount of information was available on the power profiles of combine harvesters. Table 3 shows power specifications for several combines collected from OEM data sheets. The combines are high power, and during the harvest are generally run continuously until the harvest is complete. Due to the number of functions taking place on the harvesters, and the current method of mechanical power transmission, it has been shown that the use of electric motors could prove advantageous in increasing overall efficiency and optimizing the use of space (Bernhard, 2003).

Table 3: Power specifications of combine harvesters

Make	Model	Power	
		hp	kW
Massey Ferguson	8680	260.0	193.9
John Deere	9560 STS	265.0	197.6
Massey Ferguson	9690	285.0	212.5
Challenger	CH660	285.0	212.5
New Holland	CR940	295.0	220.0
New Holland	CX840	295.0	220.0
John Deere	9660 STS	305.0	227.4
Massey Ferguson	9790	330.0	246.1
New Holland	CR960	330.0	246.1
New Holland	CX860	330.0	246.1
John Deere	9760 STS	340.0	253.5
Challenger	CH670	350.0	261.0
New Holland	CR970	370.0	275.9
New Holland	CX880	370.0	275.9
John Deere	9860 STS	375.0	279.6
Case IH	AFX8010	375.0	279.6

OPERATING REQUIREMENTS FOR A FUEL CELL POWER UNIT

Fuel cells have their highest efficiency at high voltages corresponding to lower loads through the cell polarization curve (Larminie, 2003). An equation for efficiency based on cell voltage can be seen in Equation 4.

$$\text{Efficiency} = u*(Vc/1.48)*100 \qquad \text{EQ. 4}$$

The typical power demand in agricultural vehicles is constant and high. Compared to current engine ratings, they are operated close to max RPM. To maintain a high efficiency the fuel cell stack would need to be oversized so that it would be able to run at an optimum power level. Since medium to large scale tractors are not subject to the constant unexpected variable loads seen by urban automobiles, and do not require heavy breaking, large scale hybridization would not be of much benefit (Schuller, 2002).

Power Train Differences Required to Accommodate the Fuel Cell

It is expected that due to the current series plate construction of fuel cell stacks that the vibration seen in off-road applications could be detrimental.

Temperature will also play a role for fuel cell tractors to be used in Midwest farming during the winter. Stack heaters and insulation will be required to protect the electrolyte and shorten start up times in severe cold. Depending on the operational temperature of the type of stack used cooling can also become an issue. PEM stacks currently used in automotive application have an operation range of 30-80P^{oP}C. Unless cooling is to come from a source other than a water circulated radiator a very large surface area is going to be required especially on hot summer days.

Air purity is yet another concern for fuel cell systems since the poisoning of cell catalyst is the greatest current threat to operating stacks. A series of advanced air clean up devices should be required to ensure that the stack is not polluted by particulate matter.

Aside from the effects of vibration, temperature and air purity, the concept of a fuel cell powered tractor offers greater flexibility in power train layout since the components are not mechanically linked. This would enable the designers to place the components such that the overall vehicle has the weight distributed for optimum traction. A block diagram of a fuel cell powered tractor power train can be seen in Figure 20.

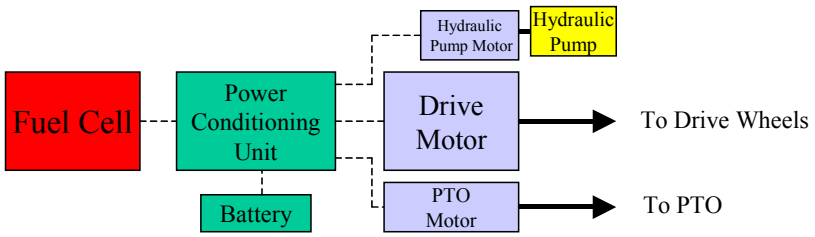

Figure 20: Block diagram of fuel cell tractor power train

The electric transmission of power affords the elimination of costly transmissions and uncouples the power generation from the usage.

Dealing with Transients

The transient response of the fuel cell stack itself is not a limiting factor. It has been shown that a PEM fuel cell can reach 90% production within 1 second (Yan et al., 2005). Turbocharged Diesel response times have been shown to be on the order of 1.7 sec (Katrasnik et al., 2003). When dealing with fuel cell systems the fuel processor has proven to be the limiting mechanism. It has been shown that the limiting process in the indirect liquid-fueled fuel cell power train is the slow response of the fuel reformer, which can take up to 20 seconds to ramp up to 99% of the flow demand (Emonts et al., 2000; Betts, 2002; Beckhaus et al., 2004).

The strategy behind a hybrid power train is to allow for the downsizing of the power plant by compensating with some other form of stored energy. This is a great strategy for vehicles that rarely run at full power such as cars, or an example found of a hybrid electric forest vehicle(Carlini et al., 1997). However, as can be seen by Figures 11 through 16 agricultural tractors are often run at full power for extended periods of time. Even in the case of the medium to large scale tractors some degree of hybridization is recommended. By designing a hybrid fuel cell system the advantage would be that you would be able to quickly provide power for any oscillatory demands, as well as be able to exceed the rated power for a short duration to overcome any abnormal obstacles.

VEHICLE ARCHITECTURE RECOMMENDATIONS

It is important to note that the basis of this study is on an analysis of power demand and load profiles only. Presented below is a comparison showing that the use of electric motors is well suited to the torque demands of agricultural work. Also discussed is recommendations by the author for fuel cell tractor prototypes in each of the three pre-designated groups.

Properties Of Diesel Engines Vs. Fuel Cell / Electric Motors

As previously mentioned several electric tractors have been developed. Their greatest shortcoming has been battery life, limiting the tractors to chore usage. If a fuel cell was used to power the electric tractor the strength of an electric tractor

could be fully realized, which is the electric motor. One of the important factors in tractor engine design is having a torque reserve so that, for example, when a plow hits a tree root, or a large stone, the engine output increases in torque as the speed drops, otherwise in the case of an IC engine it will stall. As can be seen Figure 21 electric motors are great in this regard (the electric motor in Figure 21 is a series wound DC traction motor). If we also compare the efficiency plot in Figure 21 back to the usage plots in Figures 11 through 16 we can see that if an electric motor was being used that the motor efficiency would almost always be at maximum.

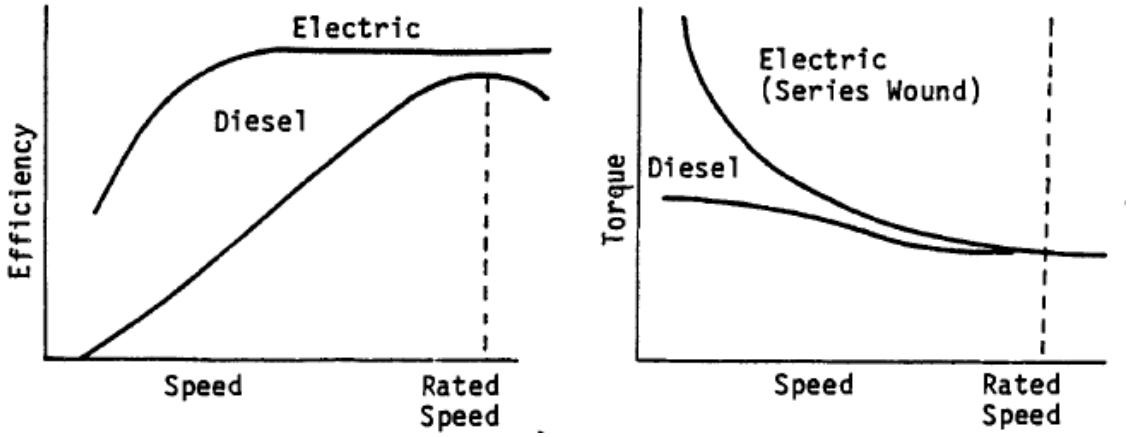

Figure 21: Comparison between electric and diesel motor characteristics, which have identical power ratings (Christianson, 1984)

During the literature review it was found that several computer models have been created to evaluate tractive efficiency of tractors as well as the draft of pulled implements (Sonnen, 1969; Clark, 1981; Dwyer, 1987). As mentioned previously implement draft can be found using the ASAE standards if soil composition is known (ASAE, 2003). There have also been several models developed to evaluate tractive efficiency and vehicle performance on an economic scale (Al-Janobi, 2002). It is recommended that a more comprehensive model be developed to evaluate possible drive train design taking into account the often variable nature of the load profile with outputs such as vehicle performance, efficiency and fuel consumption. ADVISOR is one example of a simulation program developed to evaluate different automobile power train configurations including fuel cells (Markel et al., 2002; Maxoulis et al., 2004).

Vehicle Recommendations

Without a detailed computational analysis it is difficult to determine what architecture would yield the best performance. However, from the data collected on the uses of different sized tractors and the response times of fuel processors. The following is recommended.

For small tractors to be used for personal or chore usage which would currently fall into the category of less than 20 kW it is recommended that a slightly larger

fuel cell stack of 25 kW be used with a direct drive electric motor. Compressed hydrogen would yield the fast transient response times required, and a moderate level of hybridization should be used to recoup the energy that would otherwise be lost by frequent stops and starts. Aside from the main drive motor, an additional hydraulic pump motor should be used to provide hydraulic power. An additional motor designed to operate at 540 rpm could be used to supply PTO power and enable the motor to be optimized for operation at that speed.

For medium scale tractors that currently utilize 20 to 200 kW of power the load profiles have shown to be relatively constant with predictable transients. For this class of vehicles it is also recommended that the fuel cell stack be slightly larger than the current compression engine counterpart. Studies have shown that the vehicles are most often operated at maximum power, and to obtain the highest possible efficiency out of the fuel cell stack it would be ideal to operate the stack at partial power. For ease of operation and longer hours of operation it is recommended that vehicles of this class use on board liquid fuel reformers, with a small degree of hybridization to handle unexpected transients. Since the load profiles of the operations performed by these vehicles is fairly predictable and generally continues for many hours at a time the liquid fuel option is well suited.

For ease of implementation a single electric motor could directly replace the internal combustion engine on a current tractor chassis retaining the use of the transmission. If implementation costs are not an issue there could be separate motors used for prime motive force, the hydraulic pump and each PTO connection.

The largest class of agricultural tractor evaluated is those that are over 200 kW. These vehicles would be best suited to a similar architecture as the medium scale tractors.

It is anticipated that for fuel cell vehicles to be used in agricultural applications, eventually, drawn implements that currently use PTO power could be fitted with their own electric motor(s), and a cable could be run to the implement to supply power. This would yield overall increases in efficiency since the fuel conversion of the fuel cell is greater than that of the internal combustion engine, and the efficiency of the electric motor is generally higher than that of the transmission of power through the mechanical transmission, universal joint(s) of the PTO and mechanical transmission of the implement. The elimination of the universal joints connecting the PTO outlet to the implement would also afford a greater degree of flexibility in operation.

If fuel cells were to be tested for use in large scale tractors it is recommended that combine harvesters be a starting point. The elimination of the numerous mechanical transmissions of power from the engine to the individual processes could result in much greater efficiencies. Also the size of combines would easily comply with the requirements of an indirect liquid fueled fuel cell.

CONCLUSION AND RECOMMENDATIONS

As has been shown the electric motors are a good match to the power characteristics required by agricultural work. On the basis of load profiles alone the authors would highly recommend the use of a hybrid fuel cell power train for medium to large agricultural tractors (Carlini et al., 1997).

It is recommended that further studies be performed to research the effect of energy density in tractor systems to determine if the size and weight of acceptable fuel cell systems are compatible with off road use. A vehicle simulation should be made to facilitate a parametric evaluation of possible power trains and their economical impacts.

APPENDIX

Table A1: Tractor data for small tractors with up to 20 kW of PTO power

Make	Drive	Model	Weight		Power at 540 PTO RPM		Hydraulic power		Hitch Class
			(kg)	(LB)	(kW)	(hp)	(kW)	(hp)	
Massey Ferguson	Std.	MF 1417-4	645	1422	9.9	13.3	4.1	5.4	1
Case-IH	Std.	DX18E	596	1314	10.2	13.7			1
New Holland	Std.	TZ18DA	595	1311	10.2	13.7			1
John Deere	4WD	4010	644	1420	10.4	14.0	4.9	6.6	1
Case-IH	Std.	DX22E	596	1314	12.7	17.0			1
New Holland	Std.	TZ22DA	599	1320	12.7	17.0			1
Case-IH	Std.	DX23	722	1592	13.0	17.5			1
John Deere	4WD	2210	635	1400	13.2	17.7	4.7	6.3	1
New Holland	Std.	TC23DA	722	1592	13.8	18.5			1
Massey Ferguson	4WD	1523	695	1532	13.9	18.7			1
AGCO	4WD	ST24A	710	1565	14.2	19.0			1
Case-IH	Std.	DX25E	600	1323	14.2	19.0			1
New Holland	Std.	TZ25DA	599	1320	14.2	19.0			1
AGCO	Std.	ST25	720	1588	14.5	19.5	5.1	6.9	1
Massey Ferguson	Std.	MF 1423-4	679	1498	14.5	19.5	5.1	6.9	1
AGCO	4WD	ST22A	620	1367	14.7	19.7			1
Case-IH	Std.	DX26	726	1600	14.7	19.7			1
New Holland	Std.	TC26DA	726	1600	15.3	20.5			1
Massey Ferguson	Std.	MF 1429-4	1240	2734	17.2	23.0	8.1	10.9	1
Case-IH	Std.	DX29	1122	2474	17.6	23.6			1
John Deere	FWA	790	975	2150	17.9	24.0	5.0	6.7	1
AGCO	Std.	ST30x	1147	2528	18.3	24.5	6.9	9.3	1
AGCO	4WD	ST28A	1000	2205	18.3	24.5			1
Massey Ferguson	4WD	MF 1428V-2/4	1064	2345	18.3	24.5	6.9	9.3	1
Massey Ferguson	4WD	1528	1099	2423	18.3	24.5			1
Massey Ferguson	4WD	1531	1099	2423	18.3	24.5			1
New Holland	Std.	TC29DA	1122	2474	18.6	25.0			1
AGCO	Std.	ST32	1198	2642	19.3	25.9	7.2	9.7	1
AGCO	4WD	ST33A	1000	2205	19.3	25.9			1

Make	Drive	Model	Weight		Power at 540 PTO RPM		Hydraulic power		Hitch Class
			(kg)	(LB)	(kW)	(hp)	(kW)	(hp)	
Massey Ferguson	Std.	MF 1431-4	1069	2356	19.3	25.9	7.2	9.7	1
AGCO	4WD	ST34A	1290	2844	19.4	26.0			1
Massey Ferguson	4WD	1533	1290	2844	19.4	26.0			1
Challenger	4WD	MT265B	1422	3136	19.4	26.0	9.4	12.6	1

Note: All of the data presented is from the manufacturers, since the Nebraska tests do not give results for compact tractors. Hence, max drawbar pull and max torque were unavailable.

Table A2: Tractor data for medium scale tractors with PTO power ratings between 20 kW and 200 kW

Make	Drive	Model	Weight		Power at 540 PTO RPM		Power at 1000 PTO RPM		Hydraulic power		Hitch Class	Max draw bar pull unballasted		Max torque	
			(kg)	(LB)	(kW)	(hp)	(kW)	(hp)	(kW)	(hp)		(lb)	(kN)	(lb ft)	(Nm)
Case-IH	Std.	DX33	1122	2474	20.1	26.9					1				
AGCO	Std.	ST35	1437	3168	20.1	27.0			8.4	11.3	1				
AGCO	Std.	ST35x	1399	3085	20.1	27.0			8.4	11.3	1				
Massey Ferguson	Std.	MF 1433-4	1275	2810	20.1	27.0			8.4	11.3	1				
Massey Ferguson	Std.	MF 1433V-4	1265	2788	20.1	27.0			8.4	11.3	1				
New Holland	Std.	TC33DA	1122	2474	21.3	28.6					1				
John Deere	4WD	4410	1284	2830	21.6	29.0			15.0	20.1	1				
Case-IH	Std.	D/DX35	1497	3300	21.7	29.1					1				
New Holland	Std.	TC35DA	1523	3357	21.7	29.1					1				
New Holland	Std.	TC35A	1466	3231	22.1	29.6					1				
AGCO	4WD	ST41A	1310	2888	23.1	31.0					1				
Massey Ferguson	4WD	1540	1310	2888	23.1	31.0					1				
Challenger	4WD	MT275B	1437	3169	23.1	31.0			9.4	12.6	1				
AGCO	Std.	ST40	1507	3323	24.2	32.4			8.4	11.3	1				
AGCO	Std.	ST40x	1442	3180	24.2	32.4			8.4	11.3	1				
Massey Ferguson	Std.	MF 1440-4	1361	3001	24.2	32.4			8.4	11.3	1				
Massey Ferguson	Std.	MF 1440V-4	1331	2935	24.2	32.4			8.4	11.3	1				
Case-IH	Std.	D/DX40	1531	3375	24.8	33.2					1				
New Holland	Std.	TC40DA	1557	3433	24.8	33.2					1				
New Holland	Std.	TC40A	1544	3405	26.1	35.0					1				
AGCO	Std.	ST45	2018	4448	27.6	37.0			9.6	12.9	1				
Massey Ferguson	Std.	MF1445-4	1753	3864	27.6	37.0			9.3	12.5	1				
Case-IH	Std.	D/DX45	1648	3633	28.2	37.8					1				
New Holland	Std.	TC45DA	1696	3738	28.2	37.8					1				
AGCO	4WD	ST47A	1585	3494	28.3	38.0					1				
Massey Ferguson	4WD	1547	1585	3494	28.3	38.0					1				
Challenger	4WD	MT285B	1660	3660	28.3	38.0			11.0	14.8	1				
Case-IH	FWA	DX48	1957	4315	28.8	38.6			8.6	11.5	1			96	130

Make	Drive	Model	Weight		Power at 540 PTO RPM		Power at 1000 PTO RPM		Hydraulic power		Hitch Class	Max draw bar pull unballasted		Max torque	
			(kg)	(LB)	(kW)	(hp)	(kW)	(hp)	(kW)	(hp)		(lb)	(kN)	(lb ft)	(Nm)
New Holland	FWA	TC 48DA - New	1957	4315	28.8	38.6			8.6	11.5	1			96	130
New Holland	Std.	TC45A	1567	3454	29.5	39.6					1				
Case-IH	FWA	CX 50/C50	3445	7595	30.5	40.9			12.0	16.1	2	7990	35.54	121	164
AGCO	4WD	ST52A	1625	3582	30.6	41.0					1				
Massey Ferguson	4WD	1552	1585	3494	30.6	41.0					1				
Challenger	4WD	MT295B	1690	3726	30.6	41.0			12.0	16.1	1				
Case-IH	FWA	JX 55	2756	6075	31.6	42.4			9.5	12.8	2	3680	16.37	115.3	156
Massey Ferguson	FWA	243	2327	5130	31.7	42.5			12.2	16.3	2	4310	19.17	133	180
New Holland	FWA	TN 55D	2901	6395	31.8	42.6			12.5	16.7	2	5030	22.37	136.3	185
White	FWA	6045	2216	4885	32.9	44.1			10.5	14.1	2	5115	22.75	132.1	179
Case-IH	FWA	JX 55 series II - New	2756	6075	33.7	45.2			12.2	16.4	2	5180	23.04	133.7	181
AGCO	Std.	ST55	2004	4417	34.0	45.6			12.8	17.2	1				
Massey Ferguson	Std.	MF 1455-4	1720	3791	34.0	45.6			12.8	17.2	1				
Massey Ferguson	Std.	MF 1455V-2/4	1615	3560	34.0	45.6			12.8	17.2	1				
John Deere	FWA	5210/5220	2300	5070	34.4	46.2			11.9	15.9	2			130	176
Massey Ferguson	FWA	2210	2506	5525	34.5	46.3			13.0	17.5	2			123	167
John Deere	Std.	5105 (late)	2041	4500	35.2	47.2			10.4	13.9	2			133	180
Case-IH	FWA	JX 65	2781	6130	35.6	47.7			9.5	12.8	2	3680	16.37	129.7	176
Case-IH	FWA	DX55	2125	4685	35.6	47.8			9.2	12.3	1			122	165
New Holland	FWA	TC 55 DA - New	2125	4685	35.6	47.8			9.2	12.3	1			122	165
Massey Ferguson	FWA	263	2318	5110	36.7	49.2			11.6	15.5	2	4520	20.11	161.8	219
John Deere	FWA	5205 (late)	2161	4765	37.8	50.7			11.0	14.7	2		0.00	142	193
New Holland	FWA	TN-65	2549	5620	38.6	51.8			12.5	16.7	2	7155	31.83	146.6	199
New Holland	FWA	TN 65D	2930	6460	39.1	52.4			12.5	16.7	2	6785	30.18	151.9	206
Massey Ferguson	FWA	4225	3461	7630	39.8	53.4	41.7	55.9	11.5	15.4	2	7680	34.16	174.7	237

Make	Drive	Model	Weight		Power at 540 PTO RPM		Power at 1000 PTO RPM		Hydraulic power		Hitch Class	Max draw bar pull unballasted		Max torque	
			(kg)	(LB)	(kW)	(hp)	(kW)	(hp)	(kW)	(hp)		(lb)	(kN)	(lb ft)	(Nm)
Massey Ferguson	FWA	4325 (also 4225)	3461	7630	39.8	53.4	41.7	55.9	11.5	15.4	2	7680	34.16	174.7	237
Challenger	FWA	MT 425	3461	7630	39.8	53.4	41.7	55.9	11.5	15.4	2	7680	34.16	174.7	237
Case-IH	FWA	CX 60/C60	3450	7605	41.0	55.0			11.8	15.8	2	9160	40.75	161	218
John Deere	FWA	5310/5320	2336	5150	41.7	55.9			12.1	16.2	2		0.00	168	228
Case-IH	FWA	JX 75	3073	6775	42.0	56.3			9.5	12.8	2	3930	17.48	153.3	208
New Holland	FWA	TL 70D	3740	8245	42.1	56.5			11.6	15.6	2	9065	40.32	170.4	231
Massey Ferguson	FWA	2220	2245	4950	42.8	57.3			9.7	13.0	2			169	229
Case-IH	FWA	JX 65 series II - New	2781	6130	44.6	59.8			10.6	14.2	2	4625	20.57	172.5	234
New Holland	FWA	TN 70D	2570	5665	44.6	59.8			12.5	16.7	2	7375	32.81	179.2	243
Case-IH	FWA	JX 75 series II - New	3307	7290	47.3	63.4			11.0	14.7	2	6190	27.53	153.3	208
New Holland	FWA	TN 75D	2930	6460	47.5	63.7			15.2	20.4	2	2438	10.84	202.2	274
Massey Ferguson	FWA	4233	3146	6935	48.3	64.8	50.7	68.0	12.2	16.3	2	6970	31.00	197.5	268
Massey Ferguson	FWA	4335 (also 4233)	3146	6935	48.3	64.8	50.7	68.0	12.2	16.3	2	6970	31.00	197.5	268
Challenger	FWA	MT 445	3146	6935	48.3	64.8	50.7	68.0	12.2	16.3	2	6970	31.00	197.5	268
Case-IH	FWA	JX 80U	3699	8155	48.5	65.0			14.7	19.7	2	9105	40.50	186.4	253
Massey Ferguson	FWA	4235	3713	8185	48.6	65.2	49.7	66.6	11.1	14.9	2	8545	38.01	211.5	287
John Deere	FWA	5410/5420	2624	5785	48.8	65.4			16.3	21.9	2			204	277
Case-IH	FWA	JX 85	3173	6995	49.1	65.8			9.5	12.8	2	4460	19.84	169.7	230
New Holland	FWA	TL 80D	3740	8245	49.2	66.0			11.6	15.6	2	9195	40.90	188.4	255
John Deere	FWA	6110 PQ	4300	9480	51.8	69.4			25.2	33.8	2	10145	45.13	231	313
Challenger	FWA	MT 455	3731	8225	55.6	74.5	57.8	77.5	11.5	15.4	2	8950	39.81	241.3	327
Massey Ferguson	FWA	4245 and 4243	3731	8225	55.8	74.8	57.8	77.5	11.5	15.4	2	8950	39.81	241.3	327
John Deere	FWA	5510/5520	2885	6360	56.9	76.2			16.6	22.3	2			236	320
Case-IH	FWA	JX 85 series II - New	3484	7680	57.0	76.4			13.5	18.1	2	6520	29.00	239.8	325

Make	Drive	Model	Weight		Power at 540 PTO RPM		Power at 1000 PTO RPM		Hydraulic power		Hitch Class	Max draw bar pull unballasted		Max torque	
			(kg)	(LB)	(kW)	(hp)	(kW)	(hp)	(kW)	(hp)		(lb)	(kN)	(lb ft)	(Nm)
Case-IH	FWA	JX 90U	3951	8710	60.3	80.9			14.7	19.7	2	9285	41.30	213.5	289
Case-IH	FWA	JX 95 series II - New	3454	7615	60.6	81.3			11.9	16.0	2	6500	28.91	219.7	298
Case-IH	FWA	JX 95	3454	7615	60.9	81.7			9.5	12.8	2	4115	18.30	206.4	280
Case-IH	FWA	JX 100U	3951	8710	62.0	83.1			14.7	19.7	2	9510	42.30	243.8	331
Massey Ferguson	FWA	4253 and 4255	3824	8430	62.1	83.3	64.7	86.7	11.1	14.9	2	9170	40.79	269.4	365
Challenger	FWA	MT 465	3824	8430	62.1	83.3	64.7	86.7	11.1	14.9	2	9170	40.79	269.4	365
AGCO Allis	FWA	5650	2141	4720			34.8	46.7	7.8	10.4	1	4385	19.51	123.6	168
AGCO Allis	FWA	5660	2350	5180			42.0	56.3	8.7	11.7	2	4795	21.33	136	184
Case-IH	FWA	CX 70/C70	3749	8265			46.3	62.1	14.4	19.3	2	9485	42.19	195	264
McCormick	FWA	CX-70	3749	8265			46.3	62.1	14.4	19.3	2	9485	42.19	195	264
McCormick	FWA	CX-75	3749	8265			46.3	62.1	14.4	19.3	2	9485	42.19	195	264
Case-IH	FWA	MX 80C	4799	10580			50.0	67.1	22.6	30.3	2	11080	49.29	218	296
John Deere	FWA	6120 SP	4241	9350			51.7	69.3	26.2	35.1	2	7395	32.89	231	313
Case-IH	FWA	CX 80/C80	3690	8135			54.4	73.0	13.9	18.6	2	9530	42.39	225	305
McCormick	FWA	CX-80	3690	8135			54.4	73.0	13.9	18.6	2	9530	42.39	225	305
McCormick	FWA	CX-85	3690	8135			54.4	73.0	13.9	18.6	2	9530	42.39	225	305
AGCO	Std.	LT70	3617	7975			55.8	74.9	9.5	12.7	2			235	319
AGCO Allis	Std.	8745 (Cummins engine)	3617	7975			55.8	74.9	9.5	12.7	2			235	319
White	Std.	6410	3617	7975			55.8	74.9	9.5	12.7	2			235	319
AGCO Allis	Std.	8745	3536	7795			56.2	75.3	9.1	12.2	2			240	325
Case-IH	FWA	MX 90C	5080	11200			56.2	75.4	19.8	26.5	3	11935	53.09	236	320
New Holland	FWA	TS 90 24 speed	4314	9510			56.6	75.9	16.7	22.4	2	10330	45.95	239.5	325
John Deere	FWA	6210 PQ	4359	9610			56.7	76.0	24.8	33.3	2	10695	47.57	249	338
John Deere	FWA	6220 PQ	4345	9580			56.9	76.3	32.0	42.9	2	8115	36.10	252	342
AGCO	FWA	LT75 New	4354	9600			58.9	79.0	15.9	21.3	2			240	325

Make	Drive	Model	Weight		Power at 540 PTO RPM		Power at 1000 PTO RPM		Hydraulic power		Hitch Class	Max draw bar pull unballasted		Max torque	
			(kg)	(LB)	(kW)	(hp)	(kW)	(hp)	(kW)	(hp)		(lb)	(kN)	(lb ft)	(Nm)
Massey Ferguson	FWA	6245	4230	9325			59.3	79.5	16.2	21.7	2	7890	35.10	230.1	312
Case-IH	FWA	CX 90/C90	3706	8170			60.5	81.1	14.2	19.1	2	9220	41.01	235	319
McCormick	FWA	CX-90 and CX-95	3706	8170			60.5	81.1	14.2	19.1	2	9220	41.01	235	319
New Holland	FWA	TL90D	3819	8420			60.6	81.2	11.6	15.6	2	9285	41.30	215.6	292
New Holland	FWA	TL 100D	3989	8795			61.1	81.9	10.1	13.5	2	9525	42.37	244.7	332
Massey Ferguson	FWA	6255	4454	9820			62.1	83.3	16.2	21.7	2	8970	39.90	252.8	343
John Deere	FWA	6310 PQ	4416	9735			62.1	83.3	21.7	29.1	2	9415	41.88	267	362
John Deere	FWA	6310 SP	4354	9600			62.4	83.7	25.5	34.2	2	10090	44.88	273	370
John Deere	FWA	6320 PQ	4550	10030			63.9	85.7	31.7	42.5	2	9450	42.04	265	359
AGCO Allis	FWA	8765	3921	8645			65.0	87.2	8.2	11.0	2			280	380
Case-IH	FWA	CX 100/C100	3756	8280			65.0	87.2	13.9	18.7	2	9160	40.75	268	363
McCormick	FWA	CX-100 and CX-105	3756	8280			65.0	87.2	13.9	18.7	2	9160	40.75	268	363
AGCO	FWA	LT90	4454	9820			65.4	87.7	16.6	22.2	2			322	437
AGCO	Std.	LT85	3833	8450			65.5	87.9	10.4	14.0	2			275	373
AGCO Allis	Std.	8765 (Cummins engine)	3833	8450			65.5	87.9	10.4	14.0	2			275	373
White	Std.	6510	3833	8450			65.5	87.9	10.4	14.0	2			275	373
John Deere	FWA	6403	3969	8750			65.7	88.1	13.9	18.6	2	7636	33.97	266	361
New Holland	FWA	TS 100	4300	9480			66.0	88.5	18.9	25.4	2	9780	43.50	276.4	375
John Deere	FWA	6415	4300	9480			67.6	90.7	18.3	24.5	2	9065	40.32	265	359
John Deere	FWA	6410 PQ	4391	9680			69.0	92.5	23.3	31.2	2	9480	42.17	293	397
Massey Ferguson	FWA	4360 (also 4260, 4263)	4119	9080			69.1	92.7	11.9	15.9	2	9420	41.90	270.2	366
Massey Ferguson	FWA	6265	4781	10540			70.5	94.5	16.2	21.7	2	10515	46.77	290.9	394
FENDT	FWA	410	5525	12180			70.6	94.7	22.7	30.4	3	12730	56.63	333	451
New Holland	FWA	TM 115	5334	11760			70.7	94.8	30.3	40.7	2	11690	52.00	310.9	422

Make	Drive	Model	Weight		Power at 540 PTO RPM		Power at 1000 PTO RPM		Hydraulic power		Hitch Class	Max draw bar pull unballasted		Max torque	
			(kg)	(LB)	(kW)	(hp)	(kW)	(hp)	(kW)	(hp)		(lb)	(kN)	(lb ft)	(Nm)
John Deere	FWA	6420 AQ	5039	11110			71.6	96.0	31.6	42.4	2	9915	44.10	326	442
New Holland	FWA	TS 110 24 speed	4443	9795			72.9	97.8	17.4	23.3	2	10375	46.15	323.4	438
AGCO Allis	FWA	8775	4976	10970			73.2	98.1	30.0	40.2	2			298	404
John Deere	FWA	6603	4266	9405			73.4	98.4	17.0	22.8	2	8807	39.18	333	451
AGCO	FWA	RT95	5042	11115			74.7	100.2	30.6	41.0	2			324	439
AGCO Allis	FWA	8775 (Cummins engine)	5042	11115			74.7	100.2	30.6	41.0	2			324	439
White	FWA	6710	5042	11115			74.7	100.2	30.6	41.0	2			324	439
Massey Ferguson	FWA	4370 (also 4270)	4130	9105			75.2	100.8	11.0	14.7	2	9330	41.50	316.6	429
John Deere	FWA	7220	5366	11830			75.2	100.9	29.4	39.4	2	11834	52.64	330	447
Massey Ferguson	FWA	6270	4781	10540			77.2	103.5	16.2	21.7	2	9690	43.10	316.1	429
Challenger	FWA	MT 535	4781	10540			77.2	103.5	30.6	41.0	2	9690	43.10	316.1	429
John Deere	FWA	6615	4840	10670			77.2	103.5	18.9	25.3	2	9875	43.93	311	422
Case-IH	FWA	MXM 120	5366	11830			77.6	104.1	30.6	41.0	2	12320	54.80	372.2	505
New Holland	FWA	TM 120	5366	11830			77.6	104.1	30.6	41.0	2	12320	54.80	372.2	505
FENDT	FWA	411	5525	12180			79.2	106.2	22.7	30.4	3	13375	59.49	367	498
New Holland	4WD, Articulated	TV 140 and TV 145	6675	14715			81.3	109.0	29.4	39.4	2	11010	48.97	395	536
New Holland	FWA	TM 125	5337	11765			81.8	109.7	29.3	39.3	2	11870	52.80	371.4	504
Case-IH	FWA	MXM 130	5405	11915			84.1	112.8	31.2	41.9	2	12550	55.83	348	472
New Holland	FWA	TM 130	5405	11915			84.1	112.8	31.2	41.9	2	12550	55.83	348	472
FENDT	FWA	412	5525	12180			85.5	114.7	22.7	30.4	3	12370	55.02	408	553
John Deere	FWA	7510 PQ	6024	13280			85.8	115.1	27.4	36.7	2	13818	61.47	395	536
John Deere	FWA	7320	5899	13005			86.0	115.3	29.4	39.4	2	13130	58.41	353	479
John Deere	FWA	7420	5847	12890			86.9	116.6	29.2	39.2	2	12802	56.95	414	561
Massey Ferguson	FWA	6280	5185	11430			87.2	116.9	16.2	21.7	2	11535	51.31	362.9	492
AGCO Allis	FWA	8785	5647	12450			87.3	117.1	28.2	37.8	2			388	526

Make	Drive	Model	Weight		Power at 540 PTO RPM		Power at 1000 PTO RPM		Hydraulic power		Hitch Class	Max draw bar pull unballasted		Max torque	
			(kg)	(LB)	(kW)	(hp)	(kW)	(hp)	(kW)	(hp)		(lb)	(kN)	(lb ft)	(Nm)
White	FWA	6810	5772	12725			87.9	117.8	29.5	39.5	2	11925	53.05	367	498
New Holland	FWA	TM 135	6130	13515			88.0	118.0	29.5	39.6	2	13375	59.49	392.8	533
FENDT	FWA	712 - New	6720	14815			88.1	118.1	24.5	32.8	3	15025	66.83	388	526
AGCO	FWA	RT115	5851	12900			89.8	120.4	24.2	32.4	2	10630	47.28	386.2	524
John Deere	FWA	7610 PQ	6595	14540			90.0	120.7	26.3	35.3	3	14933	66.43	420	569
Case-IH	FWA	MXM 140	5867	12935			90.1	120.8	30.5	40.9	2	13895	61.81	419.4	569
New Holland	FWA	TM 140	5867	12935			90.1	120.8	30.5	40.9	2	13895	61.81	419.4	569
John Deere	FWA	7520 IVT	6024	13280			93.8	125.8	32.0	42.9	2	13634	60.65	454	616
Massey Ferguson	FWA	6290	5169	11395			94.1	126.2	16.2	21.7	2	10925	48.60	370	502
Challenger	FWA	MT 545	5169	11395			94.1	126.2	29.5	39.5	2	10925	48.60	370	502
New Holland	FWA	TM 150	6332	13960			94.5	126.7	29.6	39.7	2	14430	64.19	438.6	595
FENDT	FWA	714 - New	6720	14815			99.1	132.9	24.5	32.8	3	15215	67.68	451	611
Case-IH	FWA	MXM 155	5860	12920			99.6	133.6	30.8	41.3	2	13915	61.90	462.5	627
New Holland	FWA	TM 155	5860	12920			99.6	133.6	30.8	41.3	2	13915	61.90	462.5	627
John Deere	FWA	7710 PQ	6836	15070			102.8	137.9	28.3	37.9	3	15820	70.37	522	708
AGCO	FWA	RT130	7271	16030			105.1	140.9	27.4	36.7	2	12950	57.60	454.6	616
Massey Ferguson	FWA	8220	7210	15895			105.3	141.2	26.7	35.8	3	14705	65.41	440.2	597
AGCO	CVT / FWA	RT135 New	7042	15525			105.9	142.1	34.9	46.8	3	13536	60.21	531	720
New Holland	FWA	TM 165	6557	14455			110.2	147.8	31.2	41.9	2	14615	65.01	487.1	660
John Deere	FWA	7720	7473	16475			112.3	150.6	29.0	38.9	3	16440	73.13	558	757
Case-IH	FWA	MX 180	8718	19220			112.6	151.0	35.4	47.5	3	19501	86.74	558	757
John Deere	FWA	7810 IVT	7344	16190			112.7	151.1	28.6	38.3	3	16698	74.28	568	770
Massey Ferguson	FWA	8240	7396	16305			113.8	152.6	26.7	35.8	3	13945	62.03	493.6	669
Challenger	FWA	MT 565	7396	16305			113.8	152.6	30.1	40.4	3	13945	62.03	498.6	676
FENDT	FWA	716 - New	6720	14815			114.1	153.0	24.5	32.8	3	15635	69.55	509	690
AGCO	FWA	RT 145	7582	16715			114.3	153.3	30.1	40.4	3	15069	67.03	478	648
White	FWA	8410	7582	16715			114.3	153.3	30.1	40.4	3	15069	67.03	478	648
Case-IH	FWA	MXM 175	7164	15795			115.0	154.2	29.7	39.8	2	16455	73.20	512.1	694

Make	Drive	Model	Weight		Power at 540 PTO RPM		Power at 1000 PTO RPM		Hydraulic power		Hitch Class	Max draw bar pull unballasted		Max torque	
			(kg)	(LB)	(kW)	(hp)	(kW)	(hp)	(kW)	(hp)		(lb)	(kN)	(lb ft)	(Nm)
New Holland	FWA	TM 175 - New	7164	15795			115.0	154.2	29.7	39.8	2	16455	73.20	512.1	694
AGCO	FWA	RT150 New	7446	16415			115.7	155.2	35.0	47.0	3	14253	63.40	551	747
Massey Ferguson	FWA	8250	8194	18065			121.7	163.2	29.8	40.0	3	16235	72.22	518.6	703
John Deere	FWA	8110	8775	19345			123.3	165.4	29.8	39.9	3	19272	85.73	586	794
Case-IH	FWA	MXM 190	7924	17470			124.8	167.4	27.5	36.9	2	17465	77.69	553.7	751
New Holland	FWA	TM 190 - New	7924	17470			124.8	167.4	27.5	36.9	2	17465	77.69	553.7	751
AGCO	FWA	DT 160	8623	19010			125.5	168.3	29.5	39.6	3	19010	84.56	538	729
AGCO Allis	FWA	9755 (Cummins engine)	8623	19010			125.5	168.3	29.5	39.6	3	17894	79.60	538	729
White	FWA	8510	8623	19010			125.5	168.3	29.5	39.6	3	17894	79.60	538	729
AGCO Allis	FWA	9755	8700	19180			126.0	168.9	26.5	35.6	3			567	769
Case-IH	FWA	MX 200	8918	19660			127.4	170.8	33.5	44.9	3	19863	88.35	660	895
John Deere	FWA	7820	7815	17230			127.5	171.0	29.2	39.1	3	17061	75.89	616	835
Challenger	FWA	MT 635	8528	18800			127.8	171.4	26.5	35.6	3			561	761
Massey Ferguson	FWA	8245	8528	18800			127.8	171.4	26.5	35.6	3			561	761
John Deere	FWA	8120	9099	20060			128.4	172.1	29.9	40.1	3	18768	83.48	632	857
Case-IH	FWA	MX 210	9160	20195			128.7	172.5	46.2	62.0	3	19579	87.09	692	938
FENDT	FWA	918	8555	18860			131.8	176.8	31.7	42.5	3	19535	86.90	533	723
Massey Ferguson	FWA	8260	8548	18845			137.1	183.9	29.8	39.9	3			589	799
Challenger	FWA	MT 645	8548	18845			137.1	183.9	29.8	39.9	3			589	799
John Deere	FWA	7920	8149	17965			138.4	185.6	30.8	41.3	3	17373	77.28	654	887
John Deere	FWA	8210	8777	19350			139.7	187.3	29.8	39.9	3	19515	86.81	667	904
John Deere	Tracked	8210T	11517	25390			140.3	188.1	28.6	38.4	3	24479	108.89	663	899
FENDT	FWA	920	8555	18860			141.6	189.9	31.7	42.5	3	19210	85.45	592	803
Case-IH	FWA	MX 220	9076	20010			141.9	190.3	34.4	46.1	3	20650	91.86	712	965
John Deere	FWA	8220	9092	20045			142.6	191.2	29.9	40.1	3	18291	81.36	706	957
AGCO Allis	FWA	9765	8700	19180			143.0	191.8	26.5	35.6	3			641	869

Make	Drive	Model	Weight		Power at 540 PTO RPM		Power at 1000 PTO RPM		Hydraulic power		Hitch Class	Max draw bar pull unballasted		Max torque	
			(kg)	(LB)	(kW)	(hp)	(kW)	(hp)	(kW)	(hp)		(lb)	(kN)	(lb ft)	(Nm)
Case-IH	FWA	MX230	9117	20100			143.2	192.0	46.6	62.5	3	19628	87.31	778	1055
New Holland	FWA	TG 210	9278	20455			144.2	193.3	46.5	62.4	3	20092	89.37	679	921
AGCO	FWA	DT 180	8838	19485			149.1	200.0	30.0	40.2	3	18618	82.82	633	858
AGCO Allis	FWA	9765 (Cummins engine)	8838	19485			149.1	200.0	30.0	40.2	3	18618	82.82	633	858
White	FWA	8610	8838	19485			149.2	200.1	30.0	40.2	3	18618	82.82	633	858
Challenger	Tracked	MT 735	12705	28010			149.6	200.7	49.4	66.3	3	26200	116.54	720	976
John Deere	Tracked	8310T	11775	25960			153.9	206.3	28.6	38.4	3	25919	115.29	729	988
John Deere	FWA	8310	9008	19860			154.5	207.3	29.8	39.9	3	18508	82.33	741	1005
Massey Ferguson	FWA	8270 (also 8170)	9795	21595			158.3	212.3	26.5	35.6	3	20765	92.37	710	963
Challenger	FWA	MT 655	9795	21595			158.3	212.3	26.5	35.6	3	20765	92.37	710	963
Case-IH	FWA	MX 240	9410	20745			159.1	213.4	34.3	46.0	3	20928	93.09	810	1098
New Holland	FWA	TG 230	9226	20340			159.3	213.6	47.4	63.5	3	19826	88.19	754	1022
AGCO Allis	FWA	9775	9002	19845			160.9	215.8	29.8	40.0	3			692	938
John Deere	Tracked	8320T	12127	26735			162.3	217.6	29.5	39.6	3	26656	118.57	780	1058
John Deere	FWA	8320	9085	20030			163.0	218.5	29.9	40.1	3	19460	86.56	760	1030
Case-IH	FWA	MX 255	9775	21550			163.4	219.2	46.2	62.0	3	21234	94.45	879	1192
Challenger	Tracked	MT 745	12710	28020			164.7	220.8	49.7	66.6	3	26433	117.58	804	1090
AGCO	FWA	DT 200	8904	19630			165.1	221.4	28.8	38.6	3	17996	80.05	716	971
AGCO Allis	FWA	9775 (Cummins engine)	8904	19630			165.1	221.4	28.8	38.6	3	17996	80.05	716	971
White	FWA	8710	8904	19630			165.1	221.4	28.8	38.6	3	17996	80.05	716	971
FENDT	FWA	924	8555	18860			167.4	224.5	33.1	44.4	3	19625	87.30	657	891
New Holland	4WD, Articulated	9282 (also 9184)	11251	24805			170.8	229.0	40.2	53.9	4	25020	111.29	746	1011
Massey Ferguson		8280	9770	21540			172.5	231.3	26.5	35.6	3	20925	93.08	801	1086
Challenger	FWA	MT 665	9770	21540			172.5	231.3	26.5	35.6	3	20925	93.08	801	1086

Make	Drive	Model	Weight		Power at 540 PTO RPM		Power at 1000 PTO RPM		Hydraulic power		Hitch Class	Max draw bar pull unballasted		Max torque	
			(kg)	(LB)	(kW)	(hp)	(kW)	(hp)	(kW)	(hp)		(lb)	(kN)	(lb ft)	(Nm)
AGCO	FWA	DT 225	8956	19745			174.0	233.4	29.4	39.4	3	18284	81.33	677	918
AGCO Allis	FWA	9785 (Cummins engine)	8956	19745			174.0	233.4	29.4	39.4	3	18284	81.33	677	918
White	FWA	8810	8956	19745			174.0	233.4	29.4	39.4	3	18284	81.33	677	918
John Deere	FWA	8420	10786	23780			175.6	235.5	29.9	40.1	3	24276	107.98	823	1116
John Deere	Tracked	8410T and 8420T	11966	26380			176.5	236.8	28.6	38.4	3	27233	121.14	844	1144
John Deere	FWA	8410	9271	20440			176.6	236.8	29.8	39.9	3	20330	90.43	829	1124
Case-IH	4WD, Articulated	STX 275	14417	31785			178.2	238.9	36.9	49.5	4	32944	146.54	953	1292
New Holland	4WD, Articulated	TJ 275	14417	31785			178.2	238.9	36.9	49.5	4	32944	146.54	953	1292
Case-IH	FWA	MX 285	9811	21630			180.6	242.2	47.7	63.9	3	20820	92.61	947	1284
Case-IH	FWA	MX 270	9480	20900			181.3	243.2	34.3	46.0	3	21665	96.37	923	1251
New Holland	FWA	TG 255	9639	21250			183.4	246.0	45.6	61.2	3	20629	91.76	831	1127
John Deere	Tracked	8520T	12374	27280			190.9	256.0	29.5	39.6	3	27960	124.37	912	1236
John Deere	FWA	8520	10796	23800			191.3	256.5	29.9	40.1	3	23197	103.19	922	1250
Challenger	Tracked	MT 755	13320	29365			191.9	257.3	50.6	67.8	3	28137	125.16	921	1249
John Deere	FWA	9120	16046	35375			196.1	263.0	26.8	36.0	3	35182	156.50	874	1185
FENDT	FWA	926	8555	18860			196.6	263.6	31.7	42.5	3	19485	86.67	864	1171

Table A3: Tractor data for large tractors with a PTO power rating in excess of 200 kW

Make	Drive	Model	Weight		Power at 1000 PTO RPM		Hydraulic power		Hitch Class	Max draw bar pull unballasted		Max torque	
			(kg)	(LB)	(kW)	(hp)	(kW)	(hp)		(lb)	(kN)	(lb ft)	(Nm)
New Holland	4WD, Articulated	9482	13608	30000	204.1	273.7	42.3	56.7	4	33490	148.97	901	1222
New Holland	FWA	TG 285	9605	21175	204.9	274.8	46.7	62.6	3	20744	92.27	925	1254
Case-IH	4WD, Articulated	STX 325	14481	31925	210.1	281.8	36.9	49.5	4	32797	145.89	1062	1440
New Holland	4WD, Articulated	TJ 325	14481	31925	210.1	281.8	36.9	49.5	4	32797	145.89	1062	1440
Challenger	Tracked	MT 765	13311	29345	211.0	283.0	49.5	66.4	3	28095	124.97	1012	1372
John Deere	FWA	9200	14959	32980	221.5	297.0	27.7	37.1	3			1020	1383
New Holland	4WD, Articulated	9684	13894	30630	224.7	301.3	41.9	56.2	4	31355	139.47	1099	1490
John Deere	FWA	9220	16558	36505	237.1	318.0	26.6	35.7	3	35831	159.38	1094	1483
New Holland	4WD, Articulated	9682	14454	31865	238.5	319.8	45.2	60.6	4	34630	154.04	1159	1571
Challenger	Tracked	MT 835	18690	41205	244.9	328.4	49.3	66.1	4	38429	170.94	1183	1604
John Deere	Tracked	9400T	19253	42445	247.5	332.0	29.8	39.9	3	42017	186.90	1153	1563
John Deere	Tracked	9420T and 9300T	19253	42445	247.5	332.0	29.8	39.9	3	42017	186.90	1153	1563
Case-IH	4WD, Articulated	STX 375	17060	37610	252.0	337.9	36.9	49.5	4	33658	149.72	1325	1796
New Holland	4WD, Articulated	TJ 375	17060	37610	252.0	337.9	36.9	49.5	4	33658	149.72	1325	1796
John Deere	FWA	9420	16895	37246	256.1	343.4	44.6	59.8	3	38409	170.85	1162	1575
John Deere	Tracked	9520T	19690	43410	266.6	357.5	30.6	41.1	3	42772	193.10	1221	1655
John Deere	Tracked	9320T	19432	42840	267.7	359.0	29.9	40.1	3	41342	183.90	1291	1750
John Deere	FWA	9520	17379	38315	267.8	359.1	26.4	35.4	3	40323	179.37	1231	1669
John Deere	Tracked	9620T New	19677	43380	271.1	363.5	28.6	38.4	3	40016	178.00	1233	1672
John Deere	FWA	9320	16583	36560	272.1	364.9	26.8	36.0	3	38306	170.39	1262	1711
Challenger	Tracked	MT 845	18897	41660	272.4	365.3	48.2	64.6	4	38250	170.14	1326	1798
John Deere	FWA	9620 New	17735	39100	276.4	370.7	28.5	38.2	3	40461	179.98	1238	1678
Case-IH	4WD, Articulated	STX 440 and 450 Quadtrac	23294	51355	297.6	399.1	36.9	49.5	4	38412	170.87	1583	2146
Case-IH	4WD, Articulated	STX 440 and 450	17838	39325	298.8	400.6	38.0	50.9	4	40035	178.08	1598	2167
New Holland	4WD, Articulated	TJ 450	17838	39325	298.8	400.6	38.0	50.9	4	40035	178.08	1598	2167
Challenger	Tracked	MT 855	19842	43745	319.4	428.3	50.6	67.9	4	42798	190.37	1581	2144
Challenger	Tracked	MT 865	20058	44220	366.1	491.0	50.6	67.9	4	43218	192.24	1757	2382

REFERENCES

Alcock, R. (1983). "Battery Powered Vehicles for Field Work." *Transactions of the American Society of Agricultural Engineers*: 10-13.

Al-Janobi, A. A., Saad A. Al-Hamed (2002). *An Object-Oriented Program to Predict Tractor and Machine System Performance*. World Congress of Computers in Agriculture and Natural Resources, Iguacu Falls, Brazil, ASAE.

ASAE (2003). "ASAE D497.4 FEB03 Agricultural Machinery Management Data."

ASAE (2003). "ASAE EP496.2 FEB03 Agricultural Machinery Management."

Beckhaus, P., A. Heinzel, et al. (2004). "Dynamics of H2 production by steam reforming." *Journal of Power Sources* **127**(1-2): 294-299.

Bernhard, B., V. R. Schlotter (2003). *Electric Drives For Combine Harvesters*. International Conference on Crop Harvesting and Processing, Louisville, Kentucky, ASAE.

Betts, D. A., Paul A. Erickson, Timothy C. Simmons and Vernon P. Roan (2002). *Identification of Response-Liniting Processes in an Indirect Methanol Fuel Cell Bus Powertrain*. Powertrain & Fluid Systems Conference & Exhibition, San Diego, CA.

Carlini, M., R. I. Abenavoli, et al. (1997). *Hybrid electric propulsion system for a forest vehicle*. Proceedings of the 1997 32rd Intersociety Energy Conversion Engineering Conference. Part 3-4 (of 4), Jul 27-Aug 1 1997, Honolulu, HI, USA, IEEE, Piscataway, NJ, USA.

Culpin, C. (1992). *Farm Machinery 12th Edition*. Cambridge, Great Britain, Blackwell Scientific Publications.

Dwyer, M. J. (1987). "Prediction of Drawbar Test Performance." *Journal of Terramechanics* **24**(2): 169-177.

Emonts, B., J. Bogild Hansen, et al. (2000). "Fuel cell drive system with hydrogen generation in test." *Journal of Power Sources* **86**(1-2): 228-236.

Gerlach, A. (1966). "Field Measurement of Tractor Transmission Forces." *Transactions of the American Society of Agricultural Engineers*: 707-712.

Gill, W. R., Glen E. Vanden Berg (1986). Mechanics of Traction and Transport. *Soil Dynamics in Tillage and Traction, Agriculture Handbook No. 316*. Washington D.C., U.S. Goverment Printing Office: 340-429.

Hansen, A. C., A. J. Walker, et al. (1986). "Power Demand Mapping of Tractor

Operations." *Transactions of the ASAE* **29**(3): 656-660.

Hansen, M. (1952). "Loads imposed on power-take-off shafts by farm implements." *Agricultural Engineering* **33**(2): 67-70.

Ihrig, H. K. (1960). "Fuel cell powerplant for electrically propelled earthmoving machinery." *Agricultural Engineering* **41**(4): 232-233.

Katrasnik, T., S. Rodman, et al. (2003). "Improvement of the dynamic characteristic of an automotive engine by a turbocharger assisted by an electric motor." *Journal of Engineering for Gas Turbines and Power* **125**(2): 590-595.

L. L. Christianson, R. A., D. Froehlich (1984). *Development and Testing of an Electric Farm Tractor*. 12th Energy Technology Conference.

Larminie, J. a. A. D. (2003). *Fuel Cell Systems Explained*. England, John Wiley and Sons Ltd.

Markel, T., A. Brooker, et al. (2002). "ADVISOR: a systems analysis tool for advanced vehicle modeling." *Journal of Power Sources* **110**(2): 255-266.

Maxoulis, C. N., D. N. Tsinoglou, et al. (2004). "Modeling of automotive fuel cell operation in driving cycles." *Energy Conversion and Management* **45**(4): 559-573.

OECD "OECD Standard Code for the Official Testing of Agricultural and Forestry Tractor Performance, Code 1."

R. L. Clark, R. L. B., A. H. Adsit, C. E. Rice (1981). *Determination of Draft and Energy Requirements of Agricultural Vehicles*. 1981 Winter Meeting of the ASAE, Chicago Illinois.

Ricketts, C. J., J. A. Weber (1961). "Tractor Engine Loading." *Agricultural Engineering* **42**: 236-239, 250, 252.

Ryu, I. H., D. C. Kim, et al. (2003). "Power efficiency characteristics of a tractor drive train." *Transactions of the American Society of Agricultural Engineers* **46**(6): 1481-1486.

SAE (1999). "SAE J708 FEB99 Agricultural Tractor Test Code."

Salokhe, V. M. and N. Ramalingam (2002). "Effect of rotation direction of a rotary tiller on draft and power requirements in a Bangkok clay soil." *Journal of Terramechanics* 39(4): 195-205.

Schuller, J. K. (2002). *Advanced Mechanical and Mechatronic Engineering Technologies and Their Potential Implementation on Mobile Agricultural Equipment*. 2002 ASAE Annual International Meeting, Chicago, Illinois.

Sonnen, F. J. (1969). "Drawbar performance of high-powered farm tractors with rear-wheel and four-wheel drive." *Journal of Terramechanics* **6**(1): 7-21.

Strange, K., L. L. Christianson, et al. (1984). "Microcomputer Goes to the Field to Gather Tractor Test Data." *Agricultural Engineering* **65**: 21-25.

Thoreson, B. P., R. Alcock, et al. (1986). "Electric Choremaster I: Test Procedures and Results." *Transactions of the ASAE* **29**(5): 1259-1265.

Vik, B., R. Alcock, et al. (1984). UElectric Tractor, Design and PerformanceU. 1984 Winter Meeting - American Society of Agricultural Engineers: Engineering the Future - Capitalizing on the New Technologies., New Orleans, LA, USA, ASAE, St. Joseph, MI, USA.

Yan, W.-M., C.-Y. Soong, et al. (2005). "Transient analysis of reactant gas transport and performance of PEM fuel cells." *Journal of Power SourcesU*143(1-2): 48-56.

Zoz, F. M., R. J. Turner, et al. (2002). "Power Delivery Efficiency: A valid measure of belt and tire tractor performance." *Transactions of the American Society of Agricultural Engineers* **45**(3): 509-518.

TASK 2: IMPULSE AND VIBRATION STUDY

TASK 2A: SOURCE IDENTIFICATION OF VIBRATION AND SHOCK ON OFF-ROAD VEHICLES

University of California, Davis

Siva Gunda
Uriel Rosa
Bryan Jenkins
Paul Erickson

INTRODUCTION

The literature review for identifying the nature and strength of the off-road vibration levels is an on-going process. Not much literature that has been published is readily available on the levels of vibrations present on the chassis of an off-road vehicle. Literature is available in the form of ride comfort, where many have studied the vibration levels on the seat of a vehicle or on the frame below the seat. The data presented in this process do not truly represent the extreme nature of the vibration levels present on the vehicles as the seat placement is usually chosen in a place (CG) where the vertical vibrations are small. Even though these levels do not truly represent the entirety of the vibration levels, they provide an indication of extreme levels and would help as an input to the experimental design for the vibrational testing on the fuel cells.

SUMMARY

The data obtained from the literature review supplemented by part of Toro's data obtained on the Workman vehicle are summarized in this report to have an understanding on the vibration levels. In presenting the summary of the data acquired through literature review and Toro's experimentation, each contribution was treated as an individual vehicle; i.e., every paper that was summarized in this report was treated as one vehicle. A brief summary of various literatures is presented to aid the understanding on how the data was generated in a specific study that was used to compile this report. The reviewed data were summarized into six categories:

Agricultural Machinery: Vehicles 1-9
Forestry Machinery: Vehicles 10-13
Military Machinery: Vehicles 14-19
Typical Off-road Machinery: Vehicles 20-23
Miscellaneous Machinery: Vehicles 24-30
Toro Workman Vehicle: Vehicles 31

Figure 1 and 2 shown in the next page are the identified peak and rms vertical acceleration found in the literature. The complete numerical summary of the various categories of vehicles is also presented in this report.

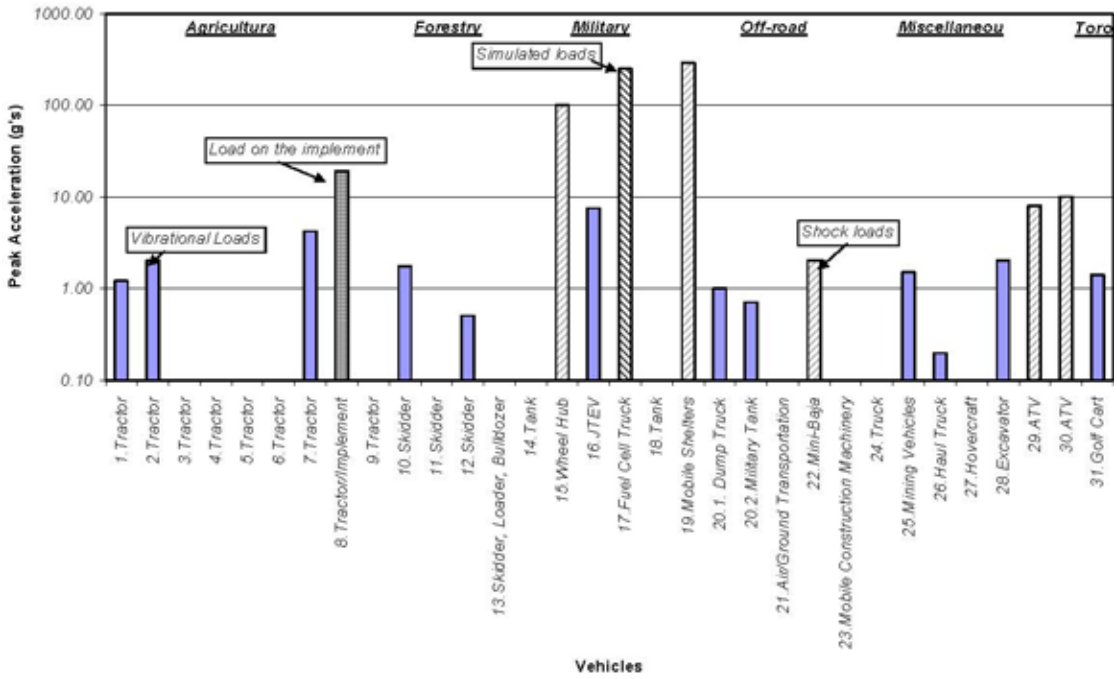

Figure 1: Peak acceleration Values of the Vehicles Researched

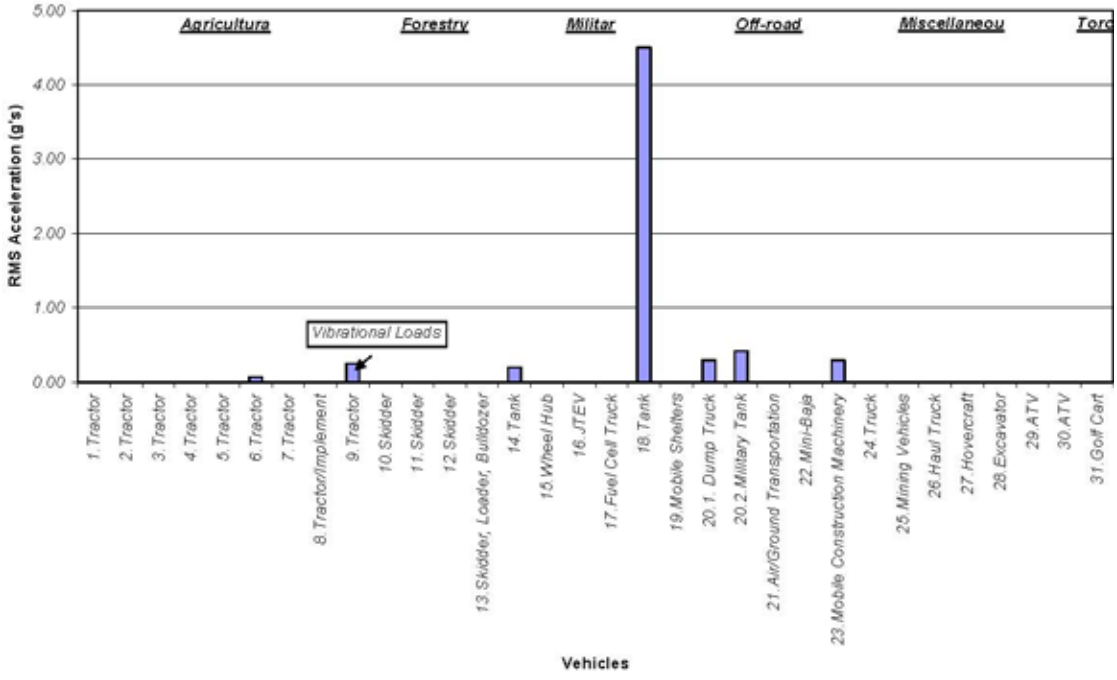

Figure 2: RMS Acceleration Values of the Vehicles Researched

AGRICULTURE MACHINERY

Vehicle 1 – Tractor

In his study of farm tractors J. Matthews [1] studied the vibration levels on the driver's seat for two models of pneumatic-tired tractor over a variety of farm surfaces and presents the excitation frequencies and amplitudes of the recorded ride characteristics. He presented measured values of peak and mean vibration levels felt in the three translational directions in a table that shown below. The vibration levels were measured while driving the tractors on five different surfaces.

Over track and pasture he reported that vertical vibrations on the two models were seen in the frequency range of 3-5 Hz and transverse vibrations at approximately 2 Hz. Over deep ploughed land (ground surface is severely undulated) vertical vibrations were seen over the range of 2-6 Hz and high levels of longitudinal vibration between 1-2 Hz were reported. Over track and rough pasture sustained oscillations at 4 Hz in pitch plane and at 2Hz in roll plane were also reported. The table below gives the strength of these induced vibrations in terms of the acceleration amplitudes.

Table 1: Measured linear and rotational vibrations of four-wheel drive tractor on unmetalled track (8 mile/hr)

Component	*Acceleration amplitude, g*	*Tractor*	*Operator*
Vertical	Mean	0·10	0·16 (160%)
	Maximum	0·5	0·7
Longitudinal	Mean	0·06	0·07 (120%)
	Maximum	0·3	0·4
Transverse	Mean	0·10	0·05 (50%)
	Maximum	0·6	0·3
Pitch		Just noticeable 2–3 c/s oscillation of < ± ¼° amplitude. Max. displacement 1°	
Roll		Max. frequency 2 c/s (not continuous). Max. angular displacement 1½°	

Vehicle 2 – Tractor

In the study by B. K. Huang et al [2] accelerations at seat and chassis were measured to quantify the vibration level in all three translation modes. It is stated that "The results indicated that for each operation the tractor acceleration in vertical, longitudinal, and transverse directions became larger with increased tractor speed, and the highest acceleration occurred at a higher frequency. In transverse vibrations, little difference was observed among the maximum acceleration verses frequency curves for different types of farm operations". For the vertical direction the frequency distribution curves indicated the vibration presence in the range of 1.5-5.5 Hz for the chassis and between

2.5-6.5 Hz for the seat. The amplitude of the vertical vibration was seen to be as high as 2g at 4 mph.

The analysis of the field data indicated that the longitudinal and transverse vibrations were much smaller than the vertical vibration. For the longitudinal the maximum acceleration was less than 1.2 g and the frequencies were distributed from 1.5-5.0 Hz with the highest concentration at 2 and 3 Hz. For the transverse vibration the maximum acceleration was less than 0.5 g and the frequencies were distributed from 1 to 4.5 Hz.

Vehicle 3 – Tractor

In their study towards improving the ride comfort by using passive seat suspension S. Rakheja et al [3] measured the vibration levels in both translation modes and rotational modes on a seat that is rigidly fixed to the cab on a tractor. They reported that the resonant frequencies of the tractor predominated at around 2.6 Hz in vertical direction, 1 Hz in transverse, 1.5-4.5 Hz in longitudinal, 1 Hz in roll and 1.5-4.5 Hz in pitch. Below are the PSD representations of their work.

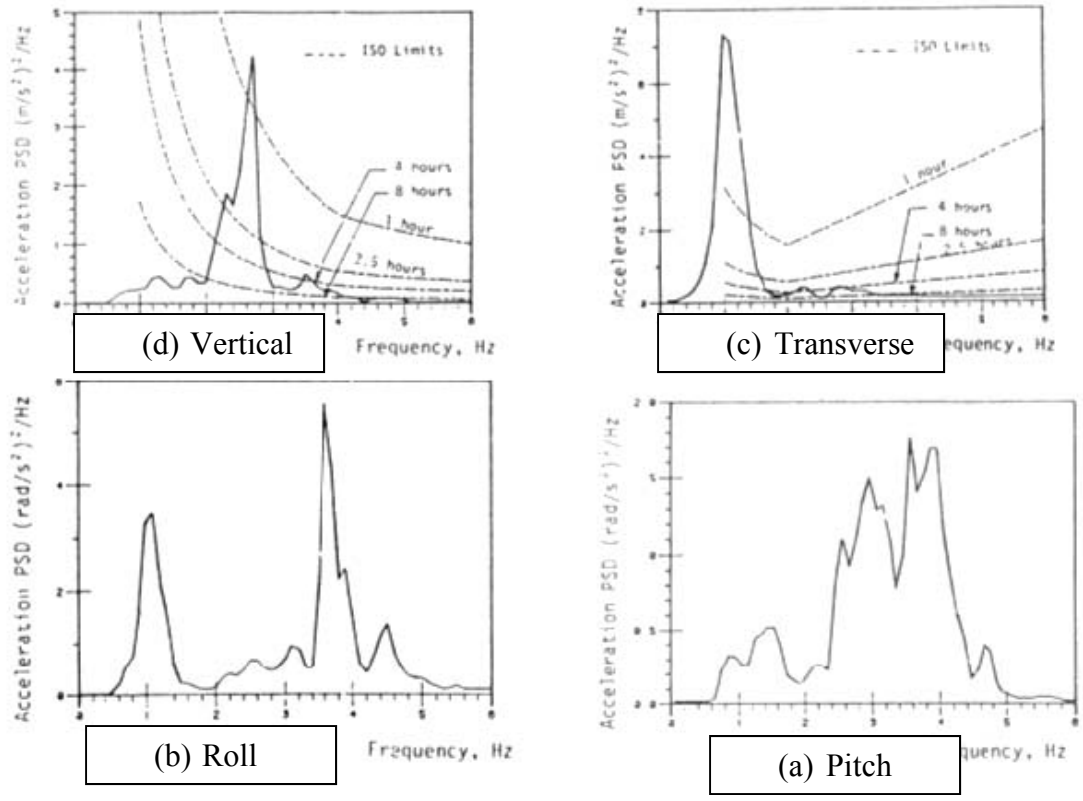

Figure 3: PSD functions of the different modes of vibration

Vehicle 4 – Tractor

In their study of roll and pitch vibration characteristics on off-road vehicles Young et al [4] measured the accelerations at seat-chassis attachment point on a pneumatic tired farm tractor. It was showed that roll accelerations in general were higher than the pitch

acceleration levels and both pitch and roll vibrations subsided after 5 Hz. It was reported that the study of J Matthew [1] addressed sustained vibration at 2 Hz in roll and at 4 Hz in pitch.

In conclusion Young et al [4] stated that, “Roll acceleration levels on a farm tractor are in general, appreciably greater than pitch acceleration levels. Acceleration levels for both roll and pitch subside remarkably for frequencies above 5 Hz. The occurrence of multiple acceleration peaks below 6 Hz for both roll and pitch probably indicates resonant frequencies in the rotational modes of multiple degree-of-freedom system with a non-constant tire spring rate characteristic of unsprung off-road vehicles”.

Vehicle 5 – Tractor

In their study of the ride vibration transfer functions of tractors, Lines et al [5] used two tractors MF 575 and MF 590 to compare between the measured and predicted responses on the tractors using simulation and field data. Though not much data was presented in terms of accelerations, he presented a plot of measured PSDs of vibration in the 3 translational directions for the tractor speed of 12 km/hr.
From the plot it can be observed that, the dominant frequencies are between 0-5Hz and the vibration level in the vertical direction is the maximum among the three translational directions, followed by longitudinal and then lateral.

Vehicle 6 – Tractor

In their study titled, “Tractor Vibrations at the operator’s”, Gerke and Hoag [6] measured the vibration levels at the man seat interface on a tractor in various working conditions. All the data recorded was presented in frequency domain as weighted rms accelerations according to the ISO 2631 standard. Vibration levels were presented for all three translational directions. Below table summaries observations from the plots provided in the study.

Table 2: Summary from Gerke and Hoag [6]

Working condition	Vehicle Speed (m/s)	Direction	Peak rms acceleration ($m/s^{2)}$	Dominant frequency / band (Hz)
Chiesel Plowing soybean ground	*2.3*	*Vertical*	*0.25*	*2.5*
Chiesel Plowing soybean ground	*2.3*	*Lateral*	*0.4*	*40*
Chiesel Plowing soybean ground	*2.3*	*Fore-aft*	*0.4*	*40*
Chiesel Plowing corn ground	*2.1*	*Vertical*	*0.22*	*2.5*
Chiesel Plowing corn ground	*2.1*	*Lateral*	*0.4*	*40*
Chiesel Plowing corn ground	*2.1*	*Fore-aft*	*0.4*	*40*
Disking chisel-plowed ground	*2.8*	*Vertical*	*0.7*	*2.5*
Disking chisel-plowed ground	*2.8*	*Lateral*	*0.4*	*2.5*
Disking chisel-plowed ground	*2.8*	*Fore-aft*	*0.4*	*2.5*

Vehicle 7 – Tractor
In their study of the effects of the implements free-play on tractor vibration, Bukta et al [7] placed a accelerometer below the driver's seat on the tractor frame and measure the vibration with and without the implements connected to the tractor's three-point hitch. A mathematical model was also developed to predict the same as mentioned above when the vehicle was moving at a speed of 6.5 km/h.

Both the measured and predicted values look to be in good agreement. From the plots of the vertical vibrations presented and from the results it is seen that the maximum peak-to-peak values of vertical vibration are 4.2 g and 3 g for the with-implement and without-implement conditions respectively. The dominant frequency was found to be the same in both cases equal to 3 Hz which was also equal to the forcing frequency.

Vehicle 8 – Tractor/Implement
In their study of vibration in cover crop rollers, Raper et al [8] measured vertical vibration levels on three kinds of alternate roller designs aimed at lowering the vibration levels felt on the roller. The plot shown below is directly taken from the study. The three different types mentioned as Long straight, Short Staggered and Curved are the three alternate designs that were looked at in the study.

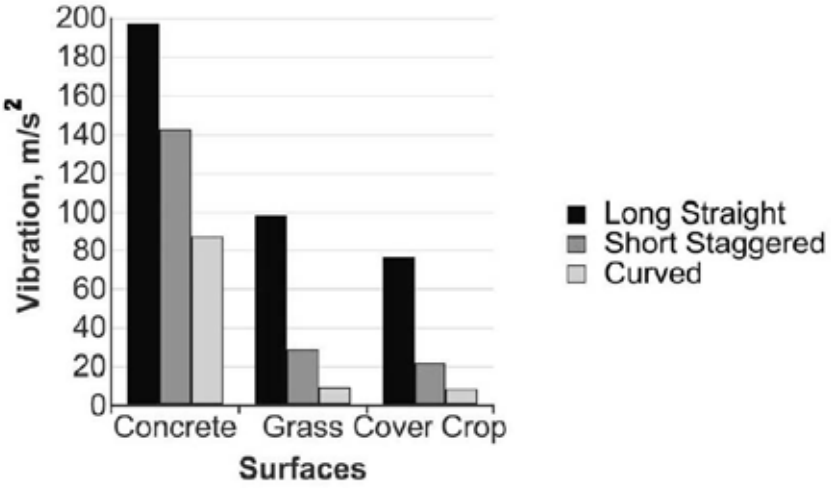

Figure 4: Vertical vibration level of various roller designs

As observed above on the cover crop the implement sees as high as 8 g of vertical vibration for the Long straight type of design.

Vehicle 9 – Tractor
In their study titled, "Ride vibration on tractor-implement system", Mehta et al [9] studied the effect off vehicle speed on the vibration level felt on the tractor at the seat driver interface in all the three translational axes. The vibration levels were measured independently for with and without the implement conditions. For tractor alone (without the implement), the vehicle was driven over three different surfaces: Tar macadam road, Farm road and Untilled field.

Ride vibrations were presented individually for both with and without the implement conditions. The plots below are directly taken from the study for the without the implement condition.

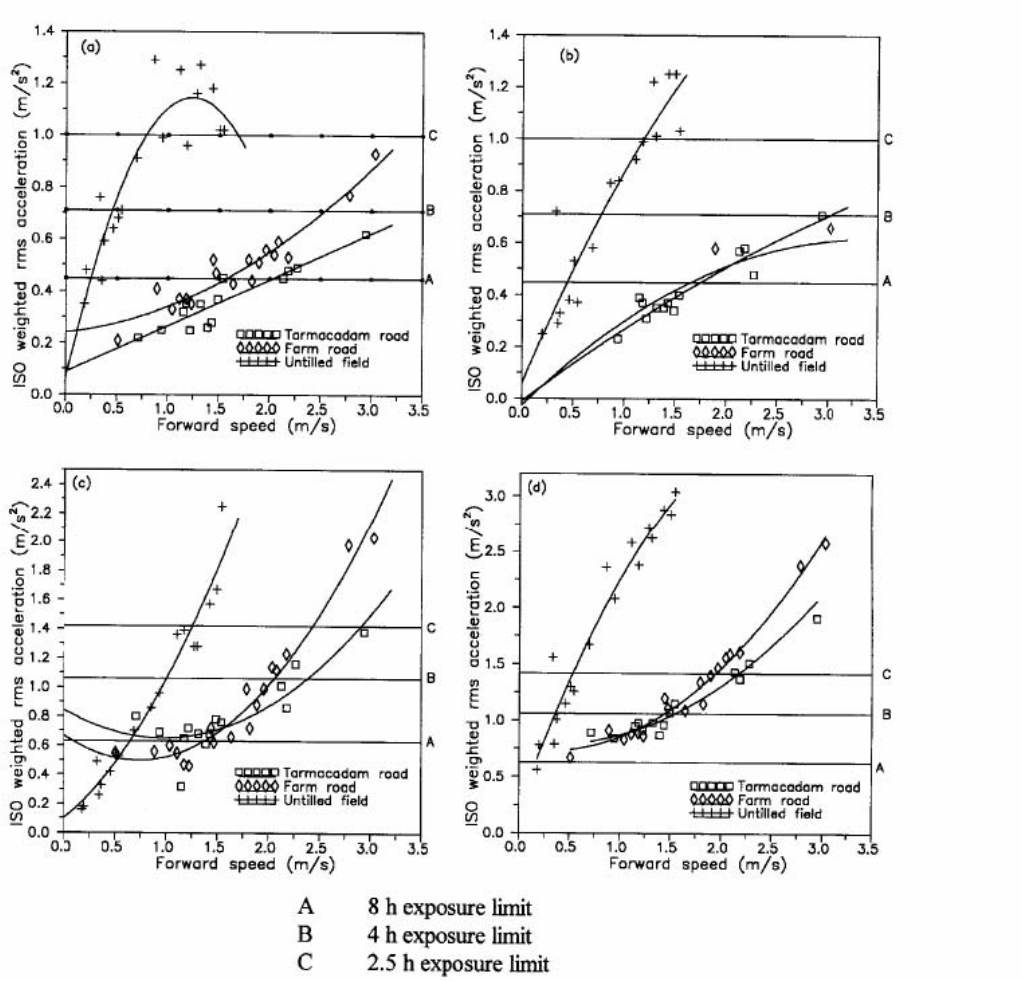

Figure 5: Variation of acceleration level with forward speed: (a) Longitudinal, (b) Lateral, (c) Vertical, (d) Sum

For the implement condition, measurements were recorded for four different situations: Tractor with MB plough (Transport), Tractor with MB plough (Ploughing), Tractor with Disc Harrow (Transport) and Tractor with Disc Harrow (Harrowing).

It is stated in the results that, “The weighted r.m.s. acceleration levels in longitudinal axis (ax) during harrowing operation, in lateral axis (ay) during transport mode and ploughing operation and in vertical axis (az) during transport mode and harrowing operation were insignificant (less than 0.01 m/s2) and therefore not recorded here. The ride vibration levels in longitudinal axis were slightly damped for tractor with MB plough and significantly (40-70%) damped for tractor with disc harrow during transport mode, as compared to tractor alone on untilled field. Because the implement damped tractor pitch motion, and since the driver was not seated at the centre of pitch, his motion in the

longitudinal axis was affected. On the untilled field, no conclusive difference in longitudinal vibration levels was found during transport mode of tractor alone and tractor with MB plough during ploughing operation. The longitudinal vibration levels during harrowing operation were insignificant." The plot below is copied from the study for the implement condition.

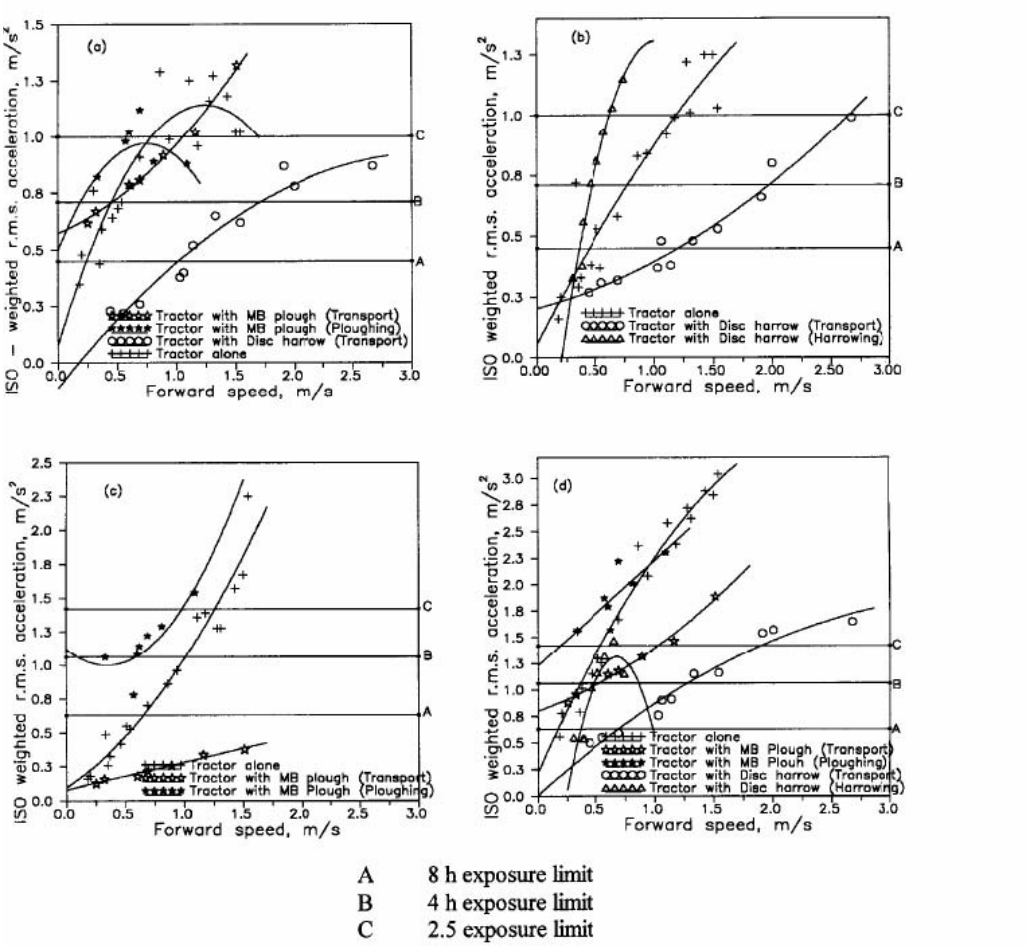

Figure 6: Variation of acceleration level with forward speed: (a) Longitudinal, (b) Lateral, (c) Vertical, (d) Sum

FORESTRY MACHINERY

Vehicle 10 – Skidder

In his study of forestry vehicles, Rummer [10] developed a mathematical model to simulate the vibration levels that are felt on a typical forestry vehicle. The terrain profile was generated from the study of Aho and Katto (1971). The studied model was of a clam- bunk skidder. Masses for each of the components and the inertial properties were estimated from the manufactures literature.

Peak vertical acceleration levels were estimated to be 1.5 g – 1.75 g @ 1 Hz at a traveling speed of 1.3 m/sec. No other kinds of vibrational data were documented.

Vehicle 11 – Skidder

In his further study of forestry vehicles Rummer [11] evaluates the computer model

developed in his previous work by comparing the results to measured acceleration values on a test track. In this work Rummer stated that “The typical prime mover for forestry applications is a rubber tired, frame-steered vehicle with the axels solidly attached to the frame”. In this paper Rummer compares measured and predicted vector-sum acceleration values under the seat location. The presented values are in g rms.
Figure 4 illustrates the comparison of the vector-sum accelerations for one of the mathematical models. The predicted values are higher than the measured values. The highest vector-sum acceleration for both predicted and measured values were observed at 1.8 Hz and are equal to 1.3 g rms and 1 g rms respectively.

Vehicle 12 – Skidder
In their study titled “Vibration attenuation performance of suspension seats for off-road forestry vehicles”, P. E. Boileau and S. Rakheja [12] reported a resonant frequency in the vertical direction at 1.8 Hz. It is stated in their study that, “Terrain-induced vibrations of forestry vehicles predominate in the frequency range of 0.5-5.0 Hz.
In their study Boileau et al provided a frequency spectrum of the vertical vibration measured on the cab floor of a skidder operating under typical conditions. The dominant frequency was measured to be in the 2.5 Hz frequency band and the maximal vertical acceleration was approximately 0.5 g.

Vehicle 13 – Skidder/Loader/Bulldozer
In their study Wilson et al [13] presented measurements both vertical and lateral vibrations in forestry vehicles for more effectively isolating operators from such vibrations. In the study Wilson et al presented recent measurements on four different forestry vehicles: Clark 667 Scarifying Skidder, Caterpillar 980 Loader, Komatsu D85 Bulldozer and Clark 664 Skidder (empty). The measurements were taken by placing accelerometers on the vehicle frame directly under the operator seat pad. All acceleration data is presented in the form of PSDs for all three directions of transverse vibrations. Wilson et al stated that “of particular significance is the relatively high level of lateral vibration compared to those in the vertical direction”.

From the figure of the PSDs presented it can be observed that in all cases the spikes PSDs are between 1.0-3.0 Hz except on the bulldozer which has a spike in the vertical direction at 6 Hz.

MILITARY MACHINERY
Vehicle 14 – Tank
In their study El-Demerdash et al [14] studied the ride performance of multi-axles combat vehicles driven at various speeds over terrain profile. Three different vehicle models were developed to study the vertical vibration and the pitching vibration levels. The terrain considered was rigid and is presented as a PSD of Gaussian stationary random process.

The PSD of the vertical vibration and the pitching vibration were shown in plots. The maximum rms accelerations felt were: Vertical acceleration was approximately .2g (two

axle model) and pitching acceleration was 1.02 rad/sec^2 (three axle model). From the PSD plots shown it is seen that the significant frequencies for both vertical and pitch vibration are between 1-2 Hz. The data was simulated for a speed of 10 m/s.

Vehicle 15 – Wheel Hub

In their study Triche et al [15] conducted a set of simulations and full-scale experiments to determine suitable shock load design requirements for in-hub (wheel) propulsion motors for hybrid and all-electric combat vehicles. It is stated that "The test was designed to represent severe on- and off-road situations that are realistic but not overly improbable, as described above".

The summary from the study as it is are replicated below.

"Drop test results are summarized by the following:

- For low speed travel with off-road tire pressures (10 to 20 psi, or 69 to 138 kPa), shock loads of 25 to 55 g's are experienced.
- For low speed travel with on-road tire pressures (20 to 30 psi or 138 to 207 kPa), the shock loads from a drop impact increase to 35 to 55 g's.
- For on- or off-road cases where the run flat is engaged (0 psi, 0 kPa), drop impacts result in shock loads >20 g's.

Curb test results are summarized by the following:

- For cross-country travel with off-road tire pressures (69 to 138 kPa, or 10 to 20 psi), shock loads of around 60 g's are experienced.
- For on-road travel with on-road tire pressures (138 to 207 kPa , or 20 to 30 psi), the shock loads from a curb impact increase to 60 to 95 g's.
- For on- or off-road cases where the run flat is engaged (0 kPa or 0 psi), curb impacts result in shock loads > 90 g's.

Pothole test results are summarized by the following:

- For cross-country travel with off-road tire pressures (69 to 138 kPa , or 10 to 20 psi),
- shock loads of 60 to 90 g's are experienced.
- For on-road travel with on-road tire pressures 138 to 207 kPa (20 to 30 psi), the shock loads from a pothole increase to 80 to 100 g's."

Vehicle 16 – JTEV

The study, "Development of a hybrid electric vehicle for the US Marine Corps" by LaPlante et al [16] intended at developing a JTEV for US Marine Corp. The study goal included extremely high ability and high speed over rough terrain. These factors influenced the design of both the mechanical and electrical system in the areas of waterproofing, material selection, vibration hardening and isolation of components. The suspension and chassis were designed to withstand the shock and vibration in the extreme conditions.

In the design of the chassis it is mentioned that by FISA specification it is designed to withstand crash imposed loads of 1.5 g lateral, 5.5 g longitudinal and 7.5 g vertical.

Vehicle 17 – Fuel Cell Truck

In their work Maturia et al [17] studied the vibration and shock considerations in the design of a truck mounted fuel cell APU system for on and off road conditions. In the work it is stated that, "there are two types of excitation sources that can affect the durability and structural integrity of the APU system: (i) tire-road dynamic interaction and (ii) engine vibration. Based on the field measurement results, the tire-road interaction is typically the more severe of these two excitations. Consequently, the design of a vibration isolation system is primarily concerned with isolating the APU and truck frame dynamics under the on-the-road vehicle operating conditions."

The developed mathematical model was studied for various aspects including the vibration prediction spectrum based on 4 g of uniform base excitation input per SAE J1455 standard titled "Joint SAE/TMC Recommended Environmental Practices for electronic equipment Design (Heavy-Duty Trucks)". Below are the plots from the above study showing the predicted steady-sated response of the APU system.

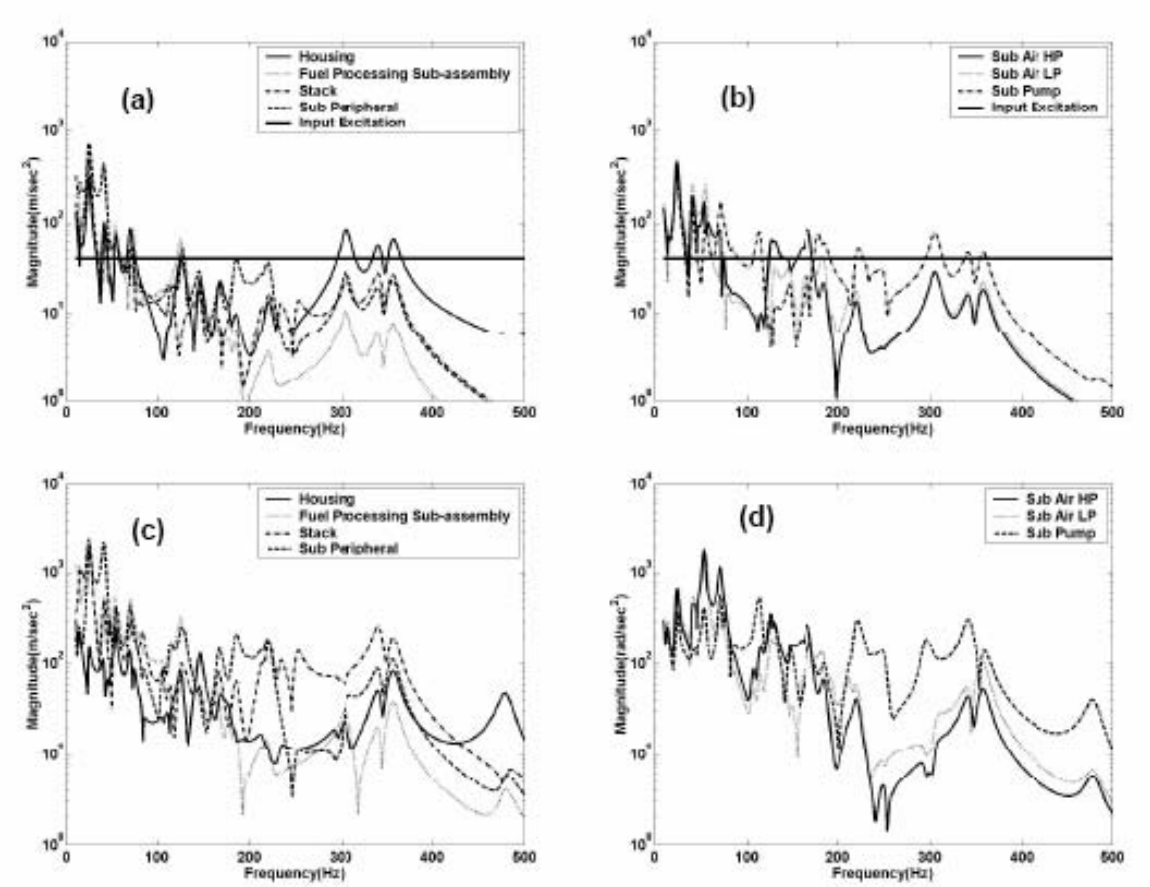

Figure 7:Predicted steady state responses for APU system per SAE J1455

The peak values in the translational vibration can be observed t be between 90-250 g occurring predominantly in the 10-60 Hz frequency band. The peak values in the rotational vibration can be observed to be approximately 2000 rad/sec2 occurring

predominantly in the 10-80 Hz frequency band.

Vehicle 18 – Tank

In their study titled, “Analysis and conceptual design of a semi-active suspension system for the M5551 tank”, Margolis and Krasnicki [18] studied the feasibility of semi-active suspensions applied to a M5551 tank. As a part of their study they reported simulated values of the change in the rms vertical and pitch accelerations with respect to speed at the CG location of the tank. For the plots presented in the study it can be seen that the peak rms values at a speed of 40 mph are: vertical – 4.5 g and pitch – 24 rad/sec2.

Vehicle 19 – Mobile Shelters

In their study titles, “Blast induced shock testing on mobile communication shelters”, Polk et al [19] measured vibration levels on the walls of the mobile shelters and reported of maximum acceleration levels sometimes exceeding 1500 g’s. Upon certain shock isolation systems, the measured results were still as high as 390 g’s in the horizontal and 292 g’s in the vertical directions.

OFF-ROAD MACHINERY

Vehicle 20 – Dump Truck/Military Tank/Hovercraft

In his study titled, “Vibration and dynamics of off-road vehicles”, Craighead [20] investigated three different off road vehicles: a 25 tonne articulated dump truck manufactured by DJB Engineering Limited, a Vickers Mk 3b/3 battle tank and a small hovercraft designed for agricultural use for vibration levels through simulations. He further validated the model by comparing the simulated values to actual measured values on the prototype vehicle mentioned above.

The results of the simulation and experimental measurements were presented for the vertical and pitch acceleration about the CG of the vehicles. Plots were also to compare the results. The observations from the plots and the results presented in the study are summarized below.

Table 3: Summary from Craighead [20]

Vehicle	Suspension	Mode of Vibration	Peak Acceleration	rms acceleration
Truck				
	Yes			
		Vertical (g)	*1.0*	*0.3*
		Pitch (rad/sec^2)	*13.0*	*4.7*
	No			
		Vertical (g)	*0.8*	*0.3*
		Pitch (rad/sec^2)	*10.0*	*3.6*
Tank				
	Torsion Bar			
		Vertical (g)	*0.7*	*0.26*
		Pitch (rad/sec^2)	*2.0*	*1.12*
	Hydrogen Gas			
		Vertical (g)	*0.4*	*0.42*
		Pitch (rad/sec^2)	*2.0*	*1.25*

Vehicle 21 – Air and Ground Transportation Vehicles
In his study titled, “Review of measured vibration and noise environments experienced by passengers in aircraft and in ground transportation systems”, Stephens [21] conducted comprehensive experimental measurements on aircrafts and various ground transportation vehicles and presented them in plots showing the comparison between various limits of vibration levels felt on these vehicles. The plots below are directly taken from his study. The descriptors used in the plots are as follows:
gp: Peak acceleration in g’s associated with a particular time history.
grms: Over all rms acceleration in g’s associated with a particular time history.

Vehicle 22 – Mini-Baja
In their study titled, “Experimental and Numerical Analysis of an off-road vehicle suspension” Buarque et al [22] presented vertical acceleration levels felt on a Mini-Baja vehicle suspension when subjected to a sinusoidal bump input. The vehicle was instrumented with a strain gauge type accelerometer mounted on the suspension and was driven over the bum at a low speed of 2.0 m/sec. The maximum vertical acceleration at such low speed was measured to be 2 g.

Vehicle 23 – Mobile Construction Machinery
In his study titled, “Survey of technical preventative measures to reduce whole-body vibration effects when designing mobile machinery”, Donati [23] presented a plot summarizing the vertical weighted rms acceleration seen on a number of mobile machinery. The plot is below is taken from his study.

Figure 8: Figure from Donati [23]

The data was recorded on the seats of these vehicles. It can be seen from the plot that some of the vehicles see a vibration level as high as 0.3 g rms.

MISCELLANEOUS

Mining

Vehicle 24 – Truck

In their study Remington et al [24] studied the exposure of vibration in mining workers. Field measurements were conducted on 61 surface coal mining vehicles by placing a tri-axial accelerometer on the seats of the vehicles. No data was presented in terms of accelerations.

Vehicle 25 – Mining Vehicles

In their study John Gniady and John Bauman stated that in construction and mining vehicles the amplitudes of vibration can be as high as 1.5 g and the typical frequencies of interest are 0-20 Hz.

Vehicle 26 – Haul Truck

In his study of a Mine haul truck, Hans modeled the stuck to simulate the vehicle dynamics. He reported that the vertical acceleration of the mainframe's CG for travel at 50Km/h is generally below 0.1 g with an occasional excursion to 0.2 g. The dominant frequency is about 1 Hz, consistent with the bounce frequency measured on haul trucks in various studies.

Hovercraft

Vehicle 27 – Hovercraft

In his study of Hovercraft ride Lovesey compared the peak vibration levels on floor of a launch (28 knot) and a small hovercraft (45 knot). The levels indicated that the ride on the hovercraft is much smoother than the launch.

The different vibration levels were summarized for the peak values and the associated frequencies on the 2 vehicles. The values presented are summarized below.

Table 4: Summary from Lovesey

Motion	Frequency (Hz)	Acceleration (g)
Heave	*1.3*	*0.14*
Sway	*12.5*	*0.05*
Shunt	*4.7*	*0.06*

Earthmoving Machinery

Vehicle 28 – Excavator

In their study Dong-wook Lee et al evaluated the operator exposure to shock and vibration in the cabin of the excavator design. The study included two different aspects which are internal vibration caused by the engine and vibration caused due to external disturbances. The external disturbances were further classified into bucket shock, traveling shock and rock braking. In the present report the values of the older design are considered to give the extreme values that the excavator cabin can feel.

Bucket shock: Peak value is approximately 2 g and the vital frequency band is 5-25 Hz
Traveling shock: It is reported in the study that this shock locates in the frequency range

of 10-20 Hz
Rock Breaking: Peak value is approximately 1 g and the vital frequency band is 30-40 Hz

Recreation Vehicles / ATVs
Vehicle 29 – ATV
In his study Breen provides an overview on the design of ATVs. In the study Breen reports that ATVs in operation are more than critically damped. From the figures presented the accelerations could get to 8 g on a vertical drop.

Vehicle 30 – ATV
In his study Sushinsky measured vertical accelerations on 14 different ATVs. He quotes that, “The vertical acceleration vector was viewed as the most important quantity in this investigation because it could be directly linked to forces acting on the target areas. In this study, the peak acceleration range was defined the sum of the peak magnitudes of negative and positive accelerations. The appropriateness of using the acceleration ranges was drawn from an examination of the acceleration profiles. The positive and the negative peak acceleration characteristically followed each other within 0.4 sec time increment”.

The accelerations were measured on eight different locations, four on the vehicle and four on the driver. The four vehicle locations and the corresponding peak values are as follows:

Front Axle: 8.7 g (Vehicle 6)
Frame: 8.0 g (Vehicle 6)
CG: 6.1 g (Vehicle 5 & 6)
Rear Axle: 10.0 g (Vehicle 6)

Toro’s Study
Vehicle 31 – Workman Vehicle
The data acquired by Toro has been shared with UC Davis to help in the design of an experimental plan for the fuel cell vibration and shock testing.
The study by Toro was done on the new Fuel Cell Hybrid Workman e2050 golf cart prototype vehicle. Vibration data was collected at Midland Hills CC, Minnesota. Various possible terrain induced excitation inputs while performing golf course or other turf maintenance such as driving over speed bumps, potholes e.t.c., were identified. The vehicle was mounted with nine tri-axial accelerometers for acquiring the vibrational data. Four accelerometers were placed on the four corners of the main frame (bed area) of the workman chassis, with a fifth one located at an approximate likely location for such a vehicle’s fuel cell (mid-mount, low, under the bed). Another four accelerometers were placed near the wheel spindles.

The data was acquired at 6 different speeds with further variability added by the load and suspension conditions. The data was collected under with and without suspension condition for each of the 6 speeds and under each suspension condition further

variability was added by empty and full load conditions.

The inputs from the five accelerometers on the frame were used to compute the vibration level at any location of the vehicle. For this the vehicle was assumed to be a rigid body. Initial analysis was done on the CG location under five different dynamic conditions, which are: Vehicle full braking (panic stop), Vehicle tree root impacts, Vehicle typical trip, Vehicle driveway curb impact and Vehicle speed bump impact. The peak translational acceleration values were identified under the above mentioned five dynamic conditions and the FFT were plotted to identify the corresponding frequency distribution.

Table 5: Peak Acceleration of te Toro Workman Vehicle

Dynamic Condition	Type of Load	Longitudinal		Lateral		Vertical	
		Peak Acceleration (G's)	Dominant Frequency (Hz)	Peak Acceleration (G's)	Dominant Frequency (Hz)	Peak Acceleration (G's)	Dominant Frequency (Hz)
Vehicle full braking (panic stop)	*Shock*	*1.8*	*0-5*	*-*	*-*	*-0.6*	*0-5*
Vehicle tree root impacts	*Oscillation*	*2.1*	*0-10*	*2.0*	*0-30*	*1.3*	*0-10*
Vehicle typical trip	*Oscillation*	*1.9*	*0-10*	*-3.0*	*0-10*	*-1.1*	*0-10*
Vehicle driveway curb impact	*Shock*	*2.3*	*0-10*	*1.9*	*0-10*	*1.2*	*0-10*
Vehicle speed bump impact	*Shock*	*3.0*	*0-10*	*-1.7*	*0-10*	*-1.4*	*0-10*

VIBRATION AND SHOCK SUMMARY BY VEHICLE CATEGORY
Agricultural Machinery: Vehicles 1-9

Transitional Acceleration

Vehicle Number	Author	Type of Load	Vertical			Longitudinal			Lateral		
			Peak Acceleration (G's)	RMS Acceleration (G's)	Dominat Frequency (Hz)	Peak Acceleration (G's)	RMS Acceleration (G's)	Dominat Frequency (Hz)	Peak Acceleration (G's)	RMS Acceleration (G's)	Dominat Frequency (Hz)
1	Matthews	Vibration	1.20	-	2-6	1.60	-	0-2	1.30	-	1-2
2	Haung	Vibration	2.00	-	1.5-6.5	1.20	-	1.5-5	0.50	-	1-4.5
3	Rekheja	Vibration	-	-	2.60	-	-	1.5-4.5	-	-	1
4	Young	Vibration	-	-	-	-	-	-	-	-	-
5	Lines	Vibration	-	-	0-5	-	-	0-5	-	-	0-5
6	Gerke	Vibration	-	0.07	0-3	-	0.04	0-40	-	0.04	0-40
7	Bukta	Vibration	4.20	-	3.00	-	-	-	-	-	-
8	Reper	Implement Vibration	19.00	-	-	-	-	-	-	-	-
9	Mehta	Vibration	-	0.25	-	-	0.14	-	-	0.14	-

Rotational Acceleration

Vehicle Number	Author	Type of Load	Pitch			Roll			Yaw		
			Peak Acceleration (rad/s^2)	RMS Acceleration (rad/s^2)	Dominat Frequency (Hz)	Peak Acceleration (rad/s^2)	RMS Acceleration (rad/s^2)	Dominat Frequency (Hz)	Peak Acceleration (rad/s^2)	RMS Acceleration (rad/s^2)	Dominat Frequency (Hz)
1	Matthews	Vibration	-	-	0-4	-	-	0-2	-	-	-
2	Haung	Vibration	-	-	-	-	-	-	-	-	-
3	Rekheja	Vibration	-	-	1.5-4.5	-	-	1.00	-	-	-
4	Young	Vibration	-	-	0-5	-	-	0-5	-	-	-
5	Lines	Vibration	-	-	-	-	-	-	-	-	-
6	Gerke	Vibration	-	-	-	-	-	-	-	-	-
7	Bukta	Vibration	-	-	-	-	-	-	-	-	-
8	Reper	Implement Vibration	-	-	-	-	-	-	-	-	-
9	Mehta	Vibration	-	-	-	-	-	-	-	-	-

Forestry Machinery: Vehicles 10-13

Transitional Acceleration

Vehicle Number	Author	Type of Load	Vertical			Longitudinal			Lateral		
			Peak Acceleration (G's)	RMS Acceleration (G's)	Dominat Frequency (Hz)	Peak Acceleration (G's)	RMS Acceleration (G's)	Dominat Frequency (Hz)	Peak Acceleration (G's)	RMS Acceleration (G's)	Dominat Frequency (Hz)
10	Rummer	Vibration	1.5-1.75	-	1.00	-	-	-	-	-	-
11	Rummer	Vibration	-	-	-	-	-	-	-	-	-
12	Boileau	Vibration	0.50	-	0-5	-	-	-	-	-	-
13	Wilson	Vibration	-	0.20	0-10	-	-	0-10	-	-	0-10

Rotational Acceleration

Vehicle Number	Author	Type of Load	Pitch			Roll			Yaw		
			Peak Acceleration (rad/s^2)	RMS Acceleration (rad/s^2)	Dominat Frequency (Hz)	Peak Acceleration (rad/s^2)	RMS Acceleration (rad/s^2)	Dominat Frequency (Hz)	Peak Acceleration (rad/s^2)	RMS Acceleration (rad/s^2)	Dominat Frequency (Hz)
10	Rummer	Vibration	-	-	-	-	-	-	-	-	-
11	Rummer	Vibration	-	-	-	-	-	-	-	-	-
12	Boileau	Vibration	-	-	-	-	-	-	-	-	-
13	Wilson	Vibration	-	-	-	-	-	-	-	-	-

Military Machinery: Vehicles 14-19

Transitional Acceleration

Vehicle Number	Author	Type of Load	Vertical			Longitudinal			Lateral		
			Peak Acceleration (G's)	RMS Acceleration (G's)	Dominat Frequency (Hz)	Peak Acceleration (G's)	RMS Acceleration (G's)	Dominat Frequency (Hz)	Peak Acceleration (G's)	RMS Acceleration (G's)	Dominat Frequency (Hz)
14	Demerdash	Vibration	100.00	0.20	1-2	-	-	-	-	-	-
15	Triche	Shock	7.50	-	-	-	-	-	-	-	-
16	LaPlante	Vibration	250.00	-	-	5.50	-	-	1.50	-	-
17	Mathurai	Vibration	-	-	10-80	-	-	-	-	-	-
18	Margolis	Vibration	-	4.50	-	-	-	-	-	-	-
19	Polk	Shock	292.00	-	-	390.00	-	-	-	-	-

Rotational Acceleration

Vehicle Number	Author	Type of Load	Pitch			Roll			Yaw		
			Peak Acceleration (rad/s^2)	RMS Acceleration (rad/s^2)	Dominat Frequency (Hz)	Peak Acceleration (rad/s^2)	RMS Acceleration (rad/s^2)	Dominat Frequency (Hz)	Peak Acceleration (rad/s^2)	RMS Acceleration (rad/s^2)	Dominat Frequency (Hz)
14	Demerdash	Vibration	-	1.02	1-2	-	-	-	-	-	-
15	Triche	Shock	-	-	-	-	-	-	-	-	-
16	LaPlante	Vibration	-	-	-	-	-	-	-	-	-
17	Mathurai	Vibration	200.00	-	10-80	-	-	-	-	-	-
18	Margolis	Vibration	-	24.00	-	-	-	-	-	-	-
19	Polk	Shock	-	-	-	-	-	-	-	-	-

Typical Off-Road Machinery: Vehicles 20-23

Transitional Acceleration

Vehicle Number	Author	Type of Load	Vertical			Longitudinal			Lateral		
			Peak Acceleration (G's)	RMS Acceleration (G's)	Dominat Frequency (Hz)	Peak Acceleration (G's)	RMS Acceleration (G's)	Dominat Frequency (Hz)	Peak Acceleration (G's)	RMS Acceleration (G's)	Dominat Frequency (Hz)
20	Craighead	Vibration	-	-	-	-	-	-	-	-	-
	Truck		1.00	0.30	-	-	-	-	-	-	-
	Tank		0.70	0.42	-	-	-	-	-	-	-
21	Stephens	Vibration	-	-	-	-	-	-	-	-	-
22	Buarque	Shock	2.00	-	-	-	-	-	-	-	-
23	Donati	Vibration	-	0.30	-	-	-	-	-	-	-

Rotational Acceleration

Vehicle Number	Author	Type of Load	Pitch			Roll			Yaw		
			Peak Acceleration (rad/s^2)	RMS Acceleration (rad/s^2)	Dominat Frequency (Hz)	Peak Acceleration (rad/s^2)	RMS Acceleration (rad/s^2)	Dominat Frequency (Hz)	Peak Acceleration (rad/s^2)	RMS Acceleration (rad/s^2)	Dominat Frequency (Hz)
20	Craighead	Vibration	-	-	-	-	-	-	-	-	-
	Truck		13.00	4.70	-	-	-	-	-	-	-
	Tank		2.00	1.25	-	-	-	-	-	-	-
21	Stephens	Vibration	-	-	-	-	-	-	-	-	-
22	Buarque	Shock	-	-	-	-	-	-	-	-	-
23	Donati	Vibration	-	-	-	-	-	-	-	-	-

Miscellaneous Machinery: Vehicles 24-30

Transitional Acceleration

Vehicle Number	Author	Type of Load	Vertical			Longitudinal			Lateral		
			Peak Acceleration (G's)	RMS Acceleration (G's)	Dominat Frequency (Hz)	Peak Acceleration (G's)	RMS Acceleration (G's)	Dominat Frequency (Hz)	Peak Acceleration (G's)	RMS Acceleration (G's)	Dominat Frequency (Hz)
	Mining		-	-	-	-	-	-	-	-	-
24	Remington	Vibration	-	-	-	-	-	-	-	-	-
25	Gniady	Vibration	1.50	-	0-20	-	-	-	-	-	-
26	Prem	Vibration	0.20	-	1.00	-	-	-	-	-	-
	Hovercraft		-	-	-	-	-	-	-	-	-
27	Lovesey	Vibration	-	-	-	-	-	-	-	-	-
	Earthmoving		-	-	-	-	-	-	-	-	-
28	Wook Lee	Vibration	2.00	-	5-40	-	-	-	-	-	-
	ATV		-	-	-	-	-	-	-	-	-
29	Breen	Shock	8.00	-	-	-	-	-	-	-	-
30	Sushinsky	Shock	10.00	-	-	-	-	-	-	-	-

Rotational Acceleration

Vehicle Number	Author	Type of Load	Pitch			Roll			Yaw		
			Peak Acceleration (rad/s^2)	RMS Acceleration (rad/s^2)	Dominat Frequency (Hz)	Peak Acceleration (rad/s^2)	RMS Acceleration (rad/s^2)	Dominat Frequency (Hz)	Peak Acceleration (rad/s^2)	RMS Acceleration (rad/s^2)	Dominat Frequency (Hz)
	Mining		-	-	-	-	-	-	-	-	-
24	Remington	Vibration	-	-	-	-	-	-	-	-	-
25	Gniady	Vibration	-	-	-	-	-	-	-	-	-
26	Prem	Vibration	-	-	-	-	-	-	-	-	-
	Hovercraft		-	-	-	-	-	-	-	-	-
27	Lovesey	Vibration	-	-	-	-	-	-	-	-	-
	Earthmoving		-	-	-	-	-	-	-	-	-
28	Wook Lee	Vibration	-	-	-	-	-	-	-	-	-
	ATV		-	-	-	-	-	-	-	-	-
29	Breen	Shock	-	-	-	-	-	-	-	-	-
30	Sushinsky	Shock	-	-	-	-	-	-	-	-	-

REFERENCES

1. Matthews, J. (1964). "Ride Comfort for Tractor Operators II. Analysis of Ride Vibrations on Pneumatic-tyred Tractors." Journal of Agricultural Engineering Research Volume 9.

2. Huang, B. K. and C. W. Suggs (1965). "Vibration Studies of Tractor Operators." Winter Meeting of ASAE, Power and Machinery Division.

3. Rakheja, S. and S. Sankar (1984). SUSPENSION DESIGNS TO IMPROVE TRACTOR RIDE: I. PASSIVE SEAT SUSPENSION. International Off-Highway & Powerplant Congress & Exposition., Milwaukee, WI, USA, SAE, Warrendale, PA, USA.

4. Young, R. E. and C. W. Suggs (1975). "ROLL AND PITCH INVESTIGATIONS OF OFF-ROAD VEHICLES." **18**(5): 841-844.

5. Lines, J. A. (1985). "The ride vibration transfer functions of tractors." Agriculture Vehicle Division.

6. Gerke, F. G. and D. L. Hoag (1980). "Tractor Vibrations at the Operator's." ASAE.

7. Bukta, A. J., Sakai, K., Sasao, A. and Shibusawa, S., (2002). "Free play as a source of nonlinearity in tractor-implement systems during transport." Transactions of the American Society of Agricultural Engineers **45**(3): 503-508.

8. Raper, R. L., Simionescu, P., Kornecki, T. S., Price and A. J., Reeves, D. W., (2004). "Reducing vibration while maintaining efficacy of rollers to terminate cover crops." Applied Engineering in Agriculture **20**(5): 581-584.

9. Mehta, C.R., Shyam, M., Singh, P. and Verma, R.N., (2000). "Ride vibration on tractor-implement system." Applied Ergonomics **31**(3): 323-328.

10. Rummer, R. B. (1989). "Computer simulation of ride dynamics for the design of forest machines." Transactions of the ASAE **32**(1): 12-16.

11. Rummer, R. B. (1988). "Designing Forest Machines for Better Ride with Computer Simulation."

12. Boileau, P.-E. and S. Rakheja (1990). "Vibration attenuation performance of suspension seats off-road forestry vehicles." International Journal of Industrial Ergonomics **5**(3): 275-291.

13. Wilson, J. N., Kirk, T. G., Lang, F. G., Tremblay, M. L. and Burton, R. T., (1986). WHOLE BODY VIBRATION IN OFF ROAD FORESTRY VEHICLES. 1986 Winter Meeting, American Society of Agricultural Engineers., Chicago, IL, USA, ASAE, St. Joseph, MI, USA.

14. El-Demerdash, S. M. and E. M. A. Rabeih (2004). "Ride Performance Analysis of Multi-Axle Combat Vehicles." SAE.

15. E. J. Triche, J. H. Beno, H. E. Tims, M. T. Worthington and J. R. Mock., (2005). "Shock Loading Experiments and Requirements for Electric Wheel Motors on Military Vehicles." SAE.

16. LaPlante, J., Anderson, C. J. and Auld, J., (1995). Development of a hybrid electric vehicle for the US Marine Corps. Proceedings of the Future Transportation Technology Conference and Exposition, Aug 7-10 1995, Costa Mesa, CA, USA, SAE, Warrendale, PA, USA.

17. P. H. Mathuria, T. C. Lim, W. S. Shepard, S. R. Bell, M. Venturi, H. H. Dobbs and E. Kallio., (2002). "Vibration and Shock Considerations in the Design of a Truck-mounted Fuel Cell APU System." SAE.

18. Margois, D. L. and E. J. Kransnicki Analysis and Conceptual Design of a Semi-Active Suspension System for the M551 Tank, U. S. Army Tank-Automotive Command Research and Development Center, Warren, Michigan.

19. Polk, J. F., Belliveau, L. J. and Guice, R. L., (1987). BLAST INDUCED SHOCK TESTING ON MOBILE COMMUNICATIONS SHELTERS. Papers Presented at the SAE Aerospace Technology Conference and Exposition., Long Beach, CA, USA, SAE, Warrendale, PA, USA.

20. Craighead, I. A. (1984). VIBRATION AND DYNAMICS OF OFF ROAD VEHICLES. Vehicle Noise and Vibration., London, Engl, r Inst of Mechanical Engineers, London, Engl by Mechanical Engineering Publ Ltd, Bury St. Edmunds, Engl.

21. Stephens, D. G. Review of Measured Vibration and Noise Environments Experienced by Passengers in Aircraft and in Ground Transportation Systems, NASA Langely Research Center.

22. F. N. Buarque, P. M. C. L. Pacheco, P. P. Kenedi and L. Xavier., (2003). Experimental and numerical analysis of an off-road vehicle suspension. 12th SAE Brazil Congress and Exposition, Sao Paulo, Brazil, Society of Automotive Engineers, Inc., Warrendale, Pennsylvania, USA.

23. Donati, P. (2002). Survey of technical preventative measures to reduce

whole-body vibration effects when designing mobile machinery. 2nd International Conference on Whole-Body Vibration Injuries, Nov 7-9 2000, Siena, Italy, Academic Press.

TASK 2B. FUEL CELL SYSTEM VIBRATION AND SHOCK SPECTRUM TESTING

Richard Lawrence
IdaTech

INTRODUCTION

The purpose of these vibration and shock spectrum experiments was to test operating conditions of the IdaTech fuel cell in the Toro Workman™ off-road vehicle. The tests focused on movement of the rear compartment where the fuel cell is mounted. The results do not reflect direct movements or impacts on the fuel cell itself.

SUMMARY

Upon observation of the data, it appears that the rear compartment of the vehicle does not sustain any g-force short time impacts greater than 117.2g. The measured g-force varies greatly depending on whether measured at accelerometers at the back of the vehicle or the front of the vehicle. The back of the vehicle sustains higher g-force on average than the front. The data can be viewed in detail for each test in the Time Domain Data graphs in the appended data section of this document. When looking at the back two accelerometers (A and D) the high g-forces can be observed in all three axis, but only for brief periods of time.

Analysis of the Average Spectrum data suggests that the vehicle does not sustain any vibrations that exceed 1g. The vibrations at the higher frequencies (above 800Hz) may be attributed to noise vibrations generated from the electric motor and generator on the vehicle. These vibrations should not be of any concern in terms of operation of the fuel cell. The frequencies originated from the terrain are considered within the range of 1-20Hz and this range is where the highest g-forces were measured. Data taken during day 2 gives more detail as a result of two additional frequencies at vibration frequencies are utilized for all 15 inputs.

Analysis of the FRF data was largely done in MEScope. The data was used to generate the vibrating modes of the storage compartment at the various measured frequencies. These were obtained from the FRF processed from recorded accelerometers data. The results of the simulations between day one and day two tests seem to vary which is most likely due to the fact that average spectrum data was only gathered for input three (the input used as a reference for the FRF analysis.) All of the day two runs have Average spectrum data for all 15 inputs.

The results from day one suggest that several of the frequencies result in vibrations in all directions, but predominantly in the z-direction. There were also vibrations in both the x and y directions, but, for the most part, these were much

smaller than the vibrations in the z-direction.

Day two's results do not match up with day one's results as expected. The results of the analysis with MEScope suggest that the majority of the vibrations occur in the horizontal directions (x-direction and y-direction) and not as much in the z-direction. It appears that the data and analysis are correct. The most likely cause for the differences in results between day one and day two is due to the lack of all the Average spectrum data for day one.

Tables 1, 2, and 3 summarize the results for the day 1 and day 2 tests. The max and minimum values were generated via observation of the time domain data. Table 1 corresponds to data from day 1. Tables 2 and 3 correspond to data taken from day 2.

Table 1: Measured acceleration and frequency data measured on Day 1 of the tests

					X-direction (g)										Peak Amplitude between 0-20Hz		RMS Vibration Frequency (Hz)
					Min.					*Max.*							
	Surface	Speed	Section	Acc. Location	A	B	C	D	E	A	B	C	D	E	(Hz)	(g)	
Run 1	grass, pavement	var.	Top 9	See fig. 2	-56.93	-7.83	-0.40	-32.05	-7.73	87.09	1.31	0.17	117.20	1.09	ND	ND	ND
Run 2	grass, pavement, gravel	var.	Bottom 9	See fig. 2	-20.35	-5.21	-0.03	-30.10	-5.63	24.91	0.90	0.05	117.20	0.75	ND	ND	ND
Run 3	grass, pavement	var.	Bottom 9	See fig. 2	-37.42	-1.06	-0.09	-25.97	-7.18	103.40	0.75	0.09	117.20	0.90	ND	ND	ND
Run 4	grass, pavement	var.	Bottom 9	See fig. 2	-38.50	-6.22	-0.45	-59.08	-7.81	114.80	0.87	0.12	117.20	1.16	ND	ND	ND
					Y-direction (g)										Peak Amplitude between 0-20Hz		RMS Vibration Frequency (Hz)
					Min.					*Max.*							
	Surface	Speed	Section	Acc. Location	A	B	C	D	E	A	B	C	D	E	(Hz)	(g)	
Run 1	grass, pavement	var.	Top 9	See fig. 2	-42.02	-86.56	-17.46	-50.36	-98.39	89.53	76.66	12.93	113.90	72.73	ND	ND	ND
Run 2	grass, pavement, gravel	var.	Bottom 9	See fig. 2	-17.68	-36.24	-3.76	-18.55	-38.24	23.50	41.56	5.07	98.42	50.09	ND	ND	ND
Run 3	grass, pavement	var.	Bottom 9	See fig. 2	-24.81	-45.62	-10.14	-36.28	-55.06	116.00	49.48	8.24	113.90	96.94	ND	ND	ND
Run 4	grass, pavement	var.	Bottom 9	See fig. 2	-40.92	-46.72	-9.44	-56.80	-68.62	114.90	43.72	11.98	113.90	93.44	ND	ND	ND
					Z-direction (g)										Peak Amplitude between 0-20Hz		RMS Vibration Frequency (Hz)
					Min.					*Max.*							
	Surface	Speed	Section	Acc. Location	A	B	C	D	E	A	B	C	D	E	(Hz)	(g)	
Run 1	grass, pavement	var.	Top 9	See fig. 2	-53.83	-76.66	-21.86	-22.21	-91.34	112.40	86.57	22.84	116.50	68.05	3.20	0.01	0.02
Run 2	grass, pavement, gravel	var.	Bottom 9	See fig. 2	-19.18	-49.37	-6.66	-29.46	-93.84	38.07	49.37	7.51	116.50	60.27	3.20	0.03	0.03
Run 3	grass, pavement	var.	Bottom 9	See fig. 2	-49.97	-53.52	-12.71	-15.83	-110.50	113.80	76.29	15.22	116.50	79.97	3.20	0.04	0.07
Run 4	grass, pavement	var.	Bottom 9	See fig. 2	-52.27	-61.02	-18.34	-60.81	-110.50	113.80	54.92	20.84	116.50	81.62	3.20	0.40	0.43

Table 2: Measured acceleration and frequency data measured on Day 2 of the tests

					X-direction (g)									
					Min.					*Max.*				
	Surface	**Speed**	**Section**	**Acc. Location**	A	B	C	D	E	A	B	C	D	E
Run 1	grass, pavement	var.	Top 9	See fig. 2	-76.79	-0.81	-6.92	-49.61	-7.88	114.80	0.13	0.95	117.20	2.89
Run 2	grass, pavement, gravel	var.	Top 9	See fig. 2	-92.85	-1.55	-6.49	-110.00	-9.09	114.80	0.12	1.29	117.20	1.12
Run 3	grass, pavement	var.	Top 9	See fig. 2	-95.66	-2.91	-10.49	-105.10	-16.38	114.80	0.35	1.17	117.20	4.01
Run 4	grass, pavement	var.	Bottom 9	See fig. 2	-93.11	-1.22	-6.36	-77.02	-10.49	114.80	0.11	0.97	117.20	0.87
					Y-direction (g)									
					Min.					*Max.*				
	Surface	**Speed**	**Section**	**Acc. Location**	A	B	C	D	E	A	B	C	D	E
Run 1	grass, pavement	var.	Top 9	See fig. 2	-80.65	-14.49	-74.67	-44.59	-76.95	116.80	11.74	105.50	113.90	110.50
Run 2	grass, pavement, gravel	var.	Top 9	See fig. 2	-84.78	-19.60	-55.27	-105.30	-78.86	116.80	17.23	82.70	113.70	110.20
Run 3	grass, pavement	var.	Top 9	See fig. 2	-93.73	-41.38	-66.06	-97.00	-79.12	116.80	40.61	108.00	113.90	109.10
Run 4	grass, pavement	var.	Bottom 9	See fig. 2	-88.74	-13.53	-61.83	-78.48	-77.35	116.80	20.18	57.57	113.90	115.40
					Z-direction (g)									
					Min.					*Max.*				
	Surface	**Speed**	**Section**	**Acc. Location**	A	B	C	D	E	A	B	C	D	E
Run 1	grass, pavement	var.	Top 9	See fig. 2	-75.26	-8.62	-58.80	-52.45	-89.45	113.80	8.11	48.25	116.50	68.59
Run 2	grass, pavement, gravel	var.	Top 9	See fig. 2	-86.34	-11.78	-48.83	-107.60	-111.40	113.80	13.13	48.28	116.50	73.87
Run 3	grass, pavement	var.	Top 9	See fig. 2	-82.16	-15.85	-66.06	-104.50	-114.50	113.80	17.16	95.87	116.50	88.30
Run 4	grass, pavement	var.	Bottom 9	See fig. 2	-87.13	-10.77	-39.23	-82.08	-102.30	113.80	10.46	33.06	116.50	74.89

Table 3: Measured acceleration and frequency data measured on Day 2 of the tests

X-direction

	Peak Amplitude between 0-20Hz										Other Peak Vibration Frequencies (Hz)										RMS Vibration Frequency (Hz)				
	A		B		C		D		E		A		B		C		D		E						
	(Hz)	(g)	(Hz)	(g)	(Hz)	(g)	(Hz)	(g)	(Hz)	(g)	(Hz)	(g)	(Hz)	(g)	(Hz)	(g)	(Hz)	(g)	(Hz)	(g)	A	B	C	D	E
Run 1	4.00	0.07	4.00	0.00	4.00	0.00	4.00	0.04	4.00	0.00	672.00	0.00	660.00	0.00	672.00	0.00	672.00	0.00	0.07	0.00	0.08	0.00	0.00	0.04	0.00
Run 2	4.00	0.01	4.00	0.00	4.00	0.83	8.00	0.00	4.00	0.00	52.00	0.03	52.00	0.00	52.00	0.00	52.00	0.02	52.00	0.00	0.05	0.00	0.00	0.03	0.00
Run 3	4.00	0.16	4.00	0.00	4.00	0.01	4.00	0.11	4.00	0.01	792.00	0.00	1360.00	0.00	60.00	0.00	32.00	0.12	60.00	0.00	0.19	0.00	0.01	0.12	0.01
Run 4	4.00	0.64	4.00	0.00	4.00	0.01	4.00	0.14	4.00	0.01	676.00	0.32	224.00	0.00	60.00	0.01	56.00	0.03	60.00	0.00	0.70	0.00	0.01	0.16	0.01

Y-direction

	Peak Amplitude between 0-20Hz										Other Peak Vibration Frequencies (Hz)										RMS Vibration Frequency (Hz)				
	A		B		C		D		E		A		B		C		D		E						
	(Hz)	(g)	(Hz)	(g)	(Hz)	(g)	(Hz)	(g)	(Hz)	(g)	(Hz)	(g)	(Hz)	(g)	(Hz)	(g)	(Hz)	(g)	(Hz)	(g)	A	B	C	D	E
Run 1	4.00	0.05	4.00	0.00	4.00	0.00	4.00	0.03	4.00	0.00	672.00	0.00	108.00	0.00	672.00	0.00	672.00	0.01	684.00	0.00	0.06	0.00	0.01	0.04	0.01
Run 2	4.00	0.01	4.00	0.00	4.00	0.01	4.00	0.00	4.00	0.00	552.00	0.04	52.00	0.03	52.00	0.00	656.00	0.07	248.00	0.01	0.09	0.04	0.08	0.12	0.06
Run 3	4.00	0.42	4.00	0.00	4.00	0.01	4.00	0.09	4.00	0.01	792.00	0.01	1340.00	0.00	772.00	0.00	32.00	0.02	780.00	0.01	0.44	0.38	0.01	0.11	0.02
Run 4	4.00	1.00	4.00	0.00	4.00	0.01	4.00	0.12	4.00	0.01	676.00	0.01	28.00	0.00	44.00	0.00	56.00	0.03	1536.00	0.00	0.00	0.00	0.01	0.13	0.01

Z-direction

	Peak Amplitude between 0-20Hz										Other Peak Vibration Frequencies (Hz)										RMS Vibration Frequency (Hz)				
	A		B		C		D		E		A		B		C		D		E						
	(Hz)	(g)	(Hz)	(g)	(Hz)	(g)	(Hz)	(g)	(Hz)	(g)	(Hz)	(g)	(Hz)	(g)	(Hz)	(g)	(Hz)	(g)	(Hz)	(g)	A	B	C	D	E
Run 1	4.00	0.06	4.00	0.00	4.00	0.00	4.00	0.04	4.00	0.00	672.00	0.00	672.00	0.00	684.00	0.00	672.00	0.00	684.00	0.00	0.07	0.00	0.00	0.05	0.00
Run 2	4.00	0.01	4.00	0.00	4.00	0.00	4.00	0.01	4.00	0.00	656.00	0.01	52.00	0.01	52.00	0.01	656.00	0.01	52.00	0.03	0.04	0.02	0.05	0.03	0.04
Run 3	4.00	0.29	4.00	0.00	4.00	0.02	4.00	0.14	4.00	0.01	792.00	0.01	96.00	0.00	776.00	0.00	32.00	0.14	148.00	0.00	0.33	0.00	0.02	0.14	0.01
Run 4	4.00	0.33	4.00	0.00	4.00	0.01	4.00	0.17	4.00	0.01	676.00	0.00	144.00	0.00	44.00	0.00	56.00	0.04	28.00	0.00	0.30	0.00	0.01	0.17	0.01

The RMS data fluctuates between runs for the day two data. This is most likely due to the inconsistent stops made during the test runs. During these stops data were still being sampled. It may be possible to obtain more accurate RMS values for the vibration frequencies by further cropping of the data to remove the periods where the vehicle was stopped.

The fuel cell is located closest to accelerometer 5, so vibrations and impacts measured at accelerometer 5 (E) are most reflective of vibrations and impacts occurring to the fuel cell.

TEST PROCEDURE

Hardware

The following hardware was used for these tests:

- Toro Workman™ Off-Road Vehicle
- Oros R36 DSP Analyzer Unit
- 3 Axis Dytran Accelerometers x5
- 350W DC-AC Converter
- Dell Laptop

Software

The following software was used for analysis of the data:

- NVGate v5.1.00017
- MEScope v5.0.2008.1031

Setup

The Accelerometers were attached to the rear compartment of Toro vehicle; one accelerometer at each corner and one at the center of the compartment towards the front of the vehicle. Figure 1 is a table of the accelerometer names, references, Oros input channels, and respective axis labels. Figure 2 is a diagram of the physical locations and orientations of the accelerometers on the Toro Off-Road Vehicle. Figure 3 is a photograph of the back of the Toro Off-Road Vehicle with the location of the accelerometers circled.

Accelerometer	Reference Letter	Oros Inputs	Axis
67	A	1	X
		2	Y
		3	Z
68	B	4	X
		5	Z
		6	Y
69	C	7	X
		8	Y
		9	Z
70	D	10	X
		11	Y
		12	Z
71	E	13	X
		14	Z
		15	Y

Figure 1: Table of Accelerometer Names

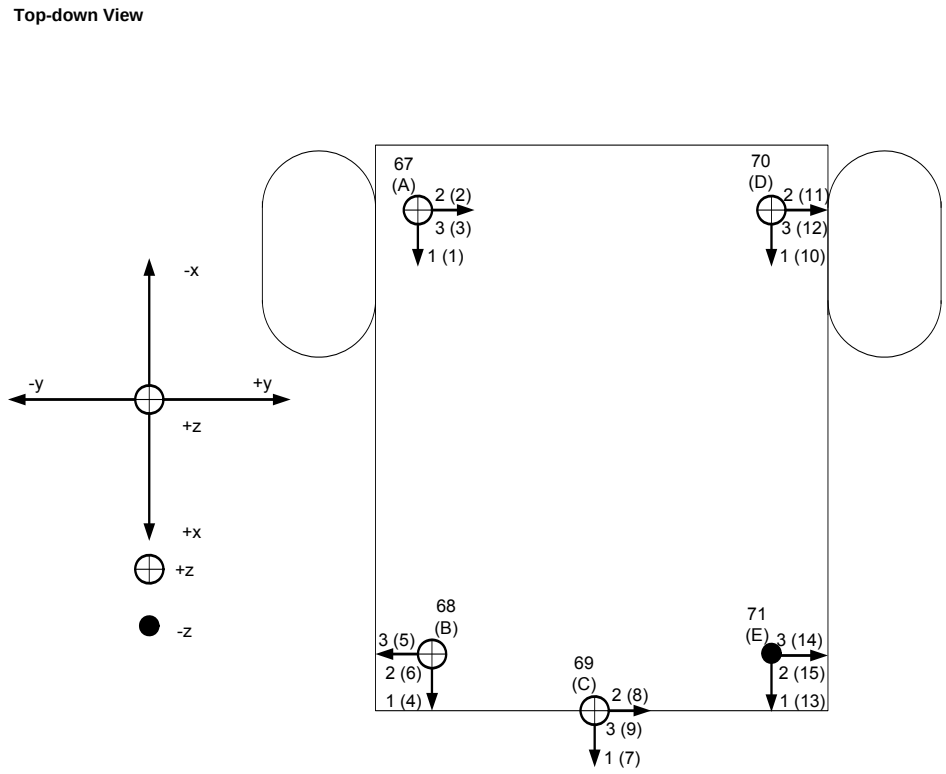

Figure 2: Diagram of the Physical Locations and Orientations of the Accelerometers

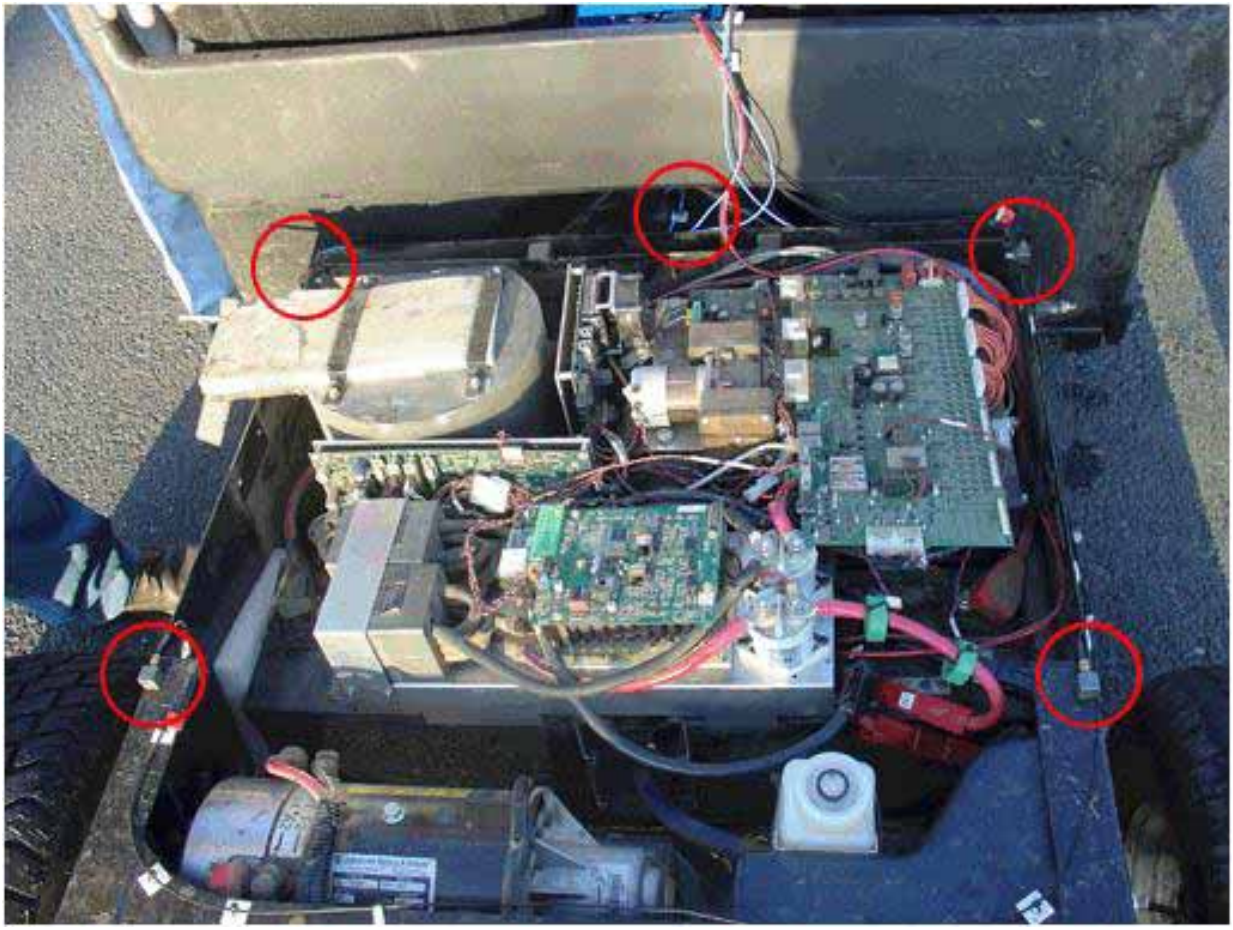

Figure 3: Photo of Accelerometers Layout

In Figure 2, the numbers on each axis correspond to the axis number for that accelerometer. The numbers within the parenthesis represents the Oros channel number used for that accelerometer axis.

A couple of things to note about the accelerometer setup:

1. Accelerometer B's axis 3 is in the –y direction
2. Accelerometer E's axis 2 is in the –z direction

Because these two accelerometers had to be mounted in a fashion that resulted in them being oriented in the negative direction for one of their axis, the data for those axis will be inverted compared to the rest of the data.

The Oros and the laptop were both powered by the 350W DC-AC converter for all the tests. The DC-AC converter was connected to the vehicle batteries.
Each accelerometer was attached to the Oros via a 3 channel cable. The vehicle was manned by two persons at all times; one to drive, and the other to monitor the equipment and data sampling.

Process

The Oros was started at the beginning of each run. It would only be stopped at the end

each run. At the end of each run the data set was saved and a new one was setup for the next run. Data was taken over the course of two days. The data sets are broken up into runs based on which set of holes on the golf course was being traveled. The course was broken up into two sections for these tests:

- Top 9 (holes 1 through 9)
- Bottom 9 (holes 10 through 18)

There were four sets of data taken each day for a total of eight data sets gathered from the course. Data was gathered throughout the duration of travel for each of the sets of holes traveled. Voice notes were recorded during day two to mark suspected points of interest and spots where the vehicle was stopped.

All data analysis was done post gathering and was done in NVGate.

TEST RESULTS

Data

The data in this section will be broken up in the order that the data were taken. There are two sections of data:

1. Day One
2. Day Two

In each of these sections there are four sets of data. The Data Set Title is the name that was given to the data set at the time of sampling. It can be used to access the appropriate set of data from within NVGate if necessary

Day One, Run One

Driver**:** Richard Lawrance
Equipment Operator**:** Robert Dailey
Data Set Title**:** Morning Run 1 Holes 1 through 9, Robert and Richard

MEScope Data

The stress points of the vehicle compartment are shown below. There are two or more sets of pictures associated with each frequency being observed. These pictures represent each peak of the oscillation at that frequency. In each picture there are the following views (in order from top left and then clockwise around the image):

- Z-axis view
- 3D view
- Y-axis view
- X-axis View

The frequencies chosen to be displayed here where based of the peaks seen in the g-forces measured in the average spectrum data. Not all of the peaks are displayed.

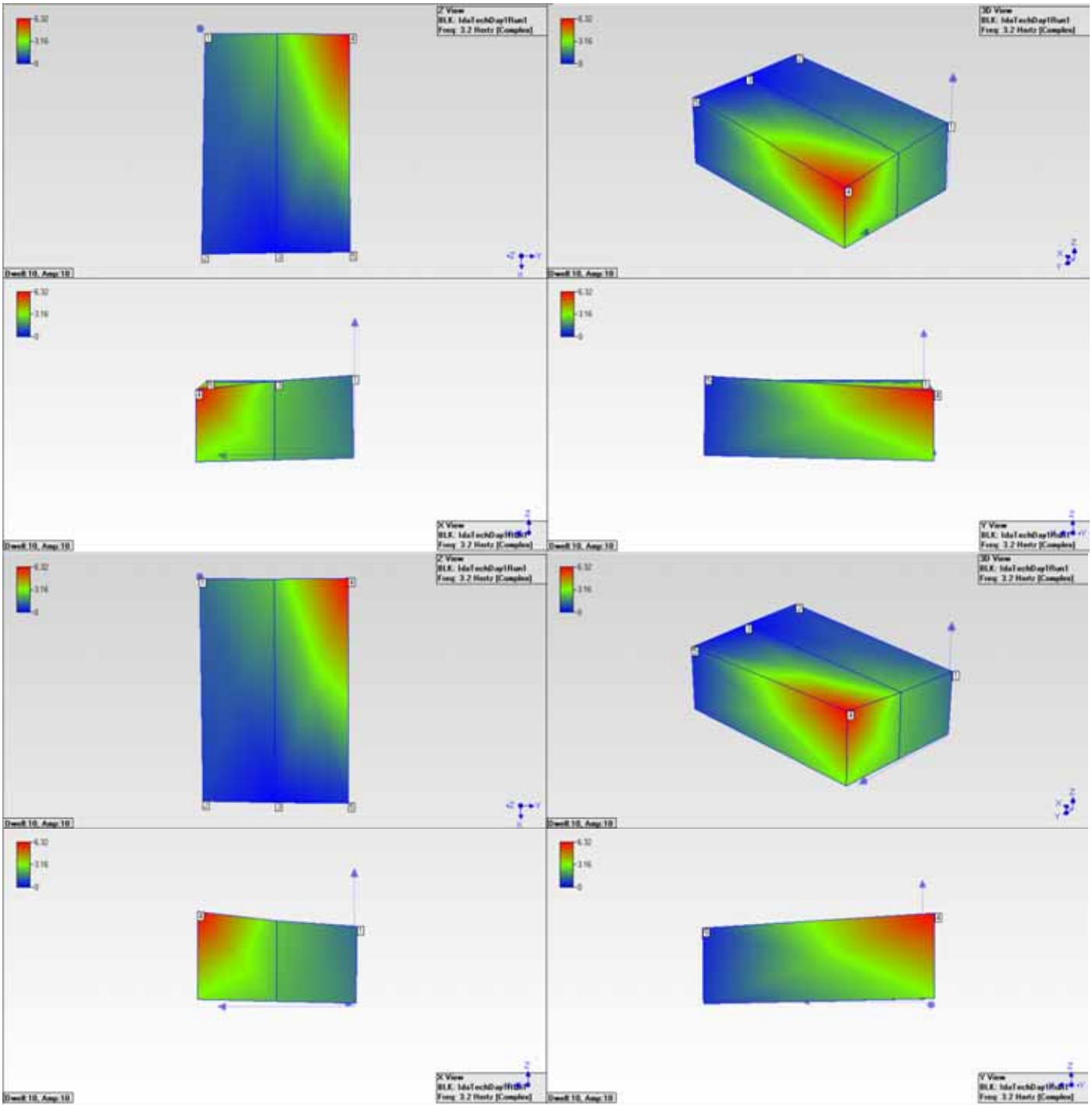

Figure 4: 3.2Hz

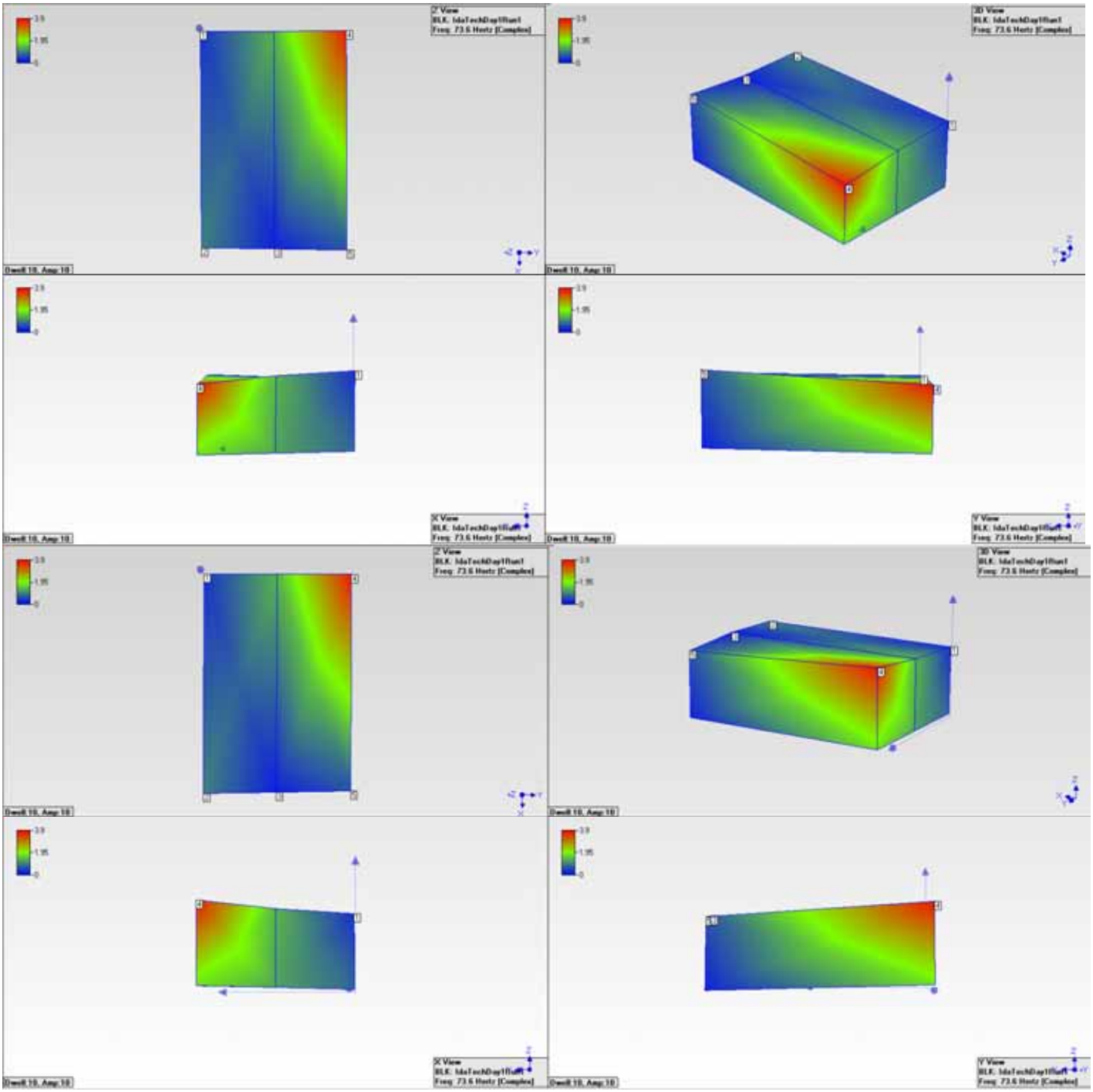

Figure 5: 73.6Hz

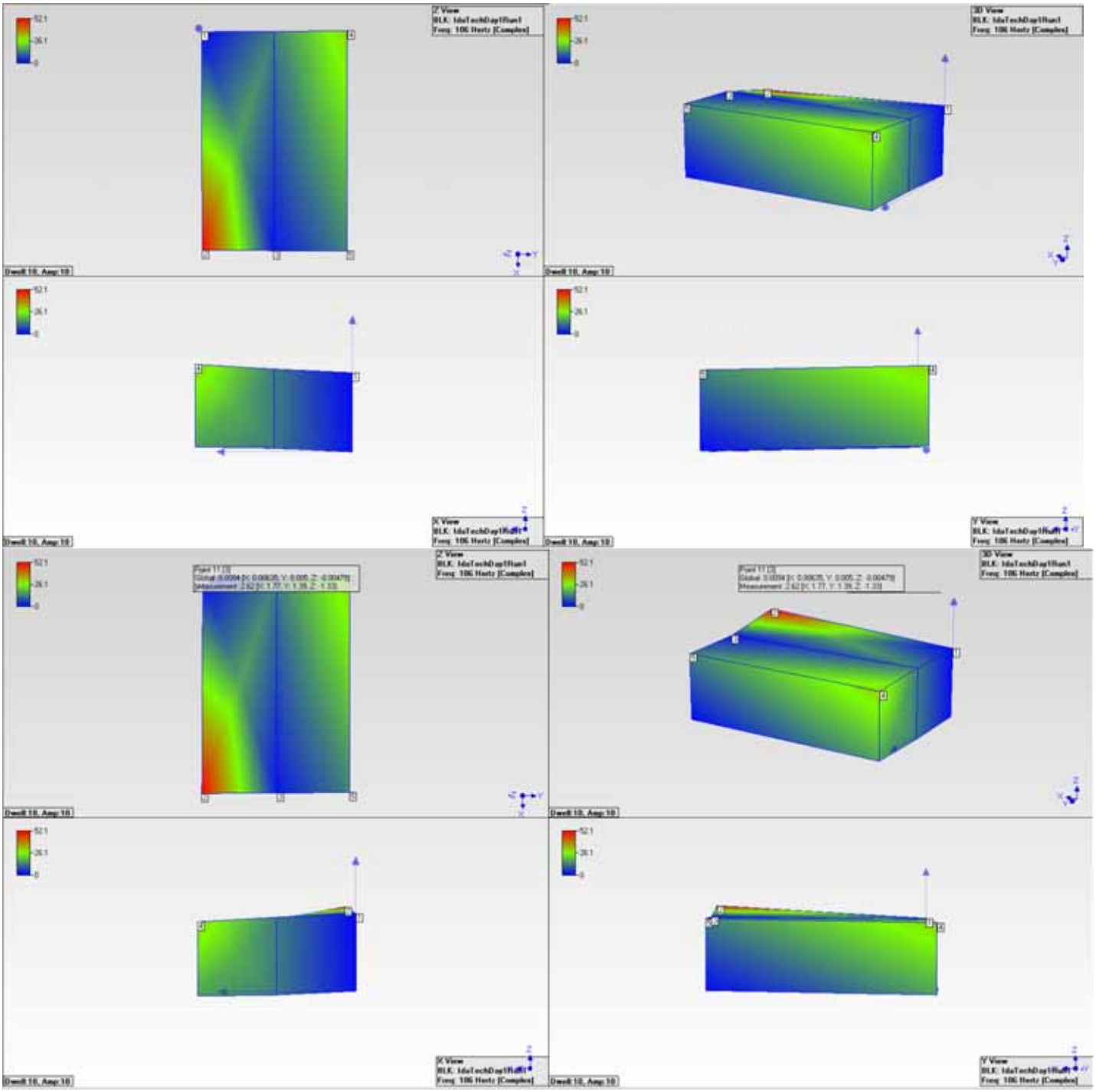

Figure 6: 106Hz

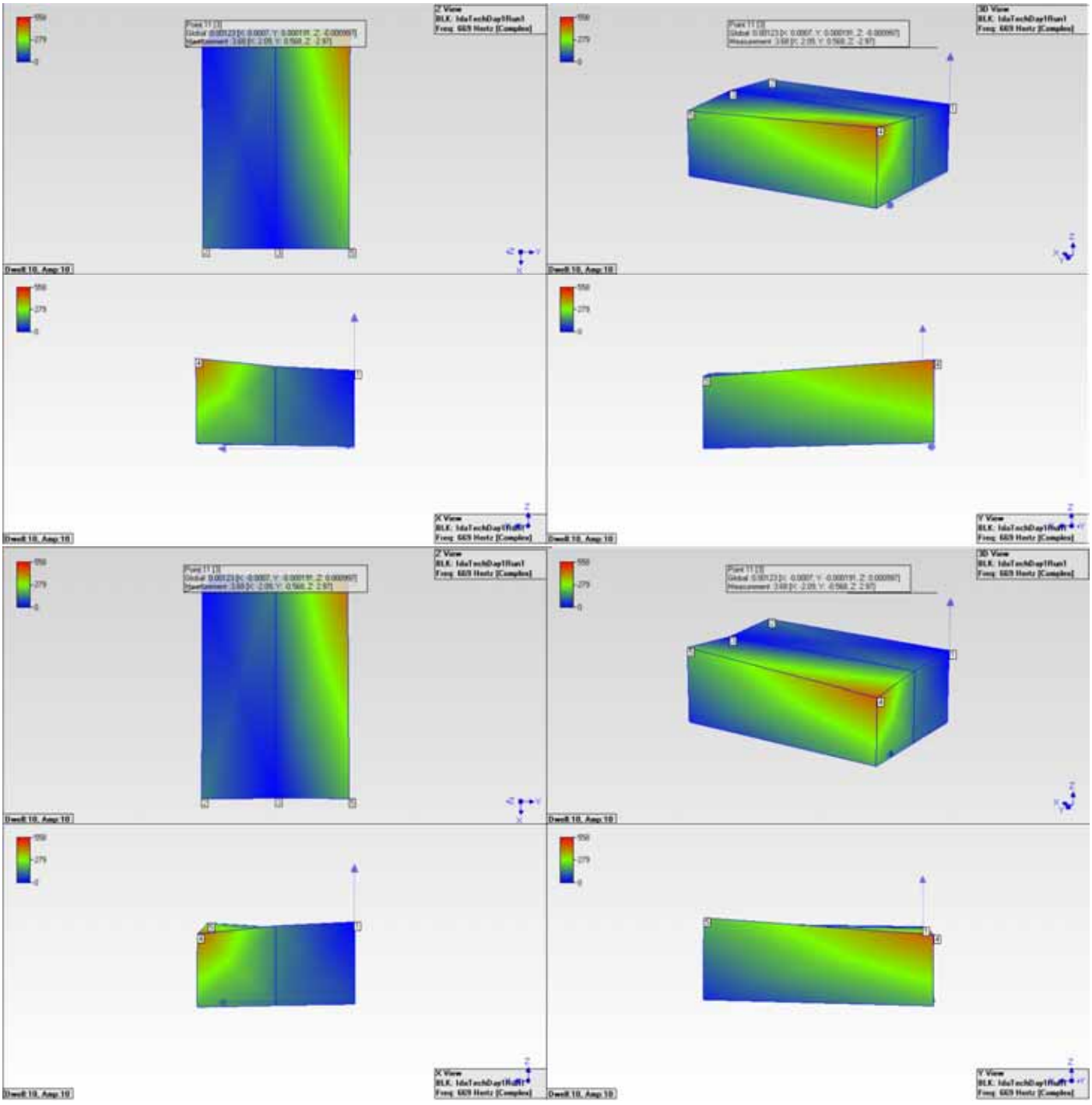

Figure 7: 669Hz

Accelerometer Data

Unless otherwise noted, the scaling for the graphs is as follows:

Time domain graph scale:

- X-axis: 6:14:43am to 6:31:06am
- Y-axis: +80g to -60g

FRF data graph scale:

- Top Graph
  - X-axis 0Hz to 1.4kHz
  - Y-axis: 0 to 10 no units
- Bottom Graph
  - X-axis 0Hz to 1.4kHz
  - Y-axis: -720° to 720°

Average spectrum graph scale:

- X-axis: 0Hz to 1.4kHz
- Y-axis: 0g to 0.006g

TIME Domain Data

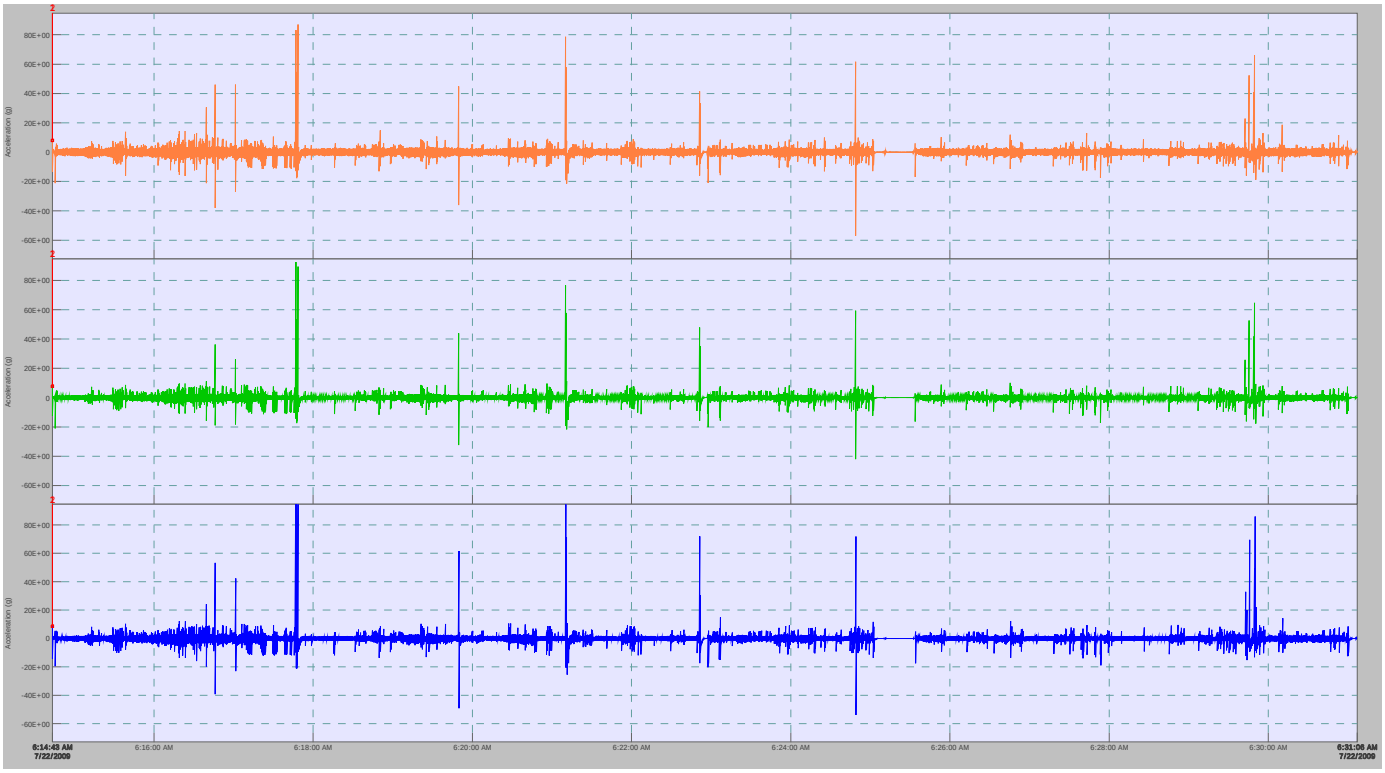

Figure 8: Accelerometer 1(#67, Reference A)

The colors are assigned as follows:

- Orange: Input 1 (x axis)
- Green: Input 2 (y axis)
- Blue: Input 3 (z axis)

Average Spectrum Data

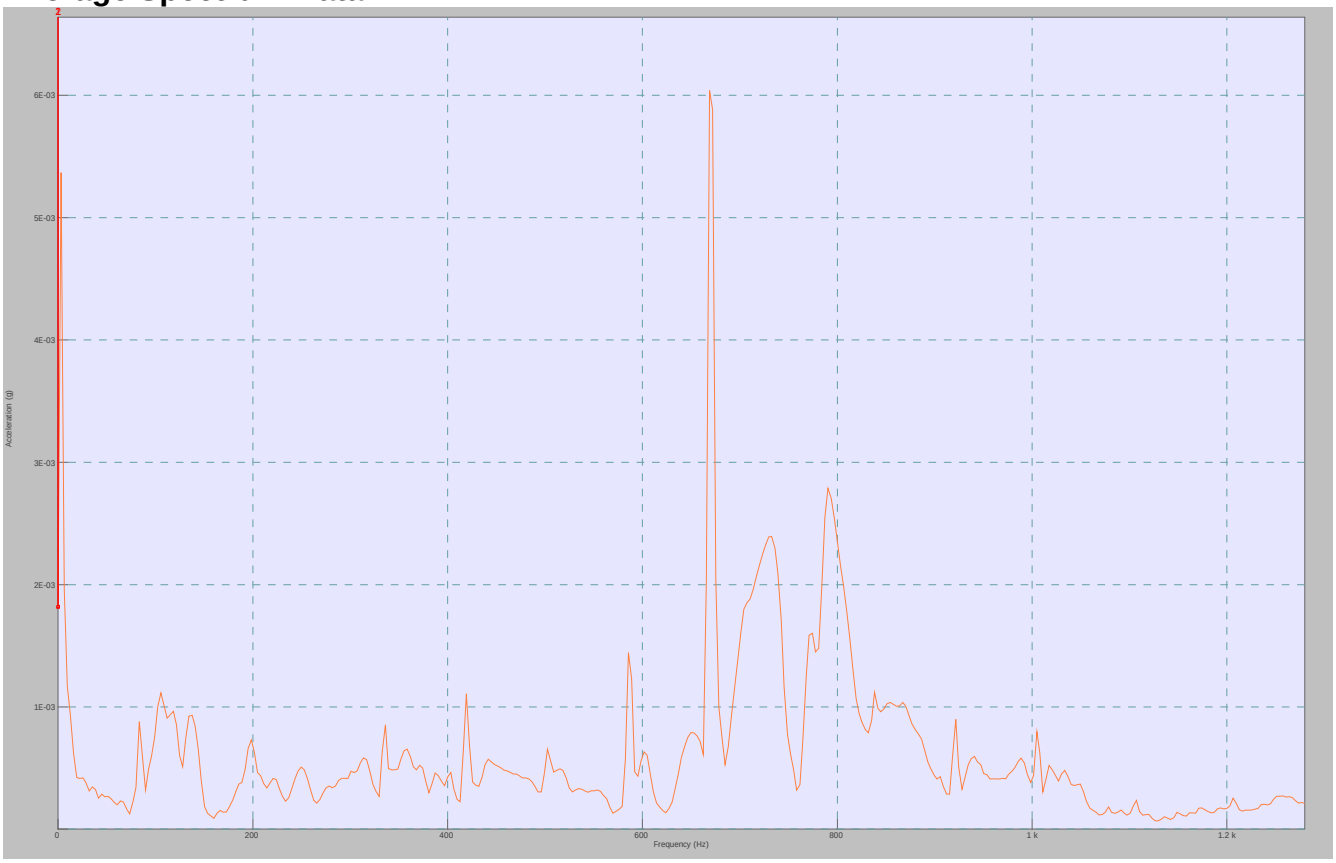

Figure 9: Accelerometer 1(#67, Reference A).This data is for the average spectrum for input 3. No other average spectrum data was gathered on day one of testing.

The graph scale data for the average spectrum data is as follows:

- x-scale 0Hz to 1.6kHz
- y-scale: 0g to 7E-3g

FRF Data

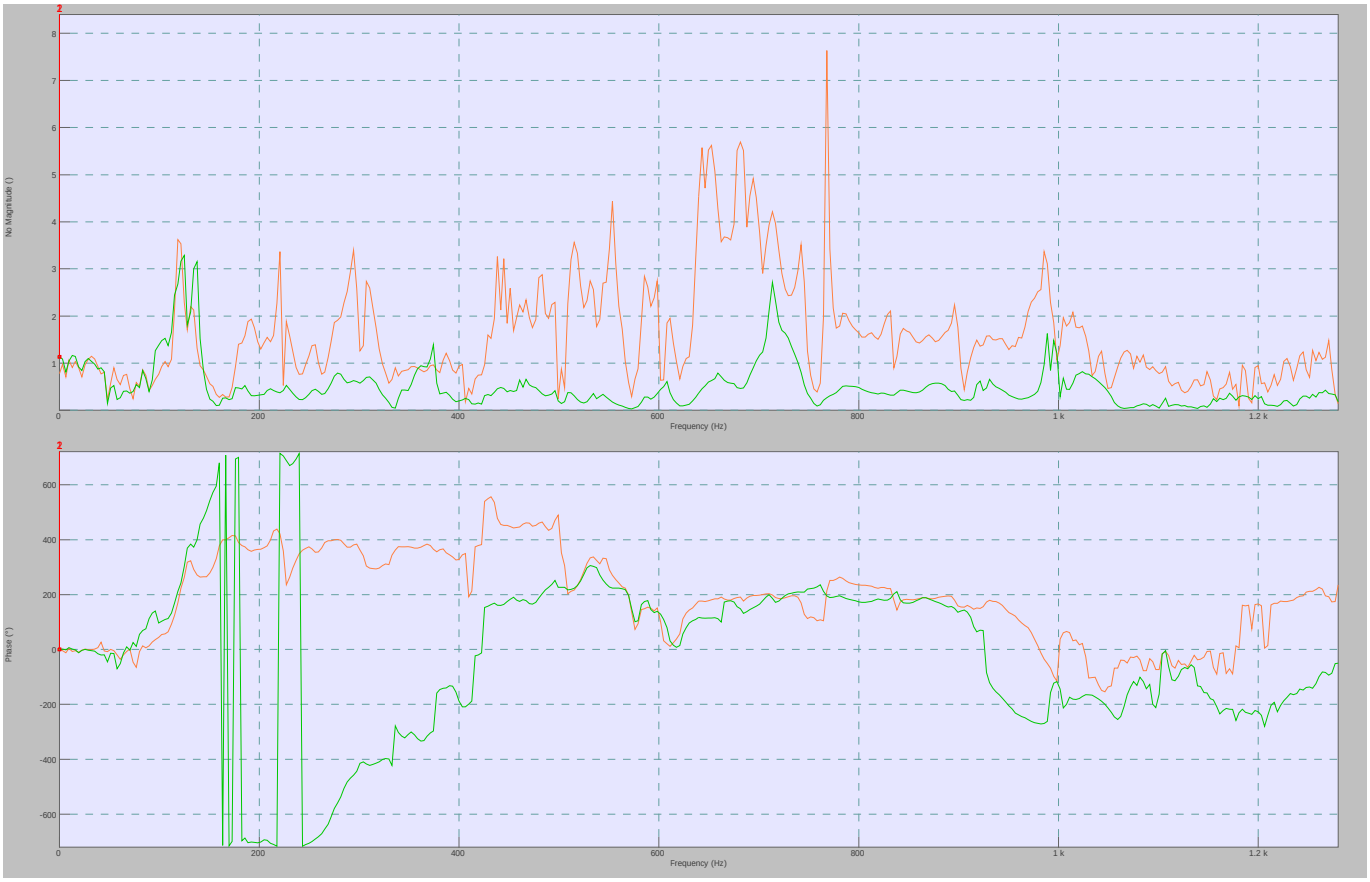

Figure 10: Accelerometer 1(#67, Reference A)

The colors are assigned as follows:

- Orange: Input 1(x axis)
- Green: Input 2 (y axis)
- *No blue for this set because there is no FRF data for input 3*
- *Reference Input: Input 3*

The graph scale data for the FRF data is as follows:

- Top Graph
  - x-scale 0Hz to 1.25kHz
  - y-scale: 0 to 8 no units
- Bottom Graph
  - x-scale 0Hz to 1.25kHz
  - y-scale: -720° to 720°

Time Domain Data

Figure 11: Accelerometer 2 (#68, Reference B)

The colors are assigned as follows:

- Orange: Input 4 (x axis)
- Green: Input 5 (z axis)
- Blue: Input 6 (y axis) *note that this data set is inverted from the rest of them

FRF Data

Figure 12: Accelerometer 2 (#68, Reference B)

The colors are assigned as follows:

- Orange: Input 4 (x axis)
- Green: Input 5 (z axis)
- Blue: Input 6 (y axis) *note that this data set is inverted from the rest of them
- Reference Input: Input 3

The graph scale data for the FRF data is as follows:

- Top Graph
  - x-scale 0Hz to 1.25kHz
  - y-scale: 0 to 250 no units
- Bottom Graph
  - x-scale 0Hz to 1.25kHz
  - y-scale: -720° to 720°

Time Domain Data

Figure 13: Accelerometer 3 (#69, Reference C)

The colors are assigned as follows:

- Orange: Input 7 (x axis)
- Green: Input 8 (y axis)
- Blue: Input 9 (z axis)

FRF Data

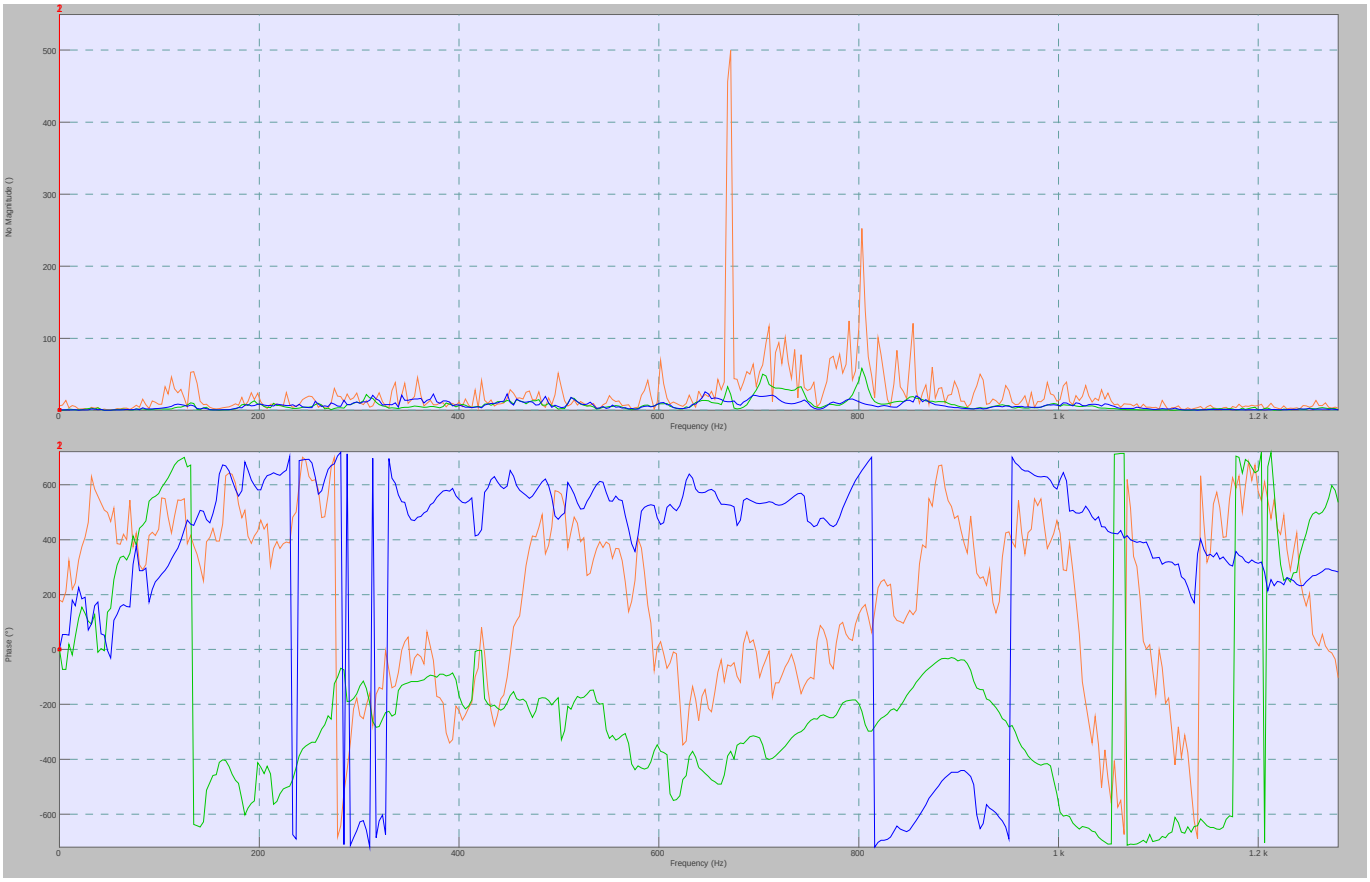

Figure 14: Accelerometer 3 (#69, Reference C)

The colors are assigned as follows:

- Orange: Input 7 (x axis)
- Green: Input 8 (y axis)
- Blue: Input 9 (z axis)
- Reference Input: Input 3

The graph scale data for the FRF data is as follows:

- Top Graph
  - x-scale 0Hz to 1.25kHz
  - y-scale: 0 to 550 no units
- Bottom Graph
  - x-scale 0Hz to 1.25kHz
  - y-scale: -720° to 720°

Time Domain Data

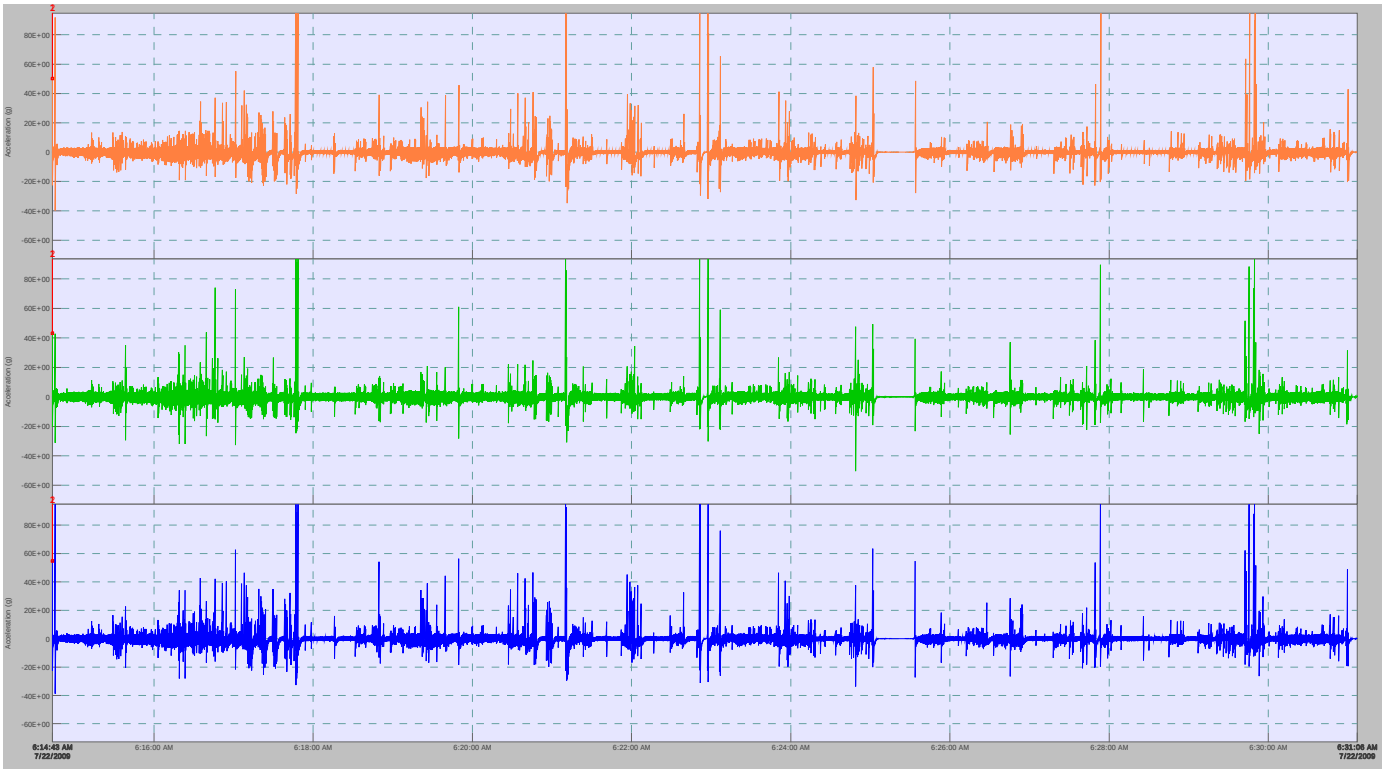

Figure 15: Accelerometer 4 (#70, Reference D)

The colors are assigned as follows:

- Orange: Input 10 (x axis)
- Green: Input 11 (y axis)
- Blue: Input 12 (z axis)

FRF Data

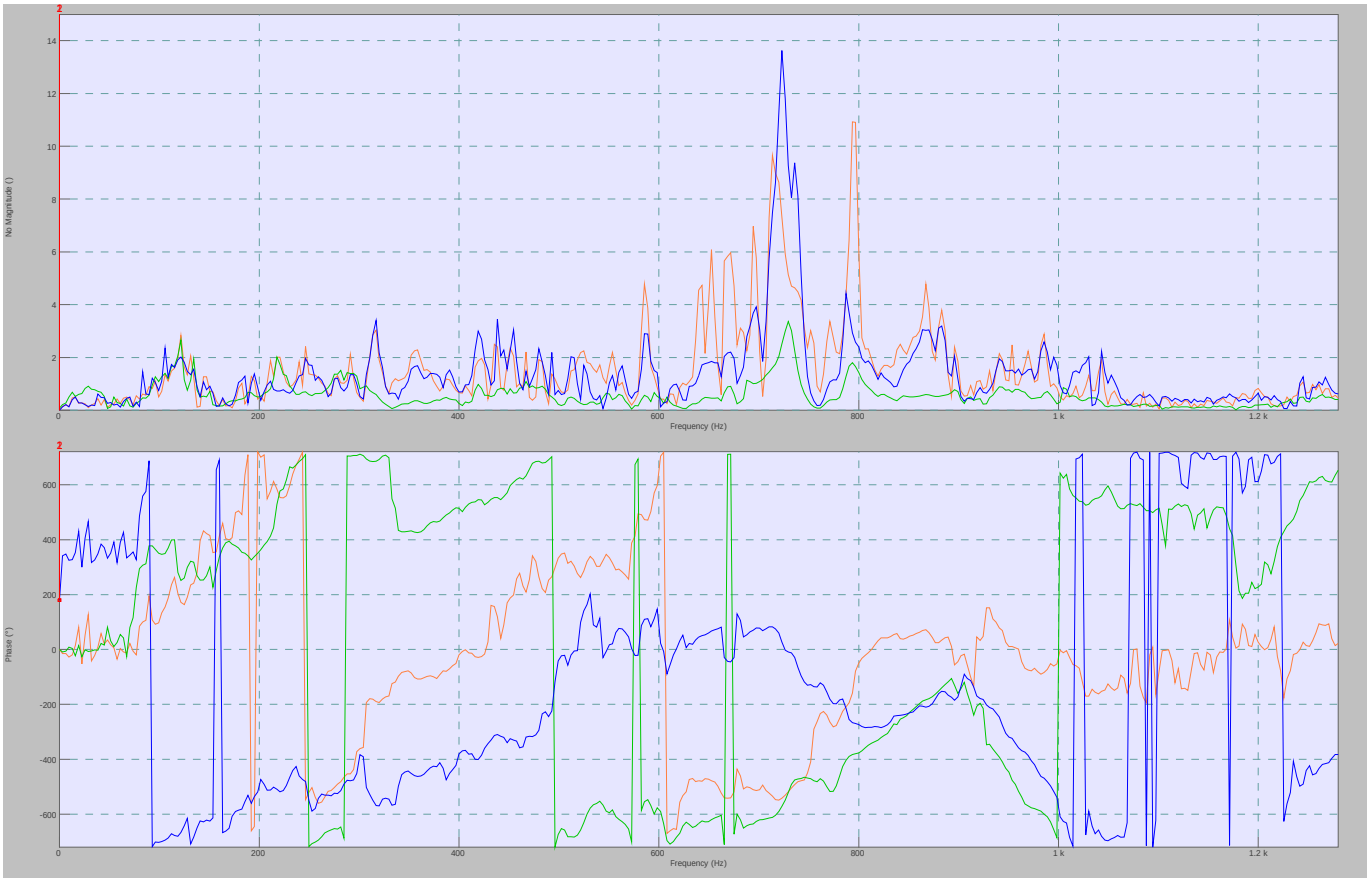

Figure 16: Accelerometer 4 (#70, Reference D)

The colors are assigned as follows:

- Orange: Input 10 (x axis)
- Green: Input 11 (y axis)
- Blue: Input 12 (z axis)
- Reference Input: Input 3

The graph scale data for the FRF data is as follows:

- Top Graph
  - x-scale 0Hz to 1.25kHz
  - y-scale: 0 to 15 no units
- Bottom Graph
  - x-scale 0Hz to 1.25kHz
  - y-scale: -720° to 720°

Time Domain Data

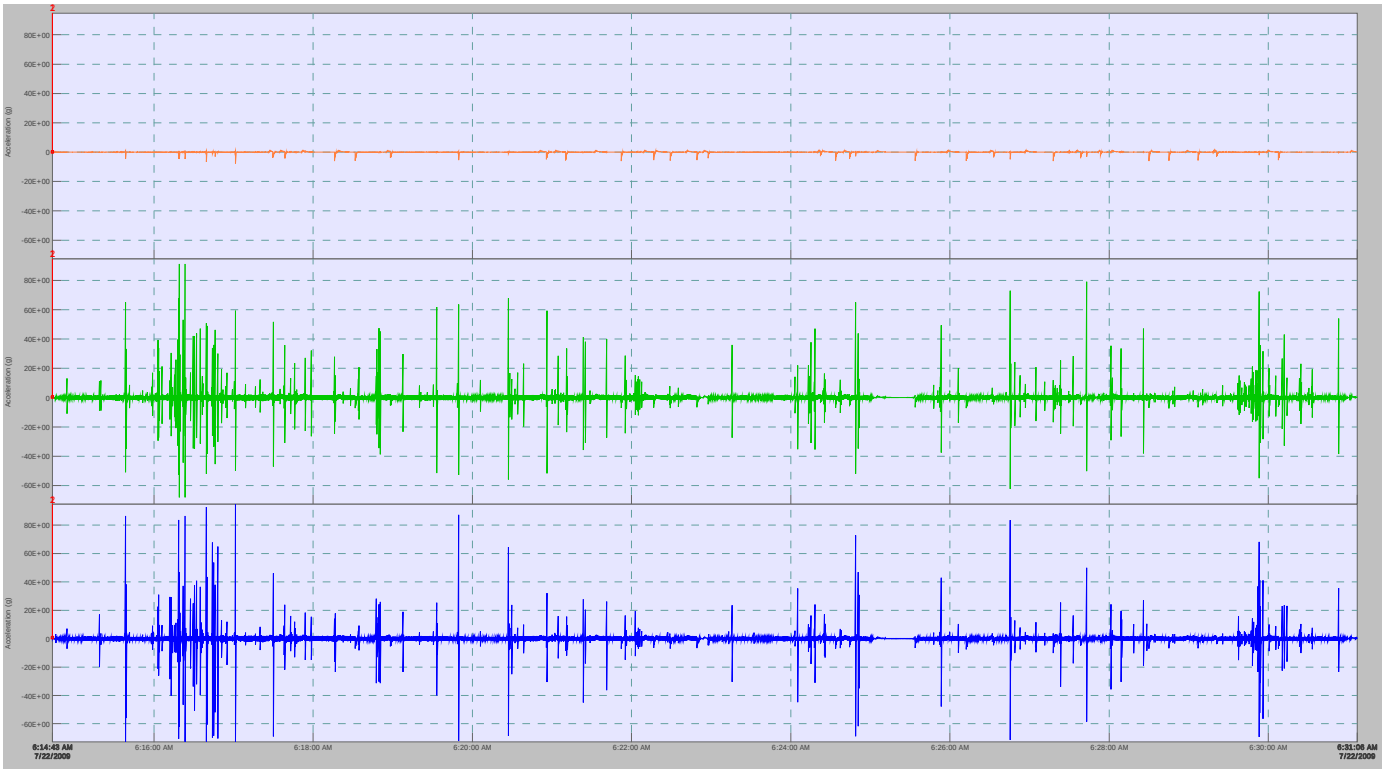

Figure 17: Accelerometer 5(#71, Reference E)

The colors are assigned as follows:

- Orange: Input 13 (x axis)
- Green: Input 14 (z axis) *note that this data set is inverted from the rest of them
- Blue: Input 15 (y axis)

FRF Data

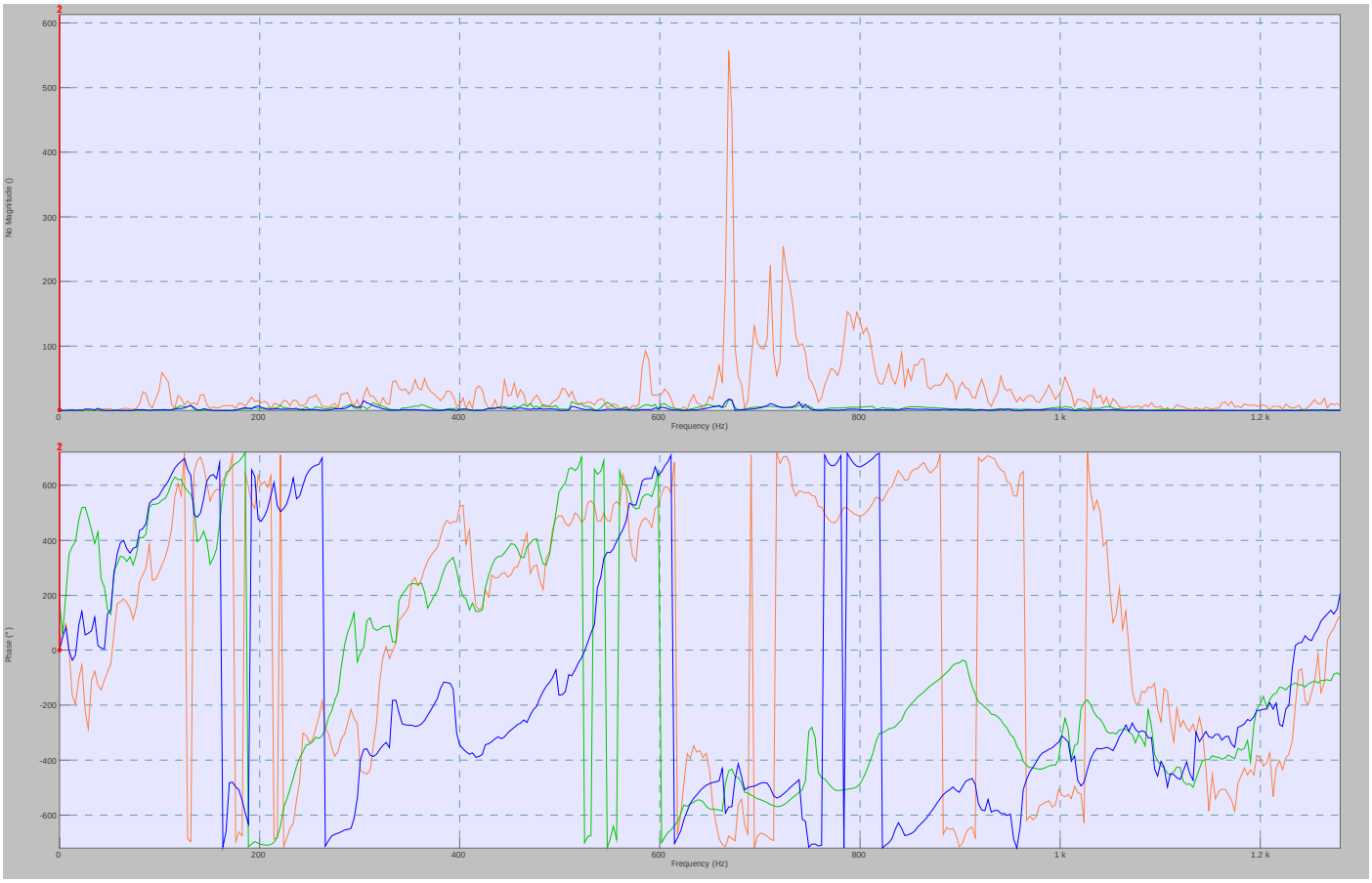

Figure 18: Accelerometer 5(#71, Reference E)

The colors are assigned as follows:

- Orange: Input 13 (x axis)
- Green: Input 14 (z axis) *note that this data set is inverted from the rest of them
- Blue: Input 15 (y axis)
- Reference Input: Input 3

The graph scale data for the FRF data is as follows:

- Top Graph
  - x-scale 0Hz to 1.25kHz
  - y-scale: 0 to 600 no units
- Bottom Graph
  - x-scale 0Hz to 1.25kHz
  - y-scale: -720° to 720°

Day One, Run Two

Driver: Richard Lawrance
Equipment Operator: Robert Dailey
Data Set Title: Morning Run 1 Holes 10 through 18, Robert and Richard

Accelerometer Data

Unless otherwise noted, the scaling for the graphs is as follows:

Time domain graph scale:
- X-axis: 7:04:54 to 7:17:41
- Y-axis: +30g to -30g

FRF data graph scale:
- Top Graph
  - X-axis 0Hz to 1.4kHz
  - Y-axis: 0 to 10 no units
- Bottom Graph
  - X-axis 0Hz to 1.4kHz
  - Y-axis: -720° to 720°

Average spectrum graph scale:
- X-axis: 0Hz to 1.4kHz
- Y-axis: 0g to 0.006g

Notes
This run was ended prematurely due to the batteries needing to have time to recharge. The data does not reflect a complete run through the bottom 9 holes of the golf course.

Time Domain Data

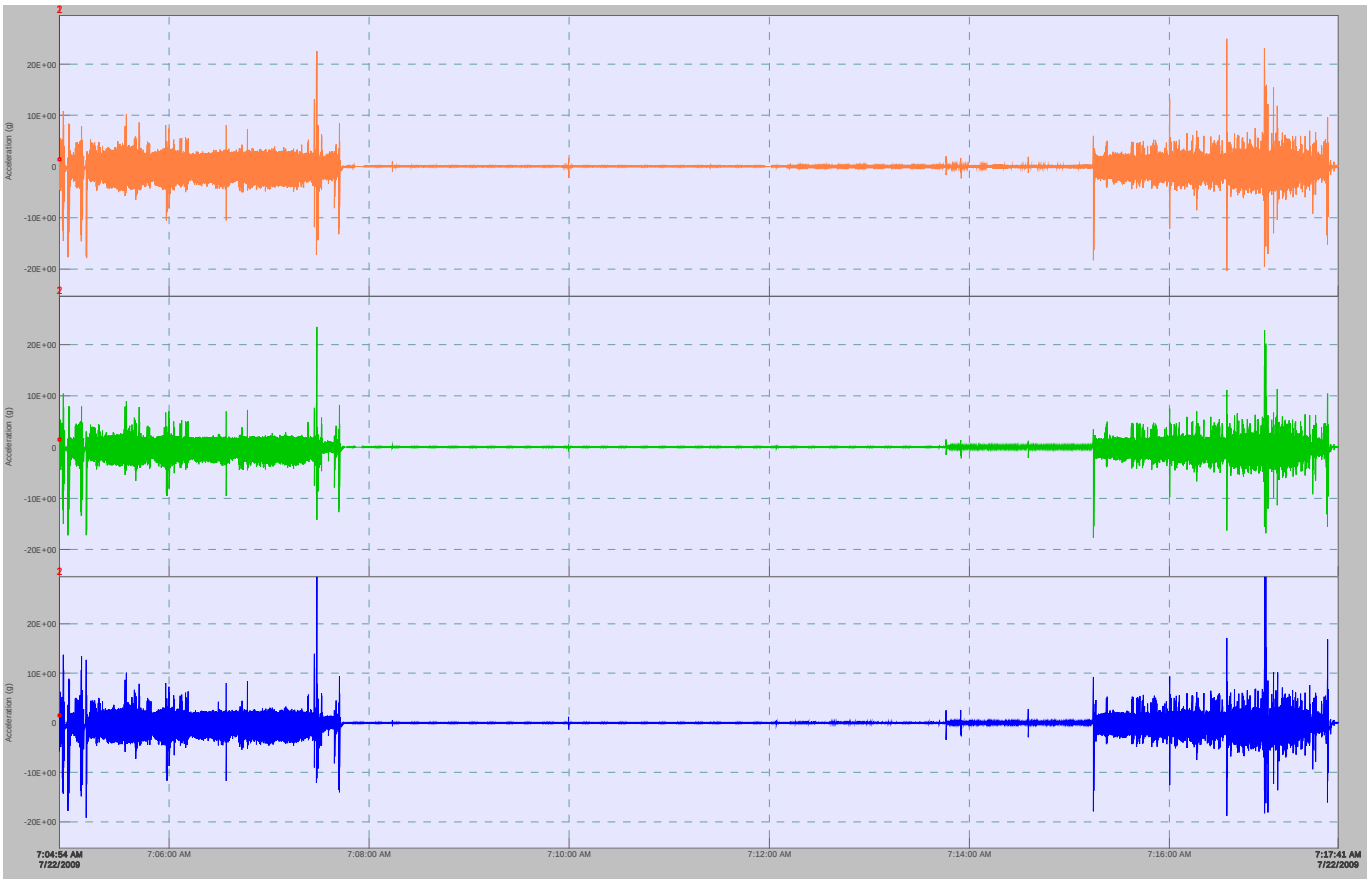

Figure 19: Accelerometer 1(#67, Reference A)

The colors are assigned as follows:

- Orange: Input 1 (x axis)
- Green: Input 2 (y axis)
- Blue: Input 3 (z axis)

Average Spectrum Data

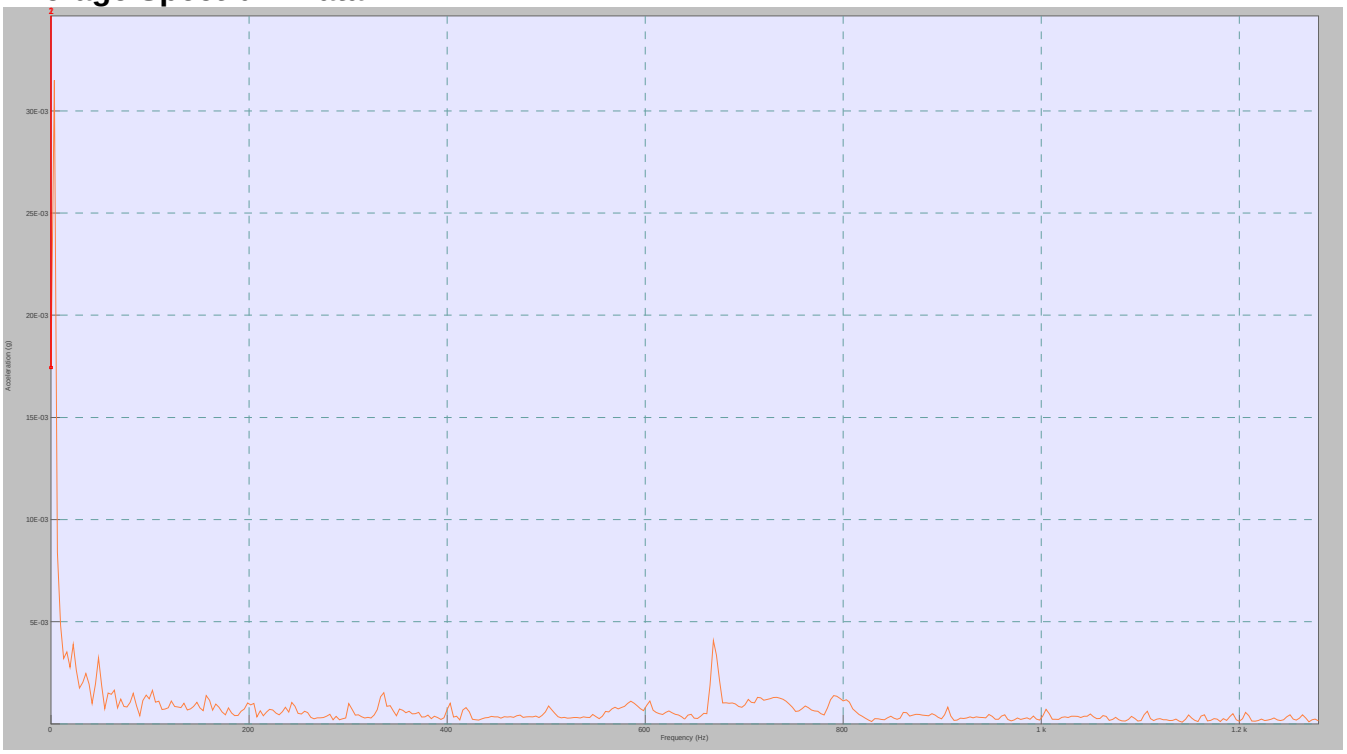

Figure 20: Accelerometer 1(#67, Reference A)

Scale Information

- X-axis: 0Hz to 1.25kHz
- Y-axis: 0g to 25E-3g

FRF Data

Figure 21: Accelerometer 1(#67, Reference A)

The colors are assigned as follows:

- Orange: Input 1 (x axis)
- Green: Input 2 (y axis)
- *No data for input 3*

The graph scale data for the FRF data is as follows:

- Top Graph
  - x-scale 0Hz to 1.25kHz
  - y-scale: 0 to 4.5 no units
- Bottom Graph
  - x-scale 0Hz to 1.25kHz
  - y-scale: -720° to 720°

Time Domain Data

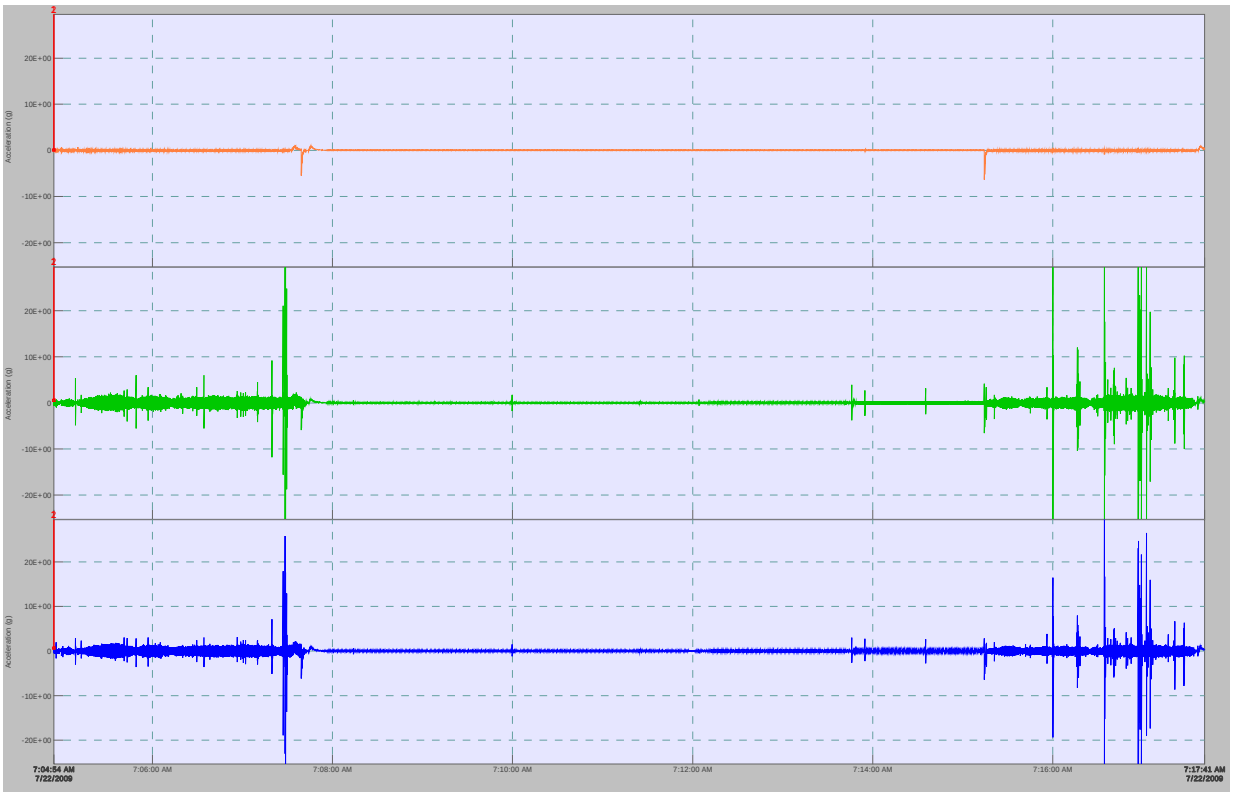

Figure 22: Accelerometer 2 (#68, Reference B)

The colors are assigned as follows:

- Orange: Input 4 (x axis)
- Green: Input 5 (z axis)
- Blue: Input 6 (y axis) *note that this data set is inverted from the rest of them

FRF Data

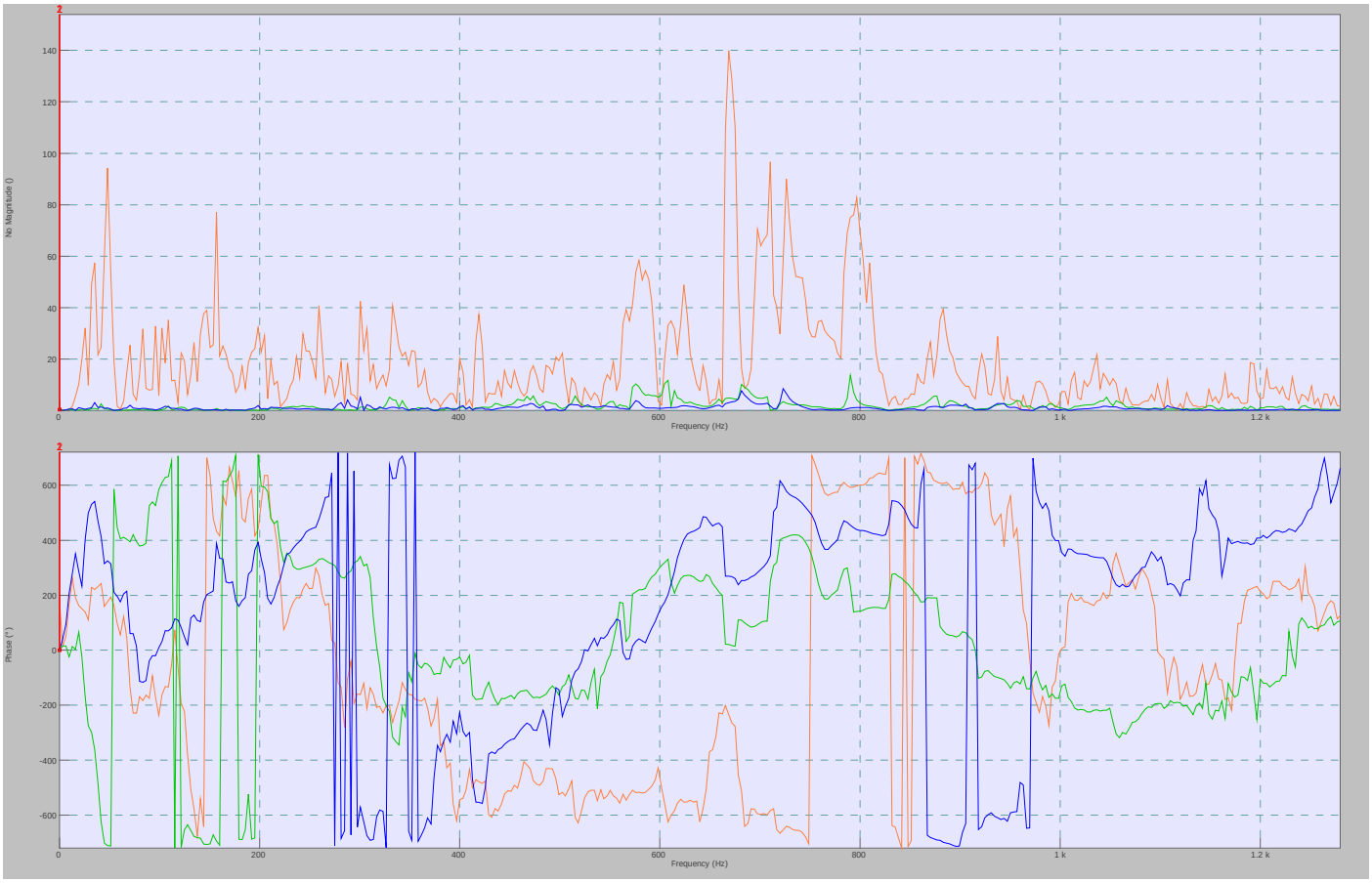

Figure 23: Accelerometer 2 (#68, Reference B)

The colors are assigned as follows:

- Orange: Input 4 (x axis)
- Green: Input 5 (z axis)
- Blue: Input 6 (y axis) *note that this data set is inverted from the rest of them

The graph scale data for the FRF data is as follows:

- Top Graph
  - x-scale 0Hz to 1.25kHz
  - y-scale: 0 to 150 no units
- Bottom Graph
  - x-scale 0Hz to 1.25kHz
  - y-scale: -720° to 720°

Time Domain Data

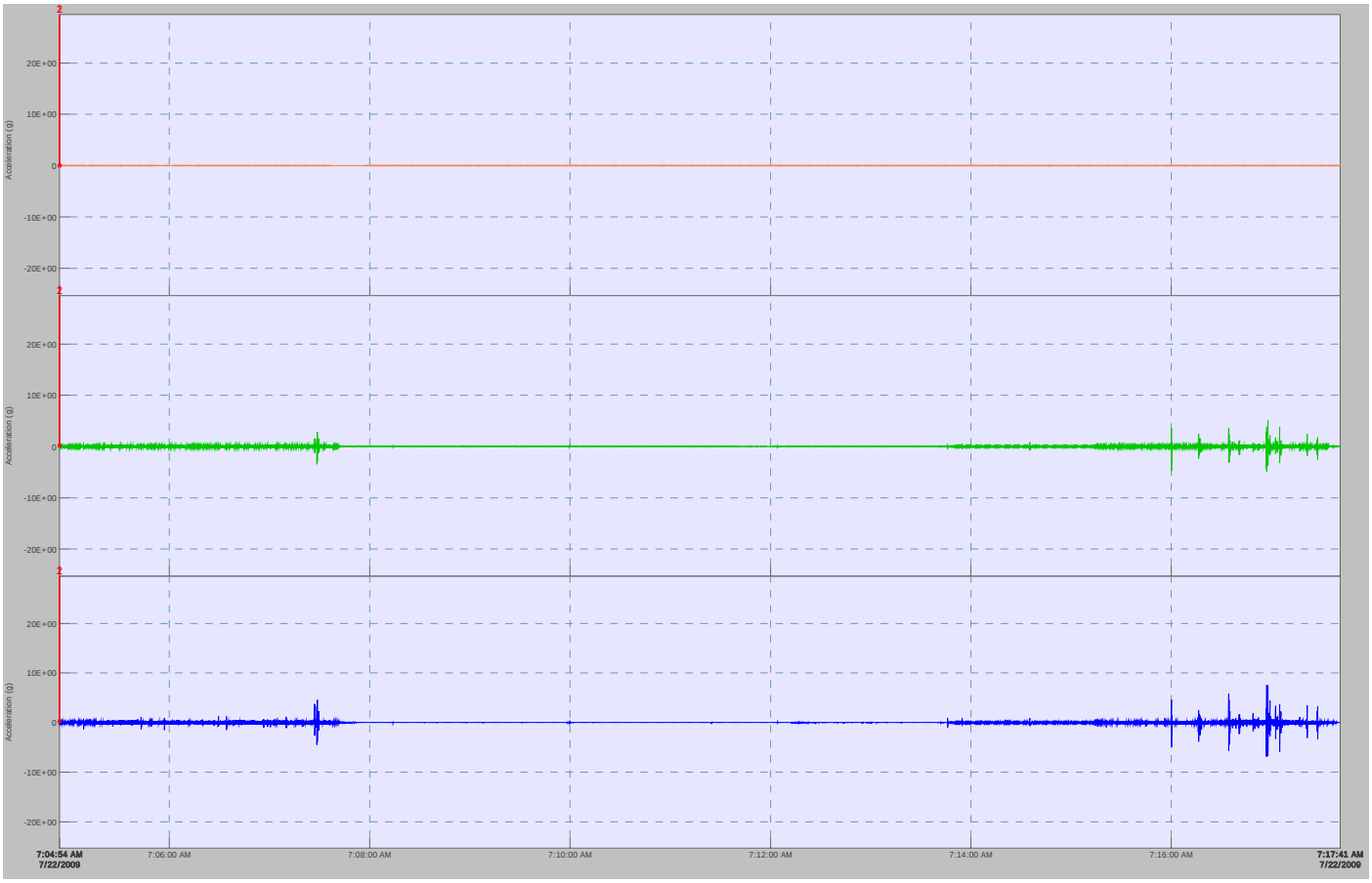

Figure 24: Accelerometer 3 (#69, Reference C)

The colors are assigned as follows:

- Orange: Input 7 (x axis)
- Green: Input 8 (y axis)
- Blue: Input 9 (z axis)

FRF Data

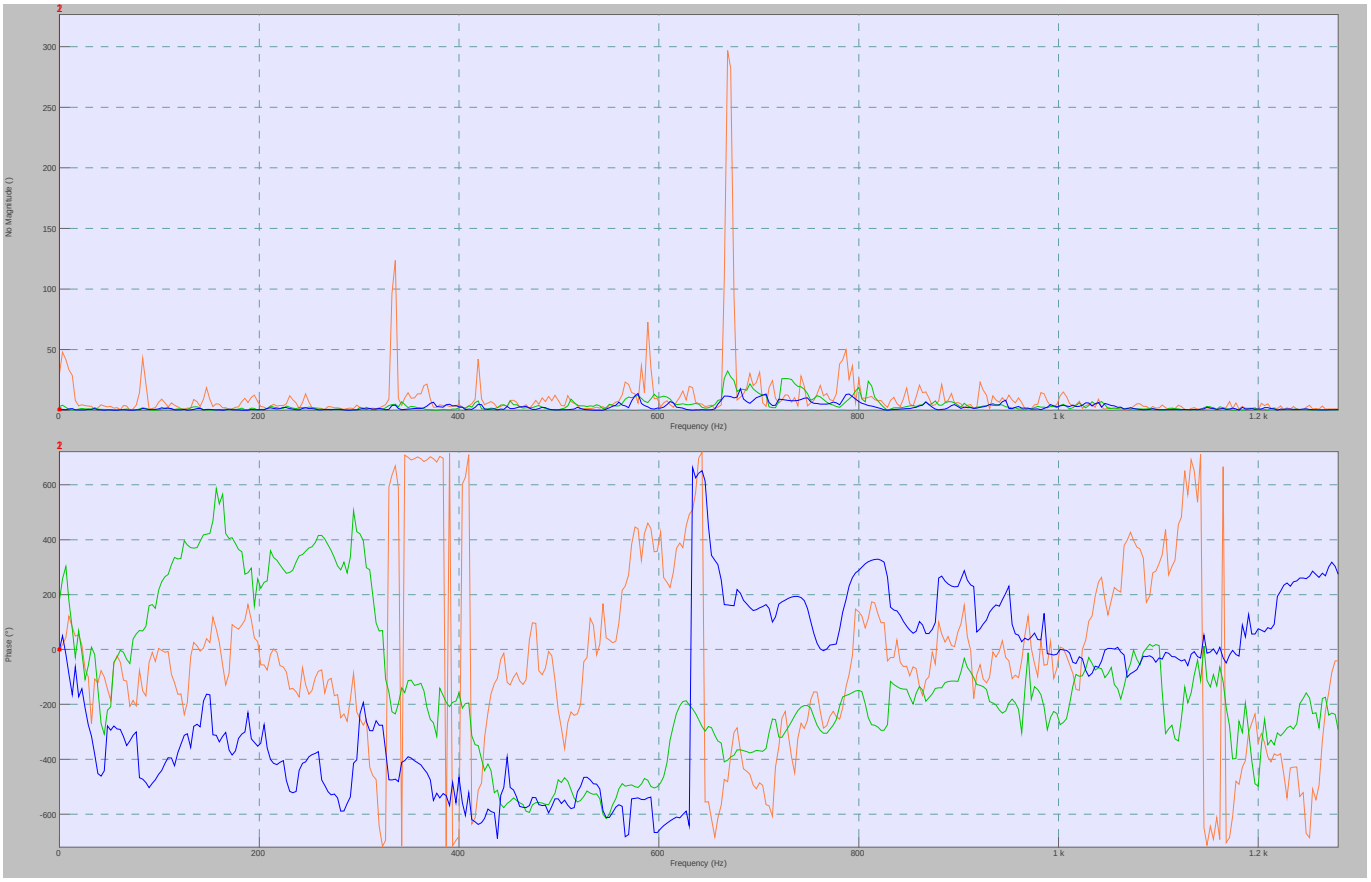

Figure 25: Accelerometer 3 (#69, Reference C)

The colors are assigned as follows:

- Orange: Input 7 (x axis)
- Green: Input 8 (y axis)
- Blue: Input 9 (a axis)

The graph scale data for the FRF data is as follows:

- Top Graph
  - x-scale 0Hz to 1.25kHz
  - y-scale: 0 to 325 no units
- Bottom Graph
  - x-scale 0Hz to 1.25kHz
  - y-scale: -720° to 720°

Time Domain Data

Figure 26: Accelerometer 4 (#70, Reference D)

The colors are assigned as follows:

- Orange: Input 10 (x axis)
- Green: Input 11 (y axis)
- Blue: Input 12 (z axis)

FRF Data

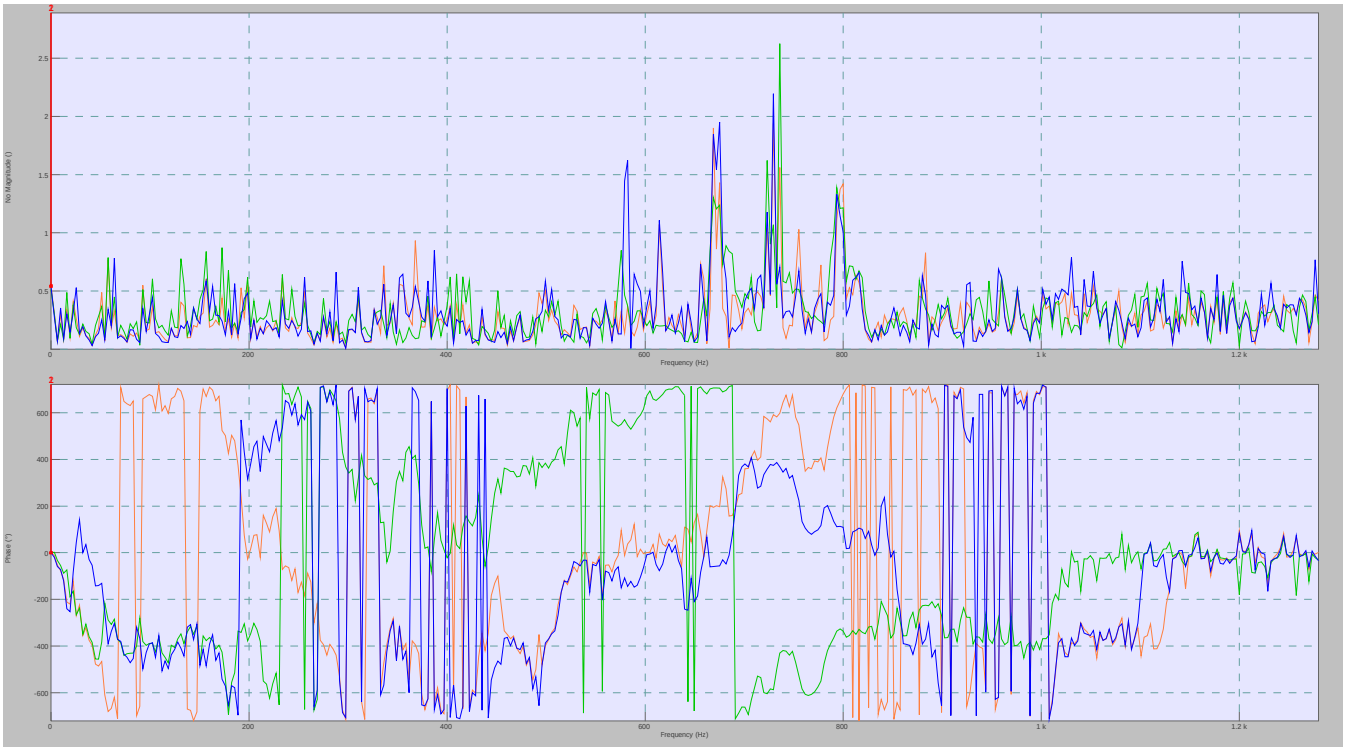

Figure 27: Accelerometer 4 (#70, Reference D)

The colors are assigned as follows:

- Orange: Input 10 (x axis)
- Green: Input 11 (y axis)
- Blue: Input 12 (z axis)

The graph scale data for the FRF data is as follows:

- Top Graph
    - x-scale 0Hz to 1.25kHz
    - y-scale: 0 to 3 no units
- Bottom Graph
    - x-scale 0Hz to 1.25kHz
    - y-scale: -720° to 720°

Time Domain Data

Figure 28: Accelerometer 5 (#71, Reference E)

The colors are assigned as follows:

- Orange: Input 13 (x axis)
- Green: Input 14 (z axis) *note that this data set is inverted from the rest of them
- Blue: Input 15 (y axis)

FRF Data

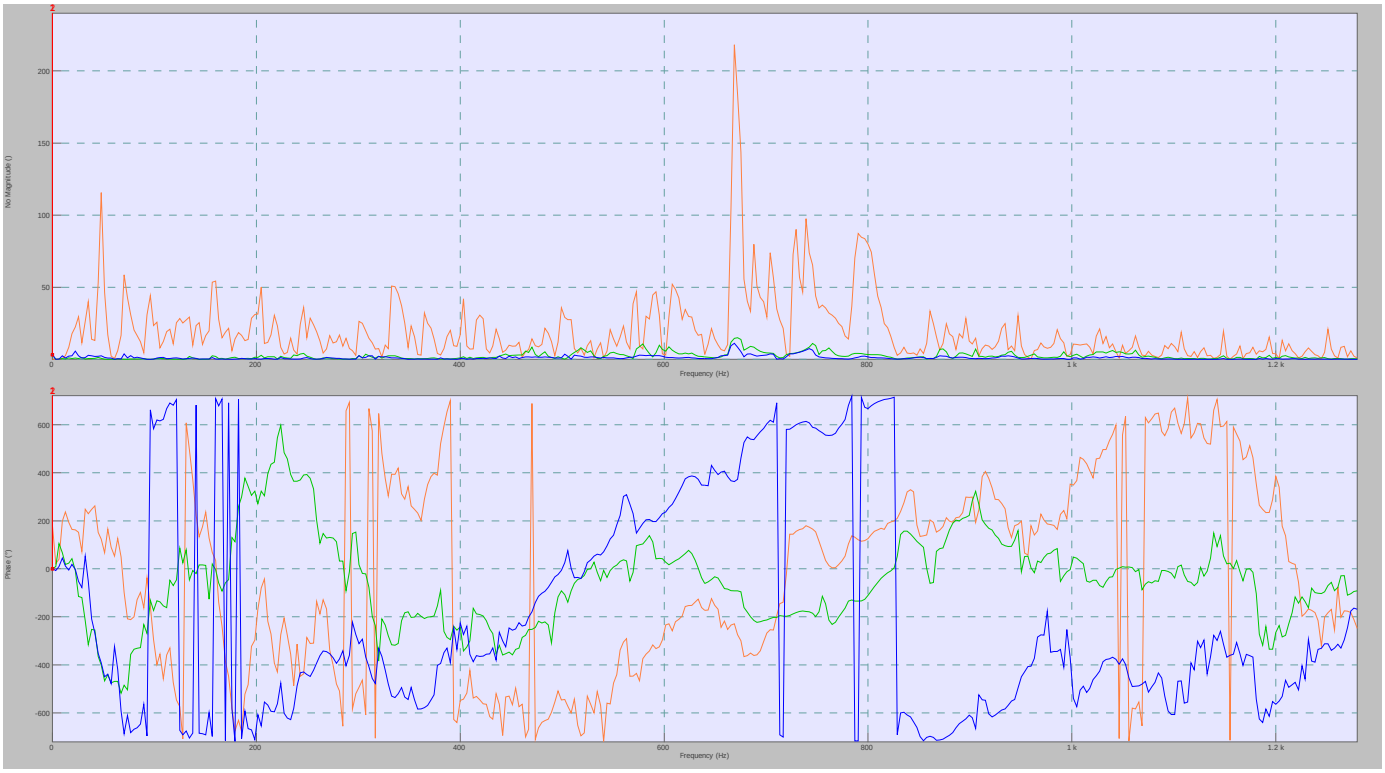

Figure 29: Accelerometer 5 (#71, Reference E)

The colors are assigned as follows:

- Orange: Input 13 (x axis)
- Green: Input 14 (z axis) *note that this data set is inverted from the rest of them
- Blue: Input 15 (y axis)

The graph scale data for the FRF data is as follows:

- Top Graph
  - x-scale 0Hz to 1.25kHz
  - y-scale: 0 to 250 no units
- Bottom Graph
  - x-scale 0Hz to 1.25kHz
  - y-scale: -720° to 720°

Day One, Run Three

Driver: Richard Lawrance
Equipment Operator: Robert Dailey
Data Set Title: Morning Run 1 Holes 10 through 18 (second try,) Robert and Richard

Accelerometer Data

Unless otherwise noted, the scaling for the graphs is as follows:

Time domain graph scale:

- X-axis: 9:55:08am to 10:13:15am
- Y-axis: +90g to -50g

FRF data graph scale:

- Top Graph
  - X-axis 0Hz to 1.4kHz
  - Y-axis: 0 to 10 no units
- Bottom Graph
  - X-axis 0Hz to 1.4kHz
  - Y-axis: -720° to 720°

Average spectrum graph scale:

- X-axis: 0Hz to 1.4kHz

Y-axis: 0g to 0.006g

Notes
This run was a repeat of run two in order to get a full set of data for holes 10 through 18.

Time Domain Data

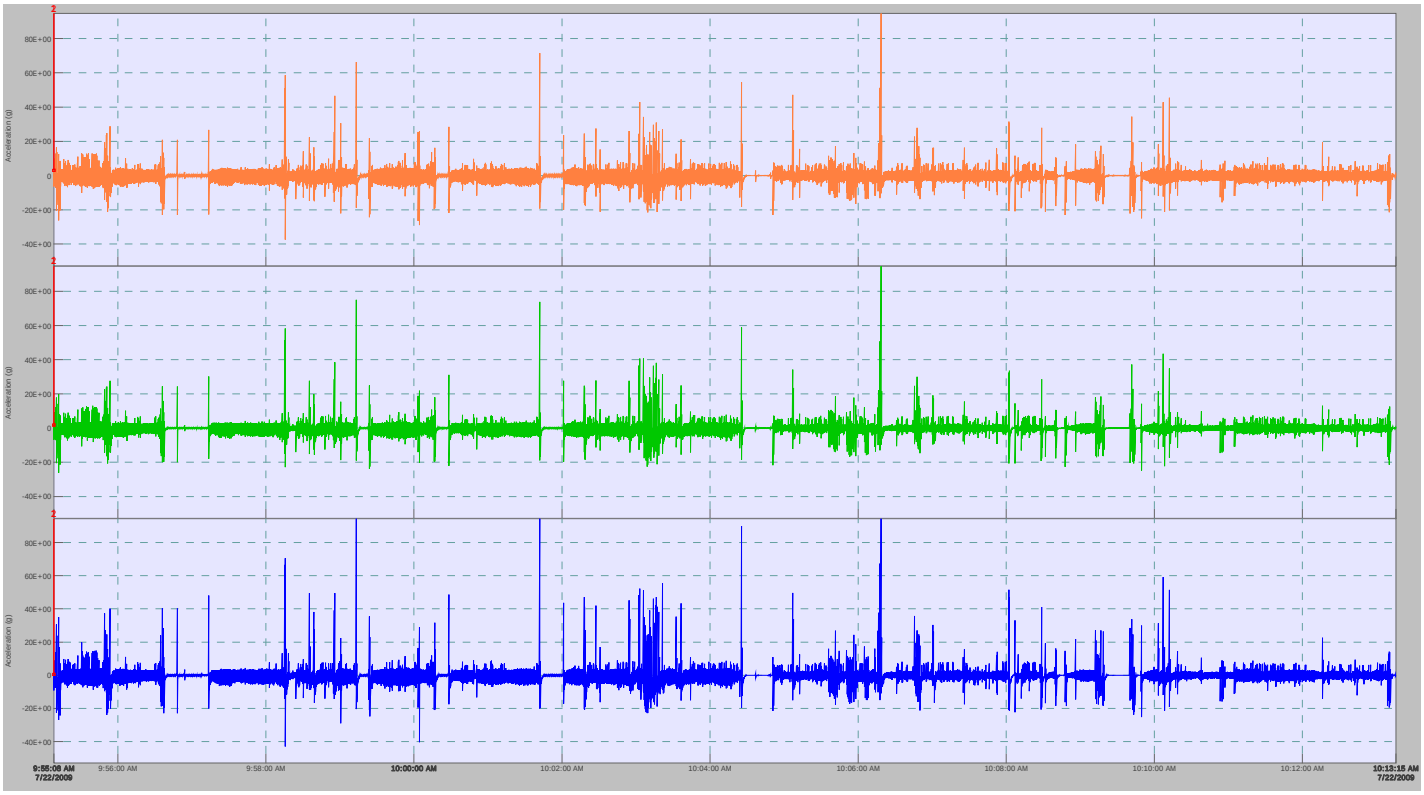

Figure 30: Accelerometer 1(#67, Reference A)

The colors are assigned as follows:

- Orange: Input 1 (x axis)
- Green: Input 2 (y axis)
- Blue: Input 3 (z axis)

Average Spectrum Data

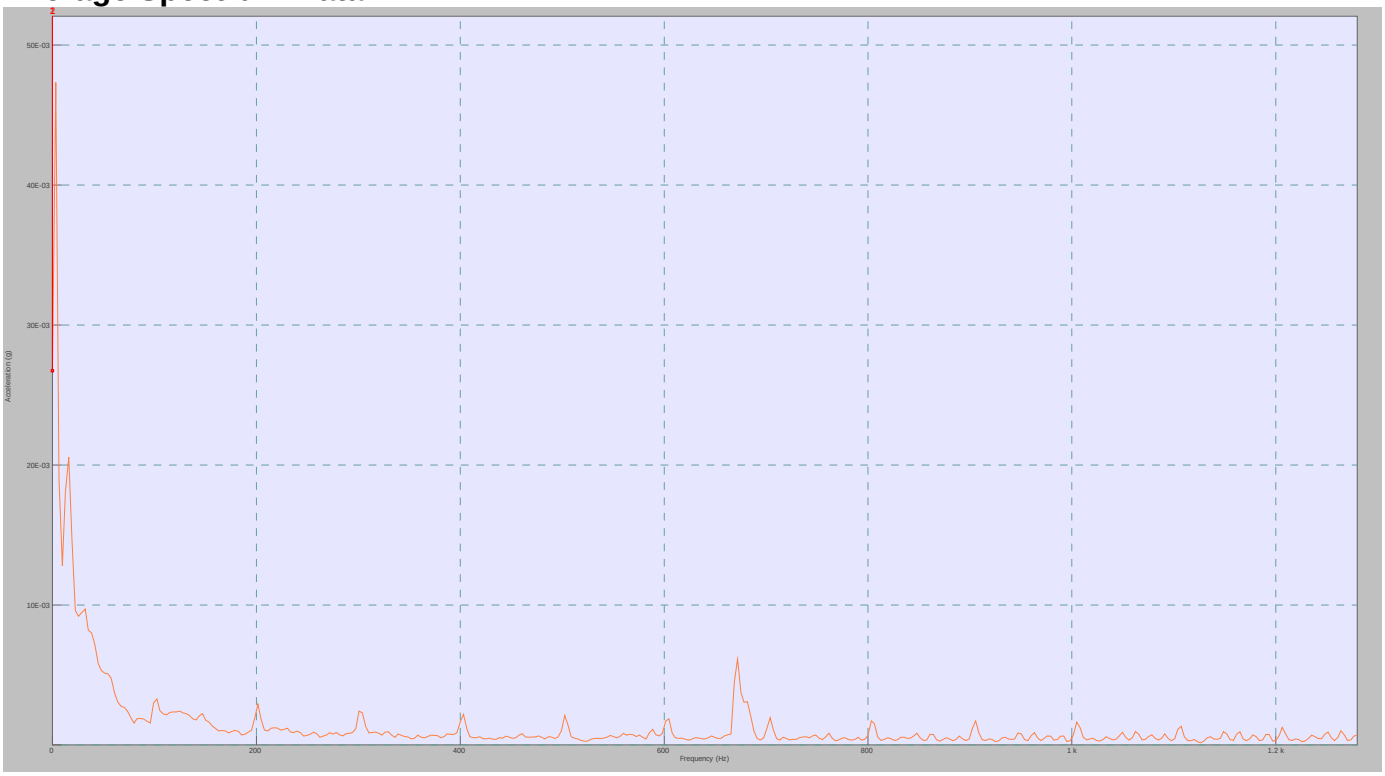

Figure 31: Accelerometer 1(#67, Reference A)

Scale Information

- X-axis: 0Hz to 1.25kHz
- Y-axis: 0g to 50E-3g

FRF Data

Figure 32: Accelerometer 1(#67, Reference A)

The colors are assigned as follows:

- Orange: Input 1 (x axis)
- Green: Input 2 (y axis)
- *No data for input 3*

The graph scale data for the FRF data is as follows:

- Top Graph
    - x-scale 0Hz to 1.25kHz
    - y-scale: 0 to 4 no units
- Bottom Graph
    - x-scale 0Hz to 1.25kHz
    - y-scale: -720° to 720°

Time Domain Data

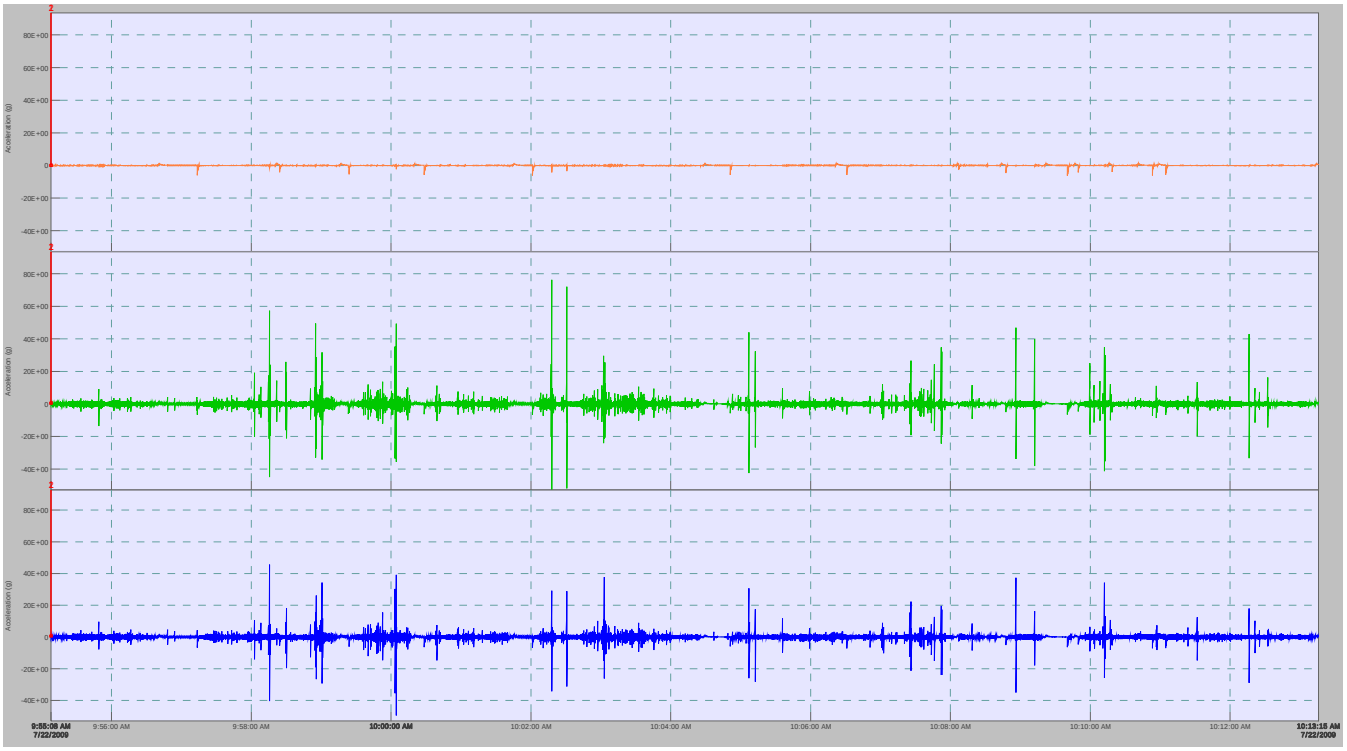

Figure 33: Accelerometer 2 (#68, Reference B)

The colors are assigned as follows:

- Orange: Input 4 (x axis)
- Green: Input 5 (z axis)
- Blue: Input 6 (y axis) *note that this data set is inverted from the rest of them

FRF Data

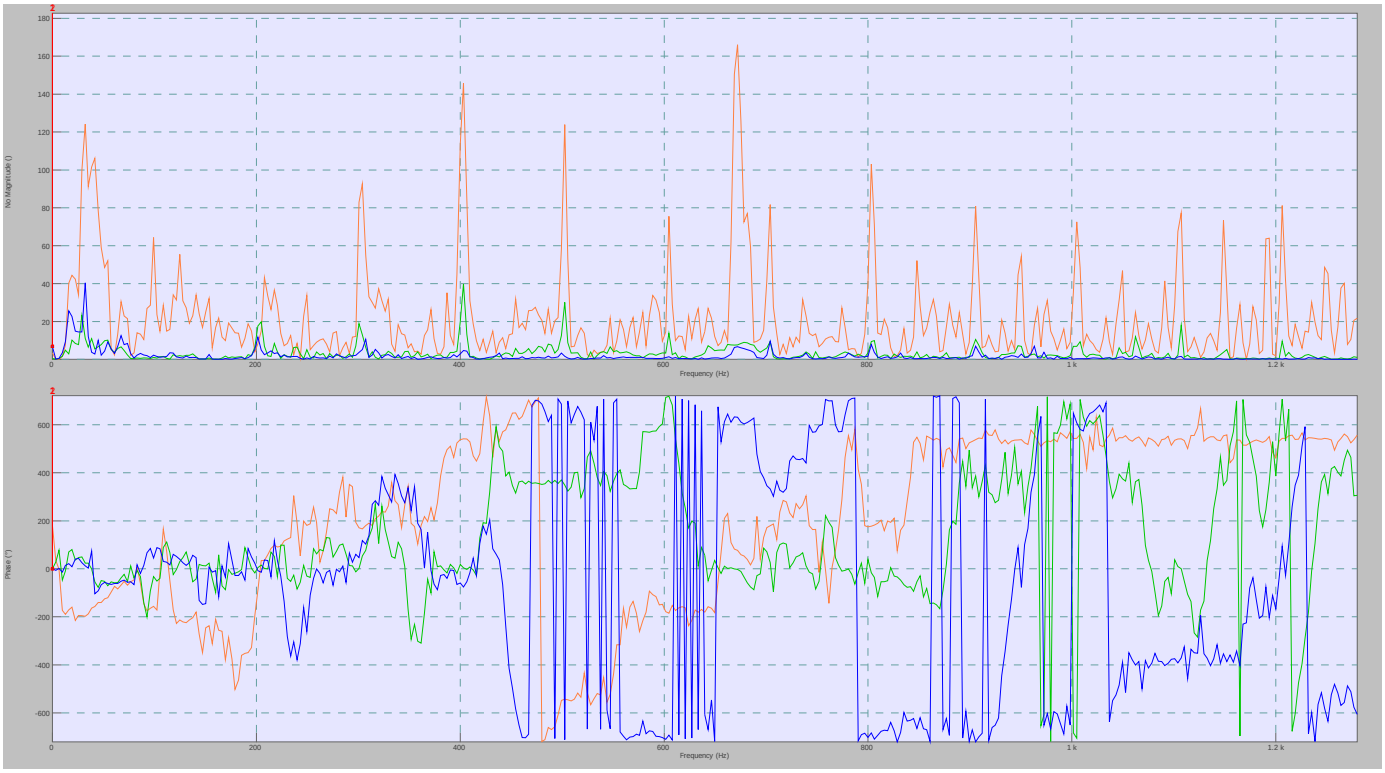

Figure 34: Accelerometer 2 (#68, Reference B)

The colors are assigned as follows:

- Orange: Input 4 (x axis)
- Green: Input 5 (z axis)
- Blue: Input 6 (y axis) *note that this data set is inverted from the rest of them

The graph scale data for the FRF data is as follows:

- Top Graph
  - x-scale 0Hz to 1.25kHz
  - y-scale: 0 to 180 no units
- Bottom Graph
  - x-scale 0Hz to 1.25kHz
  - y-scale: -720° to 720°

Time Domain Data

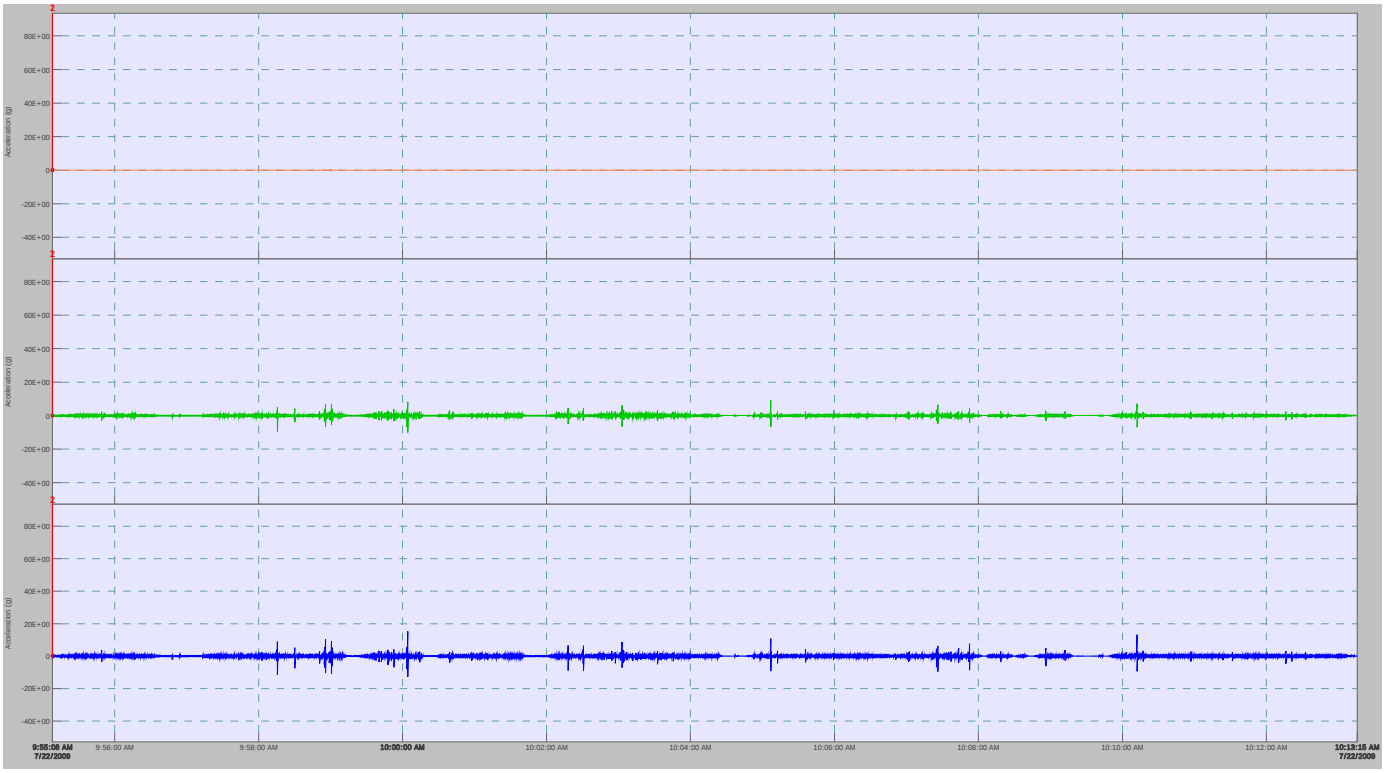

Figure 35: Accelerometer 3 (#69, Reference C)

The colors are assigned as follows:

- Orange: Input 7 (x axis)
- Green: Input 8 (y axis)
- Blue: Input 9 (z axis)

FRF Data

Figure 36: Accelerometer 3 (#69, Reference C)

The colors are assigned as follows:

- Orange: Input 7 (x axis)
- Green: Input 8 (y axis)
- Blue: Input 9 (z axis)

The graph scale data for the FRF data is as follows:

- Top Graph
    - x-scale 0Hz to 1.25kHz
    - y-scale: 0 to 475 no units
- Bottom Graph
    - x-scale 0Hz to 1.25kHz
    - y-scale: -720° to 720°

Time Domain Data

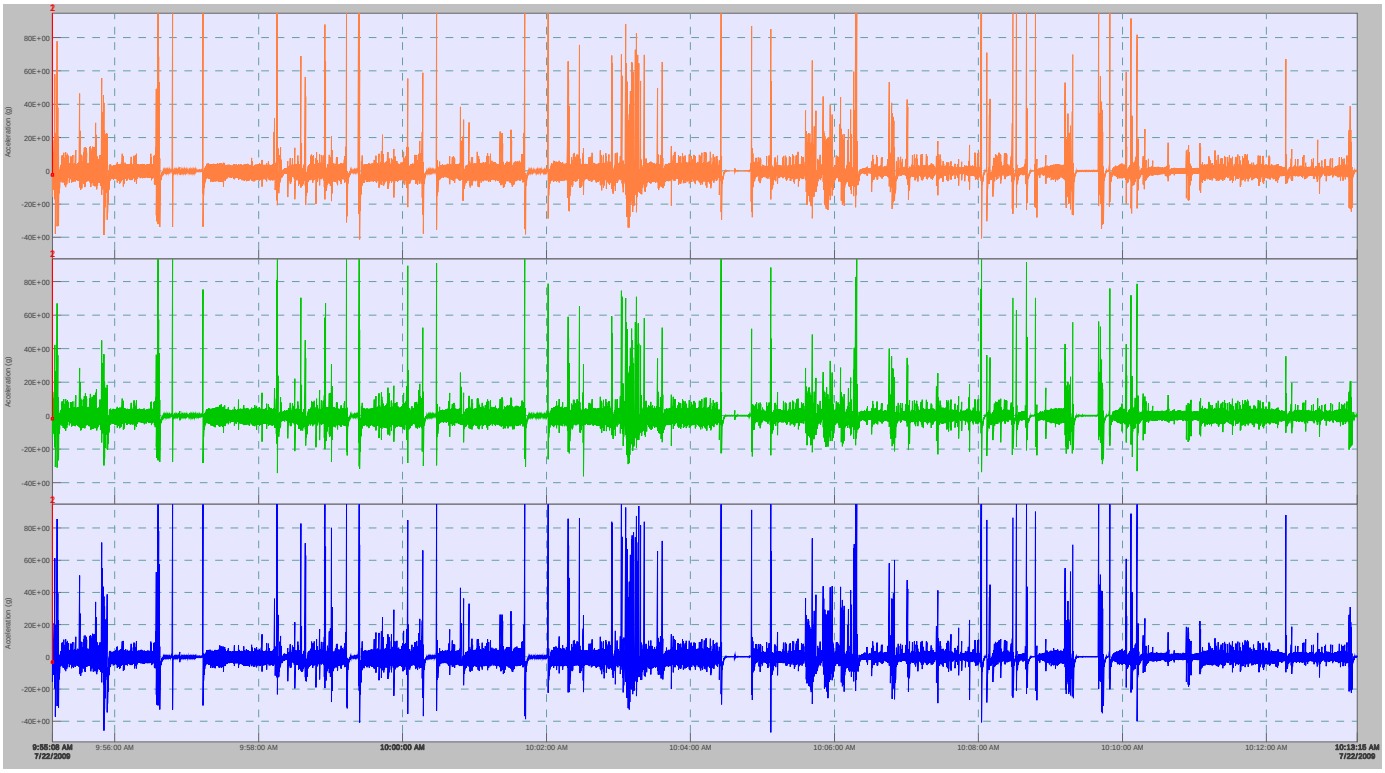

Figure 37: Accelerometer 4 (#70, Reference D)

The colors are assigned as follows:

- Orange: Input 10 (x axis)
- Green: Input 11 (y axis)
- Blue: Input 12 (z axis)

FRF Data

Figure 38: Accelerometer 4 (#70, Reference D)

The colors are assigned as follows:

- Orange: Input 10 (x axis)
- Green: Input 11 (y axis)
- Blue: Input 12 (z axis)

The graph scale data for the FRF data is as follows:

- Top Graph
    - x-scale 0Hz to 1.25kHz
    - y-scale: 0 to 4 no units
- Bottom Graph
    - x-scale 0Hz to 1.25kHz
    - y-scale: -720° to 720°

Time Domain Data

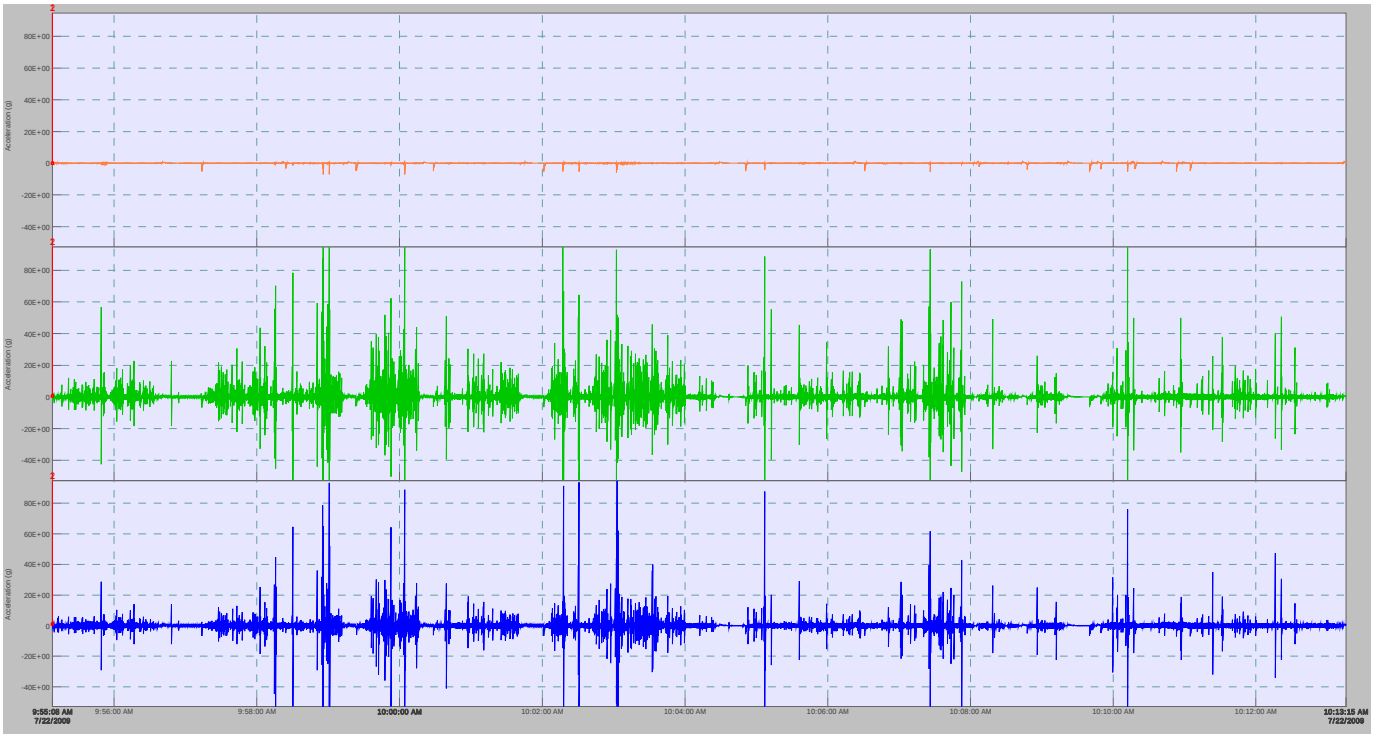

Figure 39: Accelerometer 5 (#71, Reference E)

The colors are assigned as follows:

- Orange: Input 13 (x axis)
- Green: Input 14 (z axis) *note that this data set is inverted from the rest of them
- Blue: Input 15 (y axis)

FRF Data

Figure 40: Accelerometer 5 (#71, Reference E)

The colors are assigned as follows:

- Orange: Input 13 (x axis)
- Green: Input 14 (z axis) *note that this data set is inverted from the rest of them
- Blue: Input 15 (y axis)

The graph scale data for the FRF data is as follows:

- Top Graph
    - x-scale 0Hz to 1.25kHz
    - y-scale: 0 to 275 no units
- Bottom Graph
    - x-scale 0Hz to 1.25kHz
    - y-scale: -720° to 720°

Day One, Run Four

Driver: Richard Lawrance
Equipment Operator: Robert Dailey
Data Set Title: Morning Run 1 Holes 10 through 18, Robert and Richard

Accelerometer Data
Unless otherwise noted, the scaling for the graphs is as follows:

Time domain graph scale:
- X-axis: 10:35:43am to 10:52:00amam
- Y-axis: +90g to -50g

FRF data graph scale:
- Top Graph
  - X-axis 0Hz to 1.4kHz
  - Y-axis: 0 to 10 no units
- Bottom Graph
  - X-axis 0Hz to 1.4kHz
  - Y-axis: -720° to 720°

Average spectrum graph scale:
- X-axis: 0Hz to 1.4kHz
- Y-axis: 0g to 0.006g

Notes
This was the final run of the day. It is a repeat of the bottom 9 holes.

Time Domain Data

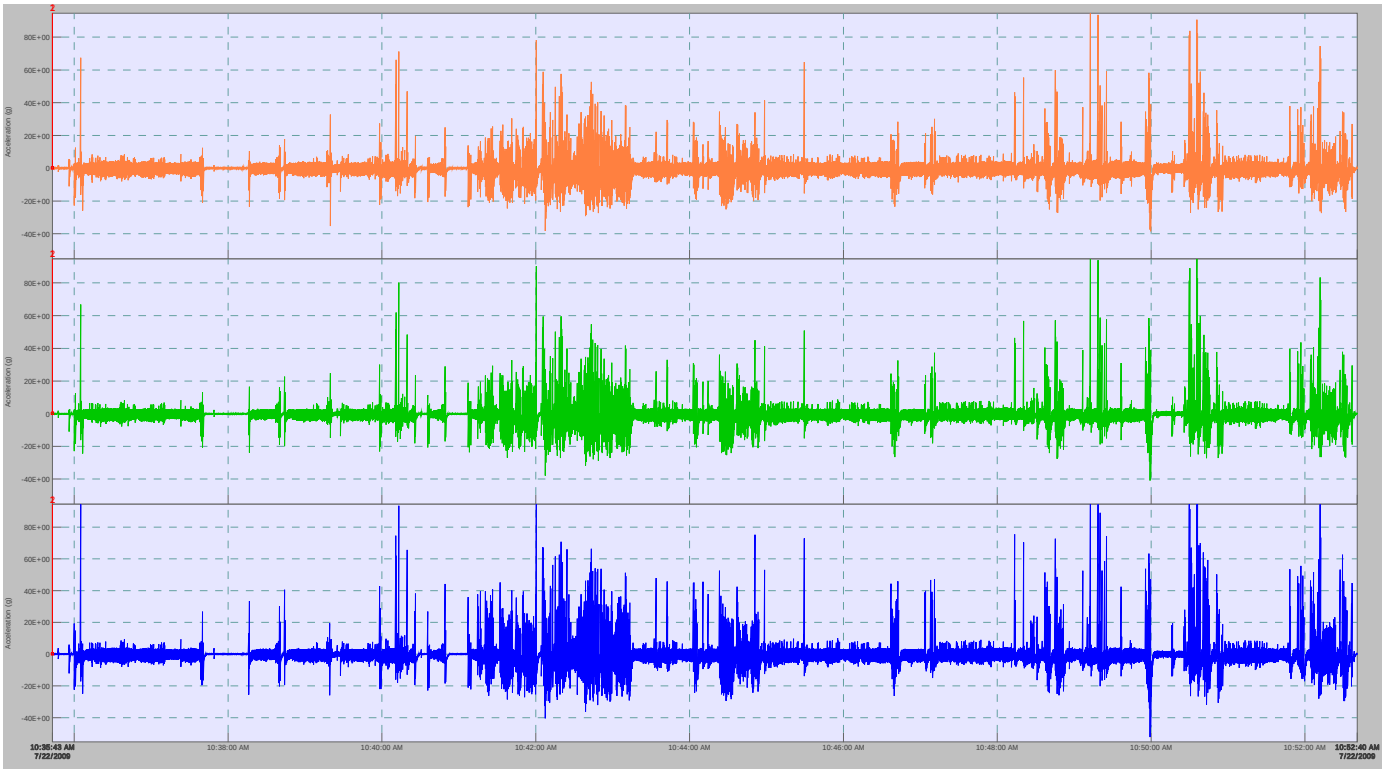

Figure 41: Accelerometer 1(#67, Reference A)

The colors are assigned as follows:

- Orange: Input 1 (x axis)
- Green: Input 2 (y axis)
- Blue: Input 3 (z axis)

Average Spectrum Data

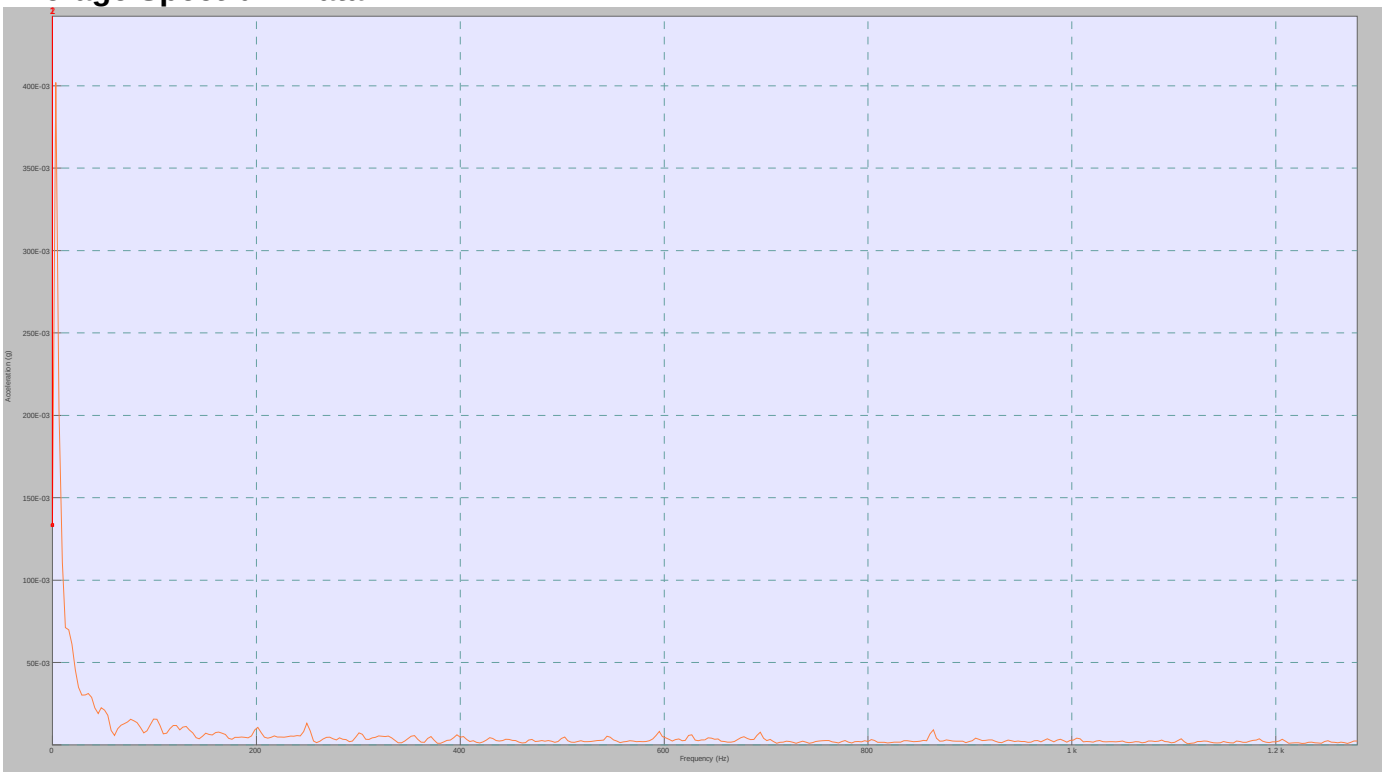

Figure 42: Accelerometer 1(#67, Reference A)

Scale Information

- Y-axis: 0g to 450E-3g
- Y-axis: 0Hz to 1.25kHz

FRF Data

Figure 43: Accelerometer 1(#67, Reference A)

The colors are assigned as follows:

- Orange: Input 1 (x axis)
- Green: Input 2 (y axis)
- *No data for input 3*

The graph scale data for the FRF data is as follows:

- Top Graph
    - x-scale 0Hz to 1.25kHz
    - y-scale: 0 to 4.5 no units
- Bottom Graph
    - x-scale 0Hz to 1.25kHz
    - y-scale: -720° to 720°

Time Domain Data

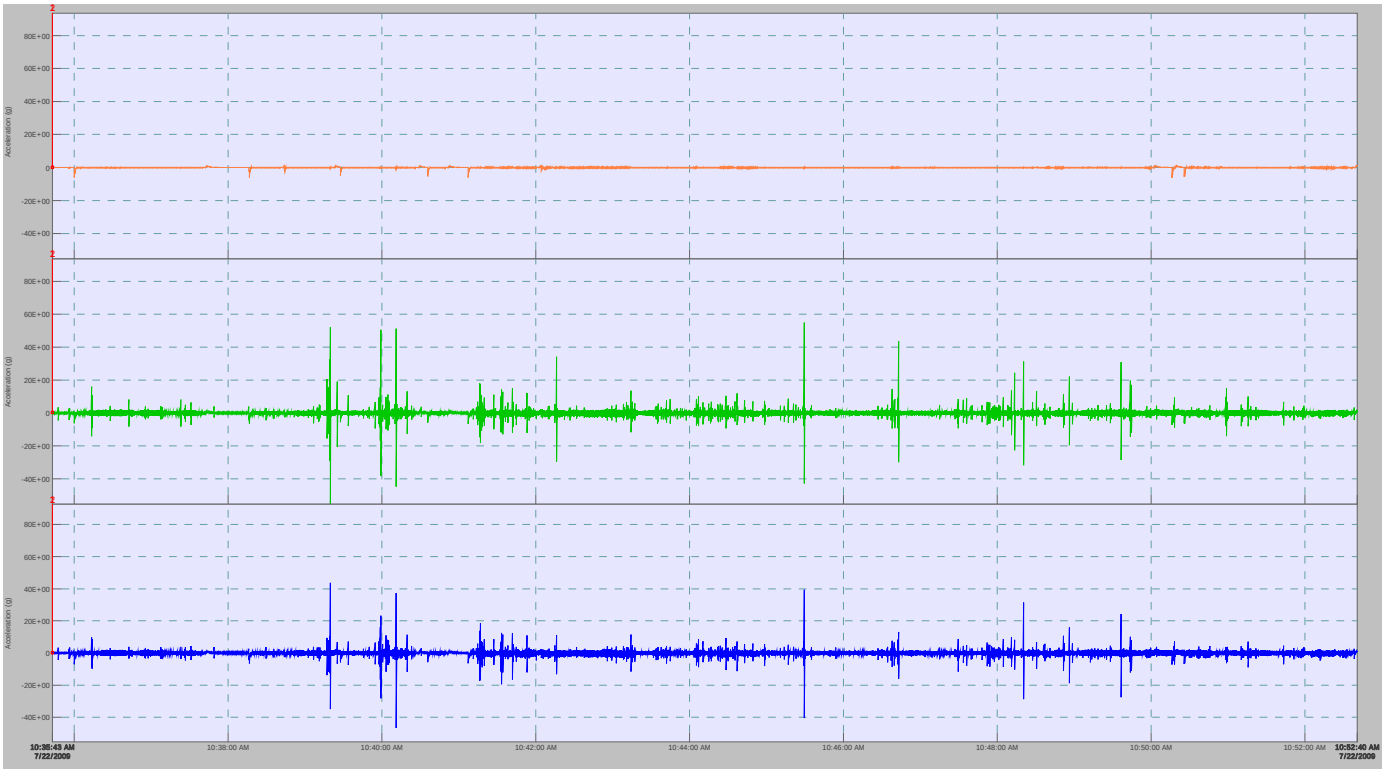

Figure 44: Accelerometer 2 (#68, Reference B)

The colors are assigned as follows:

- Orange: Input 4 (x axis)
- Green: Input 5 (z axis)
- Blue: Input 6 (y axis) *note that this data set is inverted from the rest of them

FRF Data

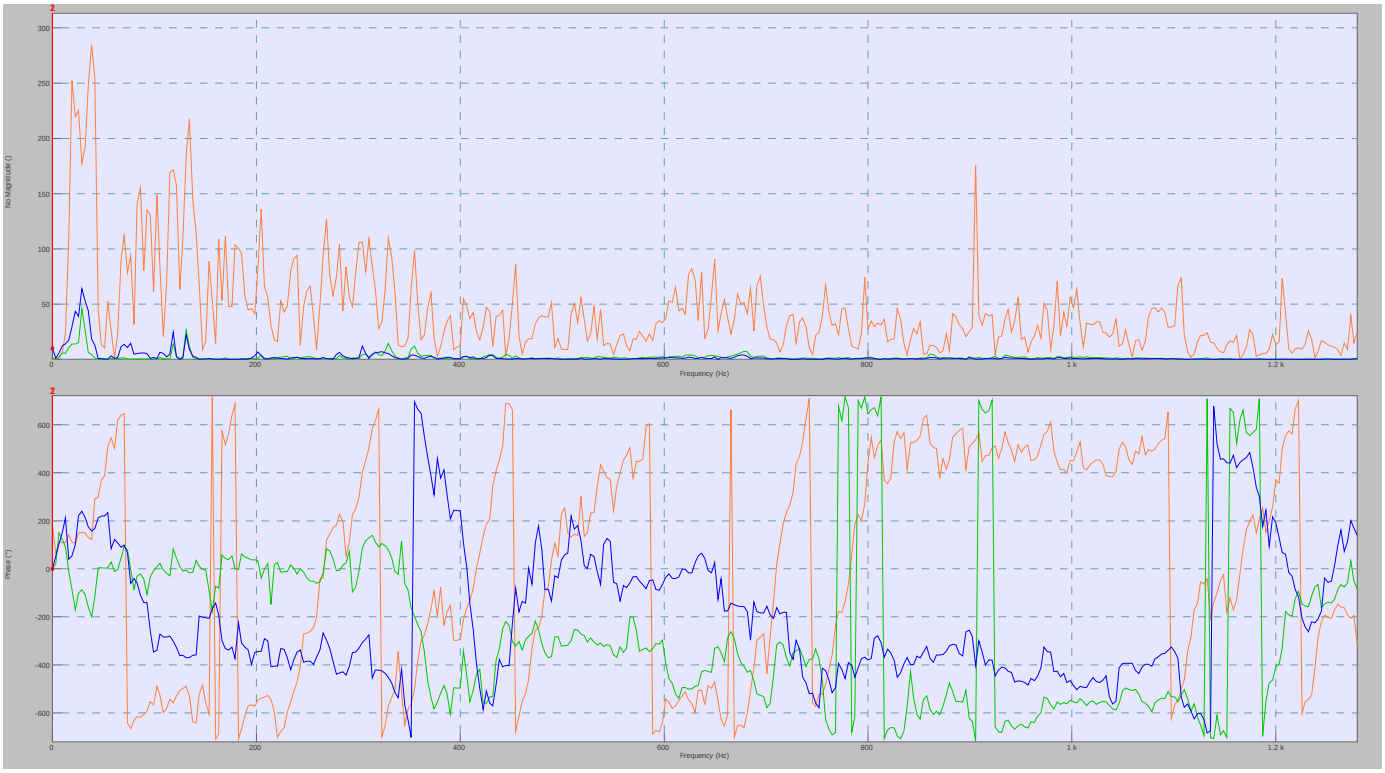

Figure 45: Accelerometer 2 (#68, Reference B)

The colors are assigned as follows:

- Orange: Input 4 (x axis)
- Green: Input 5 (z axis)
- Blue: Input 6 (y axis) *note that this data set is inverted from the rest of them

The graph scale data for the FRF data is as follows:

- Top Graph
    - x-scale 0Hz to 1.25kHz
    - y-scale: 0 to 300 no units
- Bottom Graph
    - x-scale 0Hz to 1.25kHz
    - y-scale: -720° to 720°

Time Domain Data

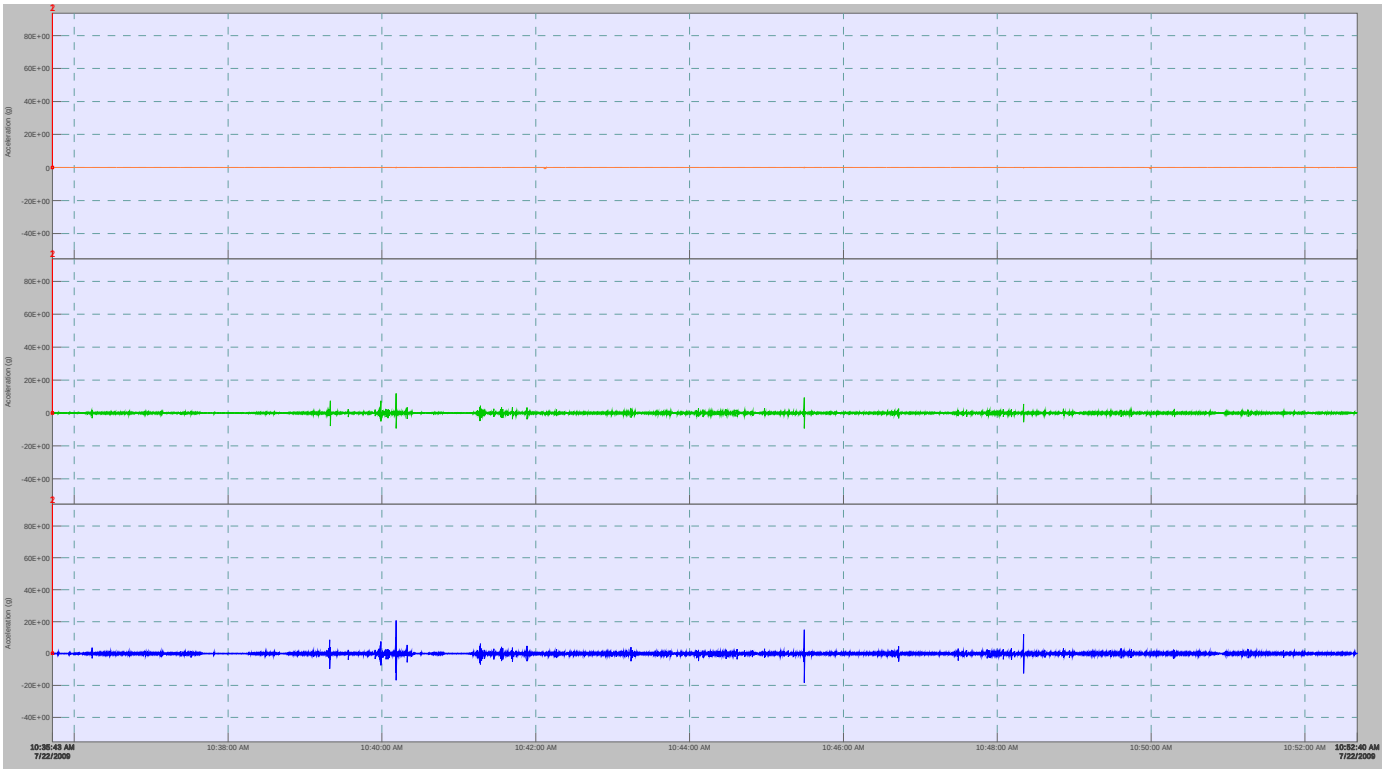

Figure 46: Accelerometer 3 (#69, Reference C)

The colors are assigned as follows:

- Orange: Input 7 (x axis)
- Green: Input 8 (y axis)
- Blue: Input 9 (z axis)

FRF Data

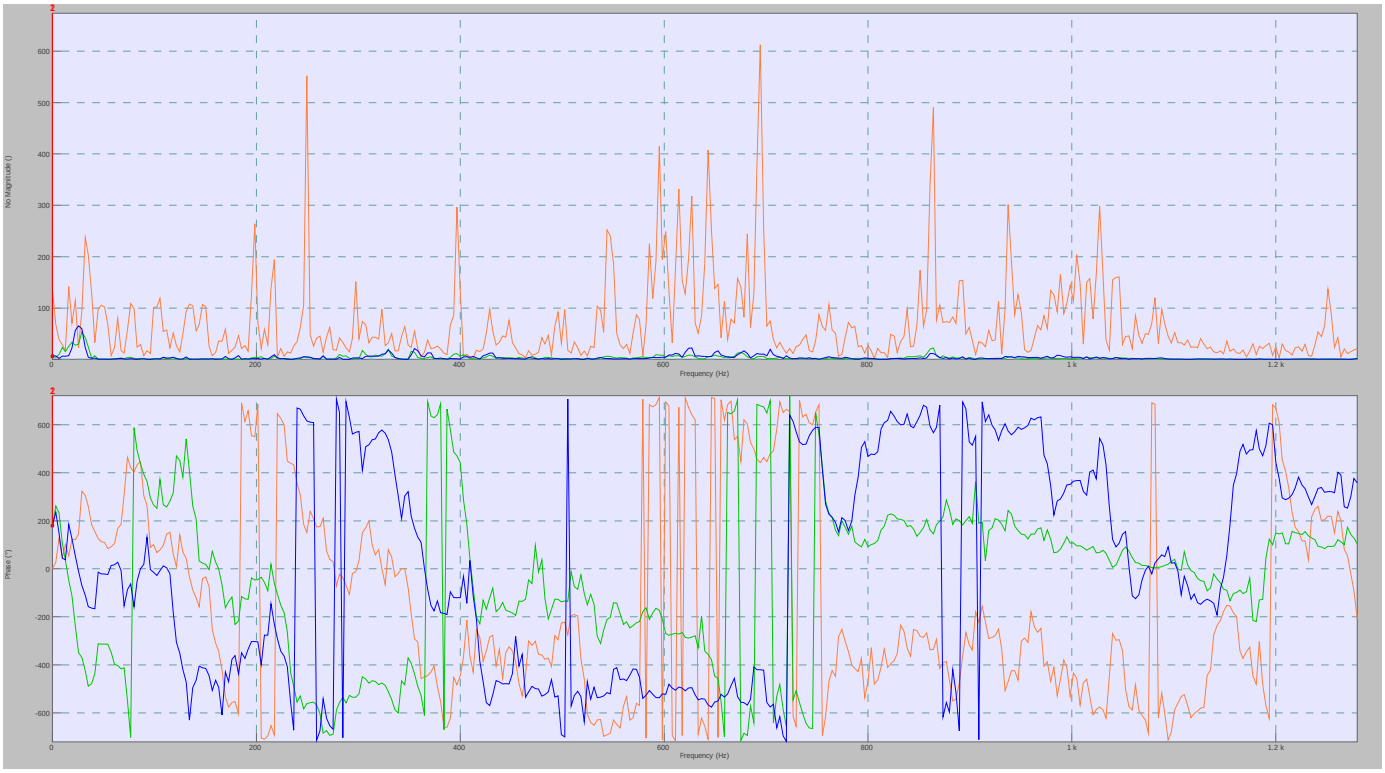

Figure 47: Accelerometer 3 (#69, Reference C)

The colors are assigned as follows:

- Orange: Input 7 (x axis)
- Green: Input 8 (y axis)
- Blue: Input 9 (z axis)

The graph scale data for the FRF data is as follows:

- Top Graph
    - x-scale 0Hz to 1.25kHz
    - y-scale: 0 to 700 no units
- Bottom Graph
    - x-scale 0Hz to 1.25kHz
    - y-scale: -720° to 720°

Time Domain Data

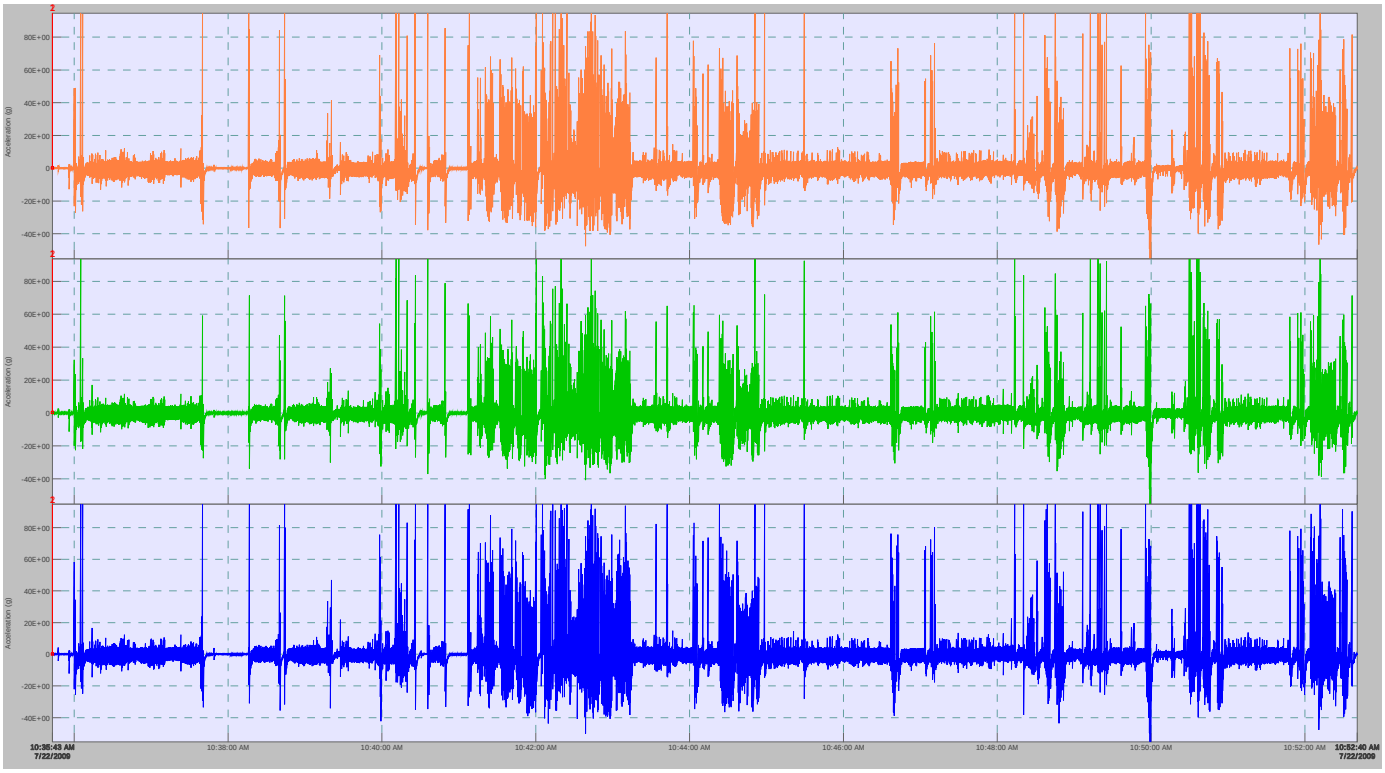

Figure 48: Accelerometer 4 (#70, Reference D)

The colors are assigned as follows:

- Orange: Input 10 (x axis)
- Green: Input 11 (y axis)
- Blue: Input 12 (z axis)

FRF Data

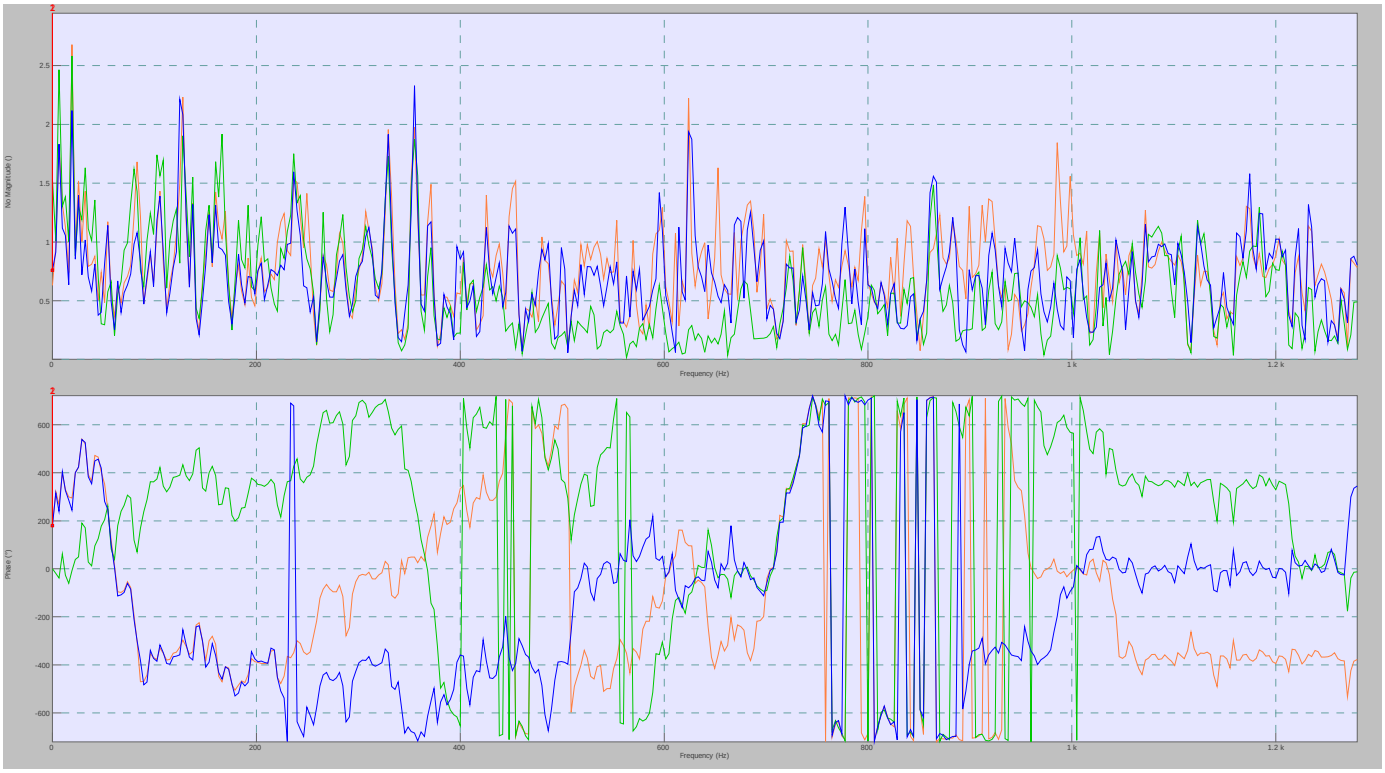

Figure 49: Accelerometer 4 (#70, Reference D)

The colors are assigned as follows:

- Orange: Input 10 (x axis)
- Green: Input 11 (y axis)
- Blue: Input 12 (z axis)

The graph scale data for the FRF data is as follows:

- Top Graph
    - x-scale 0Hz to 1.25kHz
    - y-scale: 0 to 3 no units
- Bottom Graph
    - x-scale 0Hz to 1.25kHz
    - y-scale: -720° to 720°

Time Domain Data

Figure 50: Accelerometer 5 (#71, Reference E)

The colors are assigned as follows:

- Orange: Input 13 (x axis)
- Green: Input 14 (z axis) *note that this data set is inverted from the rest of them
- Blue: Input 15 (y axis)

FRF Data

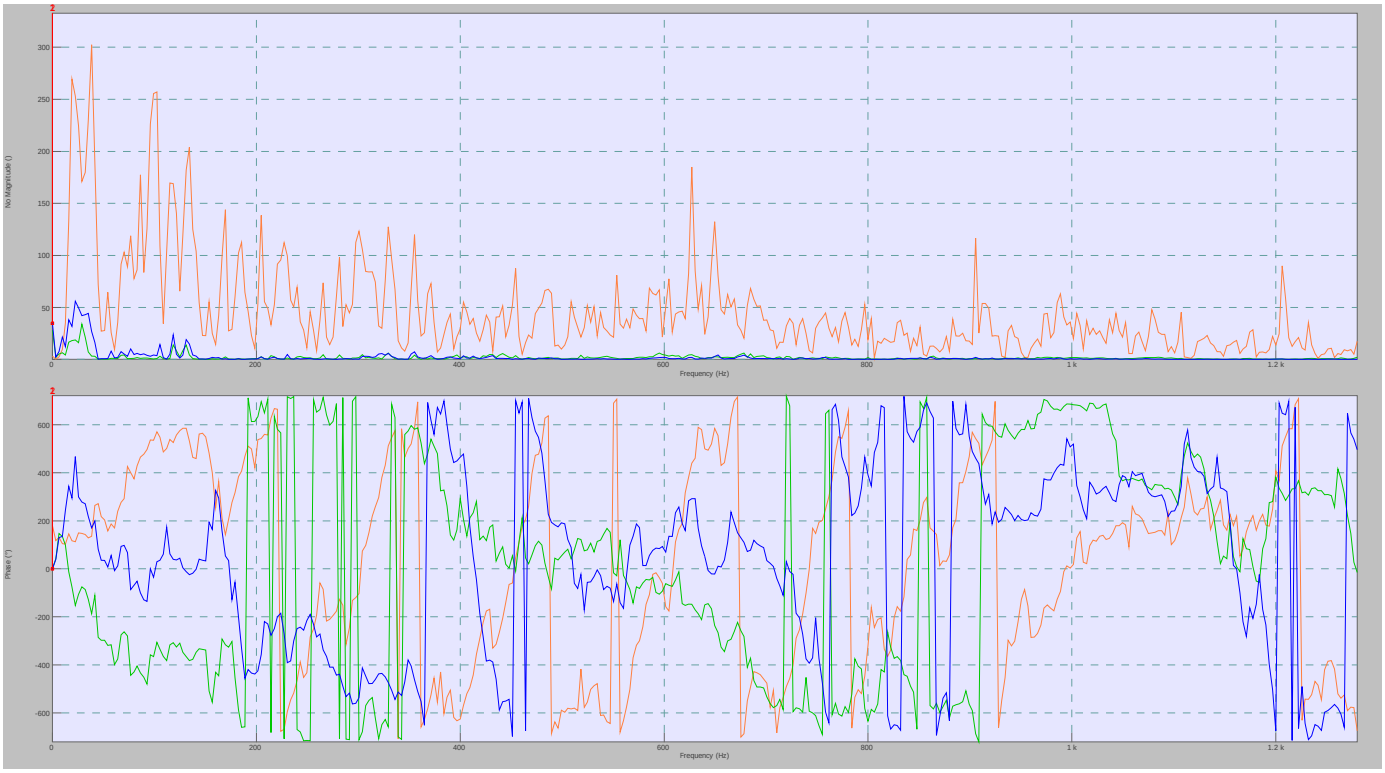

Figure 51: Accelerometer 5 (#71, Reference E)

The colors are assigned as follows:

- Orange: Input 13 (x axis)
- Green: Input 14 (z axis) *note that this data set is inverted from the rest of them
- Blue: Input 15 (y axis)

The graph scale data for the FRF data is as follows:

- Top Graph
    - x-scale 0Hz to 1.25kHz
    - y-scale: 0 to 350 no units
- Bottom Graph
    - x-scale 0Hz to 1.25kHz
    - y-scale: -720° to 720°

Day Two, Run One

Driver: Richard Lawrance
Equipment Operator: Robert Dailey
Data Set Title: Morning Run 1 Holes 1 through 9, Uriel and Richard

MEScope Data

The stress points of the vehicle compartment are shown below. There are two or more sets of pictures associated with each frequency being observed. These pictures represent each peak of the oscillation at that frequency. In each picture there are the following views (in order from top left and then clockwise around the image):

- Z-axis view
- 3D view
- Y-axis view
- X-axis View

The frequencies chosen to be displayed here where based of the peaks seen in the g-forces measured in the average spectrum data. Not all of the peaks are displayed.

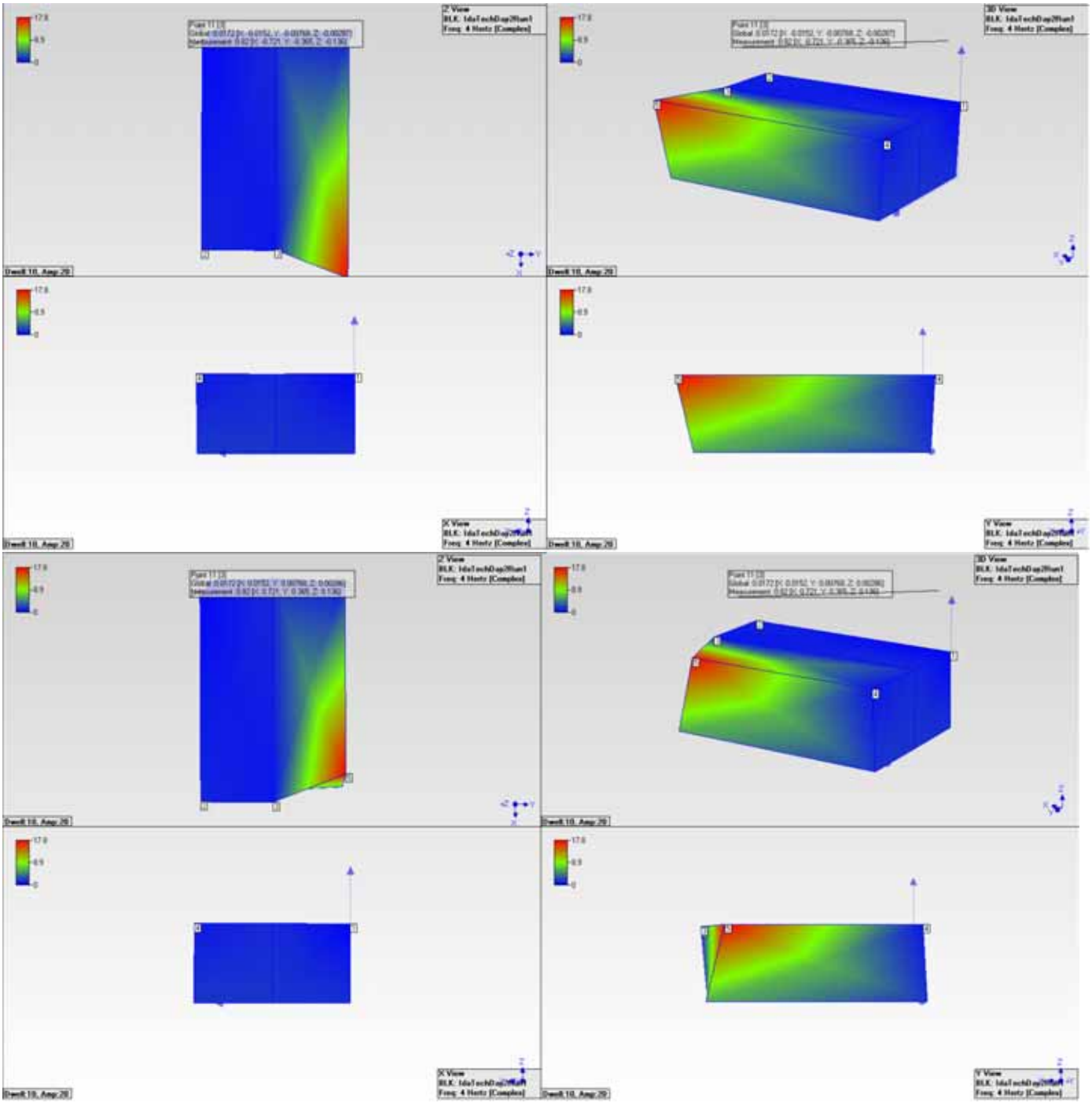

Figure 52: 4Hz

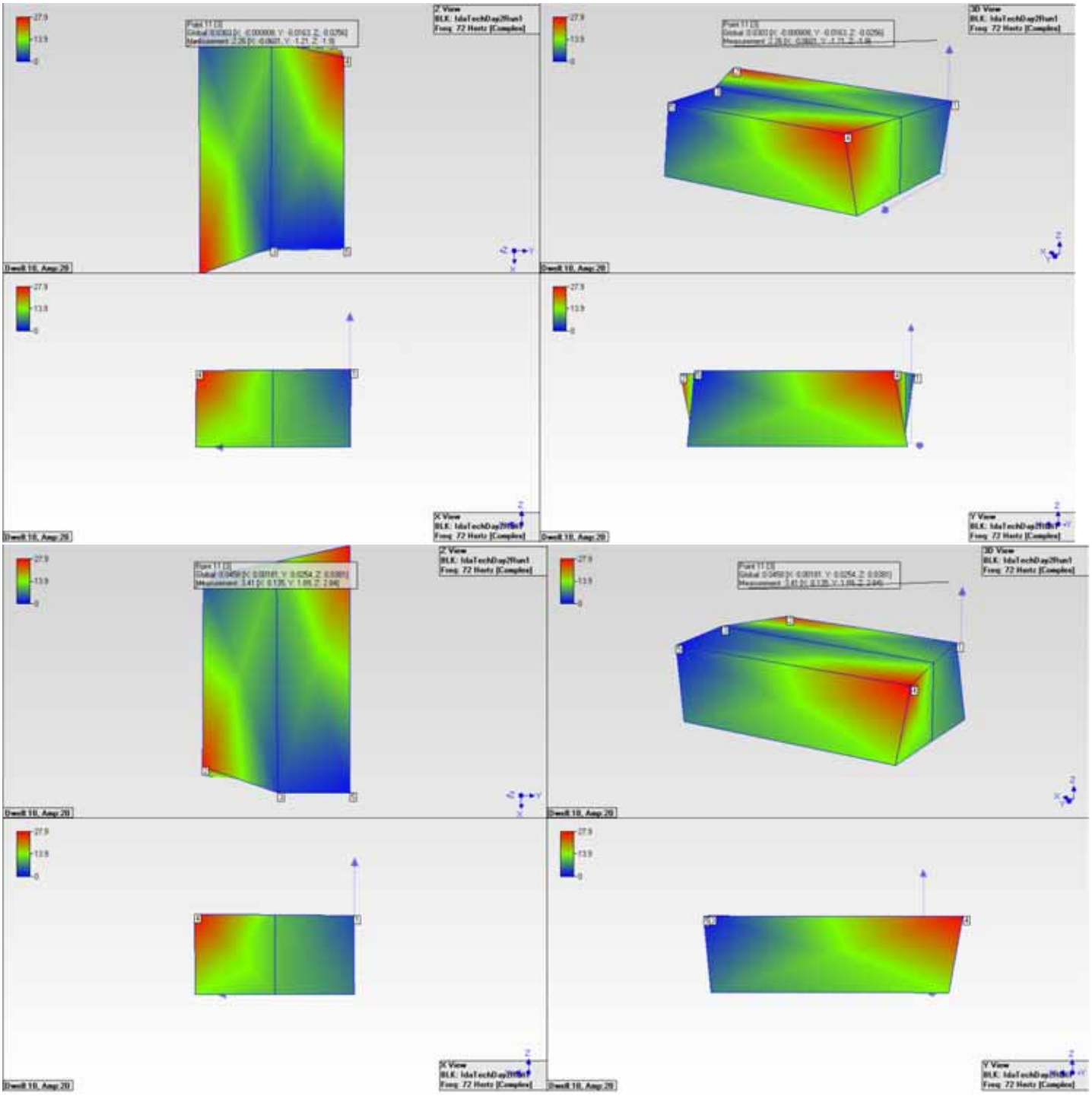

Figure 53: 72Hz

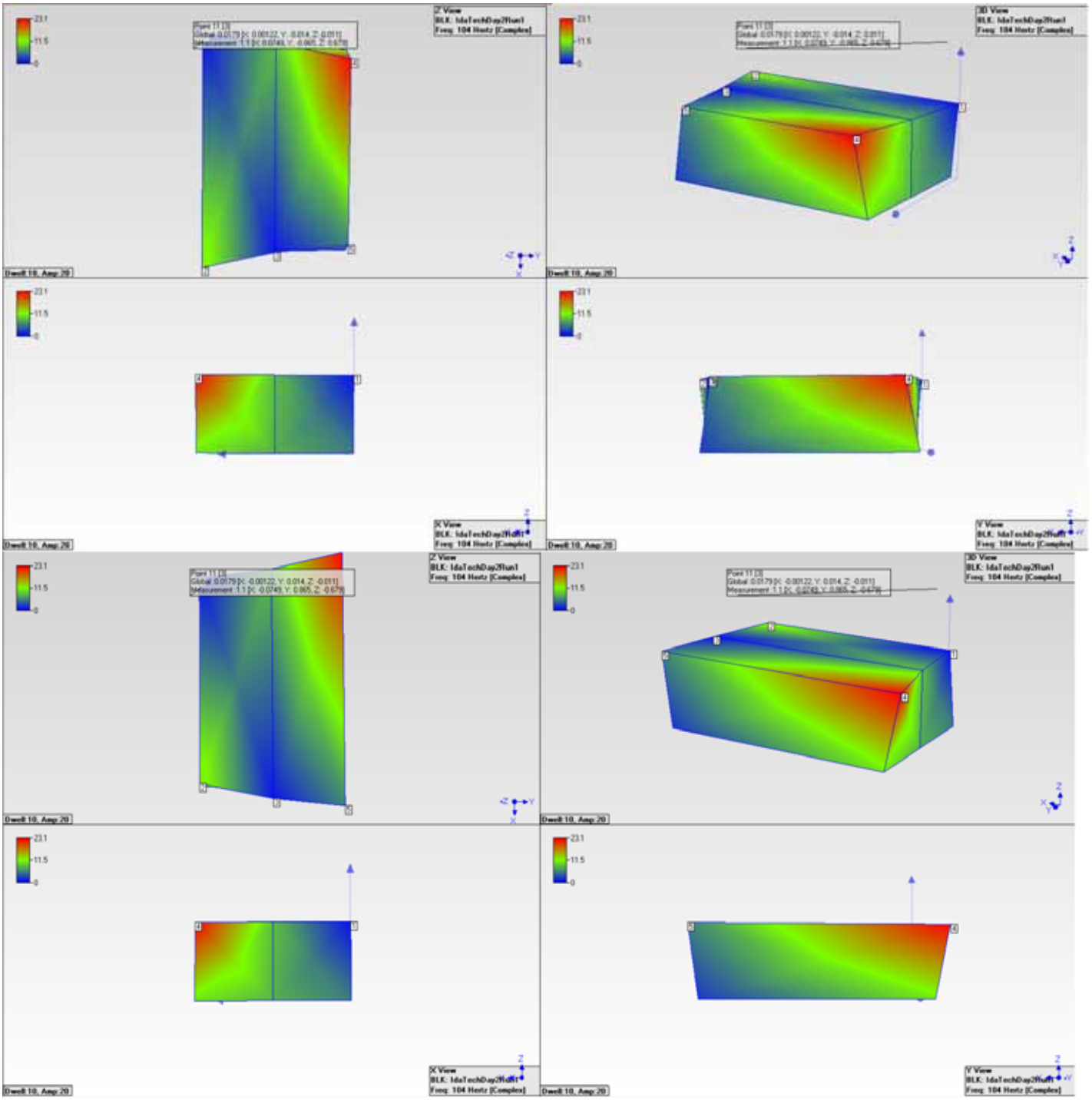

Figure 54: 104Hz

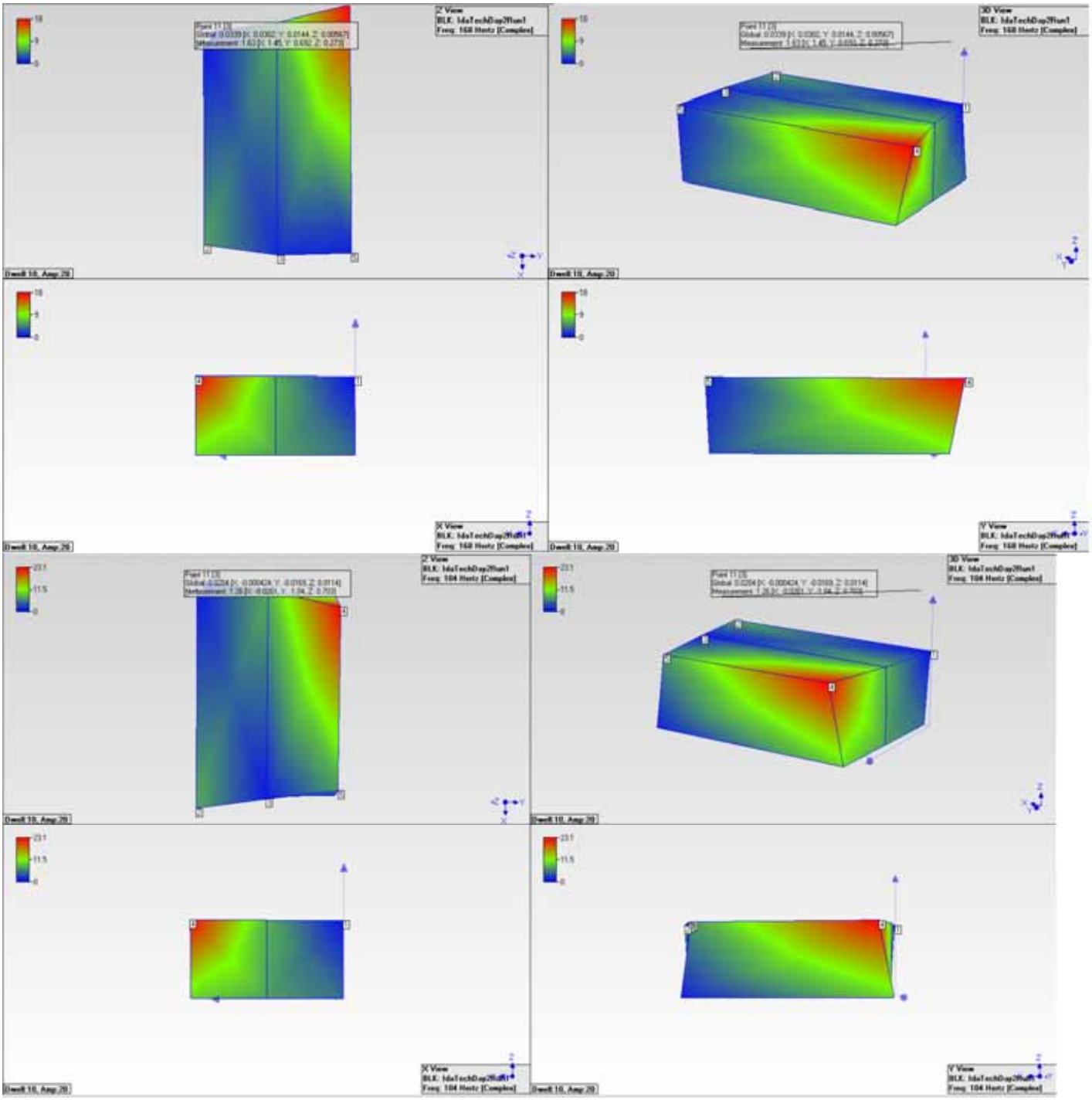

Figure 55: 668Hz

Accelerometer Data

Unless otherwise noted, the graph scales are as follows

Time domain graph scale:

- X-axis: 6:21:56am to 6:37:50am
- Y-axis: +80g to -80g

FRF data graph scale:

- Top Graph
  - X-axis 0Hz to 1.6kHz
  - Y-axis: 0 to 3.5 no units
- Bottom Graph
  - X-axis 0Hz to 1.6kHz
  - Y-axis: -720° to 720°

Average spectrum graph scale:

- X-axis: 0Hz to 1.6kHz
- Y-axis: 0g to 0.001g

Time Domain Data

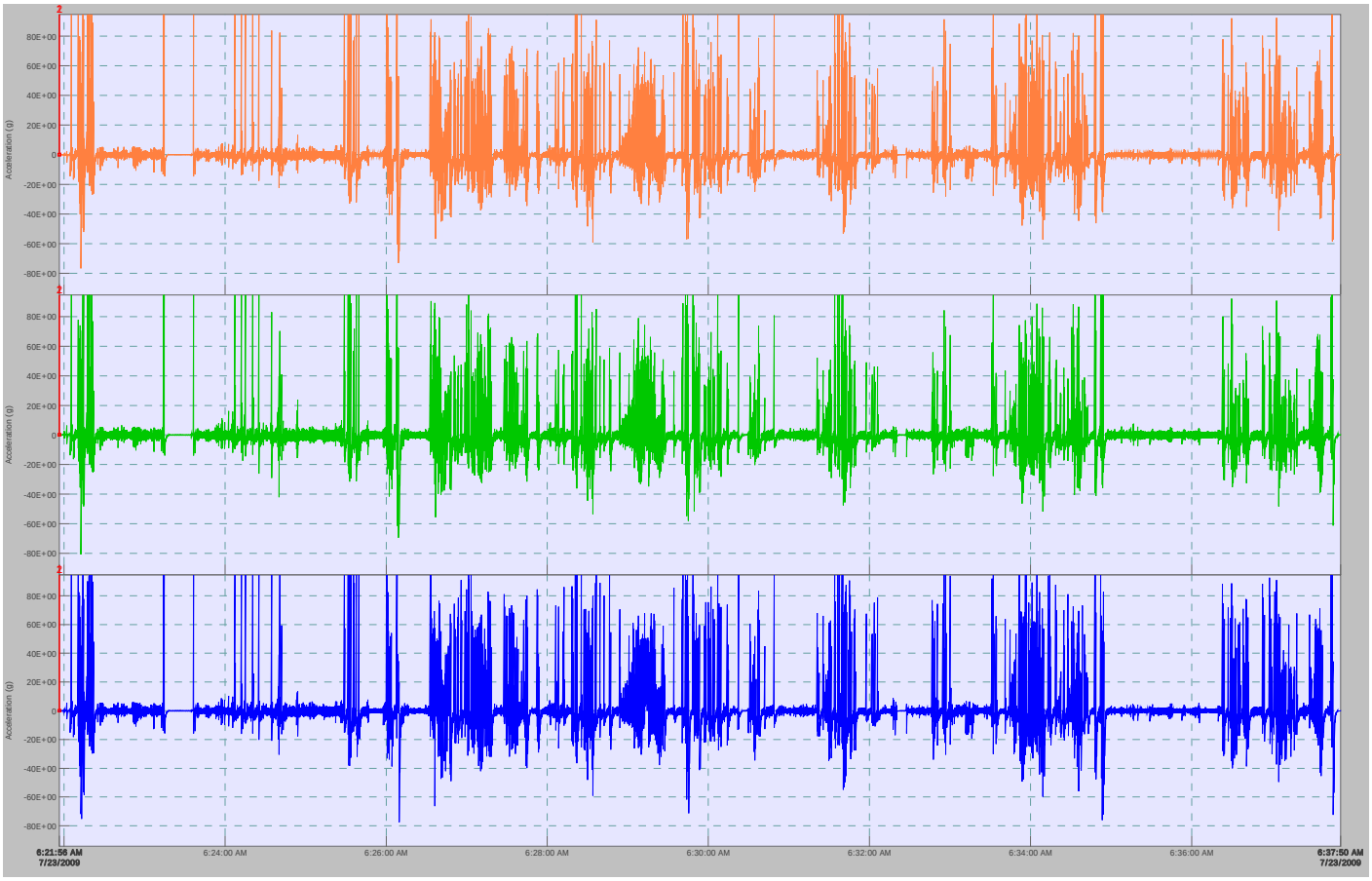

Figure 56: Accelerometer 1(#67, Reference A)

The colors are assigned as follows:

- Orange: Input 1 (x axis)
- Green: Input 2 (y axis)
- Blue: Input 3 (z axis)

Average Spectrum Data

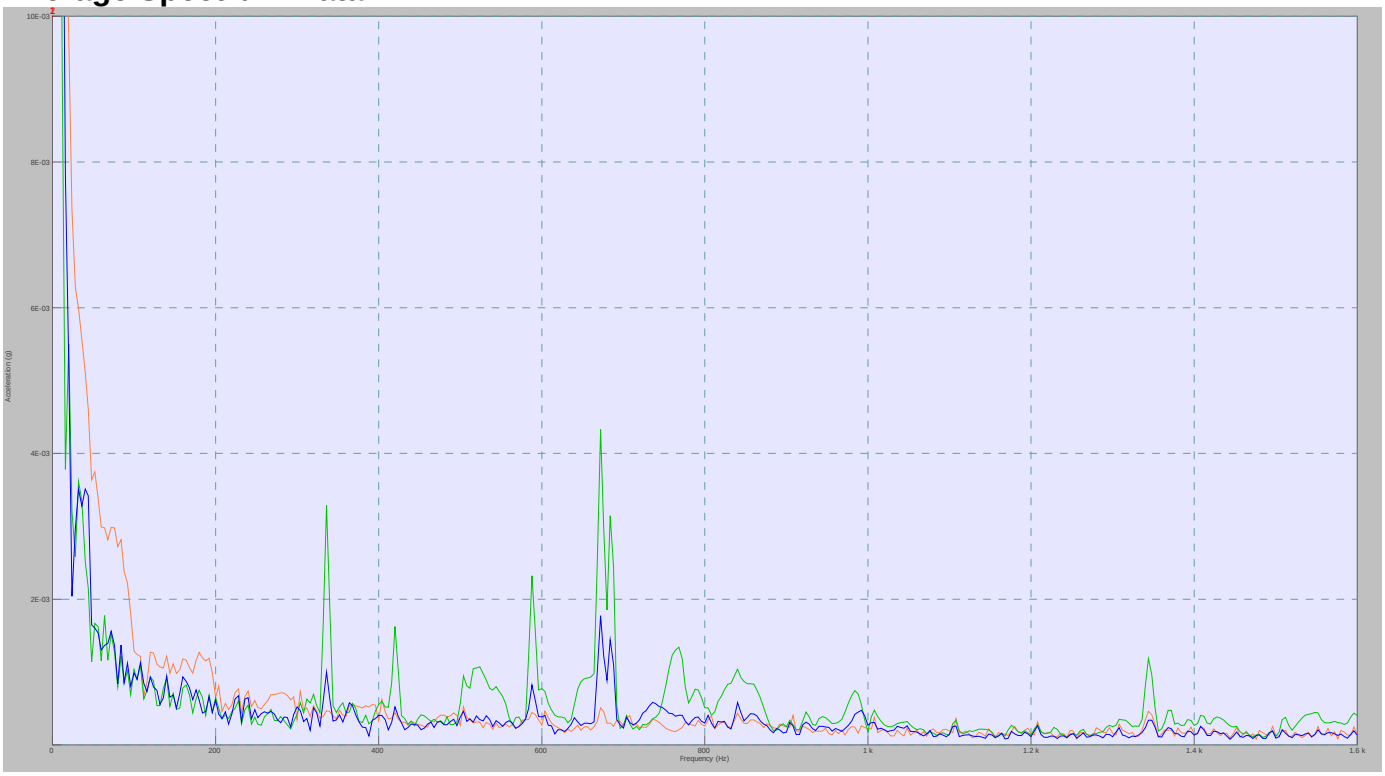

Figure 57: Accelerometer 1(#67, Reference A)

The colors are assigned as follows:

- Orange: Input 1 (x axis)
- Green: Input 2 (y axis)
- Blue: Input 3 (z axis)

FRF Data

Figure 58: Accelerometer 1(#67, Reference A)

The colors are assigned as follows:

- Orange: Input 1 (x axis)
- Green: Input 2 (y axis)
- *No FRF data for input 3*

Time Domain Data

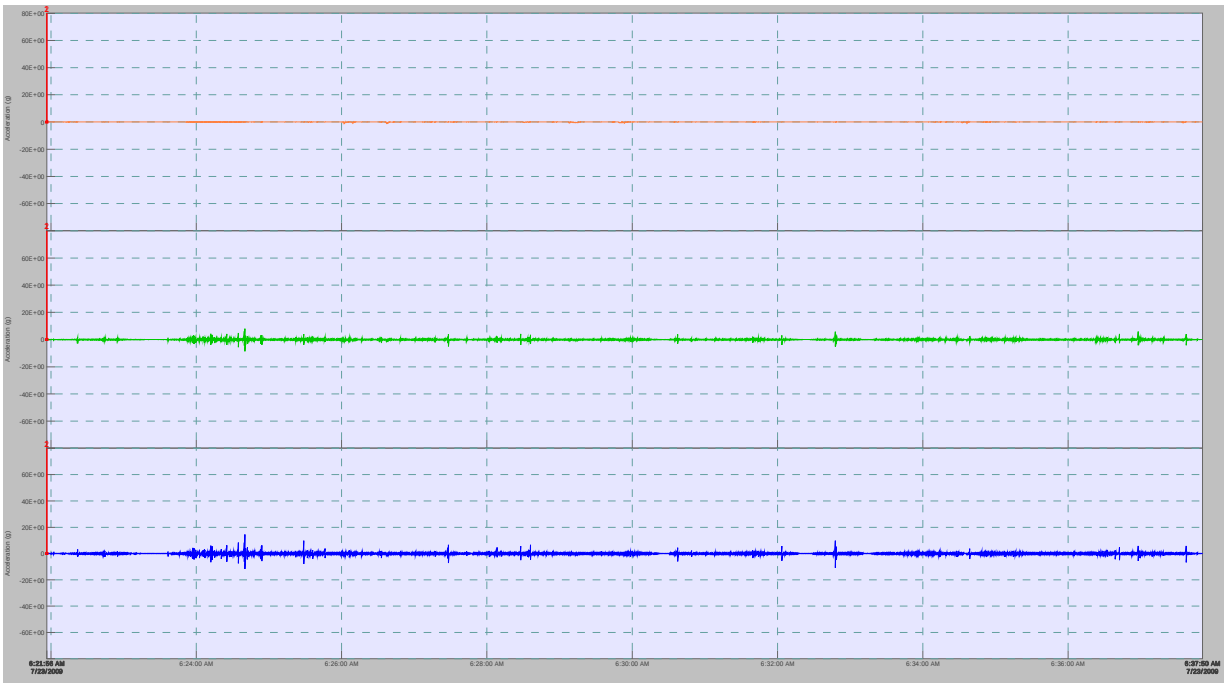

Figure 59: Accelerometer 2 (#68, Reference B)

The colors are assigned as follows:

- Orange: Input 4 (x axis)
- Green: Input 5 (z axis)
- Blue: Input 6 (y axis) *note that this data set is inverted from the rest of them

Average Spectrum Data

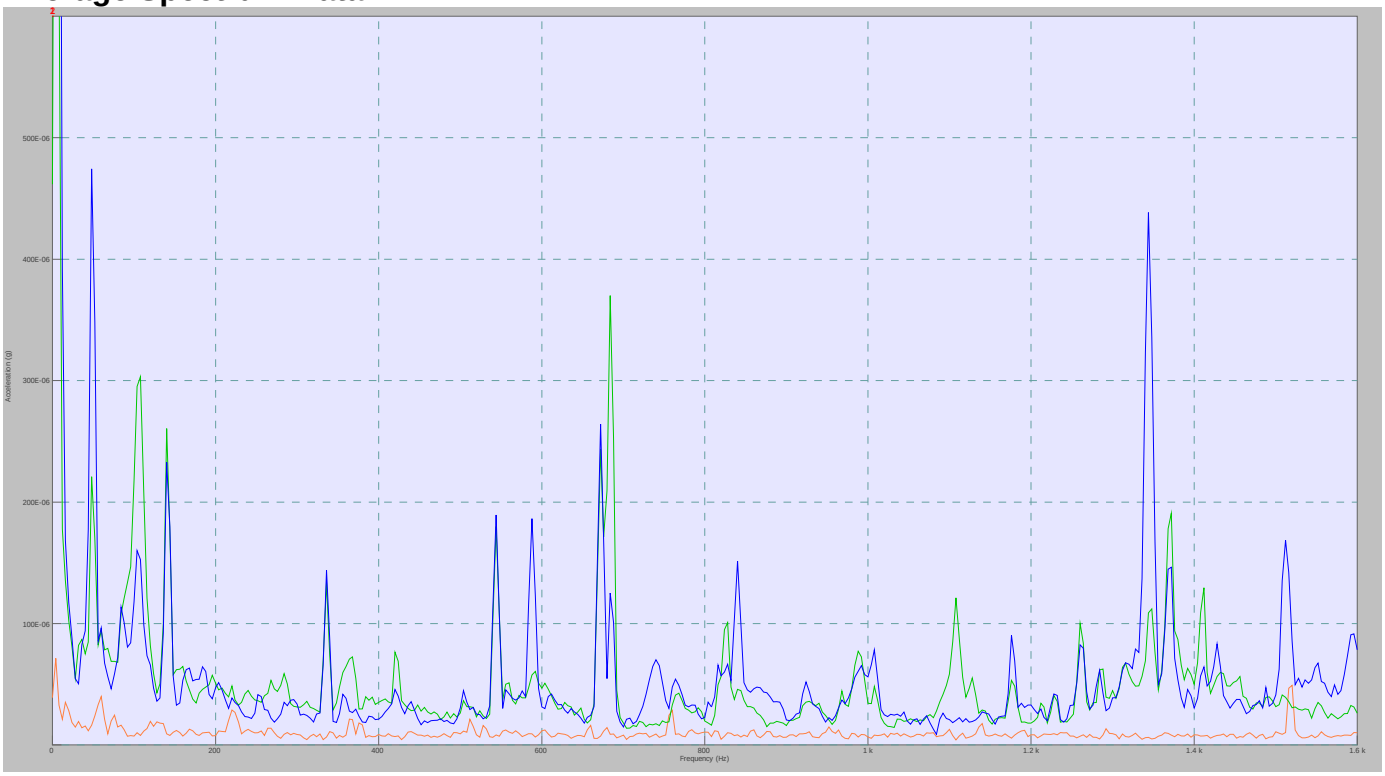

Figure 60: Accelerometer 2 (#68, Reference B)

The colors are assigned as follows:

- Orange: Input 4 (x axis)
- Green: Input 5 (z axis)
- Blue: Input 6 (y axis) *note that this data set is inverted from the rest of them

Scale information:

- X-axis: 0 to 1.6k
- Y-axis: 0 to 0.6E-3

FRF Data

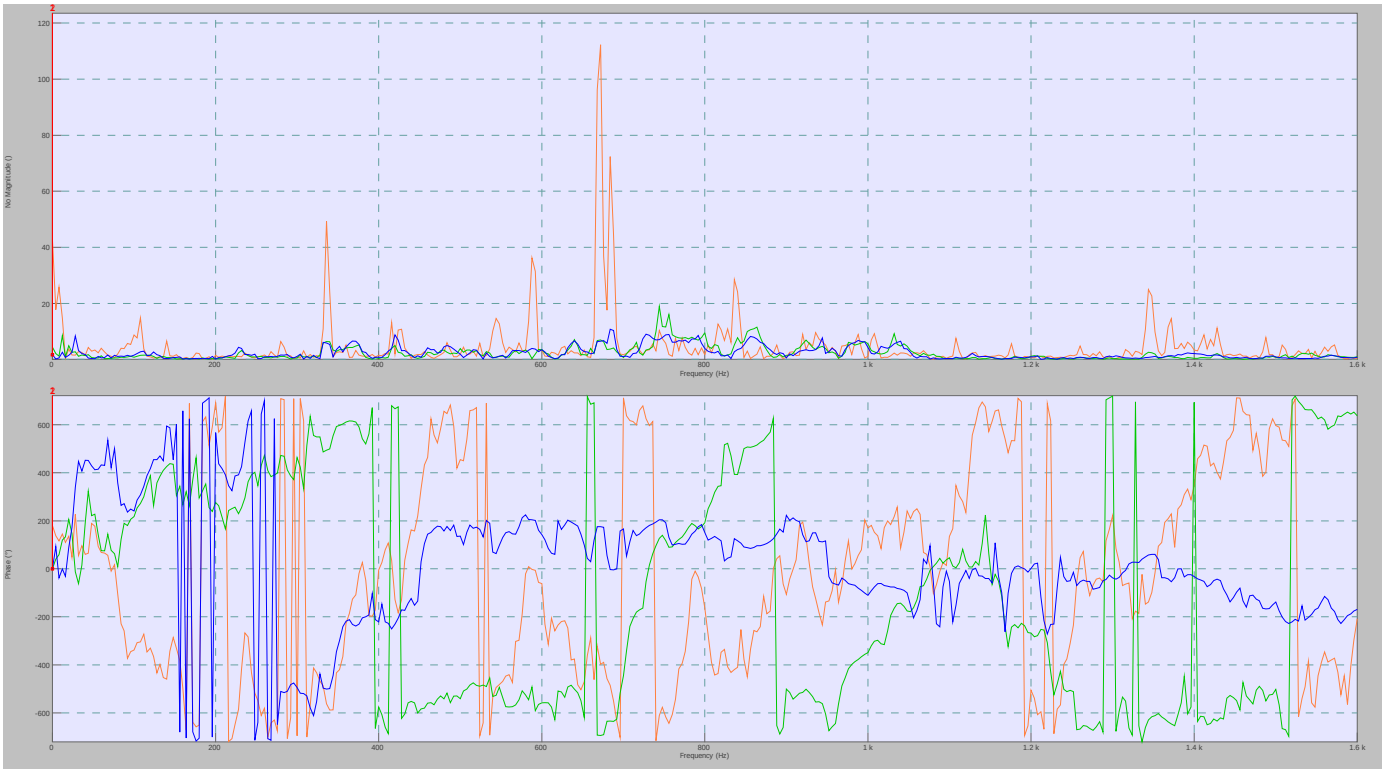

Figure 61: Accelerometer 2 (#68, Reference B)

The colors are assigned as follows:

- Orange: Input 4 (x axis)
- Green: Input 5 (z axis)
- Blue: Input 6 (y axis) *note that this data set is inverted from the rest of them

- **Time Domain Data**

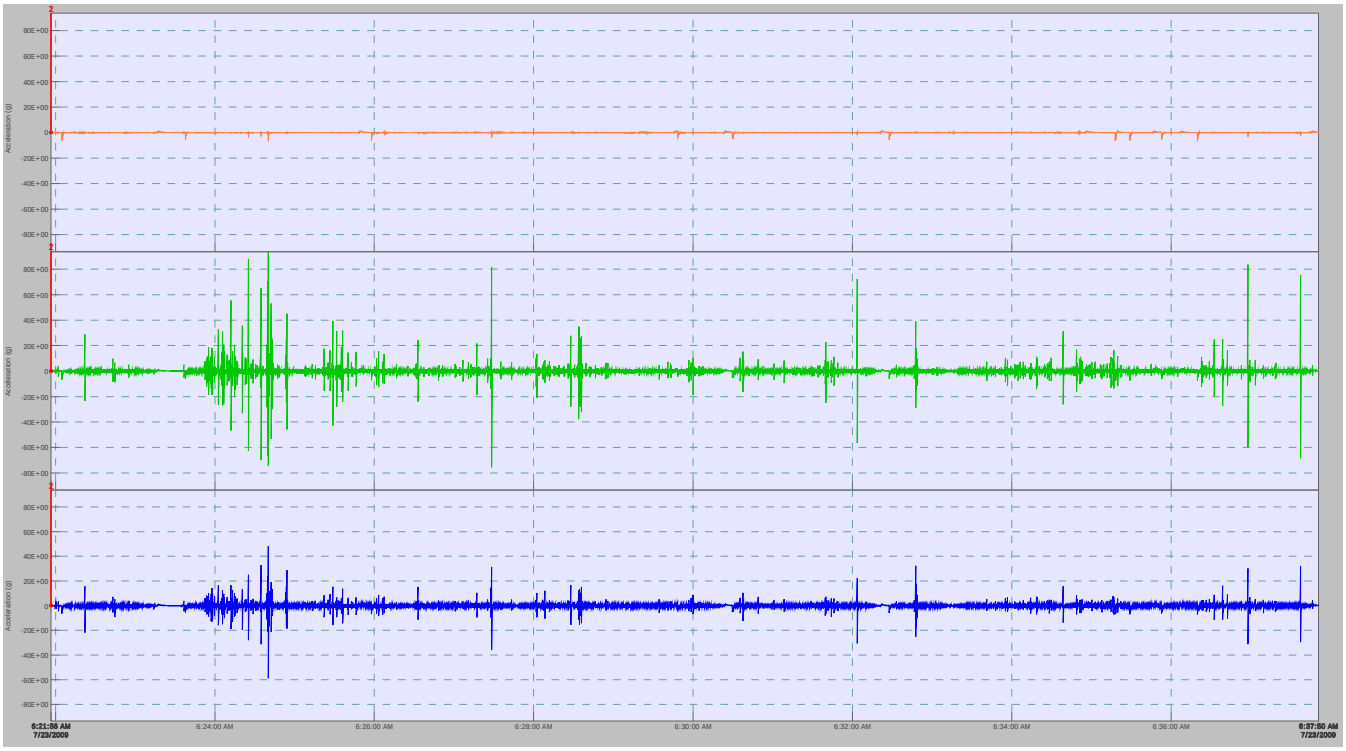

Figure 62: Accelerometer 3 (#69, Reference C)

The colors are assigned as follows:

- Orange: Input 7 (x axis)
- Green: Input 8 (y axis)
- Blue: Input 9 (z axis)

Average Spectrum Data

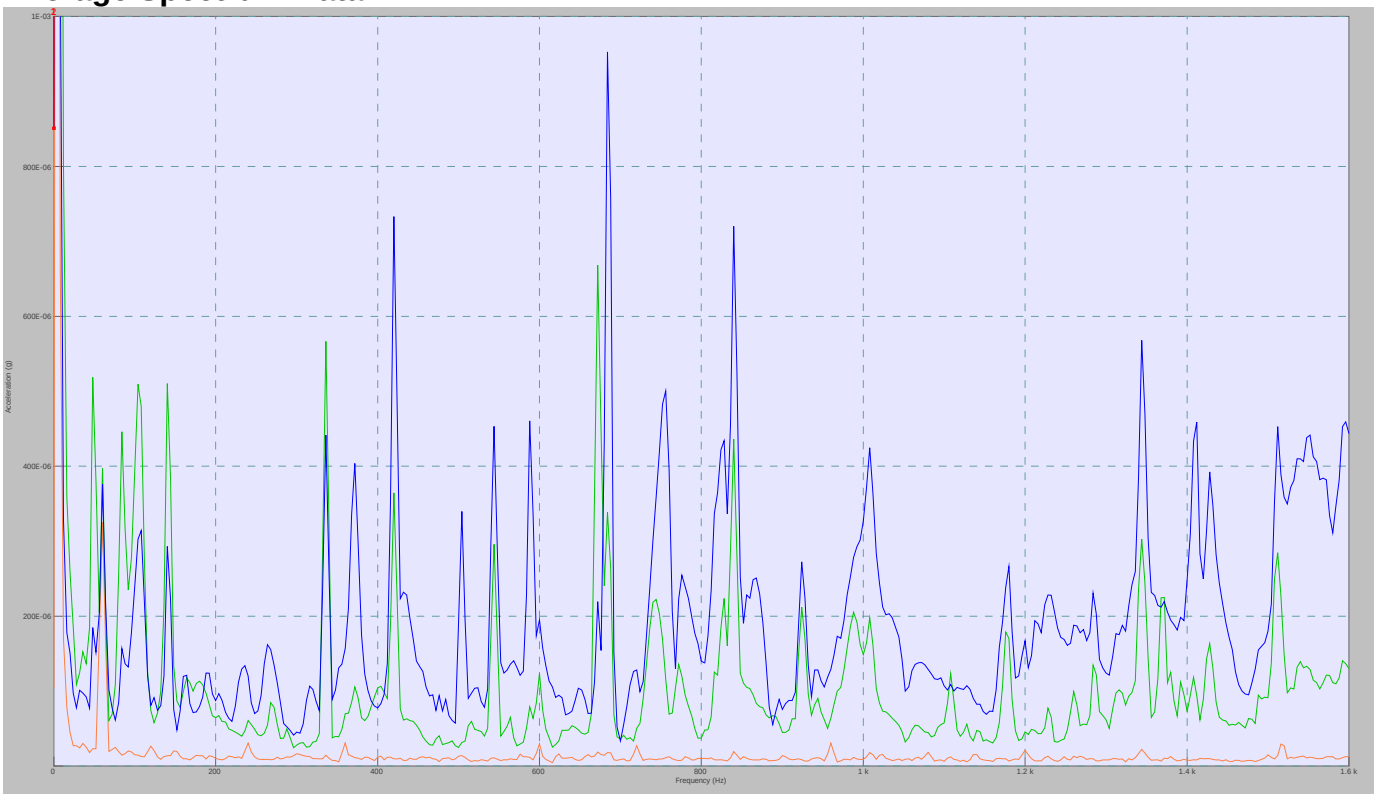

Figure 63: Accelerometer 3 (#69, Reference C)

The colors are assigned as follows:

- Orange: Input 7 (x axis)
- Green: Input 8 (y axis)
- Blue: Input 9 (z axis)

FRF Data

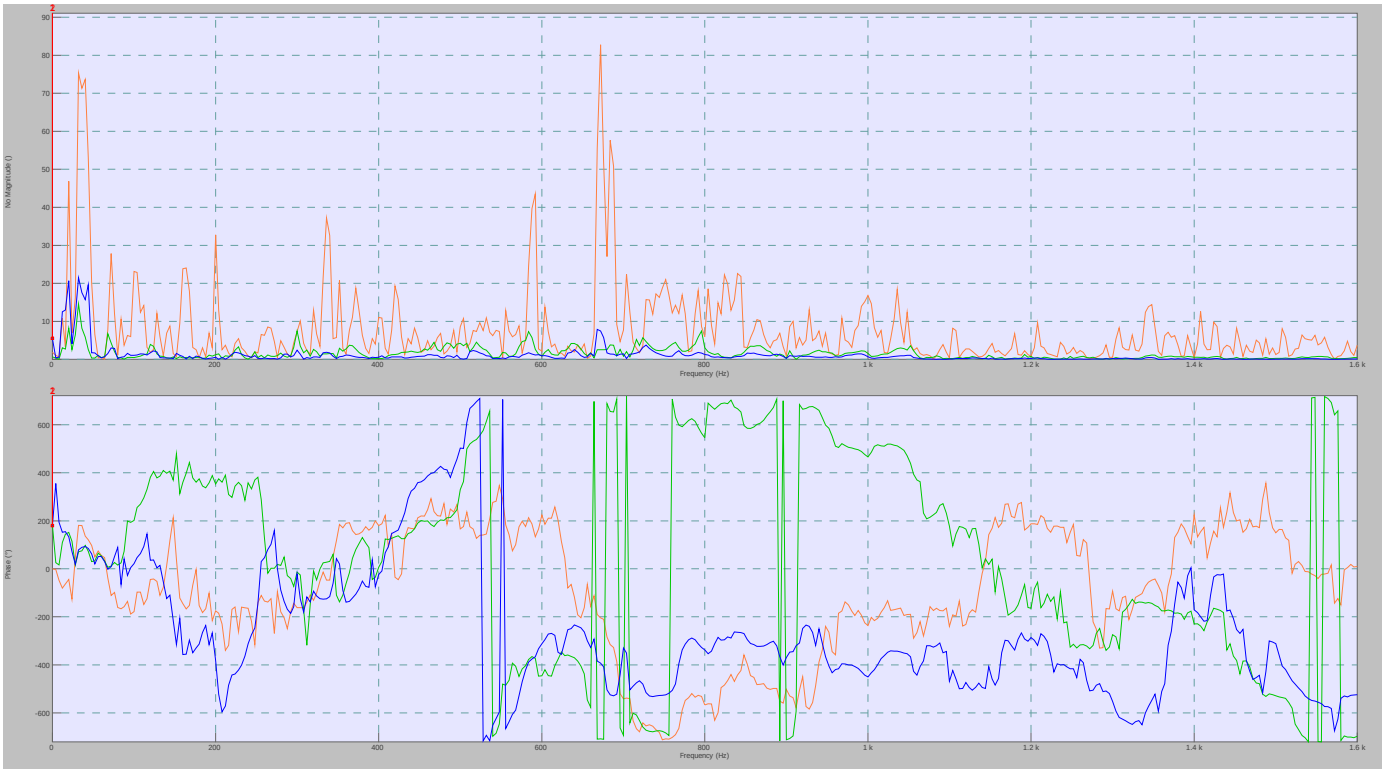

Figure 64: Accelerometer 3 (#69, Reference C)

The colors are assigned as follows:

- Orange: Input 7 (x axis)
- Green: Input 8 (y axis)
- Blue: Input 9 (z axis)

Time Domain Data

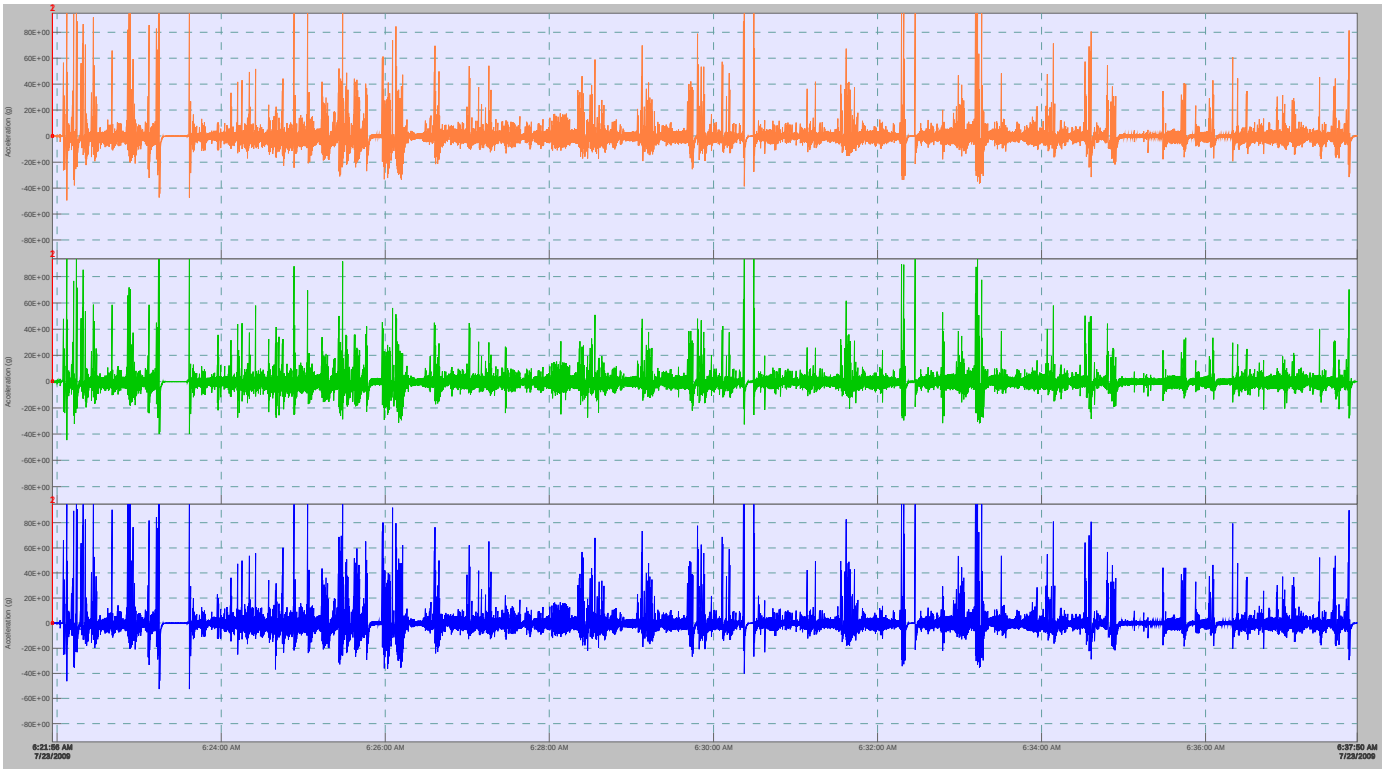

Figure 65: Accelerometer 4 (#70, Reference D)

The colors are assigned as follows:

- Orange: Input 10 (x axis)
- Green: Input 11 (y axis)
- Blue: Input 12 (z axis)

Average Spectrum Data

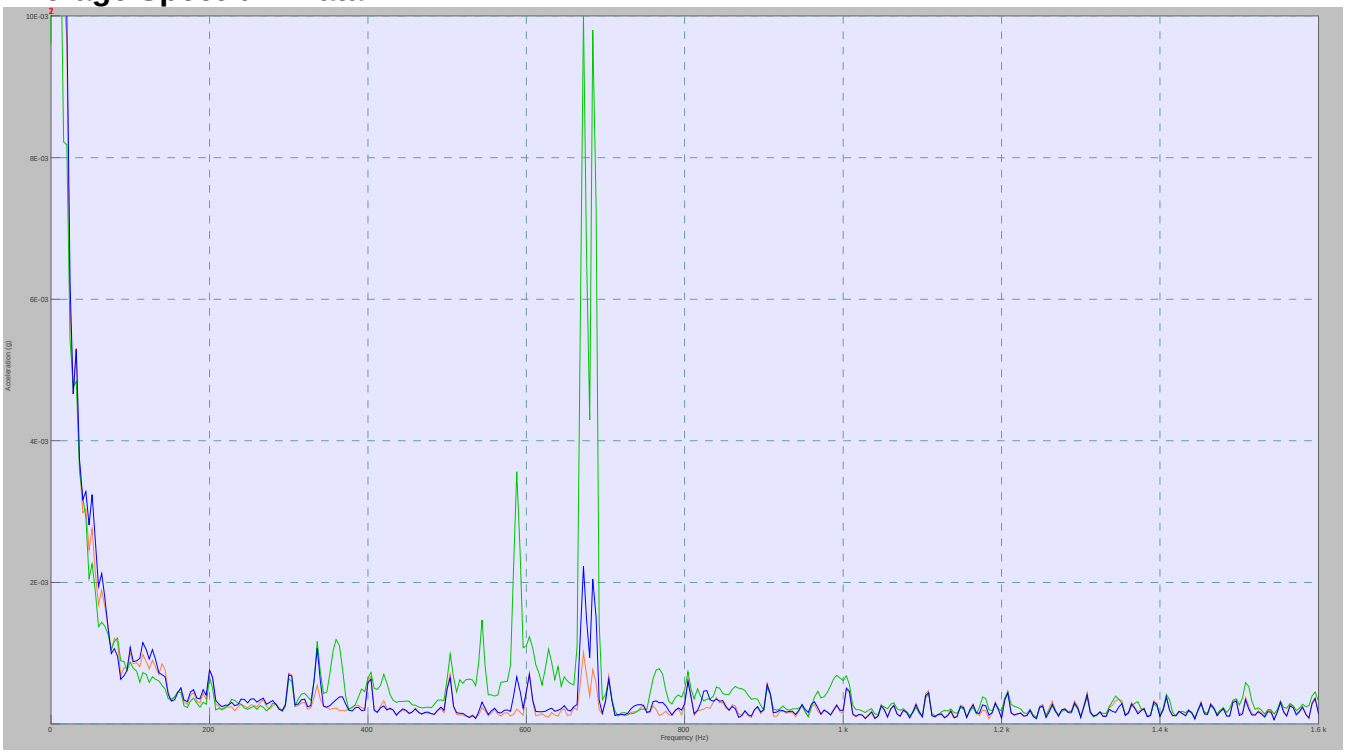

Figure 66: Accelerometer 4 (#70, Reference D)

The colors are assigned as follows:

- Orange: Input 10 (x axis)
- Green: Input 11 (y axis)
- Blue: Input 12 (z axis)

FRF Data

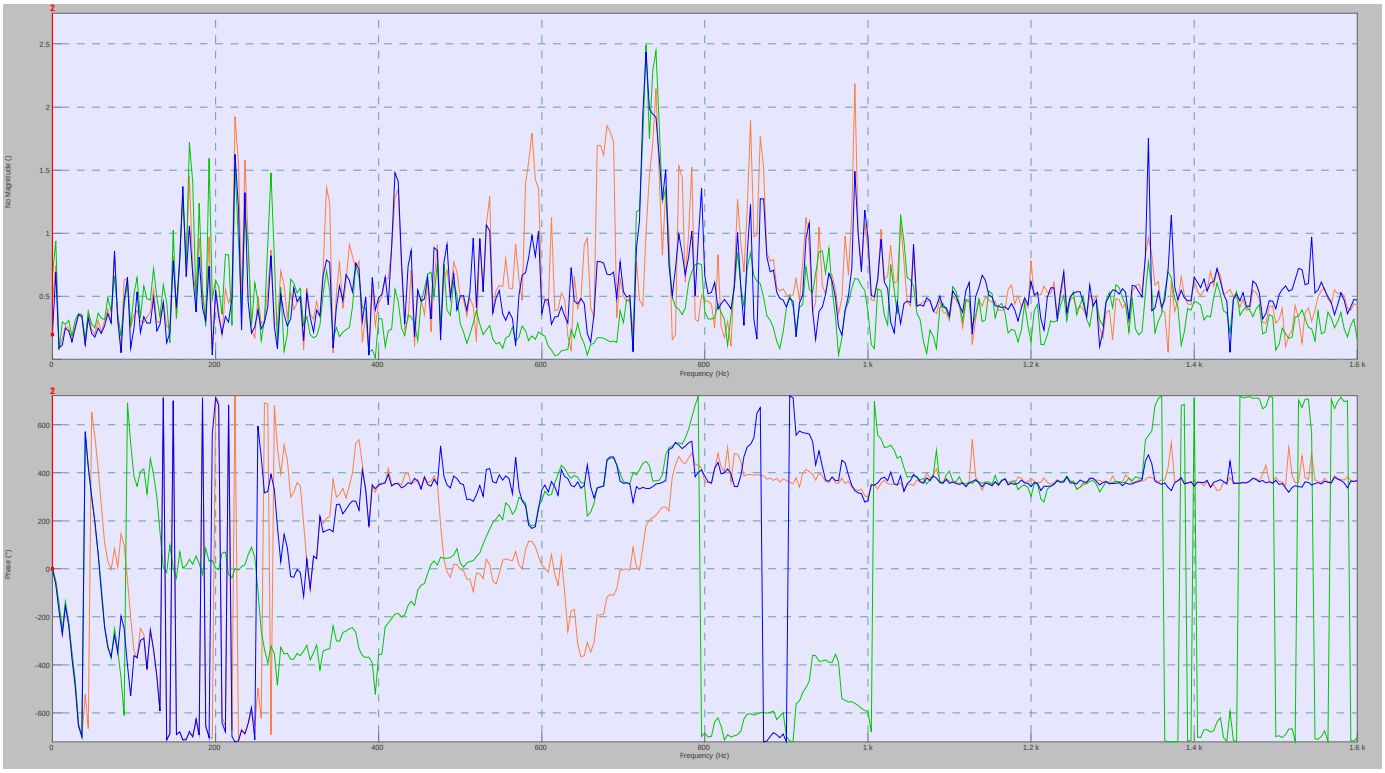

Figure 67: Accelerometer 4 (#70, Reference D)

The colors are assigned as follows:

- Orange: Input 10 (x axis)
- Green: Input 11 (y axis)
- Blue: Input 12 (z axis)

Time Domain Data

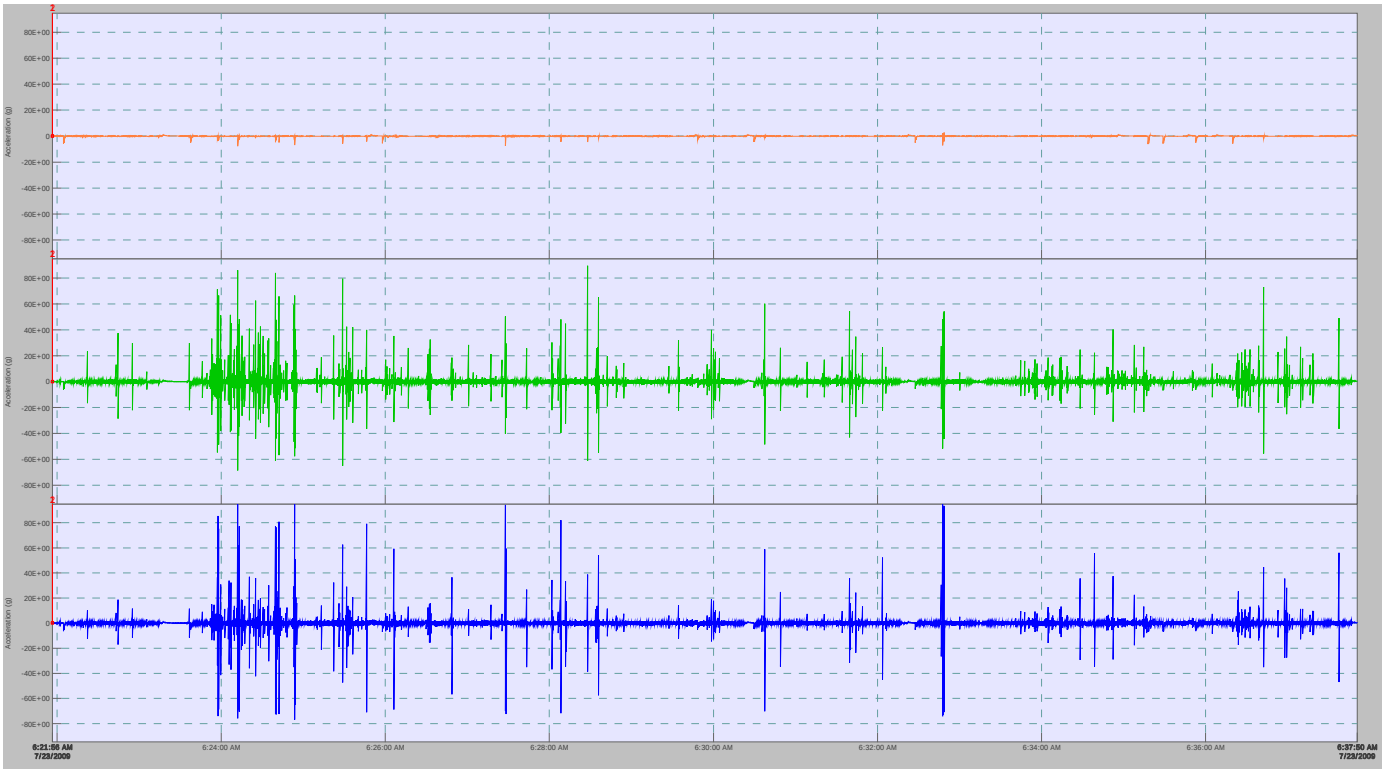

Figure 68: Accelerometer 5 (#71, Reference E)

The colors are assigned as follows:

- Orange: Input 13 (x axis)
- Green: Input 14 (z axis) *note that this data set is inverted from the rest of them
- Blue: Input 15 (y axis)

Average Spectrum Data

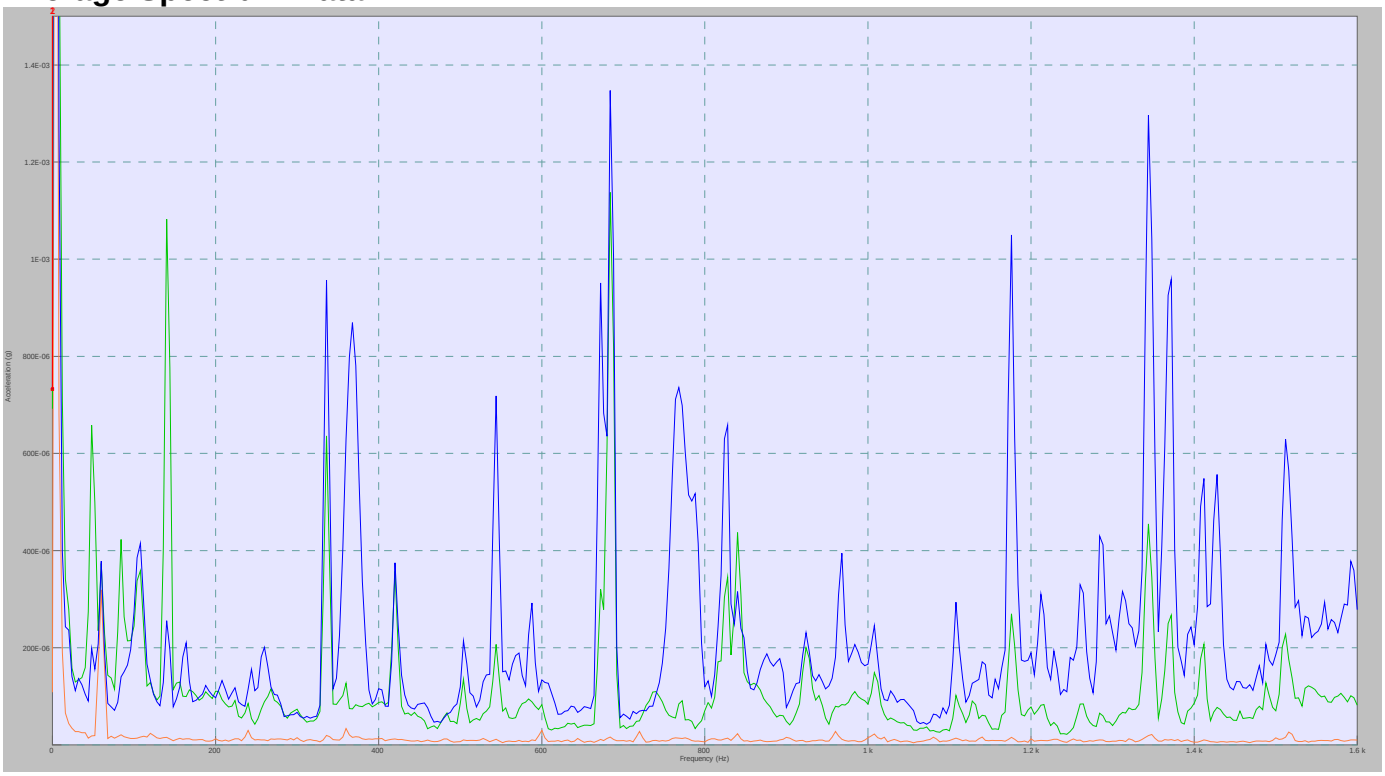

Figure 69: Accelerometer 5 (#71, Reference E)

The colors are assigned as follows:

- Orange: Input 13 (x axis)
- Green: Input 14 (z axis) *note that this data set is inverted from the rest of them
- Blue: Input 15 (y axis)

Scale Information:

- Y-axis 0g to 1.5E-3g

FRF Data

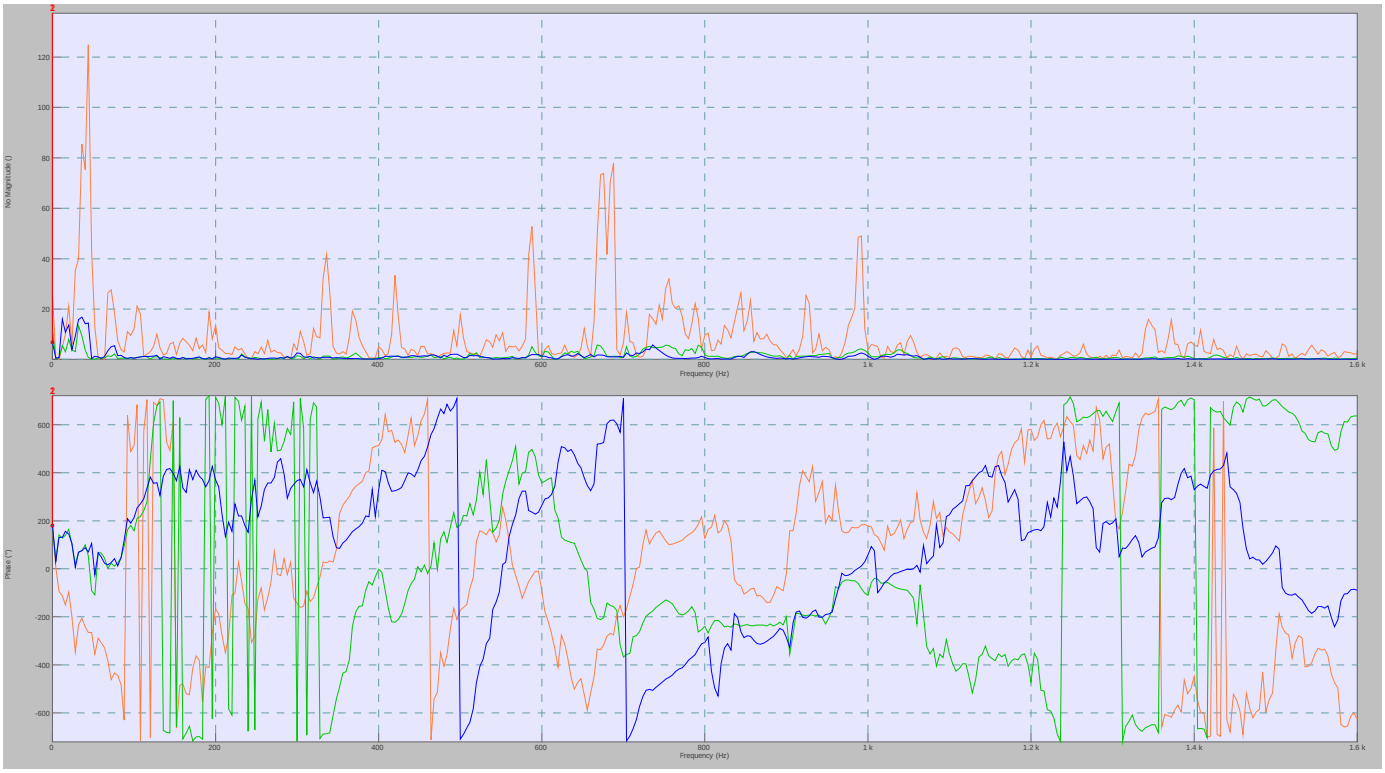

Figure 70: Accelerometer 5 (#71, Reference E)

The colors are assigned as follows:

- Orange: Input 13 (x axis)
- Green: Input 14 (z axis) *note that this data set is inverted from the rest of them
- Blue: Input 15 (y axis)

Day Two, Run Two

Driver: Richard Lawrance
Equipment Operator: Uriel Rosa
Data Set Title: Morning Run 1 Holes 1 through 9, Uriel and Richard

Accelerometer Data
Unless otherwise noted, the graph scales are as follows
Time domain graph scale:

- X-axis: 7:16:22am to 7:33:15am
- Y-axis: +90g to -50g

FRF data graph scale:

- Top Graph
    - X-axis 0Hz to 1.6kHz
    - Y-axis: 0 to 5 no units
- Bottom Graph
    - X-axis 0Hz to 1.6kHz
    - Y-axis: -720° to 720°

Average spectrum graph scale:

- X-axis: 0Hz to 1.6kHz
- Y-axis: 0g to 0.04g

Notes
This was the final run of the day. It is a repeat of the bottom 9 holes.

Time Domain Data

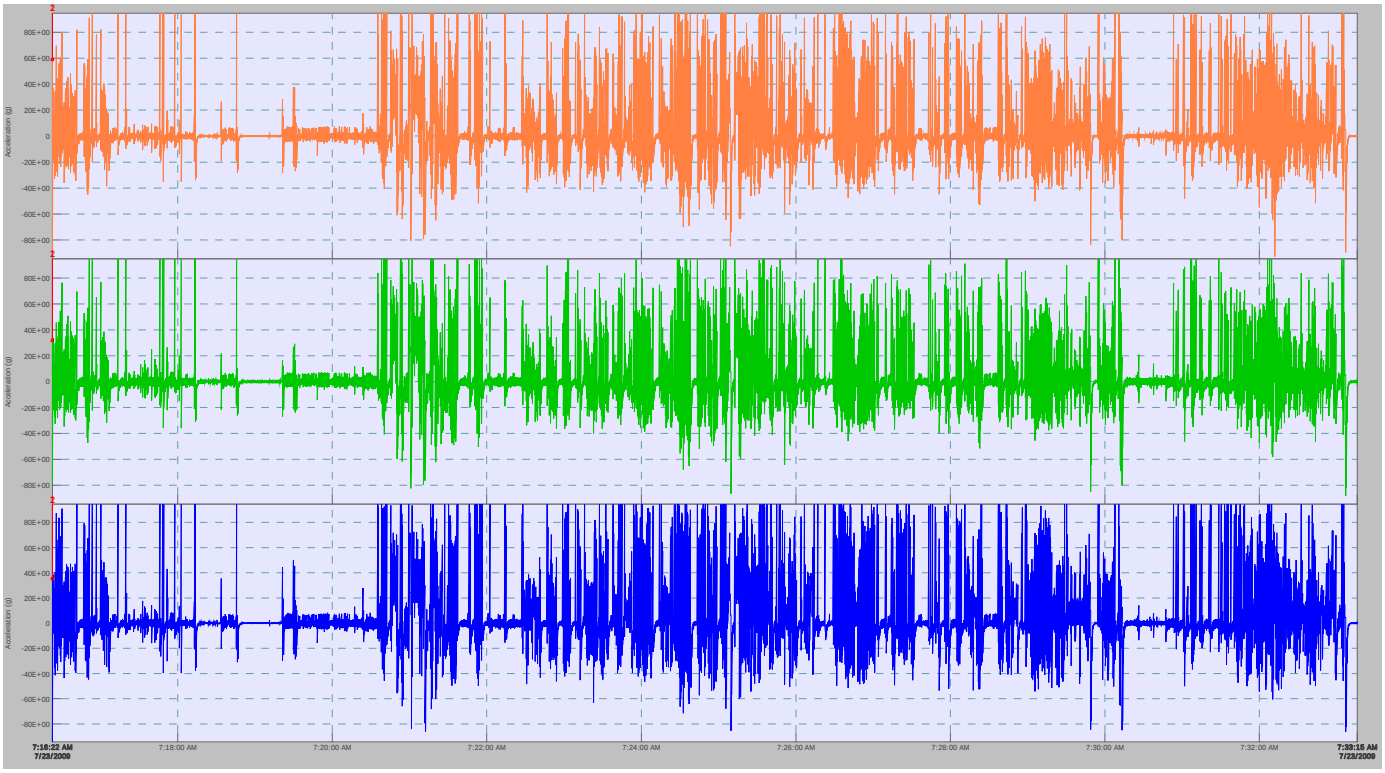

Figure 71: Accelerometer 1(#67, Reference A)

The colors are assigned as follows:

- Orange: Input 1 (x axis)
- Green: Input 2 (y axis)
- Blue: Input 3 (z axis)

Average Spectrum Data

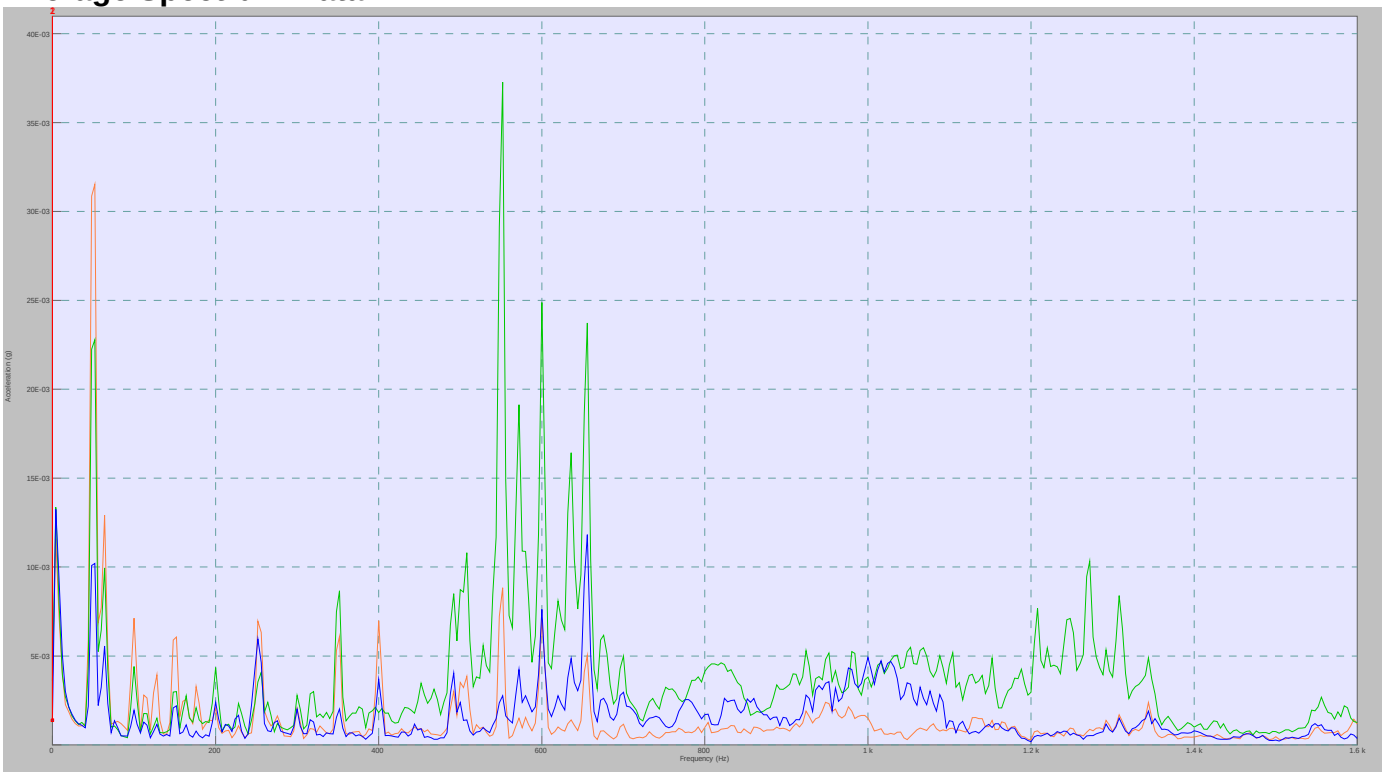

Figure 72: Accelerometer 1(#67, Reference A)

The colors are assigned as follows:

- Orange: Input 1 (x axis)
- Green: Input 2 (axis)
- Blue: Input 3 (z axis)

FRF Data

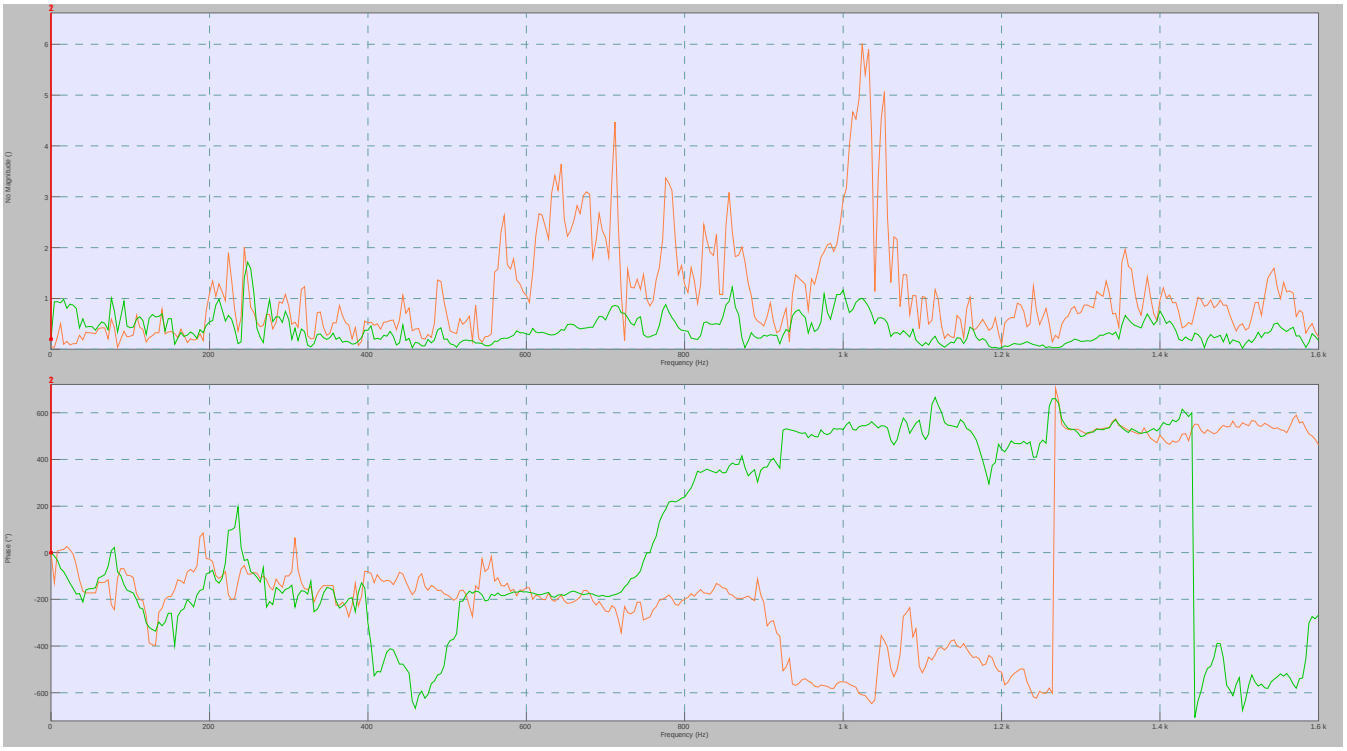

Figure 73: Accelerometer 1(#67, Reference A)

The colors are assigned as follows:

- Orange: Input 1 (x axis)
- Green: Input 2 (y axis)
- *No data for input 3*

The graph scale data for the FRF data is as follows:

- Top Graph
  - x-scale 0Hz to 1.6kHz
  - y-scale: 0 to 5 no units
- Bottom Graph
  - x-scale 0Hz to 1.6kHz
  - y-scale: -720° to 720°

Time Domain Data

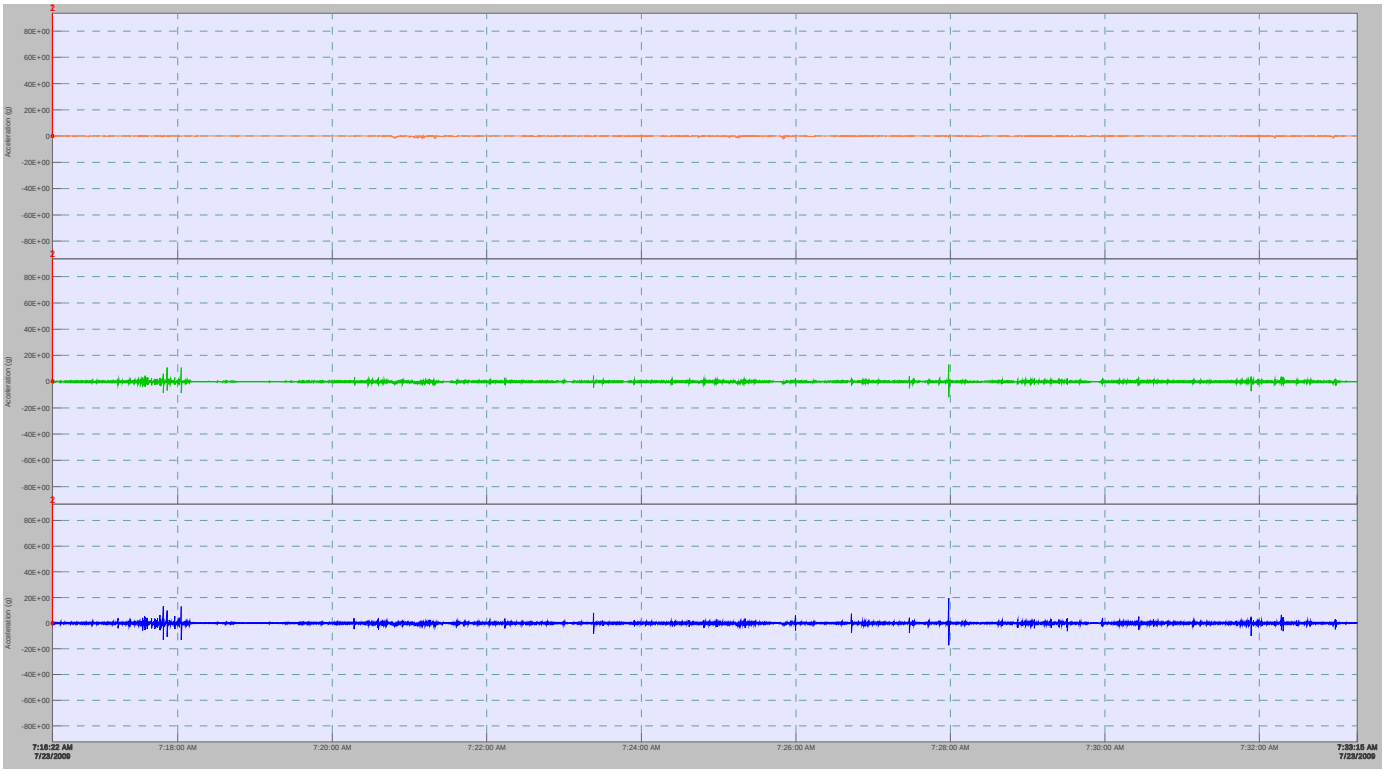

Figure 74: Accelerometer 2 (#68, Reference B)

The colors are assigned as follows:

- Orange: Input 4 (x axis)
- Green: Input 5 (z axis)
- Blue: Input 6 (y axis) *note that this data set is inverted from the rest of them

Average Spectrum Data

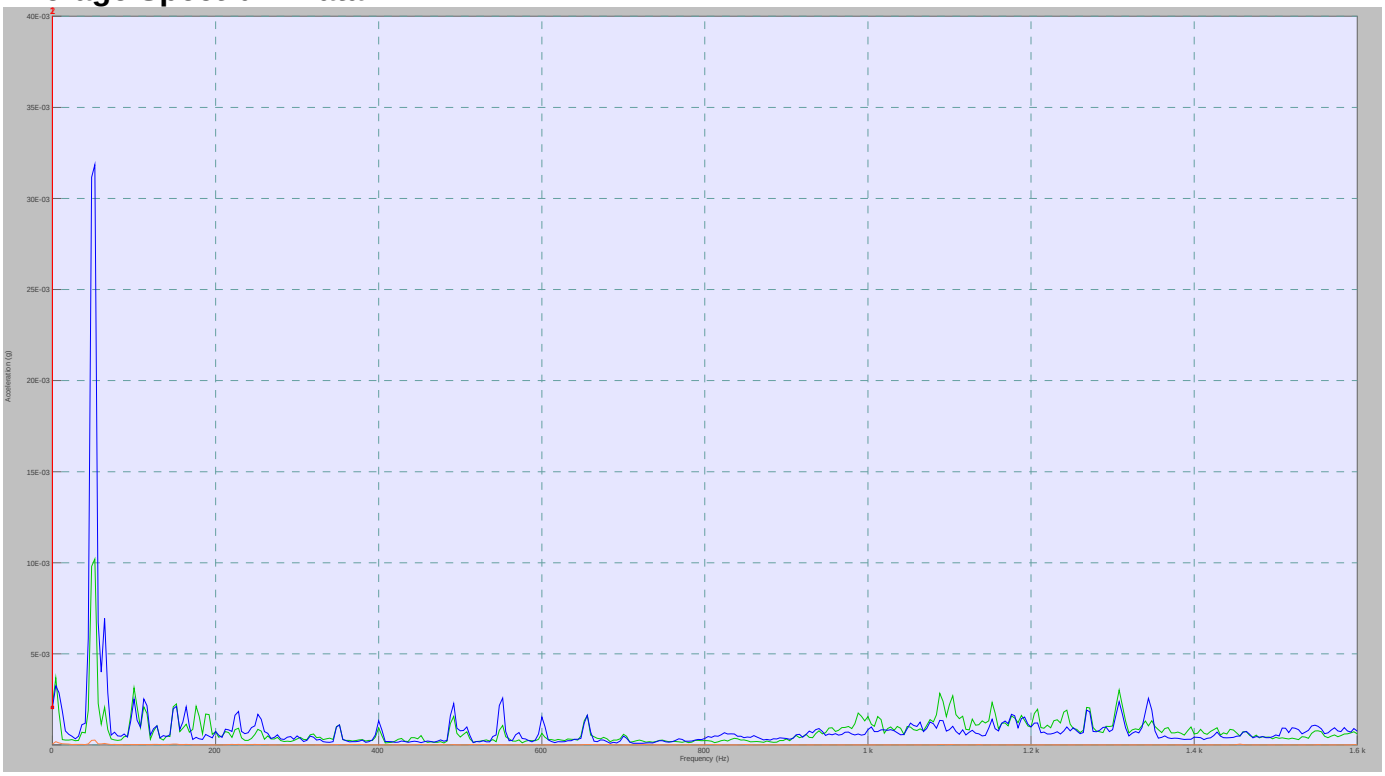

Figure 75: Accelerometer 2 (#68, Reference B)

The colors are assigned as follows:

- Orange: Input 1 (x axis)
- Green: Input 2 (z axis)
- Blue: Input 3 (y axis) *note that this data set is inverted from the rest of them

FRF Data

Figure 76: Accelerometer 2 (#68, Reference B)

The colors are assigned as follows:

- Orange: Input 4 (x axis)
- Green: Input 5 (z axis)
- Blue: Input 6 (y axis) *note that this data set is inverted from the rest of them

The graph scale data for the FRF data is as follows:

- Top Graph
  - x-scale 0Hz to 1.6kHz
  - y-scale: 0 to 700 no units
- Bottom Graph
  - x-scale 0Hz to 1.6kHz
  - y-scale: -720° to 720°

Time Domain Data

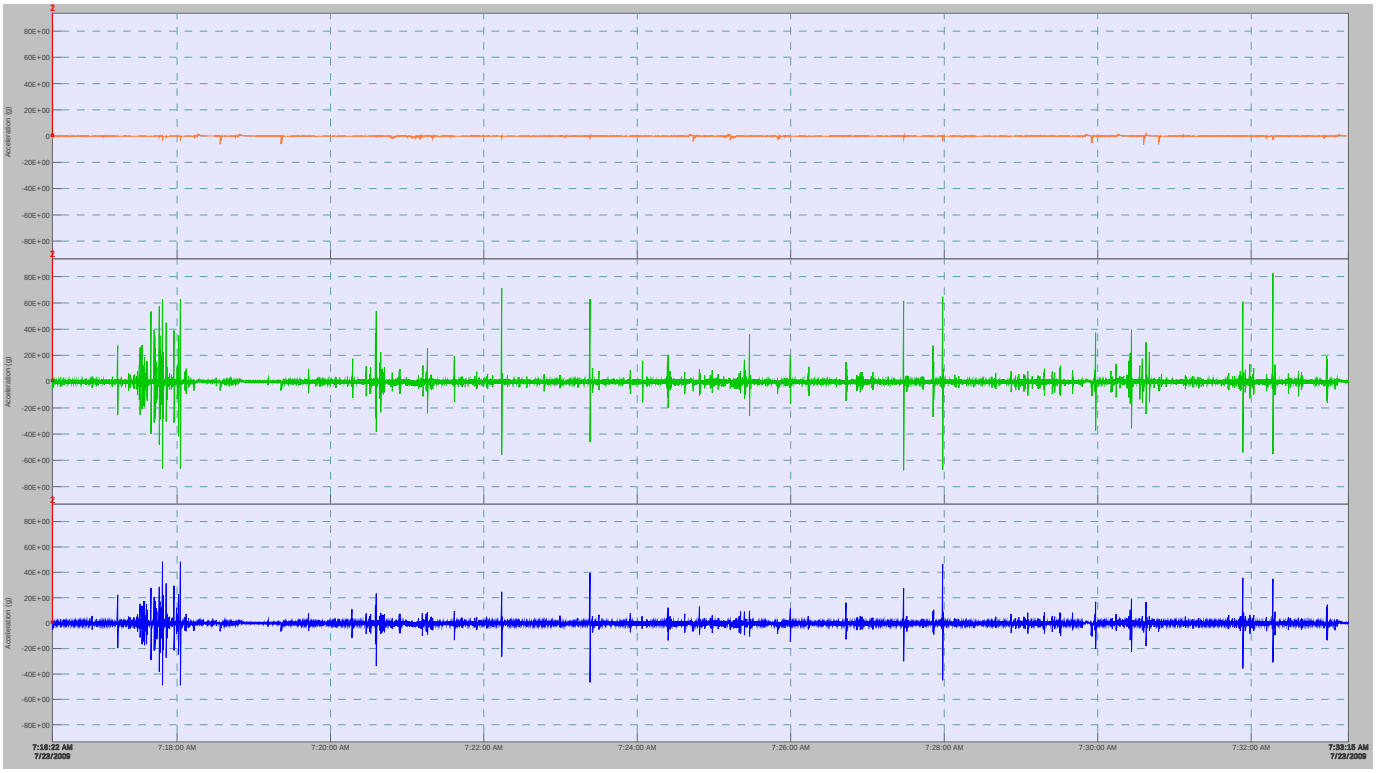

Figure 77: Accelerometer 3 (#69, Reference C)

The colors are assigned as follows:

- Orange: Input 7 (x axis)
- Green: Input 8 (y axis)
- Blue: Input 9 (z axis)

Average Spectrum Data

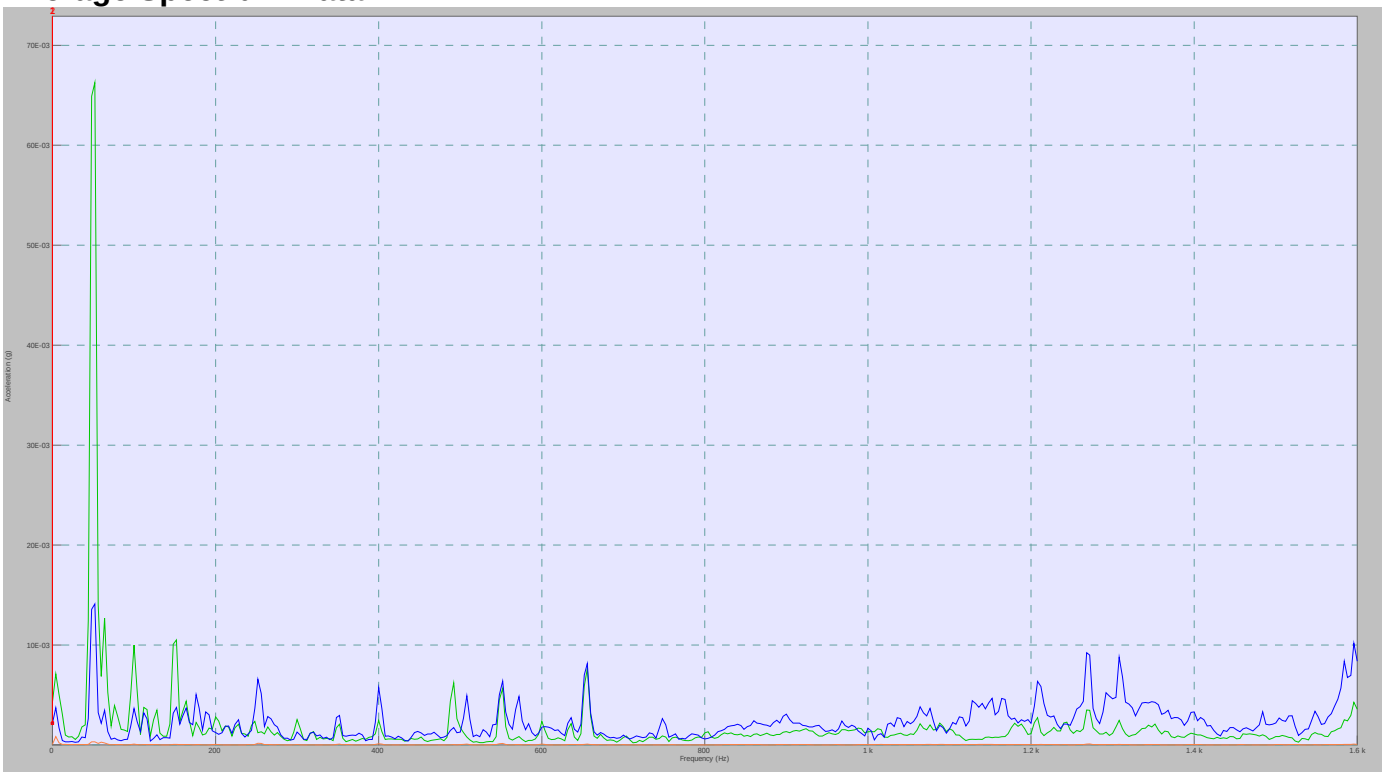

Figure 78: Accelerometer 3 (#69, Reference C)

The colors are assigned as follows:

- Orange: Input 1 (x axis)
- Green: Input 2 (y axis)
- Blue: Input 3 (z axis)

Scale information:

- X-axis: 0Hz to 1.6kHz
- Y-axis: 0g to 70E-3

FRF Data

Figure 79: Accelerometer 3 (#69, Reference C)

The colors are assigned as follows:

- Orange: Input 7 (x axis)
- Green: Input 8 (y axis)
- Blue: Input 9 (z axis)

The graph scale data for the FRF data is as follows:

- Top Graph
    - x-scale 0Hz to 1.6kHz
    - y-scale: 0 to 200 no units
- Bottom Graph
    - x-scale 0Hz to 1.6kHz
    - y-scale: -720° to 720°

Time Domain Data

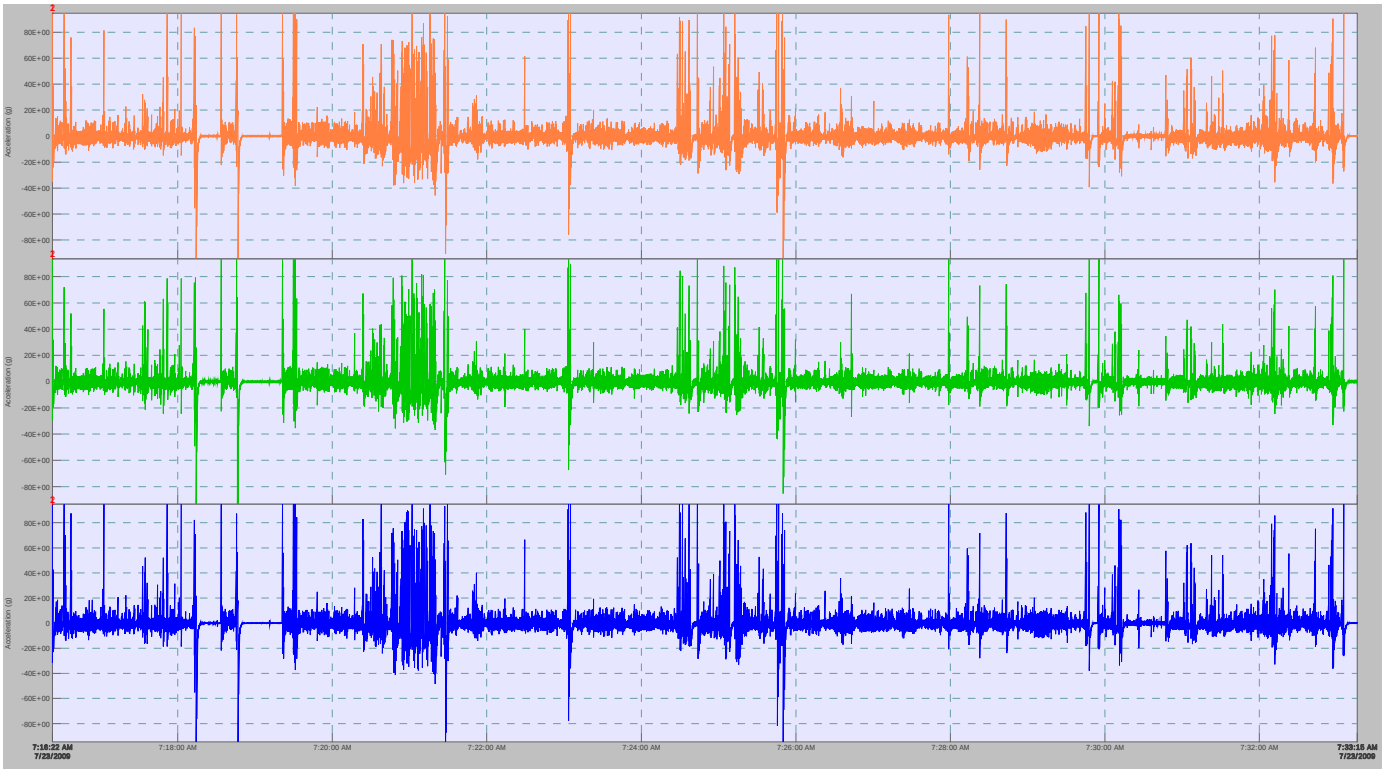

Figure 80: Accelerometer 4 (#70, Reference D)

The colors are assigned as follows:

- Orange: Input 10 (x axis)
- Green: Input 11 (y axis)
- Blue: Input 12 (z axis)

Average Spectrum Data

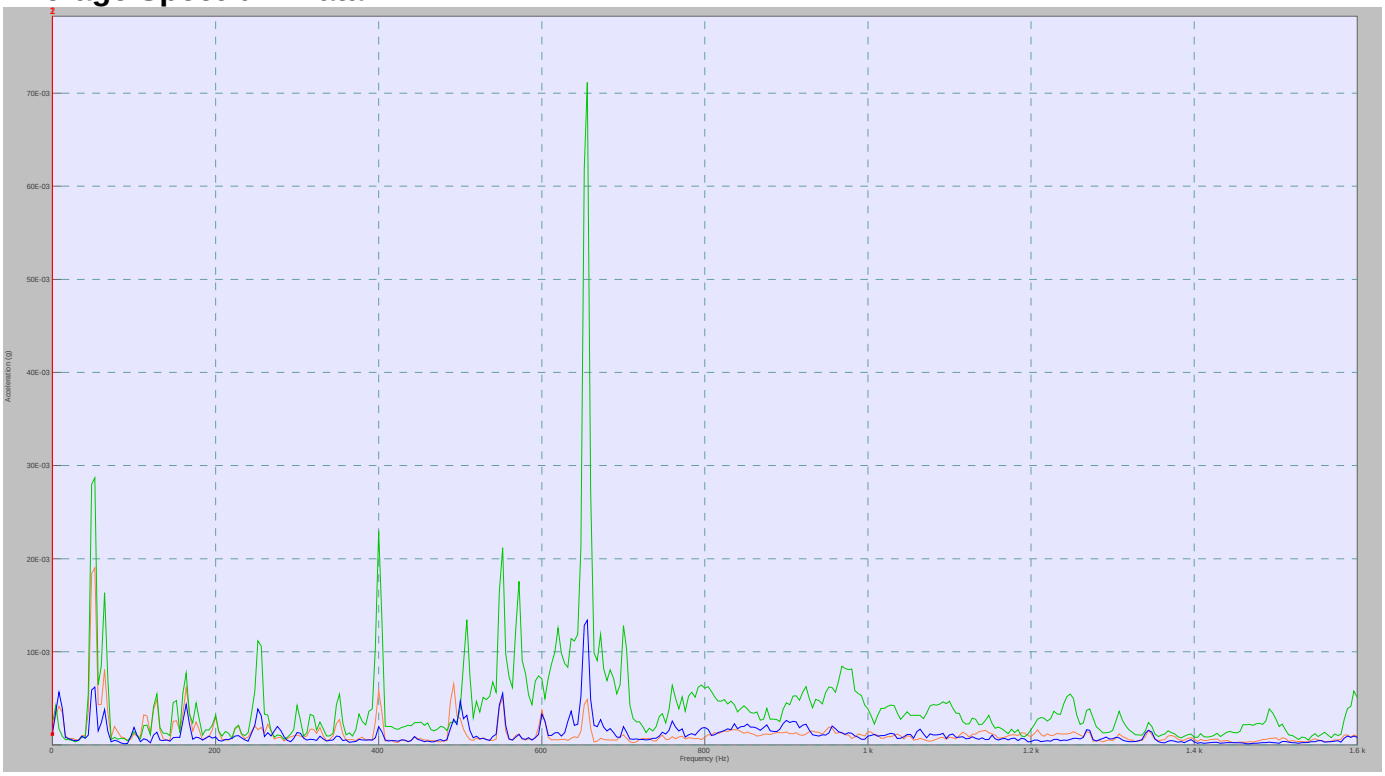

Figure 81: Accelerometer 4 (#70, Reference D)

The colors are assigned as follows:

- Orange: Input 1 (x axis)
- Green: Input 2 (y axis)
- Blue: Input 3 (z axis)

Scale Information:

- Y-axis: 0g to 80E-3g
- X-axis: 0Hz to 1.6kHz

FRF Data

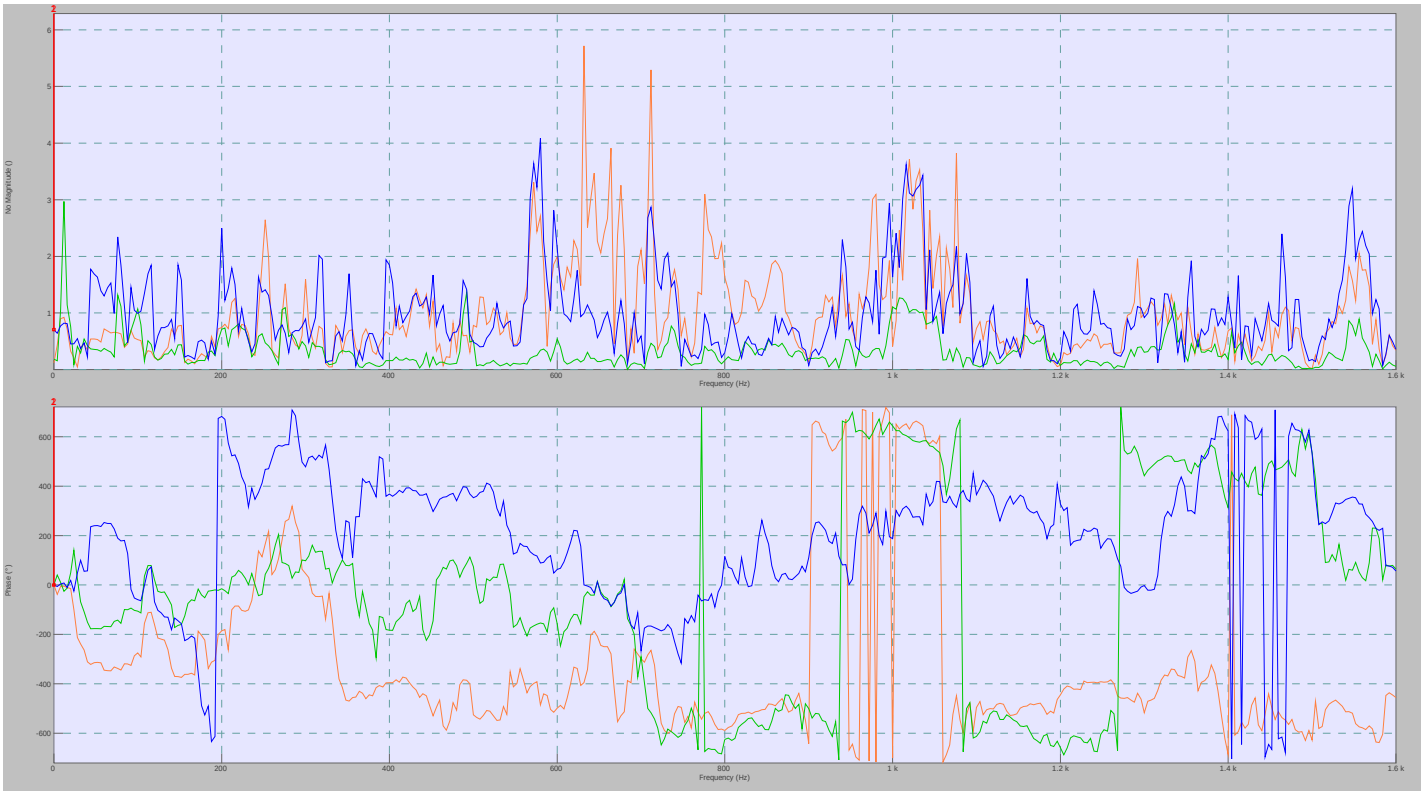

Figure 82: Accelerometer 4 (#70, Reference D)

The colors are assigned as follows:

- Orange: Input 10 (x axis)
- Green: Input 11 (y axis)
- Blue: Input 12 (z axis)

The graph scale data for the FRF data is as follows:

- Top Graph
    - x-scale 0Hz to 1.6kHz
    - y-scale: 0 to 6 no units
- Top Graph
    - x-scale 0Hz to 1.6kHz
    - y-scale: -720° to 720°

Time Domain Data

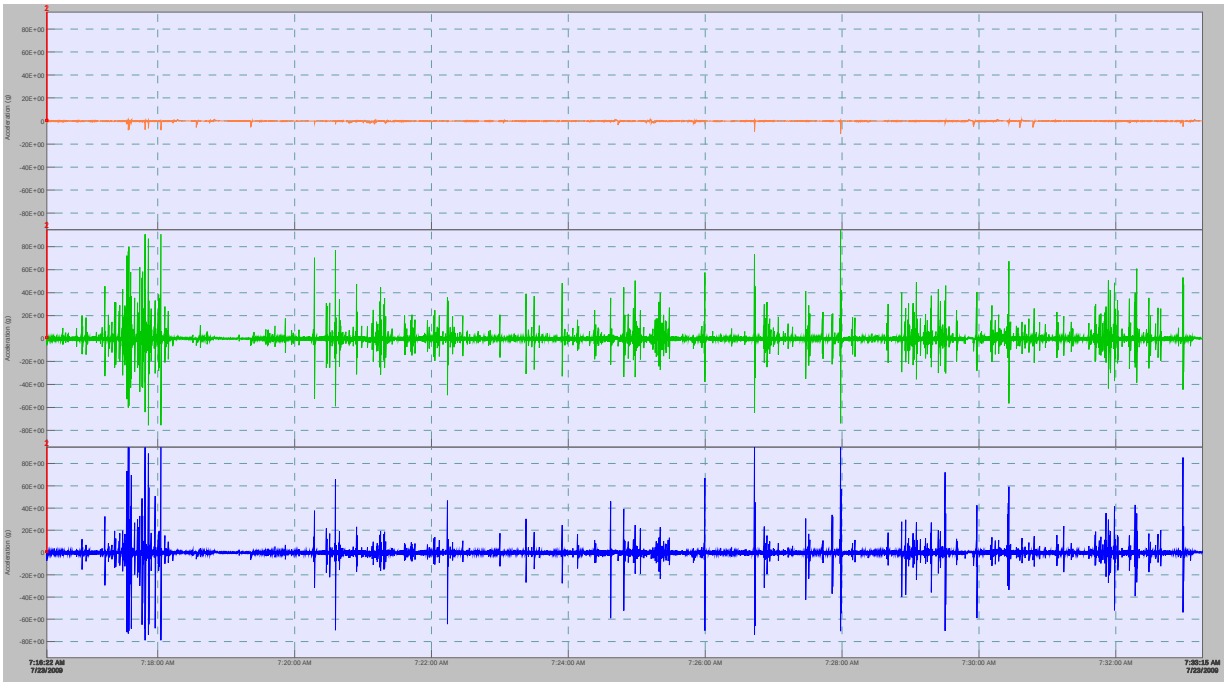

Figure 83: Accelerometer 5 (#71, Reference E)

The colors are assigned as follows:

- Orange: Input 13 (x axis)
- Green: Input 14 (z axis) *note that this data set is inverted from the rest of them
- Blue: Input 15 (y axis)

Average Spectrum Data

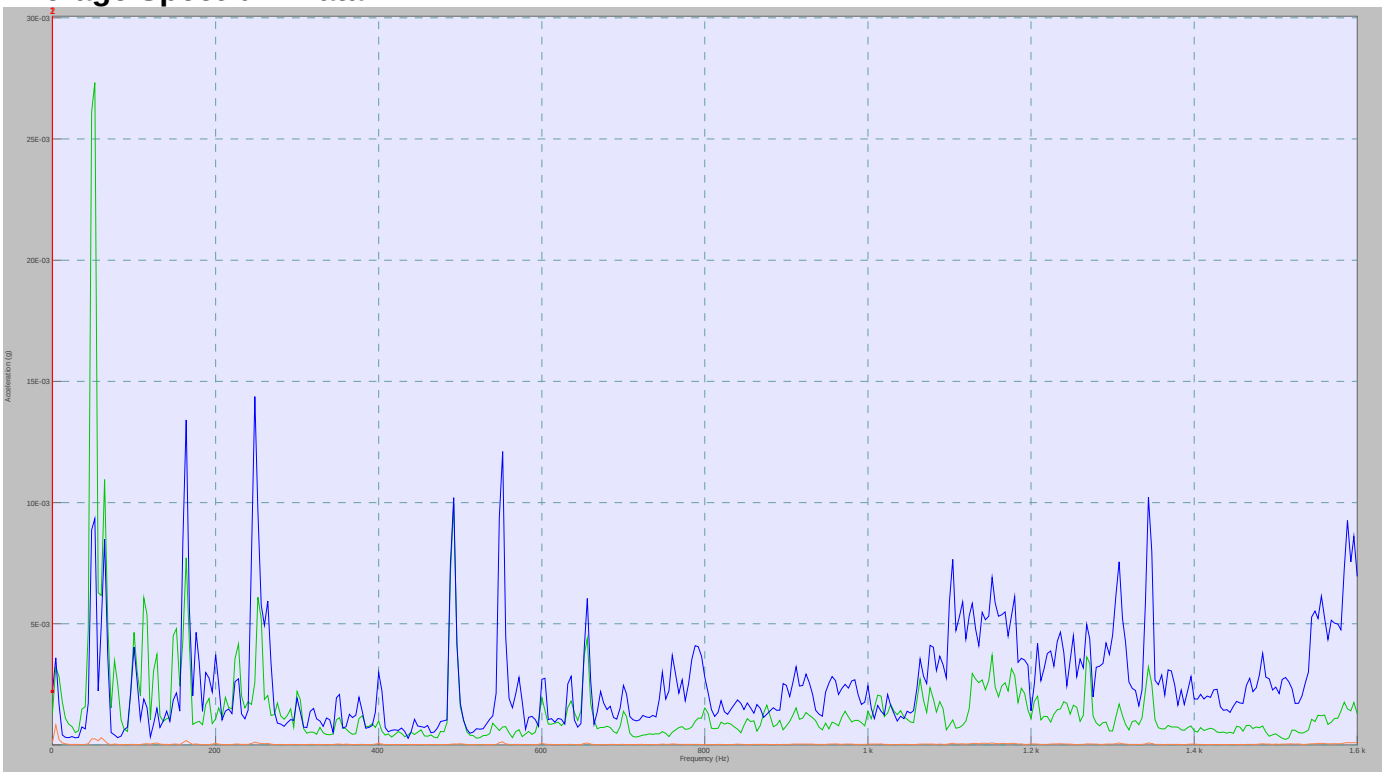

Figure 84: Accelerometer 5 (#71, Reference E)

The colors are assigned as follows:

- Orange: Input 1 (x axis)
- Green: Input 2 (y axis)
- Blue: Input 3 (z axis)

Scale Information:

- X-axis: 0Hz to 1.6kHz
- Y-axis: 0g to 30E-3g

FRF Data

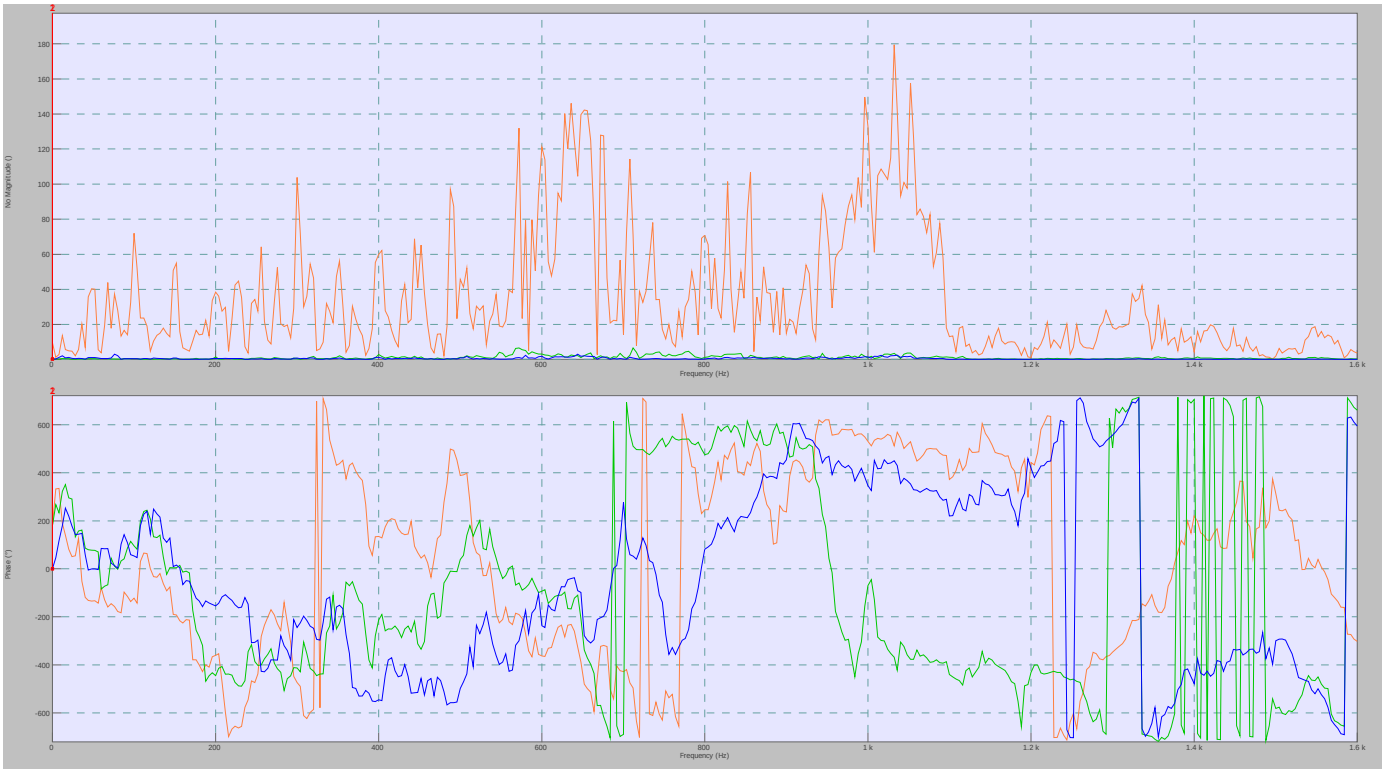

Figure 85: Accelerometer 5 (#71, Reference E)

The colors are assigned as follows:

- Orange: Input 13 (x axis)
- Green: Input 14 (z axis) *note that this data set is inverted from the rest of them
- Blue: Input 15 (y axis)

The graph scale data for the FRF data is as follows:

- Top Graph
    - x-scale 0Hz to 1.6kHz
    - y-scale: 0 to 200 no units
- Bottom Graph
    - x-scale 0Hz to 1.6kHz
    - y-scale: -720° to 720°

Day Two, Run Three

Driver: Richard Lawrance
Equipment Operator: Robert Dailey
Data Set Title: Morning Run 1 Holes 10 through 18, Robert and Richard

Accelerometer Data
Unless otherwise noted, the graph scales are as follows
Time domain graph scale:

- X-axis: 8:29:19am to 8:44:47am
- Y-axis: +90g to -50g

FRF data graph scale:

- Top Graph
    - X-axis 0Hz to 1.4kHz
    - Y-axis: 0 to 10 no units
- Bottom Graph
    - X-axis 0Hz to 1.4kHz
    - Y-axis: -720° to 720°

Average spectrum graph scale:

- X-axis: 0Hz to 1.4kHz

Y-axis: 0g to 0.006g

Notes
This was the final run of the day.

Time Domain Data

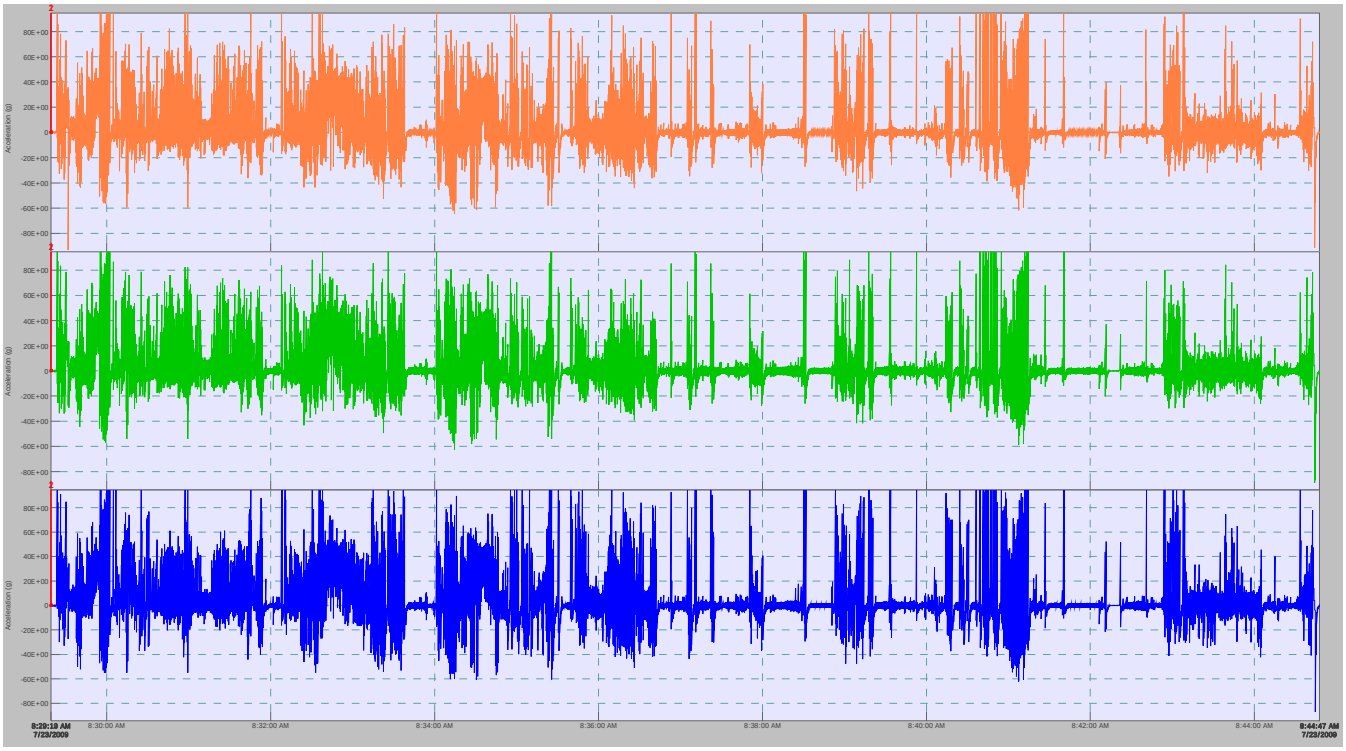

Figure 86: Accelerometer 1(#67, Reference A)

The colors are assigned as follows:

- Orange: Input 1 (x axis)
- Green: Input 2 (y axis)
- Blue: Input 3 (z axis)

Average Spectrum Data

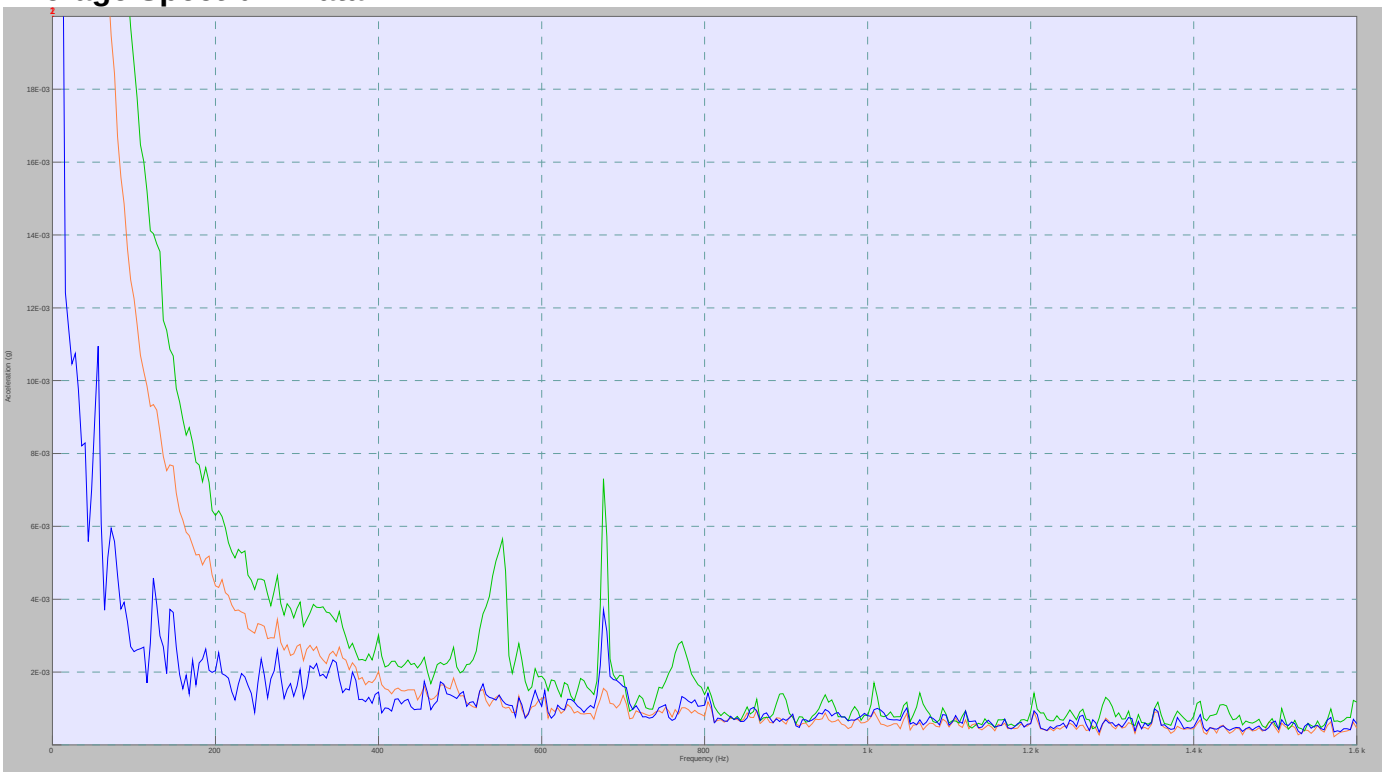

Figure 87: Accelerometer 1(#67, Reference A)

The colors are assigned as follows:

- Orange: Input 1 (x axis)
- Green: Input 2 (axis)
- Blue: Input 3 (z axis)

Scale Information:

- X-axis: 0Hz to 1.6kHz
- Y-axis: 0g to 20E-3g

FRF Data

Figure 88: Accelerometer 1(#67, Reference A)

The colors are assigned as follows:

- Orange: Input 1 (x axis)
- Green: Input 2 (y axis)
- *No data for input 3*

The graph scale data for the FRF data is as follows:

- Top Graph
    - x-scale 0Hz to 1.6kHz
    - y-scale: 0 to 1.5 no units
- Bottom Graph
    - x-scale 0Hz to 1.6kHz
    - y-scale: -720° to 720°

Time Domain Data

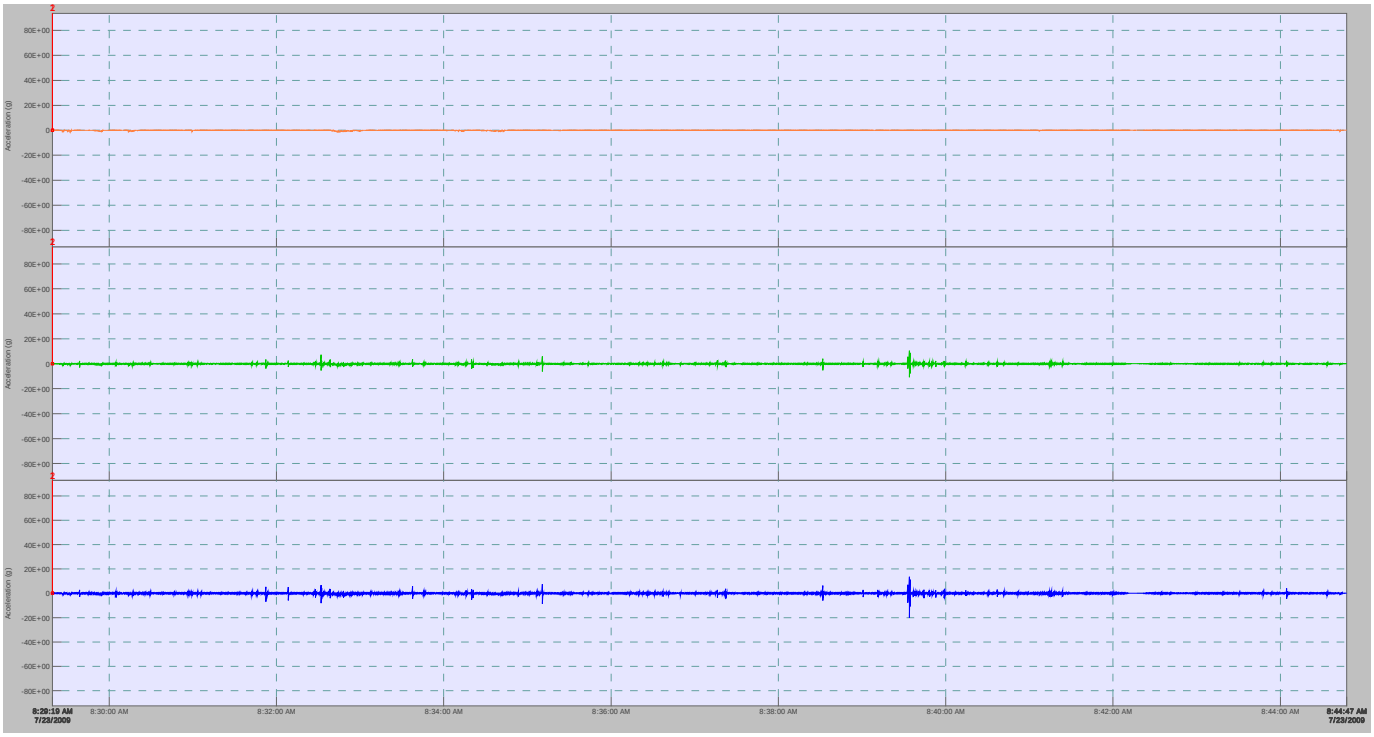

Figure 89: Accelerometer 2 (#68, Reference B)

The colors are assigned as follows:

- Orange: Input 4 (x axis)
- Green: Input 5 (z axis)
- Blue: Input 6 (y axis) *note that this data set is inverted from the rest of them

Average Spectrum Data

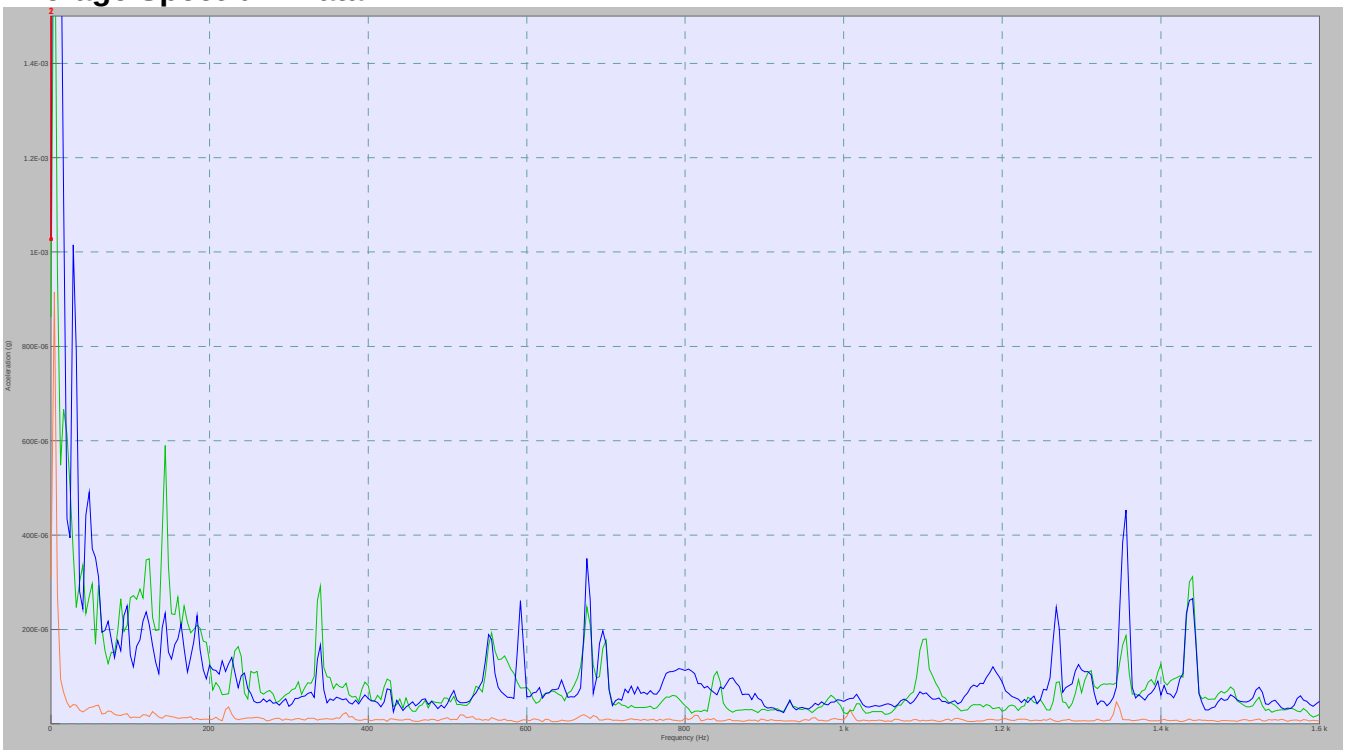

Figure 90: Accelerometer 2 (#68, Reference B)

The colors are assigned as follows:

- Orange: Input 1 (x axis)
- Green: Input 2 (z axis)
- Blue: Input 3 (y axis) *note that this data set is inverted from the rest of them

Scale Information:

- X-axis: 0Hz to 1.6kHz
- Y-axis: 0g to 1.5E-3g

FRF Data

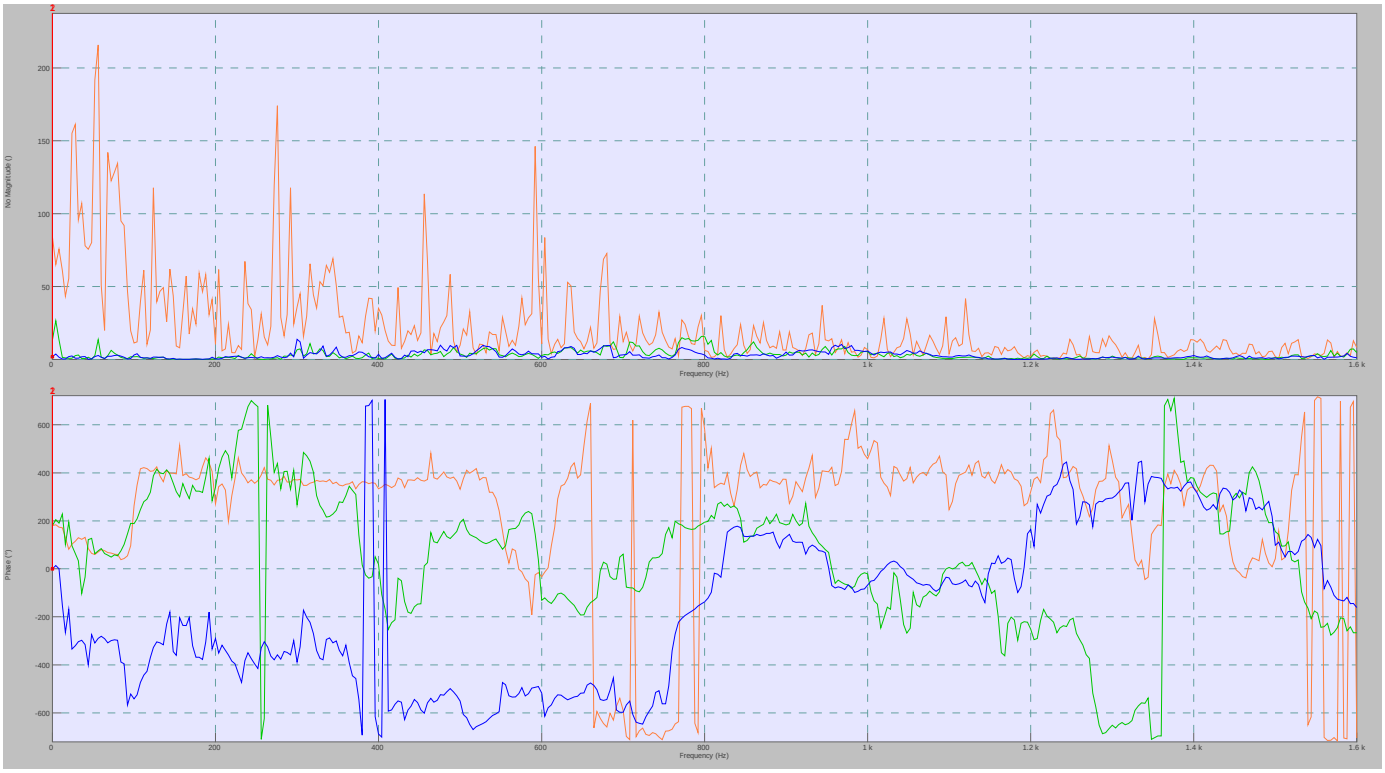

Figure 91: Accelerometer 2 (#68, Reference B)

The colors are assigned as follows:

- Orange: Input 4 (x axis)
- Green: Input 5 (z axis)
- Blue: Input 6 (y axis) *note that this data set is inverted from the rest of them

The graph scale data for the FRF data is as follows:

- Top Graph
    - x-scale 0Hz to 1.6kHz
    - y-scale: 0 to 237 no units
- Bottom Graph
    - x-scale 0Hz to 1.6kHz
    - y-scale: -720° to 720°

Time Domain Data

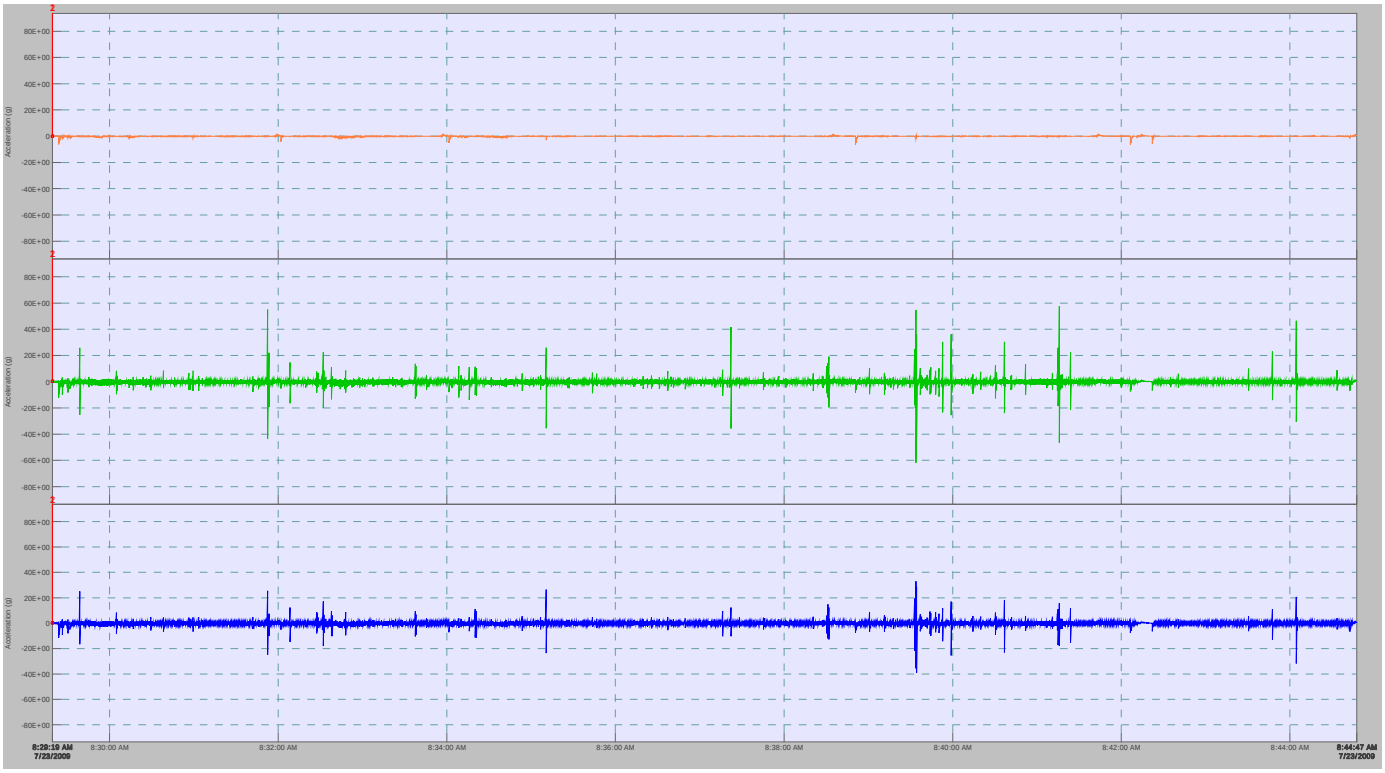

Figure 92: Accelerometer 3 (#69, Reference C):

The colors are assigned as follows:

- Orange: Input 7 (x axis)
- Green: Input 8 (y axis)
- Blue: Input 9 (z axis)

Average Spectrum Data

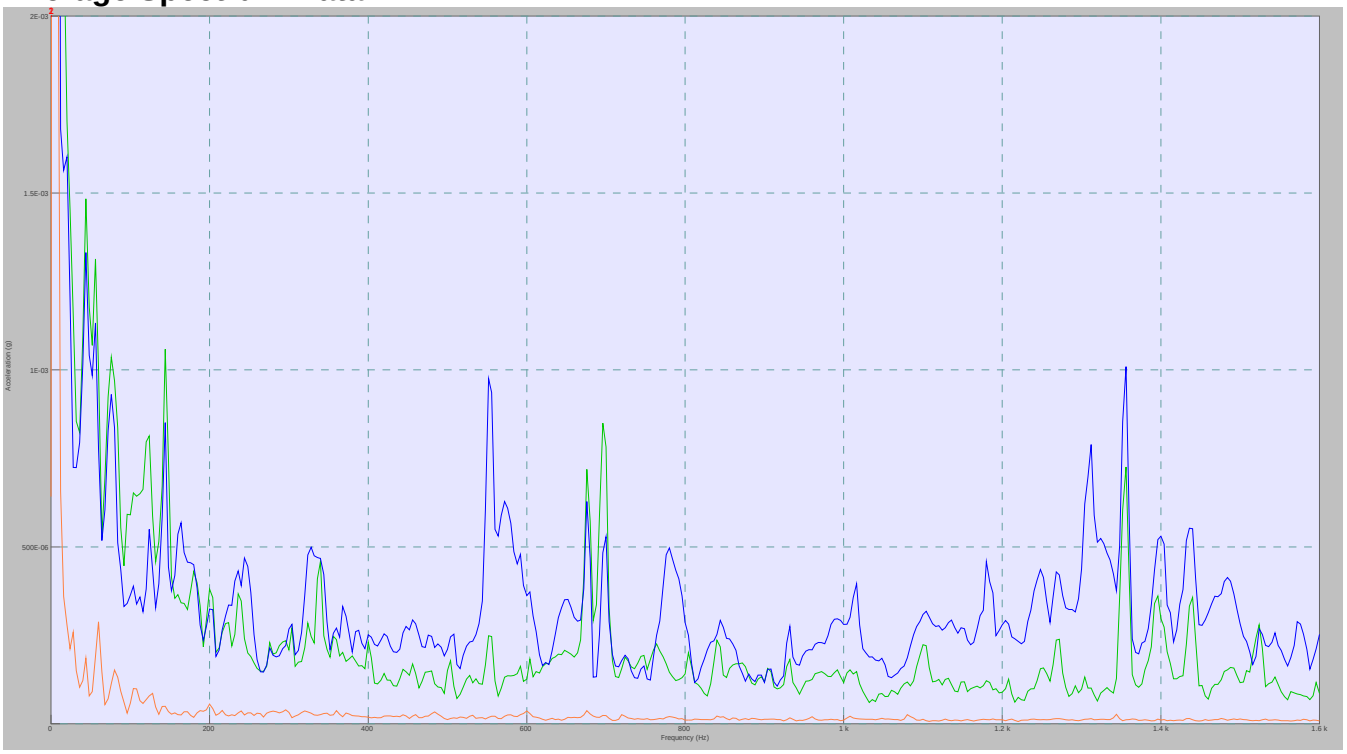

Figure 93: Accelerometer 3 (#69, Reference C)

The colors are assigned as follows:

- Orange: Input 1 (x axis)
- Green: Input 2 (axis)
- Blue: Input 3 (z axis)

Scale Information:

- X-axis: 0Hz to 1.6kHz
- Y-axis: 0g to 2E-3g

FRF Data

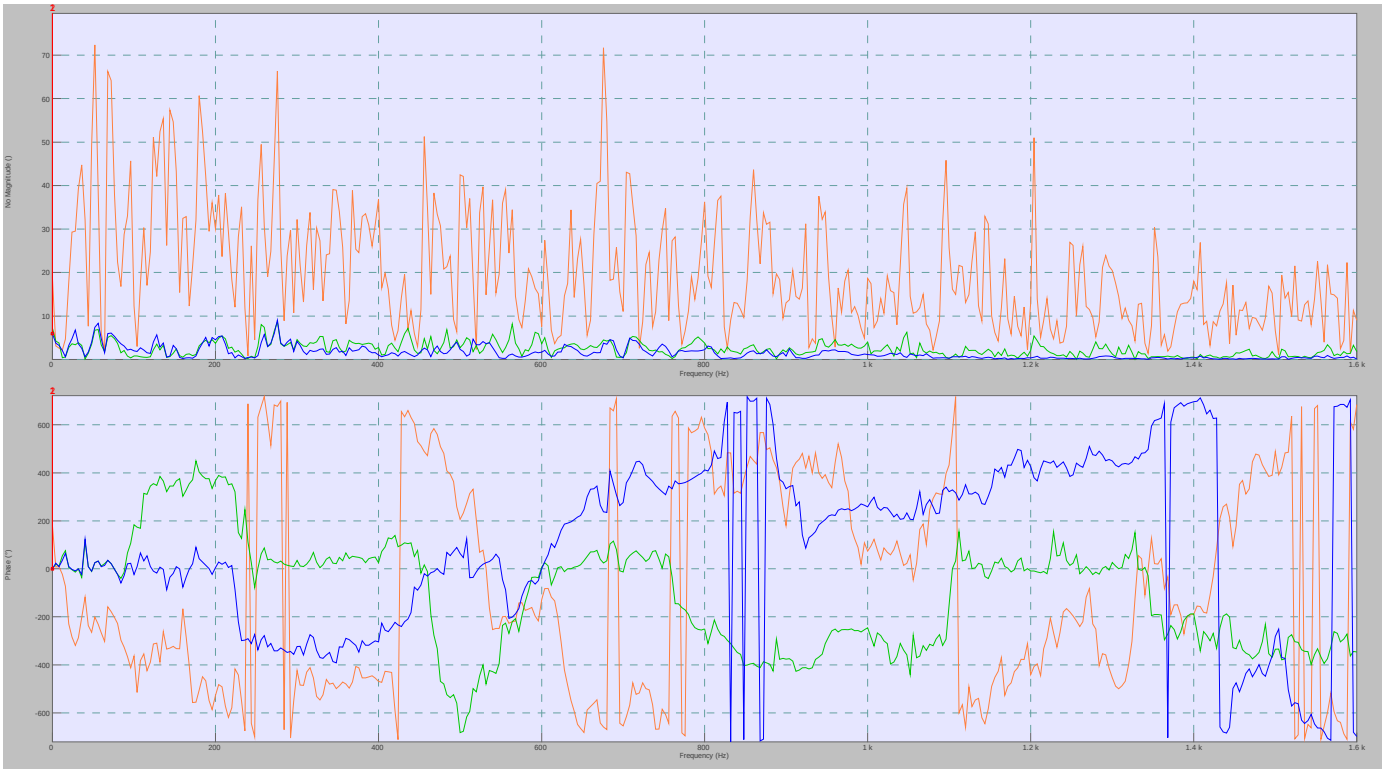

Figure 94: Accelerometer 3 (#69, Reference C)

The colors are assigned as follows:

- Orange: Input 7 (x axis)
- Green: Input 8 (y axis)
- Blue: Input 9 (z axis)

The graph scale data for the FRF data is as follows:

- Top Graph
    - x-scale 0Hz to 1.6kHz
    - y-scale: 0 to 80 no units
- Bottom Graph
    - x-scale 0Hz to 1.6kHz
    - y-scale: -720° to 720°

Time Domain Data

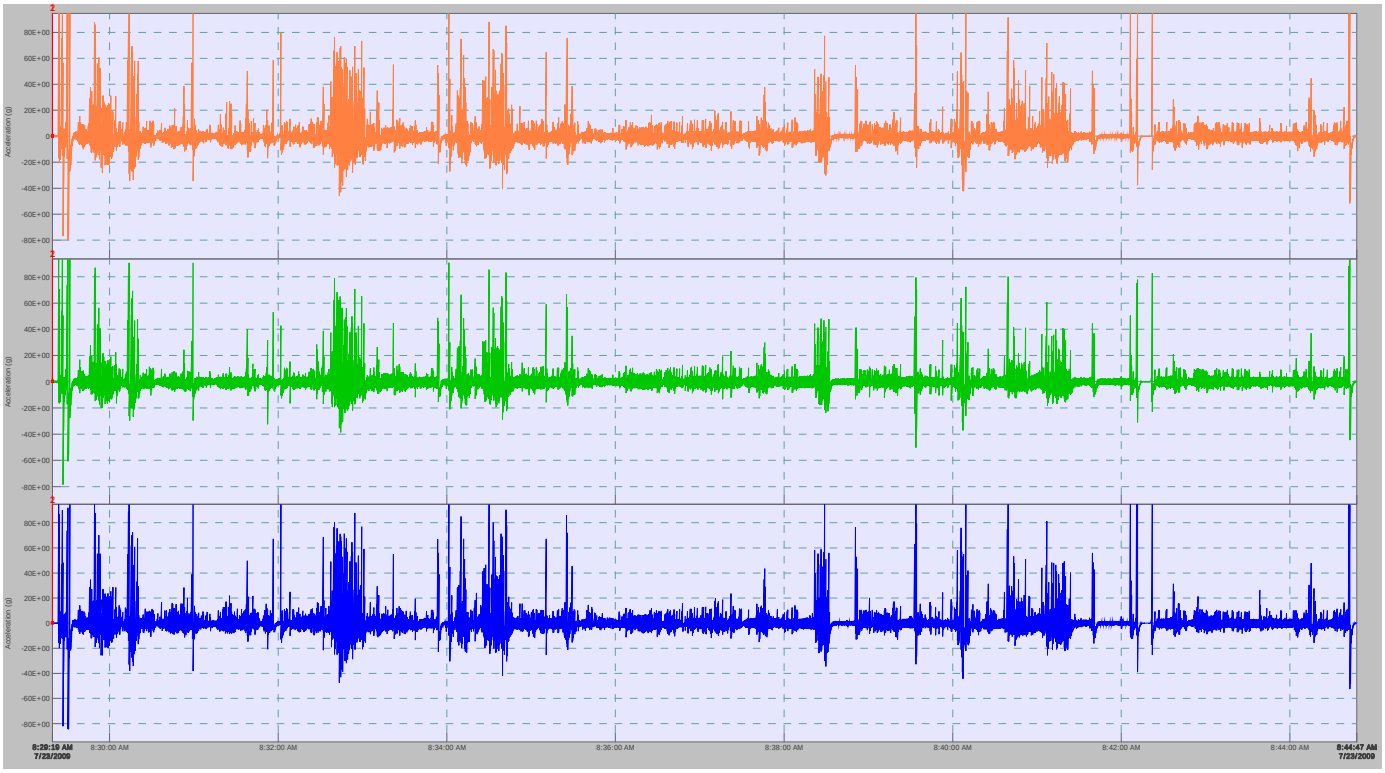

Figure 95: Accelerometer 4 (#70, Reference D)

The colors are assigned as follows:

- Orange: Input 10 (x axis)
- Green: Input 11 (y axis)
- Blue: Input 12 (z axis)

Average Spectrum Data

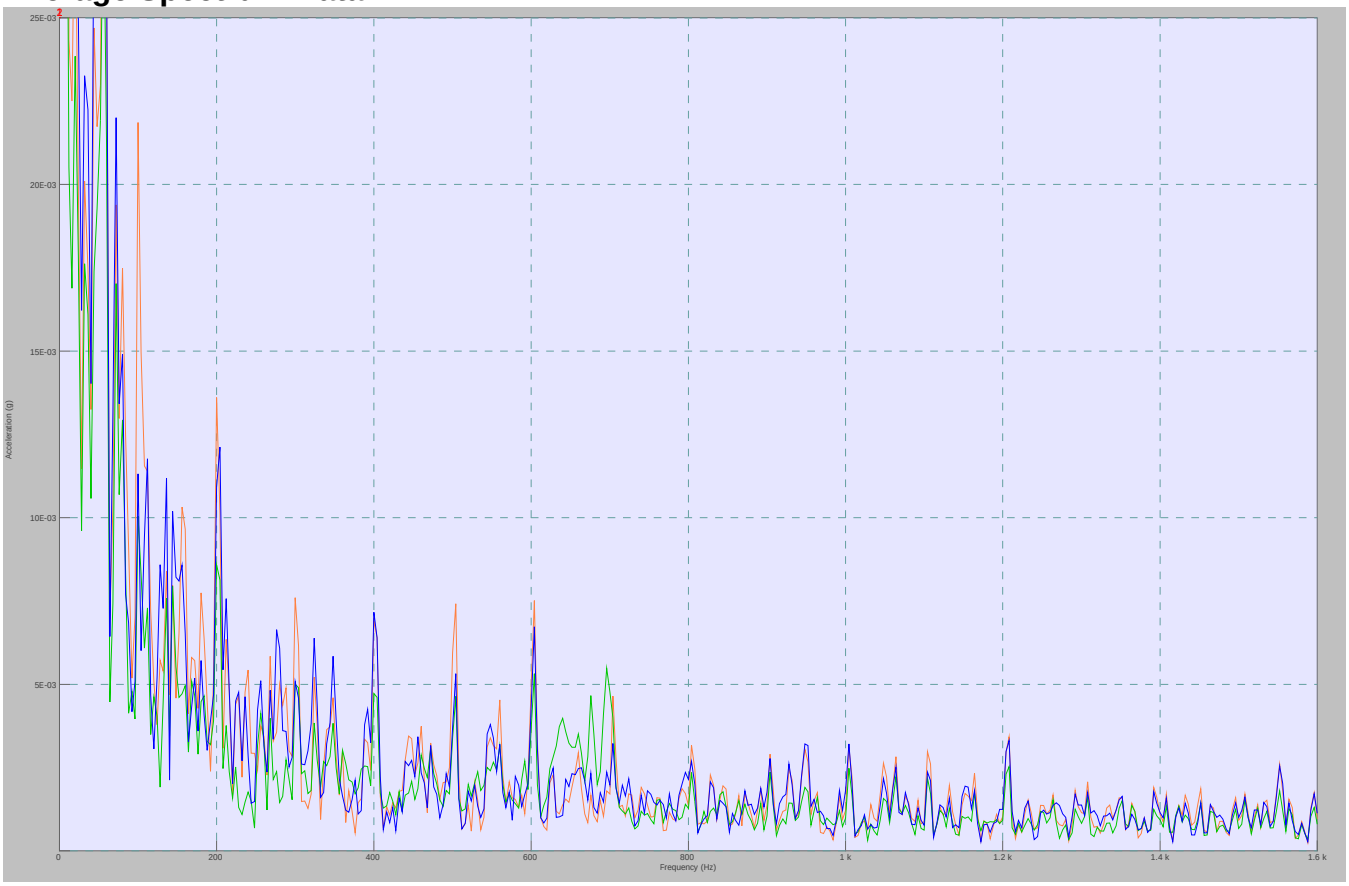

Figure 96: Accelerometer 4 (#70, Reference D)

The colors are assigned as follows:

- Orange: Input 1 (x axis)
- Green: Input 2 (axis)
- Blue: Input 3 (z axis)

Scale Information:

- X-axis: 0Hz to 1.6kHz
- Y-axis: 0g to 25E-3g

FRF Data

Figure 97: Accelerometer 4 (#70, Reference D)

The colors are assigned as follows:

- Orange: Input 10 (x axis)
- Green: Input 11 (y axis)
- Blue: Input 12 (z axis)

The graph scale data for the FRF data is as follows:

- Top Graph
    - x-scale 0Hz to 1.6kHz
    - y-scale: 0 to 2 no units
- Bottom Graph
    - x-scale 0Hz to 1.6kHz
    - y-scale: -720° to 720°

Time Domain Data

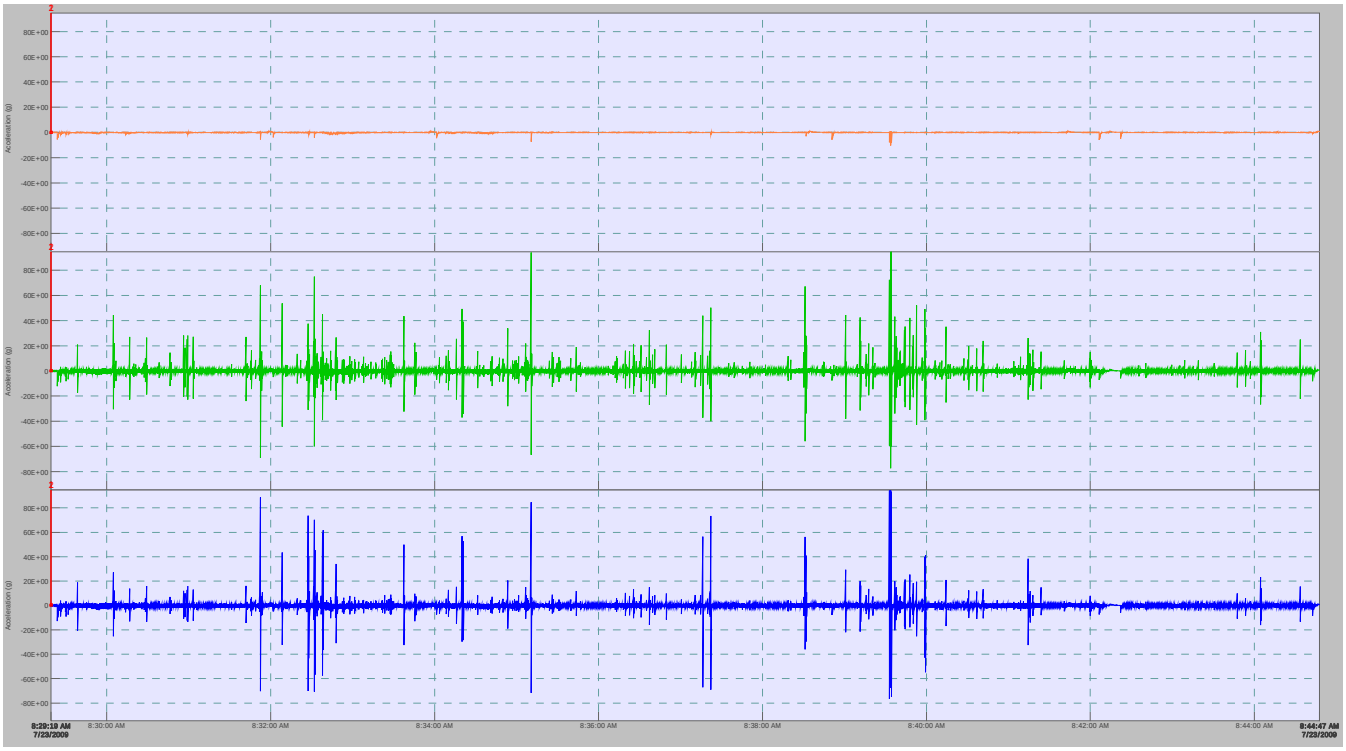

Figure 98: Accelerometer 5 (#71, Reference E)

The colors are assigned as follows:

- Orange: Input 13 (x axis)
- Green: Input 14 (z axis) *note that this data set is inverted from the rest of them
- Blue: Input 15 (y axis)

Average Spectrum Data

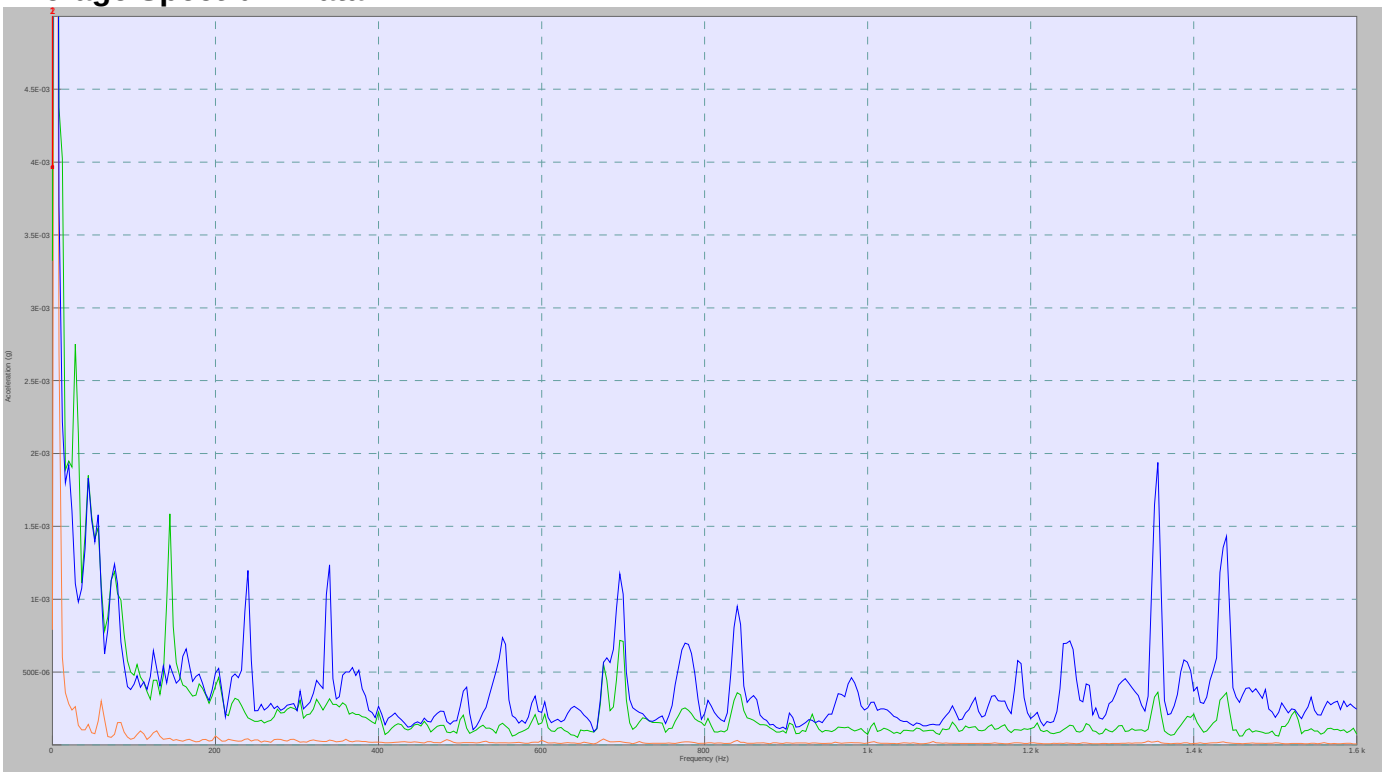

Figure 99: Accelerometer 5 (#71, Reference E)

The colors are assigned as follows:

- Orange: Input 1 (x axis)
- Green: Input 2 (axis)
- Blue: Input 3 (z axis)

Scale Information:

- X-axis: 0Hz to 1.6kHz
- Y-axis: 0g to 5E-3g

FRF Data

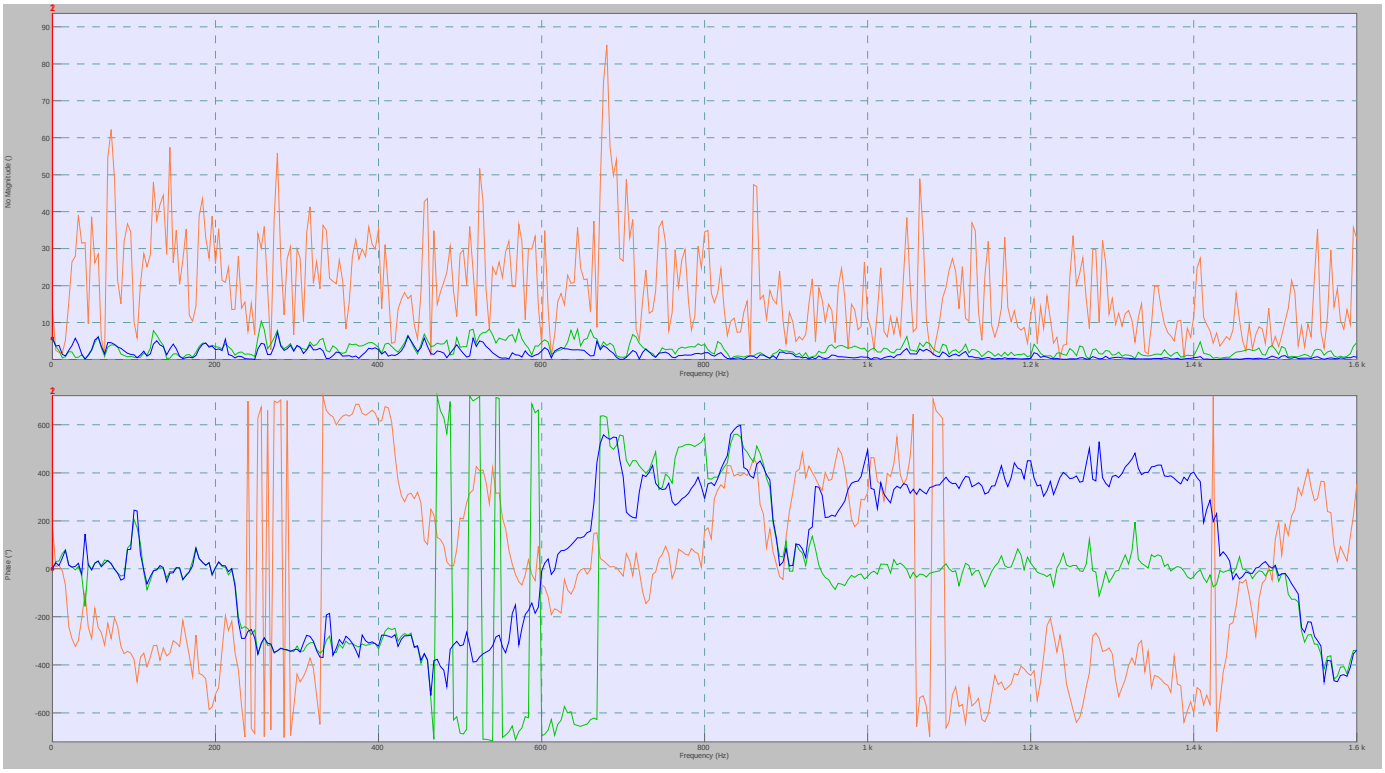

Figure 100: Accelerometer 5 (#71, Reference E)

The colors are assigned as follows:

- Orange: Input 13 (x axis)
- Green: Input 14 (z axis) *note that this data set is inverted from the rest of them
- Blue: Input 15 (y axis)

The graph scale data for the FRF data is as follows:

- Top Graph
    - x-scale 0Hz to 1.6kHz
    - y-scale: 0 to 94 no units
- Bottom Graph
    - x-scale 0Hz to 1.6kHz
    - y-scale: -720° to 720°

Day Two, Run Four

Driver: Richard Lawrance
Equipment Operator: Robert Dailey
Data Set Title**:** Morning Run 1 Holes 1 through 9, Robert and Richard

Accelerometer Data
Unless otherwise noted, the graph scales are as follows
Time domain graph scale:

- X-axis: 10:35:43am to 10:52:00am
- Y-axis: +90g to -50g

FRF data graph scale:

- Top Graph
    - X-axis 0Hz to 1.4kHz
    - Y-axis: 0 to 10 no units
- Bottom Graph
    - X-axis 0Hz to 1.4kHz
    - Y-axis: -720° to 720°

Average spectrum graph scale:

- X-axis: 0Hz to 1.4kHz
- Y-axis: 0g to 0.006g

Notes
This was manned by Robert and Richard. The top nine holes were repeated.

Time Domain Data

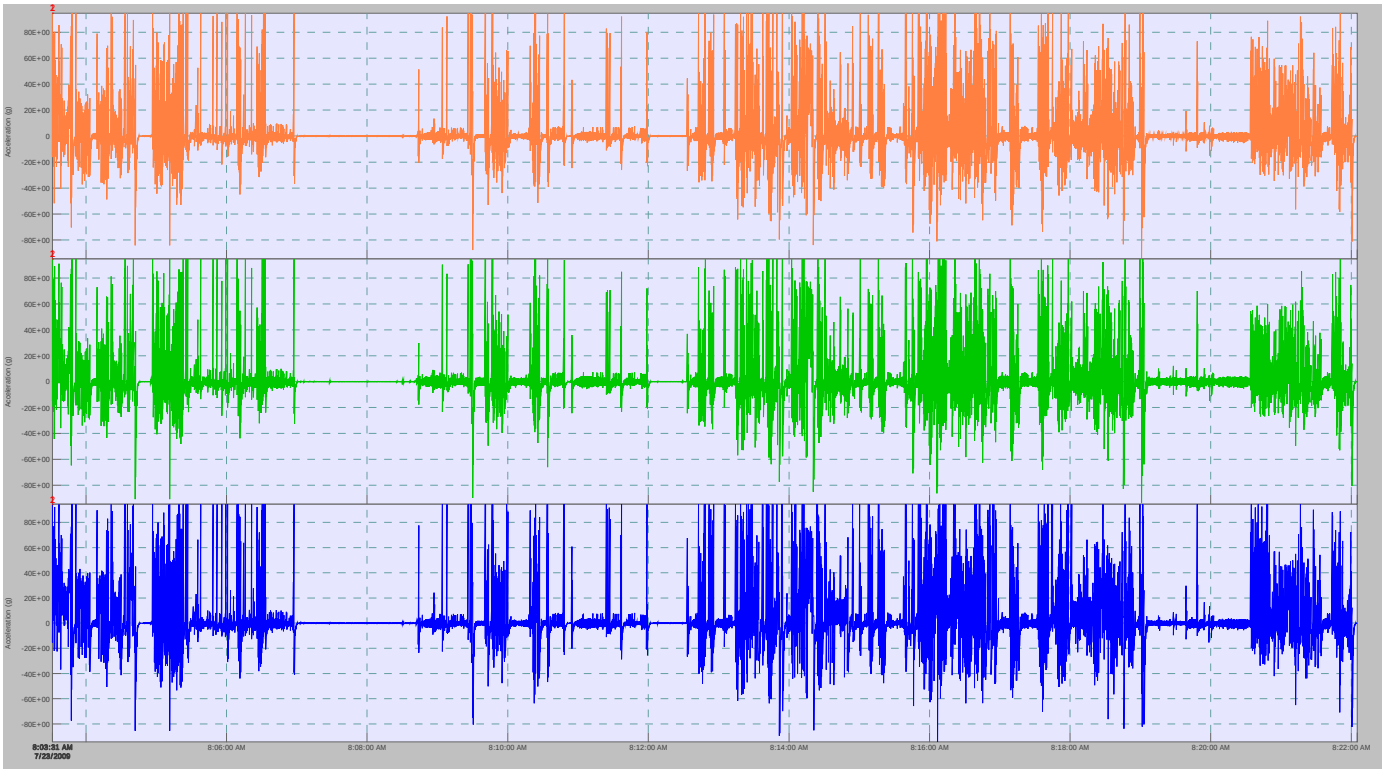

Figure 101: Accelerometer 1(#67, Reference A)

The colors are assigned as follows:

- Orange: Input 1 (x axis)
- Green: Input 2 (y axis)
- Blue: Input 3 (z axis)

Average Spectrum Data

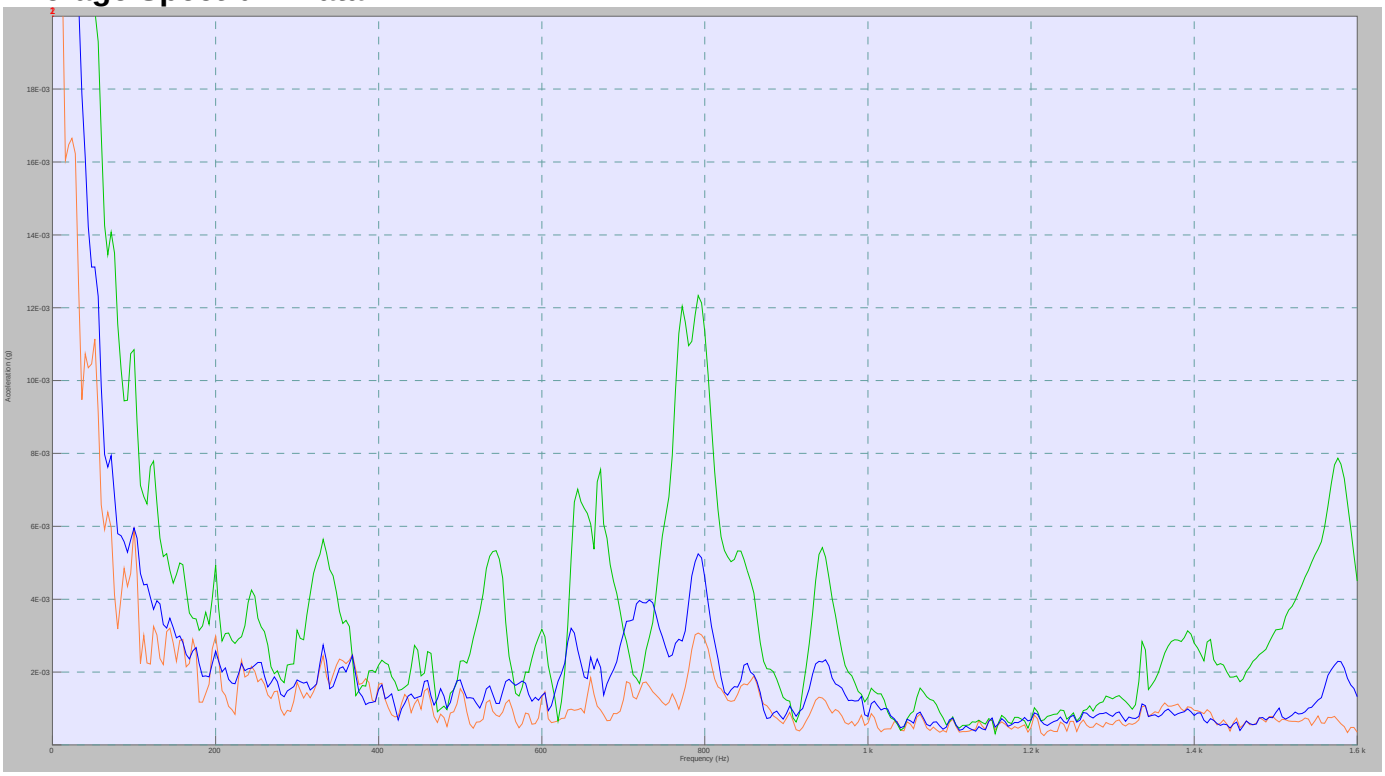

Figure 102: Accelerometer 1(#67, Reference A)

The colors are assigned as follows:

- Orange: Input 1 (x axis)
- Green: Input 2 (y axis)
- Blue: Input 3 (z axis)

Scale Information:

- X-axis: 0Hz to 1.6kHz
- Y-axis: 0g to 20E-3g

FRF Data

Figure 103: Accelerometer 1(#67, Reference A)

The colors are assigned as follows:

- Orange: Input 1 (x axis)
- Green: Input 2 (y axis)
- *No data for input 3*

The graph scale data for the FRF data is as follows:

- Top Graph
  - x-scale 0Hz to 1.6kHz
  - y-scale: 0 to 3 no units
- Bottom Graph
  - x-scale 0Hz to 1.6kHz
  - y-scale: -720° to 720°

Time Domain Data

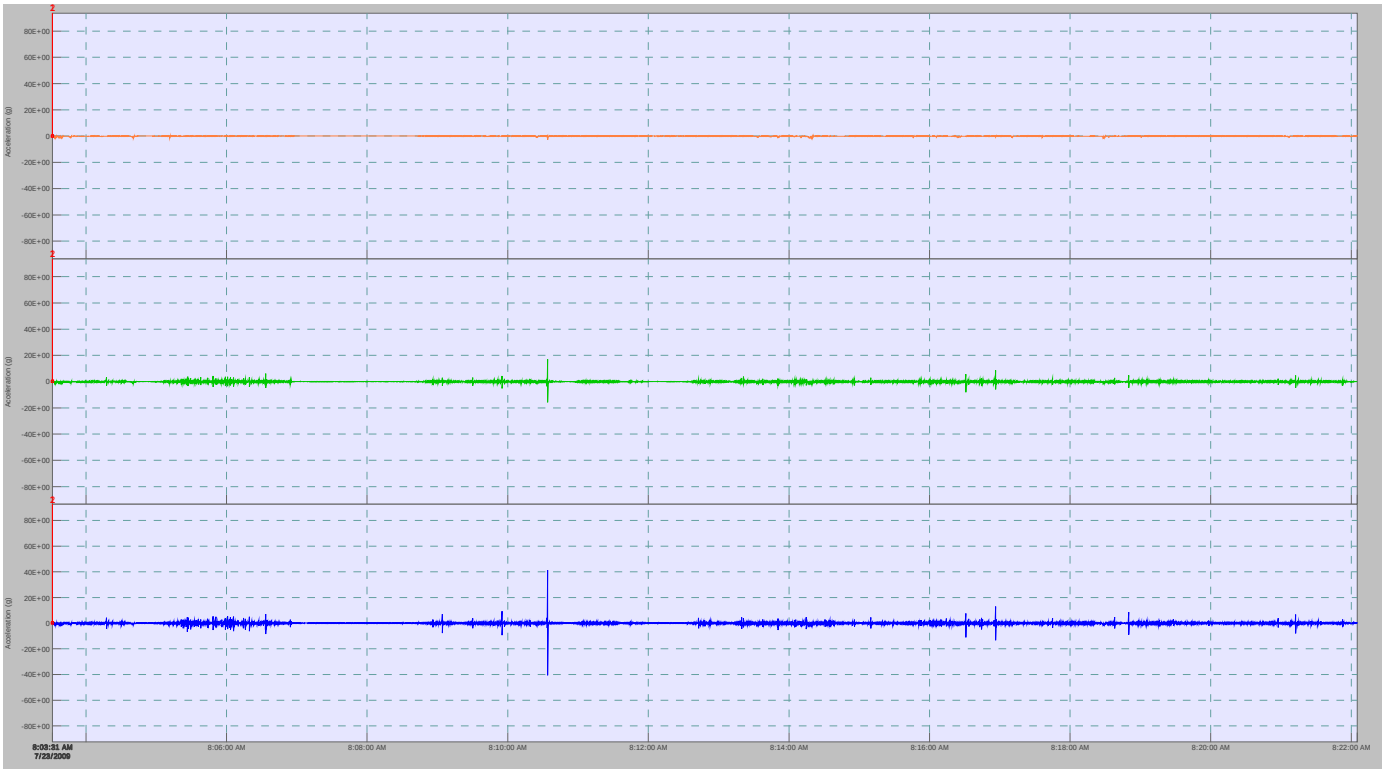

Figure 104: Accelerometer 2 (#68, Reference B)

The colors are assigned as follows:

- Orange: Input 4 (x axis)
- Green: Input 5 (z axis)
- Blue: Input 6 (y axis) *note that this data set is inverted from the rest of them

Average Spectrum Data

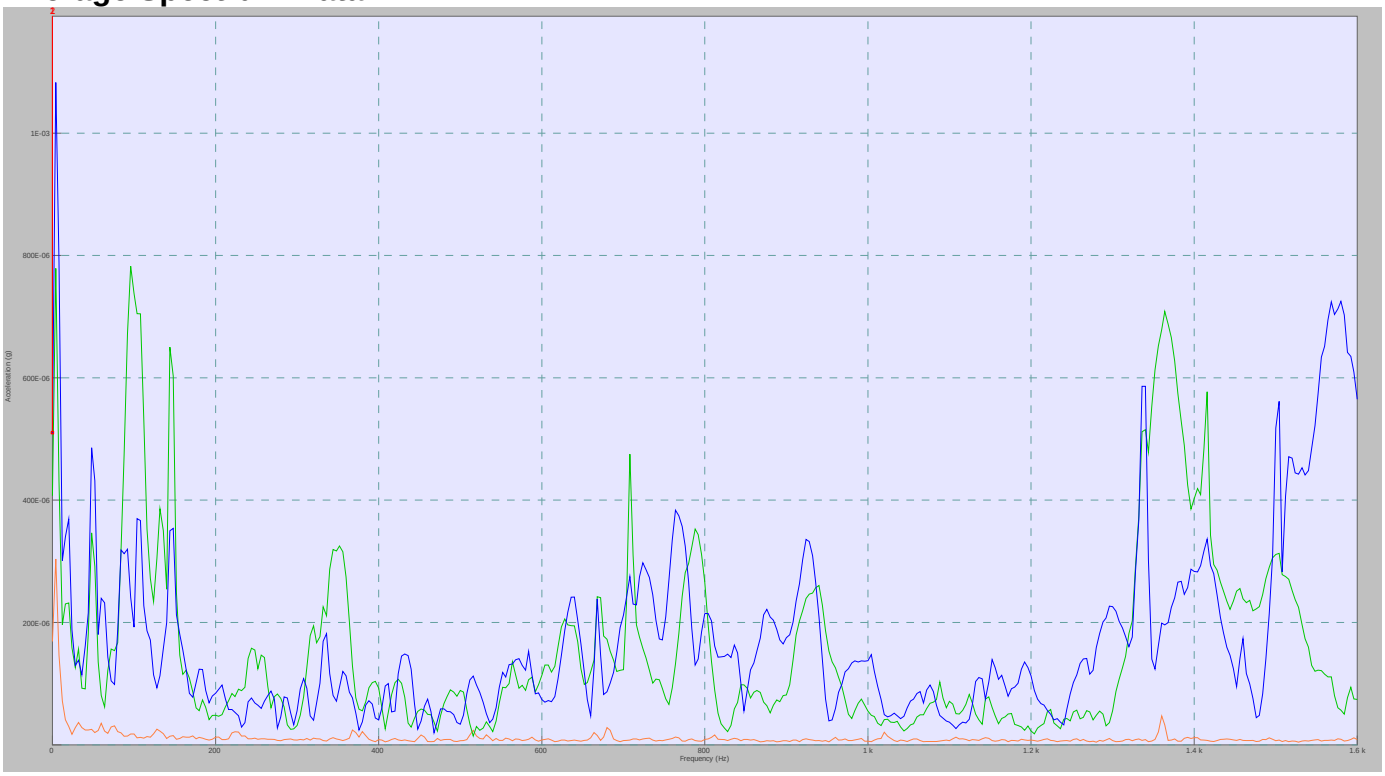

Figure 105: Accelerometer 2 (#68, Reference B)

The colors are assigned as follows:

- Orange: Input 1 (x axis)
- Green: Input 2 (z axis)
- Blue: Input 3 (y axis) *note that this data set is inverted from the rest of them

Scale Information:

- X-axis: 0Hz to 1.6kHz
- Y-axis: 0g to 1.2E-3g

FRF Data

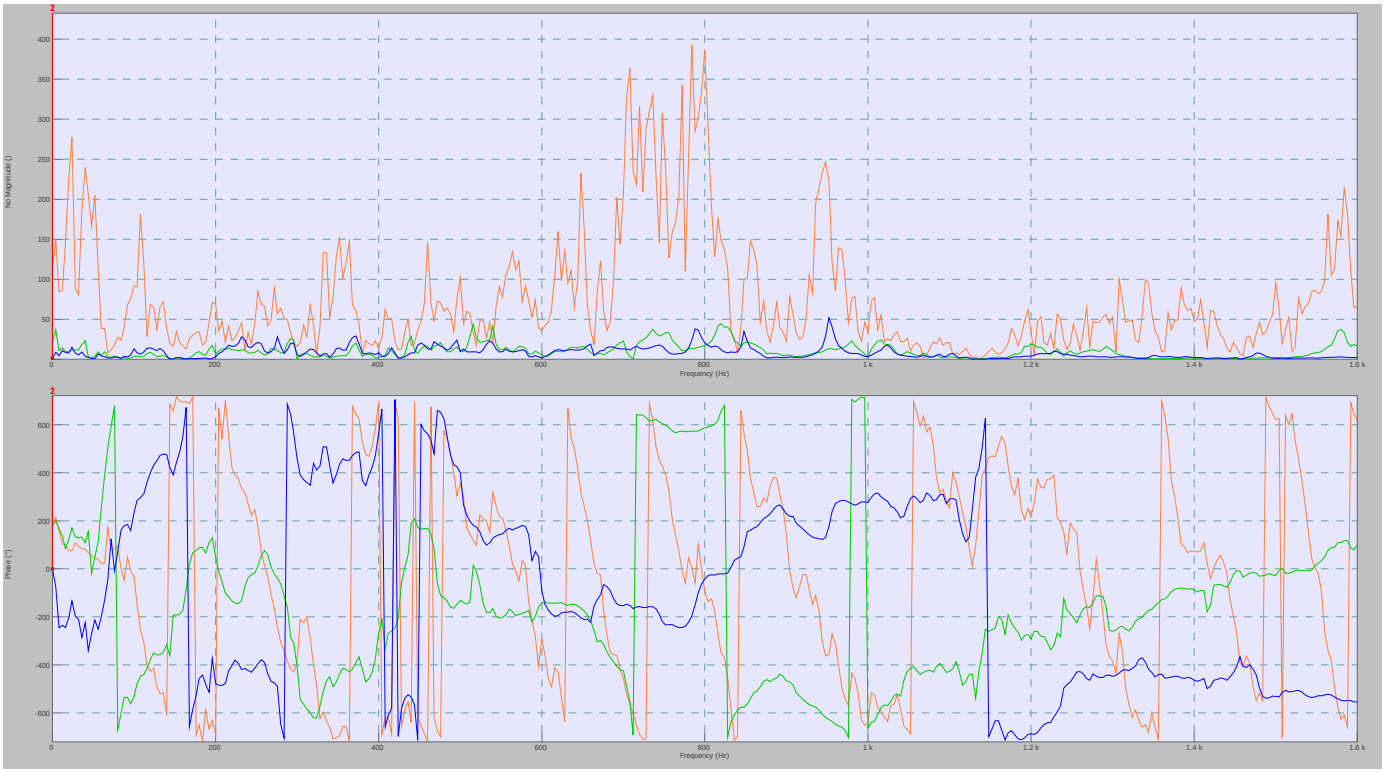

Figure 106: Accelerometer 2 (#68, Reference B)

The colors are assigned as follows:

- Orange: Input 4 (x axis)
- Green: Input 5 (z axis)
- Blue: Input 6 (y axis) *note that this data set is inverted from the rest of them

The graph scale data for the FRF data is as follows:

- Top Graph
    - x-scale 0Hz to 1.6kHz
    - y-scale: 0 to 430 no units
- Bottom Graph
    - x-scale 0Hz to 1.6kHz
    - y-scale: -720° to 720°

Time Domain Data

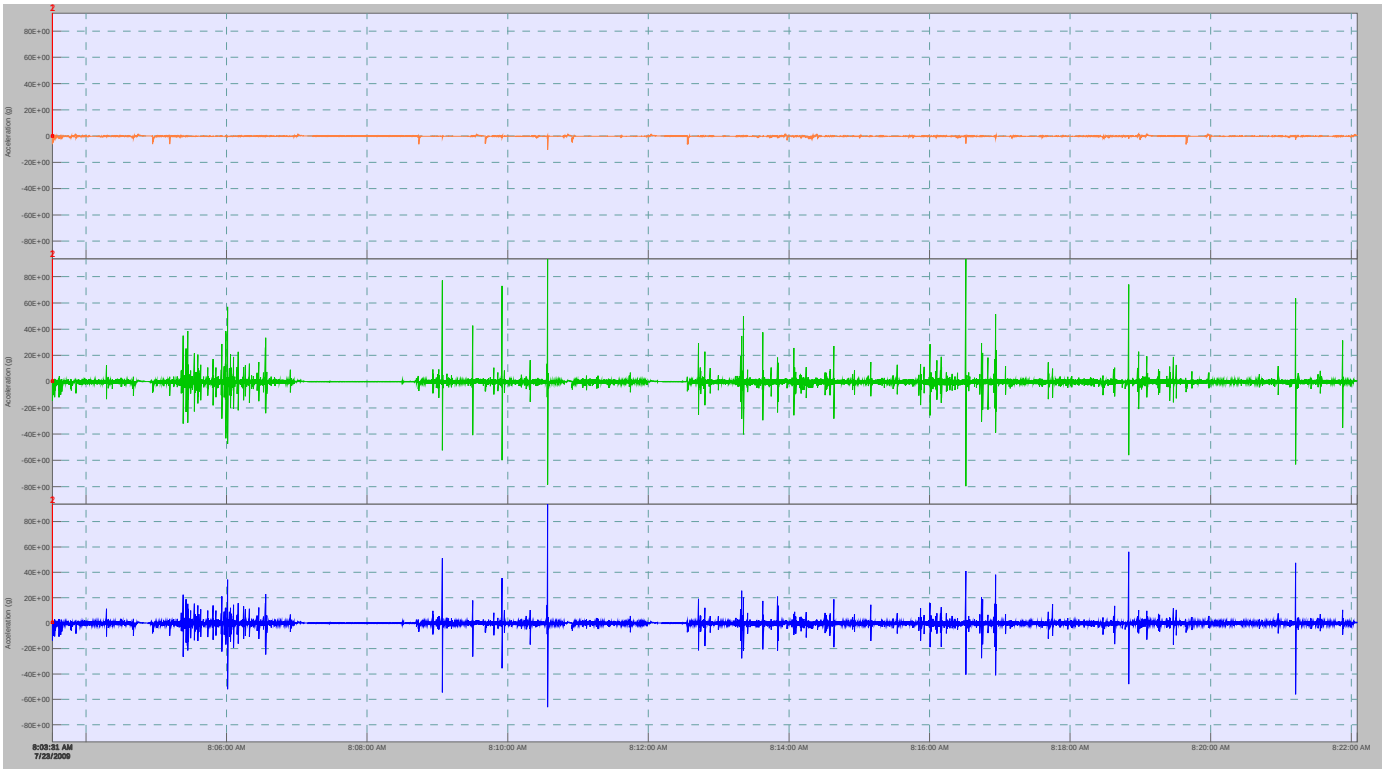

Figure 107: Accelerometer 3 (#69, Reference C)

The colors are assigned as follows:

- Orange: Input 7 (x axis)
- Green: Input 8 (y axis)
- Blue: Input 9 (z axis)

Average Spectrum Data

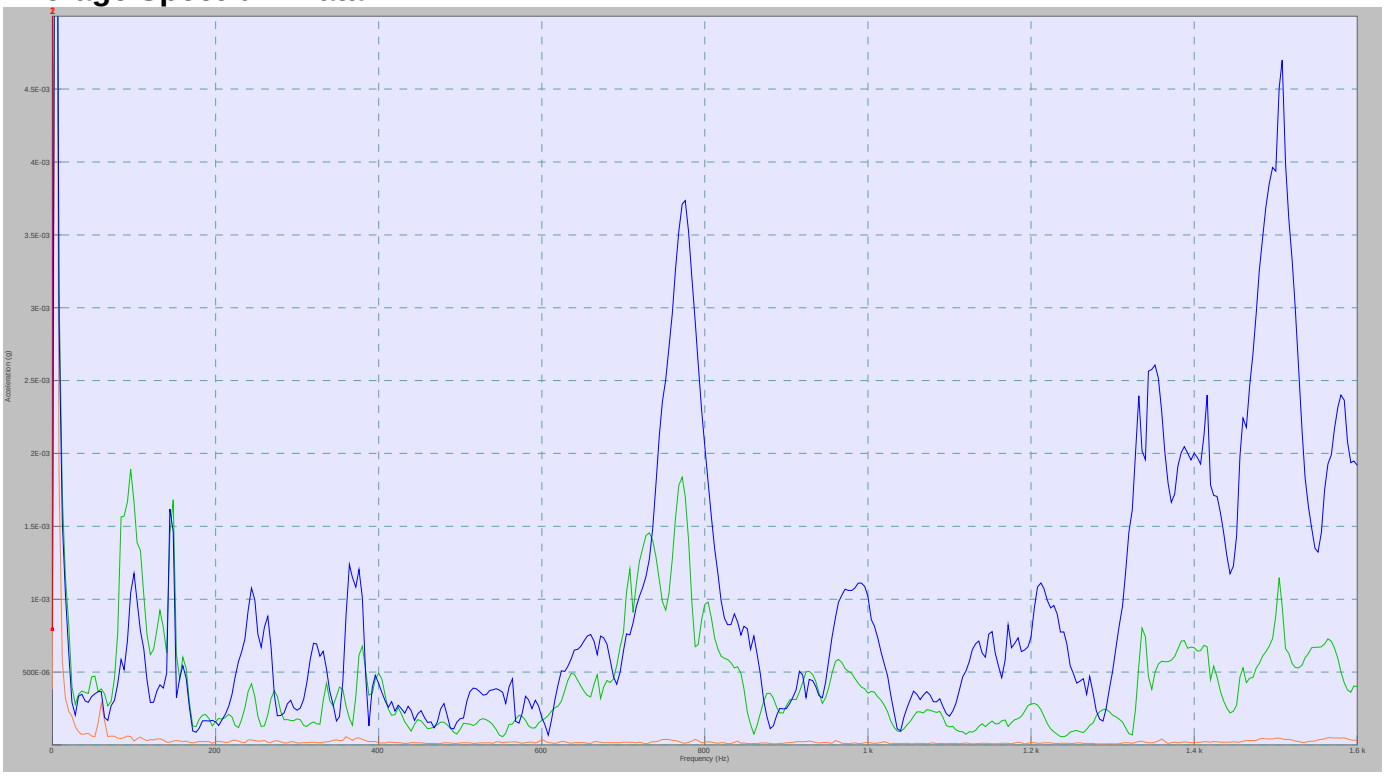

Figure 108: Accelerometer 3 (#69, Reference C)

The colors are assigned as follows:

- Orange: Input 1 (x axis)
- Green: Input 2 (axis)
- Blue: Input 3 (z axis)

Scale Information:

- X-axis: 0Hz to 1.6kHz
- Y-axis: 0g to 5E-3g

FRF Data

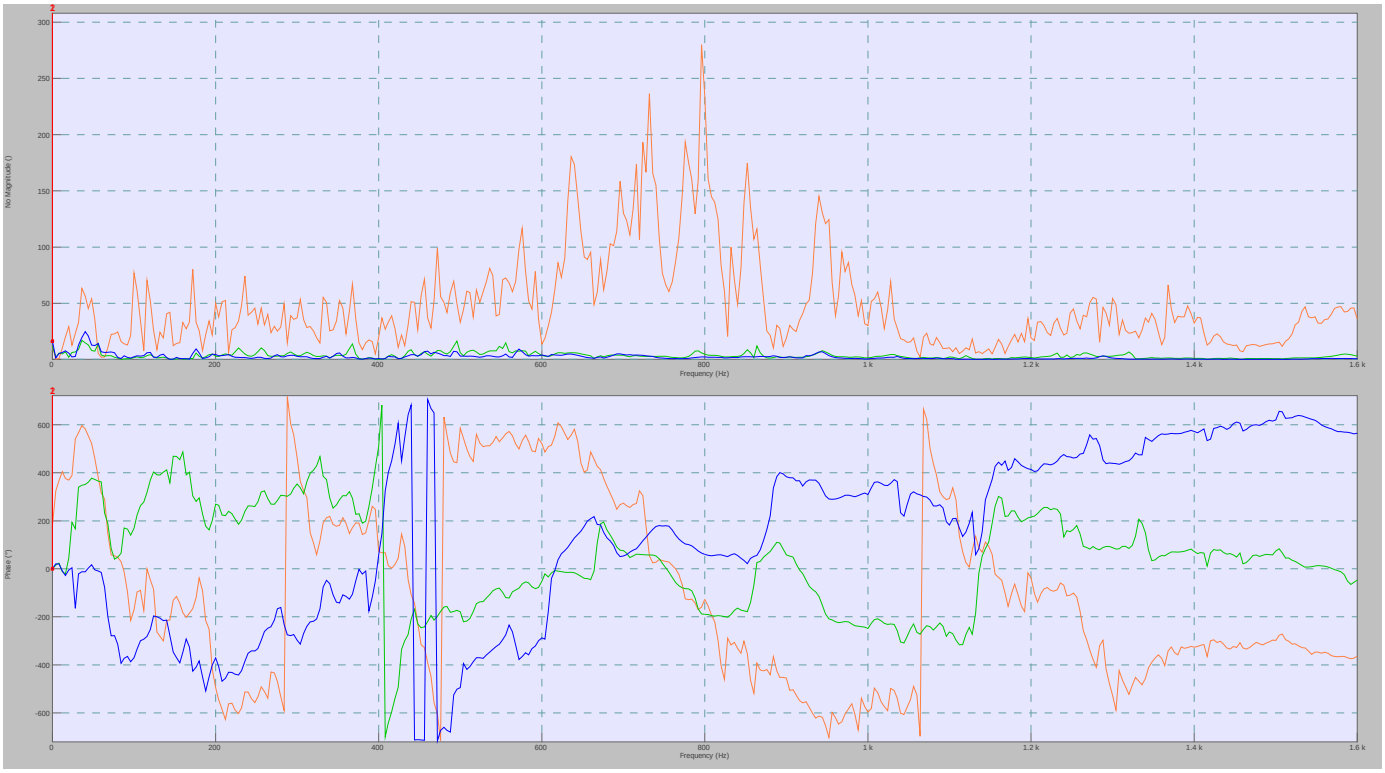

Figure 109: Accelerometer 3 (#69, Reference C)

The colors are assigned as follows:

- Orange: Input 7 (x axis)
- Green: Input 8 (y axis)
- Blue: Input 9 (z axis)

The graph scale data for the FRF data is as follows:

- Top Graph
    - x-scale 0Hz to 1.6kHz
    - y-scale: 0 to 308 no units
- Bottom Graph
    - x-scale 0Hz to 1.6kHz
    - y-scale: -720° to 720°

Time Domain Data

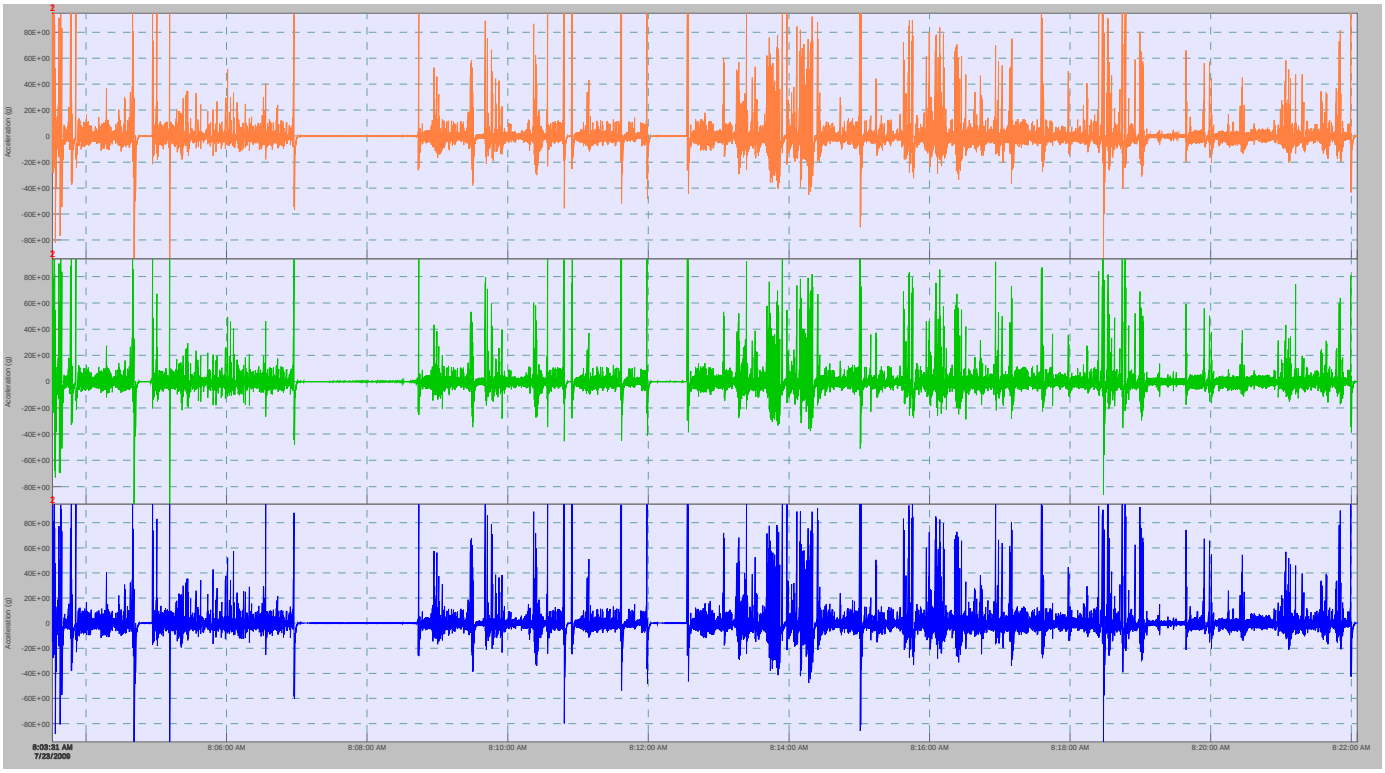

Figure 110: Accelerometer 4 (#70, Reference D)

The colors are assigned as follows:

- Orange: Input 10 (x axis)
- Green: Input 11 (y axis)
- Blue: Input 12 (z axis)

Average Spectrum Data

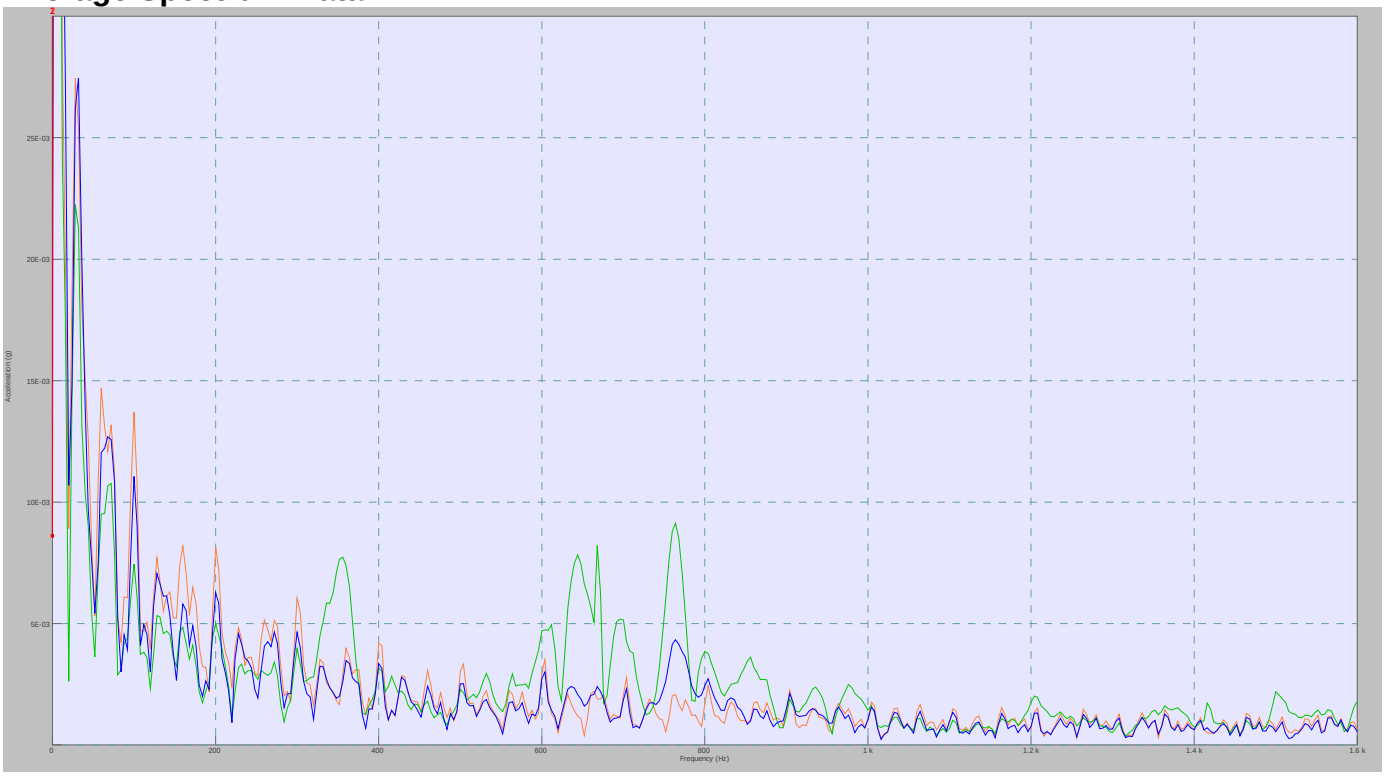

Figure 111: Accelerometer 4 (#70, Reference D)

The colors are assigned as follows:

- Orange: Input 1 (x axis)
- Green: Input 2 (axis)
- Blue: Input 3 (z axis)

Scale Information:

- X-axis: 0Hz to 1.6kHz
- Y-axis: 0g to 30E-3g

FRF Data

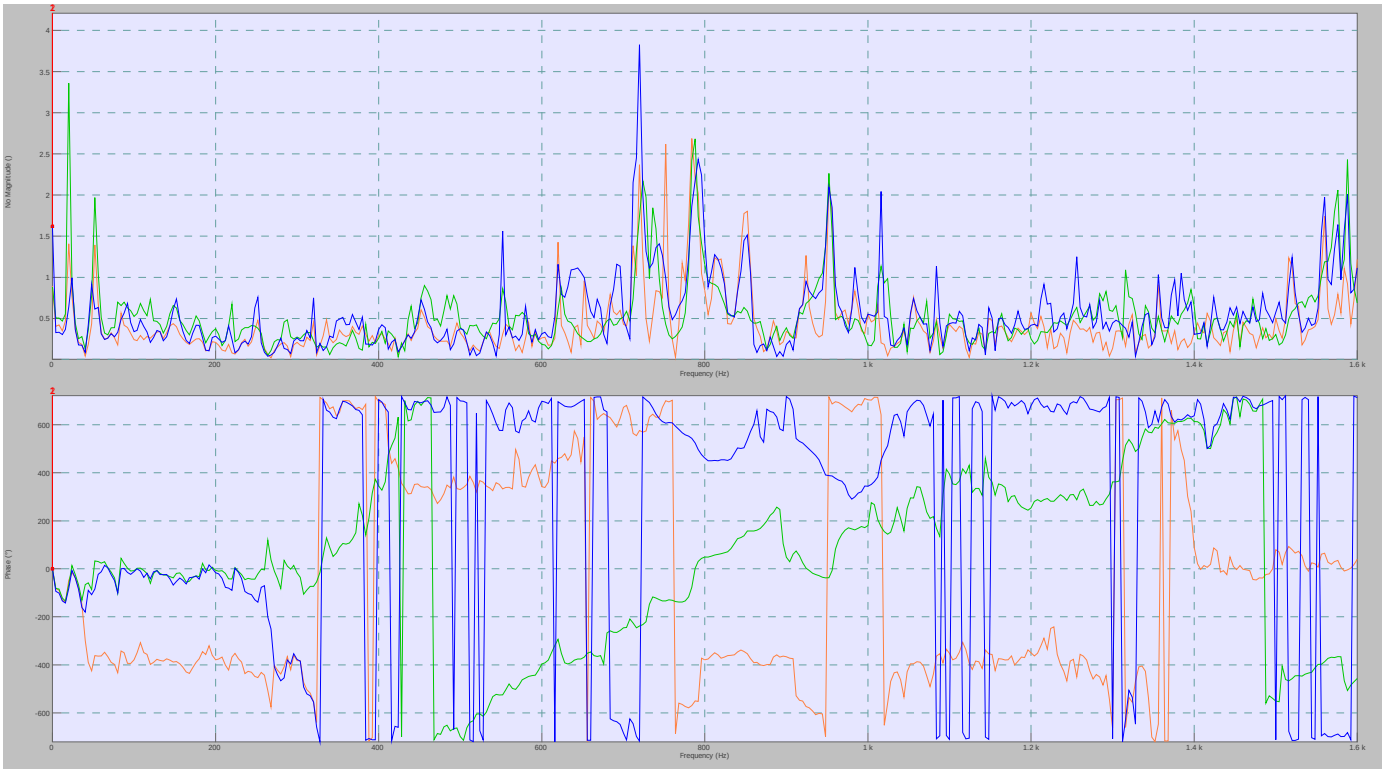

Figure 112: Accelerometer 4 (#70, Reference D)

The colors are assigned as follows:

- Orange: Input 10 (x axis)
- Green: Input 11 (y axis)
- Blue: Input 12 (z axis)

The graph scale data for the FRF data is as follows:

- Top Graph
    - x-scale 0Hz to 1.6kHz
    - y-scale: 0 to 4 no units
- Bottom Graph
    - x-scale 0Hz to 1.6kHz
    - y-scale: -720° to 720°

Time Domain Data

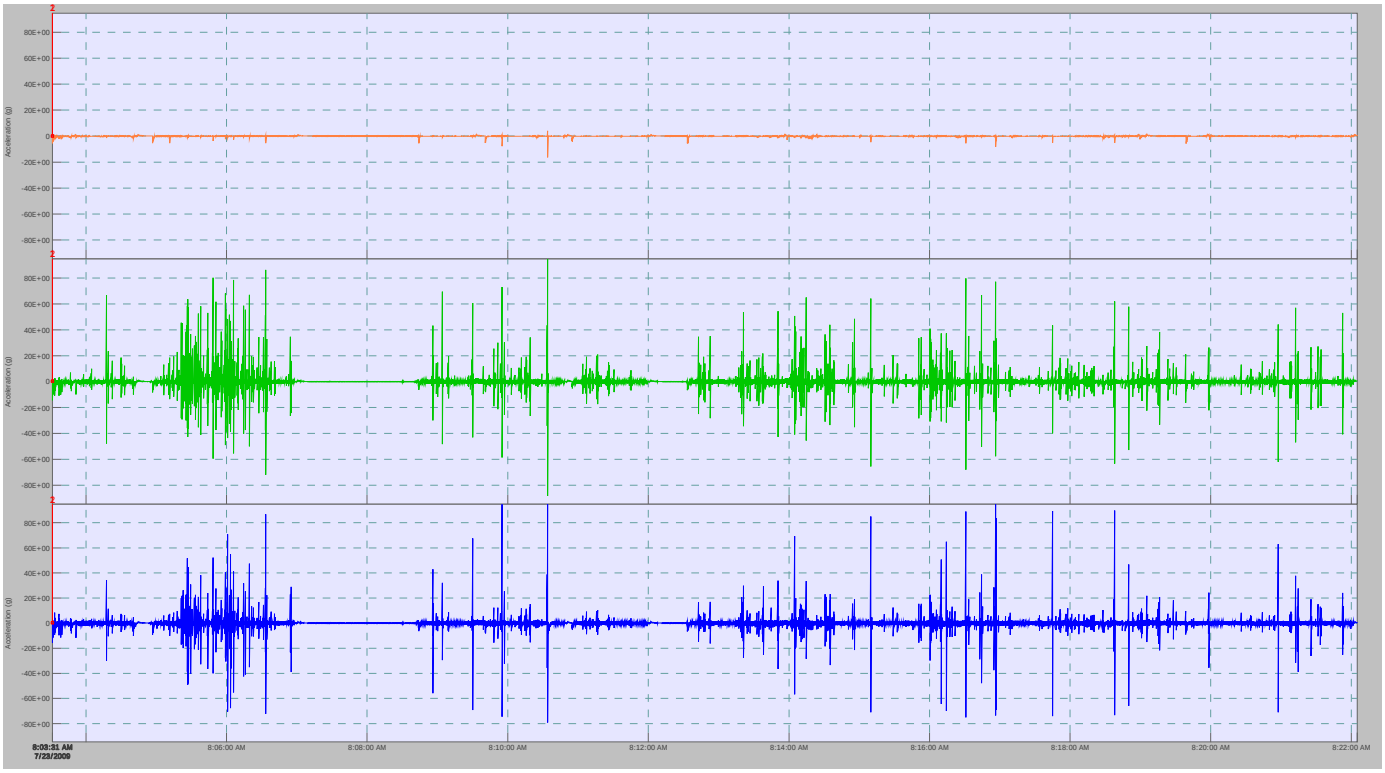

Figure 113: Accelerometer 5 (#71, Reference E)

The colors are assigned as follows:

- Orange: Input 13 (x axis)
- Green: Input 14 (z axis) *note that this data set is inverted from the rest of them
- Blue: Input 15 (y axis)

Average Spectrum Data

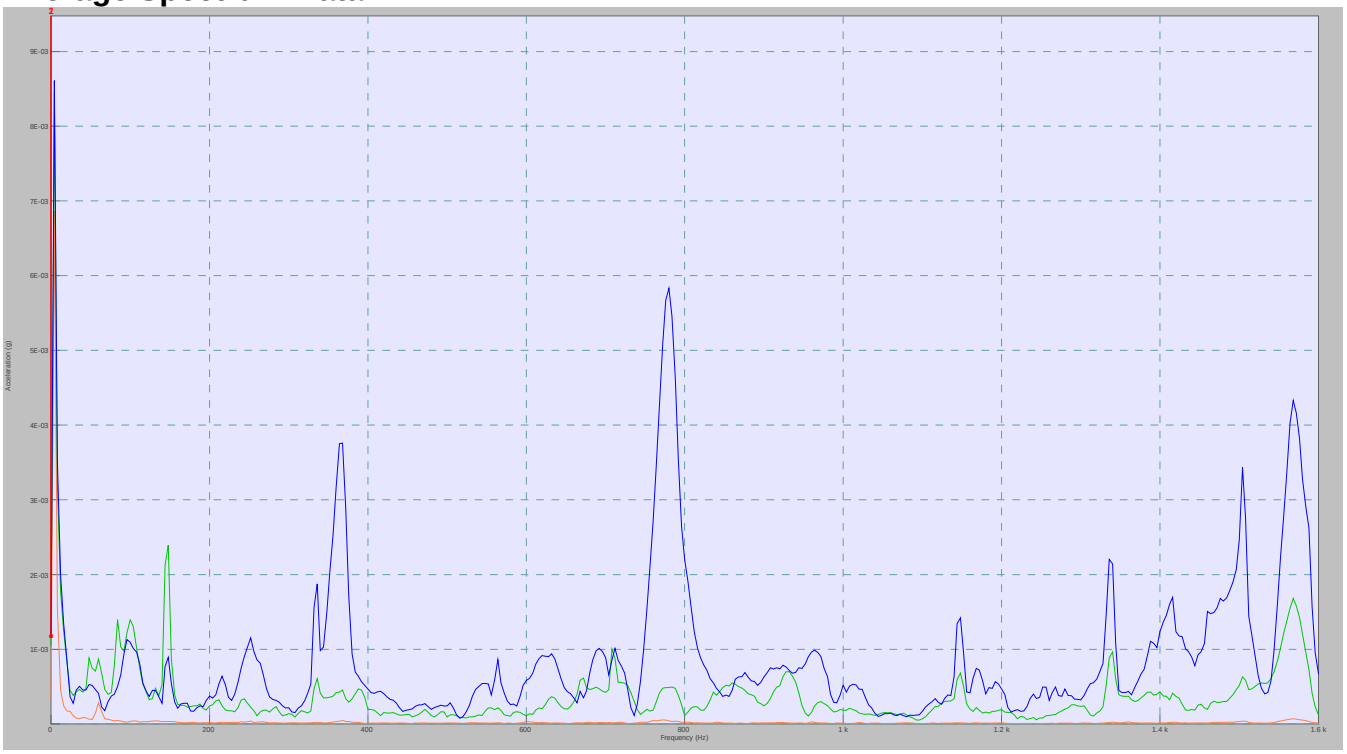

Figure 114: Accelerometer 5 (#71, Reference E)

The colors are assigned as follows:

- Orange: Input 1 (x axis)
- Green: Input 2 (axis)
- Blue: Input 3 (z axis)

Scale Information:

- X-axis: 0Hz to 1.6kHz
- Y-axis: 0g to 9E-3g

FRF Data

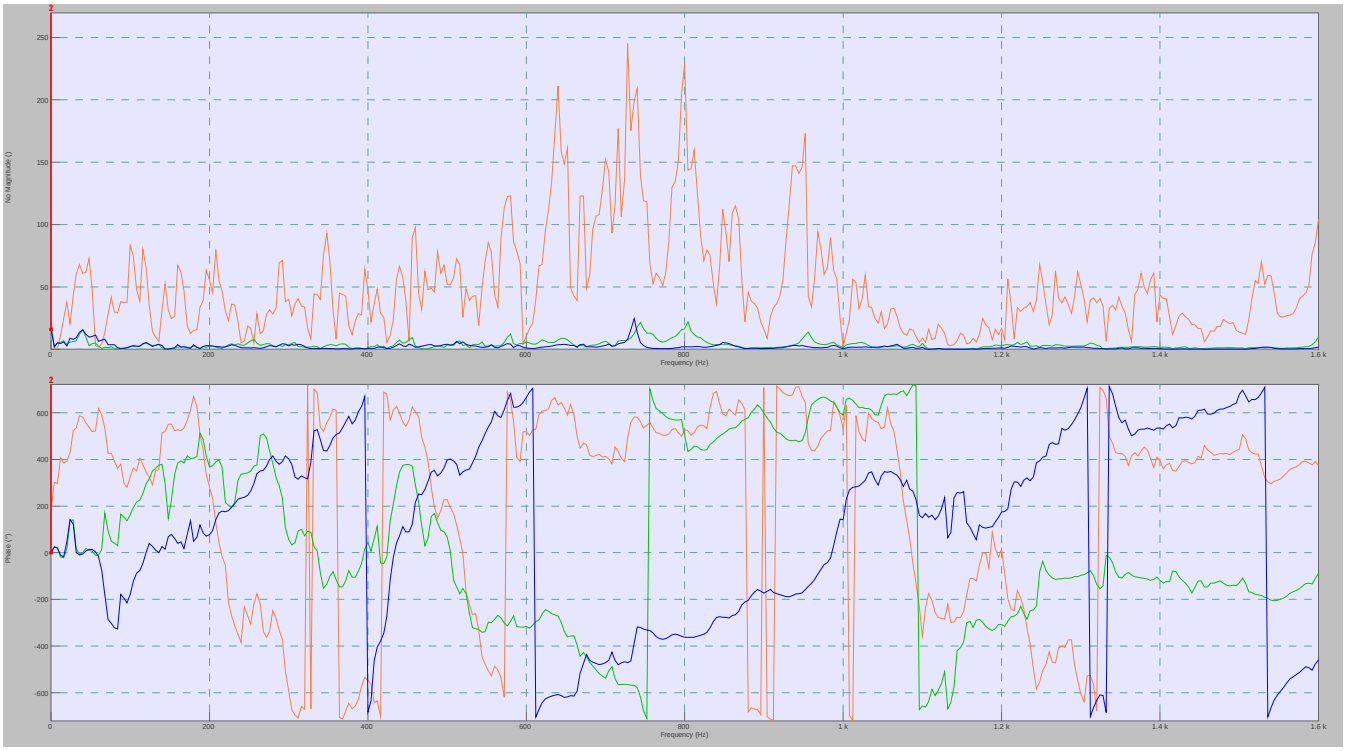

Figure 115: Accelerometer 5 (#71, Reference E)

The colors are assigned as follows:

- Orange: Input 13 (x axis)
- Green: Input 14 (z axis) *note that this data set is inverted from the rest of them
- Blue: Input 15 (y axis)

The graph scale data for the FRF data is as follows:

- Top Graph
    - x-scale 0Hz to 1.6kHz
    - y-scale: 0 to 270 no units
- Bottom Graph
    - x-scale 0Hz to 1.6kHz
    - y-scale: -720° to 720°

CONCLUSION

The conclusion that can be drawn data is that the vibration effects from the vehicle driving off road are fairly small overall. It appears that the brief impacts over time may be of more concern than the vibrations caused on the vehicle. This conclusion is drawn from the fact that while they were brief, there were impacts that resulted in measurements of more than 117.2g-force. On the other hand, the vibrations never seem to have a magnitude greater than 1g-force. Vibrations that were attributed to road travel were between the 0Hz and 20Hz range. While vibrations could be measured in all three axis, the amplitude of these vibrations were very small, the max being 9.97E-01 in the z axis during run 4 on day two.

It may also be beneficial to add some additional angle braces in the compartment of the vehicle. This may assist in reducing the horizontal vibrations measured. While the fuel cell stack could benefit from being mounted on vibration isolators to minimize the transfer of the horizontal vibrations into the structure of the stack, it does not seem to be of great concern if the stack is tightly attached to the chassis.

TASK 3 – AIR QUALITY STUDY

TASK 3.A - CHARACTERIZATION OF AIR CONTAMINATION IN OFF ROAD APPLICATIONS FOR FUEL CELL VEHICLES

Donaldson Co., Inc.
Prepared by Kevin Seguin

INTRODUCTION

When ambient air is used as a source of oxygen for the cathode in fuel cells, the life, durability and performance of the fuel cells are affected by air quality. The cathode catalyst and the electrolyte can be temporarily or permanently poisoned or damaged by contaminants that are present in the atmosphere such as sub-micrometer particulate matter, sulfur compounds, volatile organic compounds (VOCs), salts and oxides of nitrogen (NOx) etc. The concentration and type of these atmospheric contaminants vary with location, time of day and season. The removal of these contaminants is beyond the capability of current air contamination control systems (particulate filters) used in power plants such as engines and gas turbines. Therefore to maximize the performance, life and durability of PEM fuel cells, a new class of air contamination control is required.

The contamination of the cathode side of a PEM fuel cell can be divided into two main categories. The first category is poisoning of the catalyst by compounds that adsorb to the catalyst and occupy sites. Examples are VOCs and carbon monoxide. These compounds would be oxidized at elevated temperatures, but the operating temperature of most PEM fuel cells is about 80-120°C, thus preventing oxidation. The second category is either local or uniform contamination of the cathode/membrane interface by contaminant ions[1]. Examples of contaminant ions are sodium, potassium, calcium, copper, zinc and magnesium. It has been found that contamination of the cathode side of a PEM fuel cell is even more serious than that of the anode side[1]. The electrolyte in PEM fuel cells is acidic, and base gases and particles such as ammonia, salts and limestone etc. may be harmful to the electrolyte. In general, the contamination issue for fuel cells is very different than that of traditional power systems such as internal combustion engines and gas turbines. Large particulate matter is filtered out of the combustion air in engines to prevent wear, but CO and VOCs are not of concern as they are fuels for the combustion process. Sub-micron particulate matter and chemicals are not filtered from the combustion air in engines, as they are harmless. If the same level of filtration is applied to the cathode air in PEM fuel cells, contaminant ions and chemicals may permanently degrade the fuel cell.

Air contaminants vary with location in both composition and magnitude. Particulate matter for example, varies nine orders of magnitude in concentration from calm days over the ocean to a windy day in the desert. In addition, the size distribution of the particulates varies depending on the source of the particulate matter. Figure 1 describes in general terms how the contaminants vary with environmental conditions and

location[1].

GEOGRAPHIC AREA	URBAN Major metropolitan areas with heavy industry and motor vehicles	RURAL/ ARCTIC Forest, tundra and agriculture	OFF-SHORE AND MARITIME	DESERT	TROPICAL
ENVIRONMENTAL CONDITIONS	Rain, fog, smog, snow. 28°F to 100°F (-2°C to +38°C). Corrosive chemicals, VOCs, SO2, gummy soot particles, NOx, NH3, and dried salts.	Snow, freezing rain, frost. -40°F to 90°F (-40°C to +32°C). Dry, noncorrosive fibrous particles, ammonia, SO2, and blowing dust.	Wet and dry salt, corrosive particles. 0°F to 90°F (-18°C to +32°C). Blowing rain, salts, sea spray, fog, snow and ice.	Dry, sunny. 32°F to 122°F (0°C to +50°C). Sandstorms, whirlwinds, dry, corrosive particles, clays and salts.	Heavy rainfall. 40°F to 122°F (+5°C to 50°C). Fibrous noncorrosive particles, molds and insects.
PARTICLE CONCENTRATION (µg/m^3)	50 – 175	<150	<135	>350,000	<135
PARTICLE SIZE RANGE (Micrometers)	0.01 – 30	0.01 – 75	0.01 – 10	0.01 – 500	0.01 - 10

Figure 1: Types of Contaminants vs. Geographic area

Volatile Organic Compounds (VOCs) such as unburned hydrocarbon emissions from internal combustion engines vary greatly in concentration depending on location and the sources of emissions. Urban areas in cold climates experience days with significantly elevated levels of VOCs due to cold started internal combustion engines. Areas where two cycle internal combustion engines are operated have high concentrations of carbon monoxide and VOCs. A city can have relatively low average concentrations of VOCs, but have local areas where the concentrations are elevated. Sulfur compounds in the air are found wherever fuels containing sulfur are combusted, agricultural areas such as hog farms or industrial sources such as pulp mills. Typical average concentrations of a few select pollutants in various cities listed in Figure 2 illustrates the variation that can occur between locations. In extreme situations such as in battlefields, warfare gases and other pollutants can be present in the air in concentrations listed in Figure 3[1].

	SO2 (ppb)	PM10 (µg/m^3)	Benzene (ppb)
Perth, Australia	2.0	21	
London, UK	11.0	29	1.8
Rome, Italy	1.0	52	3.7
Paris, France	5.0		
Berlin, Germany	6.0	31	2.8
Shanghai, China	20.0		
Delhi, India	9.0	162	
Taipei, Taiwan	4.0	44	
Moscow, Russia	41.0		
Cairo, Egypt	26.0		
Stockholm, Sweden	2.0	25	
New York, US	9.0	17	3.0
Los Angeles, US	2.0	139	1.0
Houston, US	2.6	29	0.8
Minneapolis, US	9.8	25	0.5
Vancouver, Canada	2.0	14	0.7
Mexico City, Mexico	28.0	53	
Sao Paulo, Brazil	16.0	54	

Figure 2: Average ambient air contaminants vs. Location

Contaminant	Concentration (PPM)
Carbon Monoxide	20
Sulfur Dioxide	0.5
Benzene	50
Propane	90
Nitrogen Dioxide	0.4
Cyanogan Chloride (CNCL)	780-1560
Hydrogen Cyanide (HCN)	1780-3560
Sulfur Mustard	15
Sarin	170-340

Figure 3: Concentrations of Contaminants in a Battlefield

LITERATURE SEARCH

Particulate Contaminants

Particulate matter (PM) is typically in the size range of 10 nanometers to 100 micrometers in diameter. $PM_{2.5}$ refers to the concentration of “fine” particles that are less than 2.5 microns. PM_{10} referse to the concentraions of ‘coarse” particles, less than 10 microns in diameter Particulate matter can also be classified as primary or secondary particles. Primary particles, such as dust from roads or elemental carbon (soot) from diesel fuel or wood combustion, are emitted directly into the air. Secondary particles are formed in the atmosphere from gaseous emissions such as sulfates formed from SO2, or nitrates formed from NO_x emissions from automobiles, power plants and other industrial combustin sources. The USEPA[2] has reported the average concentration in ambient environments od PM_{10} ranges from 20-40 $\mu g/m^3$. Much higher

concentrations are found in more polluted urban environments. In addition, off road vehicles are subject to higher concentration from road or soil dust.

Barris[3] reported an average ambient range of 10-139 μg/m^3. Paved roads ranged from 139 μg/m^3 to 57 mg/m^3, and dirt roads from 139 μg/m^3 to 6113 mg/m^3.

Condition	Dust Concentration (mg/m3)
Avg. Ambient	0.010-0.139
95th % Ambient	0.089
99th % Ambient	0.112
Paved Roads	0.139-57
Dirt Roads	0.139-6113
Dust Storms	0.1-176
Worst Dust Storm	3000
0 Visibility	883
20x0 Visibility	17657

Table 1: Range of Dust Concentrations in Various Engine Environments

Besse[4] studied the particle size distribution as a function of height above a dirt road traveled by Light Armored Vehicles (LAVs). A sampling system was set up to take samples from 1-3 meters above the ground at 0.3 meter intervals. The stand was located 2 meters from the road. They found that there was only a minor shift toward the smaller particles as height increased (Table 2). As expected, the weight percent at each height decreased with increasing height (Table 3). The increase at 1.6 meters was attributed to air currents caused by the vehicles body configuration or exhaust system.

Particle Size Distribution as a Function of Height									
Height (m)	4	5	6	7	8	9	10	15	20
0	330	222	178	139	107	87.9	74.2	47.3	23
1	435	278	222	173	134	109	92.5	48.9	29.9
1.3	434	285	229	179	140	115	97.1	51.9	31.8
1.6	493	322	257	199	153	124	103	52	30.6
2	498	329	264	206	159	128	107	54.4	32.7
2.3	476	307	246	191	148	121	101	53.6	32.6
2.6	491	318	253	197	152	124	104	55.1	33.6
3	514	348	280	217	166	134	112	55.6	32.8

Table 2: Particle size distribution as a function of height

Height, m	Percentage, %
1	20.8
1.3	14.5
1.6	18.4
2	13.5
2.3	10.7
2.6	9.4
3	9.7
3.3	3.0

Table 3: Weight percentage of total airborne particulate at each height

Chemical Contaminants

Basic make Up of Air

Air is widely established to contain 78.03-78.08% nitrogen, 20.95-20.99% oxygen, 0.94% argon, 0.03-0.04% carbon dioxide, 0.001-0.002% neon, 0.0005% helium, 0.0001% krypton, 0.00005% hydrogen, and 0.000009% xenon, and this basic composition is relatively constant. Other compounds maybe present and the concentrations and nature of these compounds can vary widely from location to location and in a specific location from day to day based on atmospheric conditions and local activity.

Measuring Contaminants

Chemical contaminants are usually reported as either mass per volume of air such as micrograms per cubic meter ($\mu g/m^3$), or part per billion by volume (ppb). Part per billion is defined as the volume of the gaseous contaminant divided by the volume of air times one billion.

$$ppb = \frac{V_c}{V_a} \times 10^9$$

The number of molecules in a given volume of air at constant temperature and pressure will always be constant. This concept is known as Avogadro's law. Most Chemical detectors are concentration dependant and measure the number of molecules of a particular species in a given volume. The concentration is then reported as part per billion or part per million. This measurement is useful for determining the relative amount of one contaminant to the next. The value of the measurement in ppb will also be independent of temperature and pressure since the volume of both the contaminant and air will increase proportionally with increased temperature and decrease proportionally with increased pressure.

The ideal gas law further describes the relationship between a volume (V) of gas at a given temperature (T), and pressure (P), and the number of molecules or moles (n).

$$PV = nRT$$

R is the ideal gas constant and is dependent on the units of measurement. The mass (m) of a contaminant can be calculated from the number of moles divided by the molecular weight (M).

$$n = \frac{m}{M}$$

Therefore,

$$PV = \frac{m}{M}RT$$

The mass of a contaminant in a specific volume is then dependant on pressure, temperature, and the molecular weight of the contaminant. The value is usually assumed to be at standard temperature and pressure, 760 mmHg, and 25ºC. At this temperature and pressure, ppb can be converted to $\mu g/m^3$ with the equation[5]:

$$\mu g/m^3 = \frac{C_{ppb}M}{24.5}$$

Reported Levels of Various Contaminants

Chemical contaminants in the air can be divided up in to three classes 1) acid gases 2)

base gases 3) volatile organic compounds (VOCs). Acid gases are gases that will form acids when mixed with water. Common examples are sulfur dioxide (SO_2) which will form sulfuric acid (H_2SO_4) when dissolved in water, and nitrogen oxide (NO) or nitrogen dioxide (NO_2) which will form nitrous acid (HNO_2) and nitric acid (HNO_3) when dissolved in water. Nitrogen oxide and nitrogen dioxide are often combined and referred to as oxides of nitrogen and represented as NO_x. Base gases are gases that will form base solutions with water such as ammonia (NH_3) which forms ammonium (NH_4OH) when dissolved in water. Acid and base gases can also combine to form salts and can agglomerate to form secondary particles. Organic compounds are a broad class of compounds containing carbon chains or rings and hydrogen, and often also contain other elements such as oxygen, nitrogen, sulfur, etc. Volatile organic compounds are compounds that readily evaporate under room temperature and pressure. VOCs are common and ubiquitous. They are solvents used in paints and building materials, aerosols, fuels such as gasoline and diesel fuel, petroleum distillates and other industrial products. They are also emitted from plants and animals by off gassing or respiration. Acid gases and VOCs have been found to be particularly detrimental to fuel cell performance.

The USEPA[2] has set national air quality standards for six principal air pollutants nitrogen dioxide (NO_2), ozone (O_3), sulfur dioxide (SO_2), particulate matter (covered in section 2.1), carbon monoxide (CO), and lead (Pb). Typical concentrations, as given by the EPA are given in Table 4.

Contaminant	Concentration in ppb ($\mu g/m^3$)
Nitrogen dioxide	10-40 (19-75)
Sulfur dioxide	1.0-10 (2.6-26)
Ozone	50-200 (98-391)
Carbon monoxide	2-6 (2.3-6.8)
Lead	0-0.1 (0.8)

Table 4: Average Annual Concentration of Principal Air Pollutants

The EPA defines toxic air pollutants as those compounds that may cause serious health problems[6]. Typical examples of toxic air pollutants are benzene, perchloroethylene, and methylene chloride. Most toxic air pollutants, like those listed, are anthropogenic, but some are also released from natural sources such as forest fires. The Clean Air Act identifies 188 compounds from industrial sources. The EPA and state agencies monitor selected compounds and have compiled data to establish risk assessments and create maps that model ambient concentrations for a given compound across the nation. Table 5 shows some compounds of interest with the highest, median, and lowest concentrations. Concentration maps, shown in Appendix A, illustrate how widespread common VOCs are in the atmosphere. All of these compounds could adversely affect fuel cell performance.

Compound	Highest ppb (µg/m^3)	Media ppb (µg/m^3)	Lowest ppb (µg/m^3)
Acetaldehyde	2.6 (4.75)	0.07 (0.13)	0.0006 (0.001)
Acrolein	0.26 (0.6)	0.15 (0.34)	$6.6x10^{-5}$ ($1.5x10^{-4}$)
Benzene	1.5 (4.76)	0.2 (0.65)	0.15 (0.48)
Carbon tetrachloride	0.15 (0.94)	0.14 (0.88004)	0.14 (0.88000)
Ethylene dichloride	0.035 (0.14)	0.015 (0.062002)	0.015 (0.062000)
Formaldehyde	5.6 (6.81)	0.38 (0.46)	0.20 (0.25)
Methylene chloride	0.85 (2.94)	0.045 (0.17)	0.043 (0.15)
Perchloroethylene	0.20 (1.39)	0.022 (0.149)	0.020 (0.140)
Tetrachloroethane	0.16 (1.08)	0.012 (0.084)	0.012 (0.0810)

Table 5: Concentrations of common pollutants as measured by the EPA

Jacobson[7] reported concentrations of variable gases in polluted and clean troposphere.

Compound	Clean Troposphere	Polluted Troposphere
Inorganic		
Carbon monoxide	40-200 (46-229)	2000-10000 (2286-11428)
Sulfur dioxide	0.02-1 (0.05-2.6)	1-30 (2.6-78)
Nitric oxide	0.005-0.1 (0.006-0.12)	0.05-300 (0.06-367)
Nitrogen dioxide	0.01-0.3 (0.019-0.56)	0.2-200 (0.84-845)
CFC-12	0.55 (2.7)	0.55 (2.7)
Organic		
Methane	1800 (1175)	1800-2500 (1175-1632)
Ethane	0-2.5 (0-3.1)	1-50 (1.2-61)
Ethene	0-1 (0-1.1)	1-30 (1.1-34)
Formaldehyde	0.1-1 (0.12-1.2)	1-200 (1.2-245)
Toluene		1-30 (3.8-112)
Xylene		1-30 (4.3-130)
Methylene chloride	0.61 (2.10)	0.61 (2.1)

Table 6: Concentration of variable gases in clean and polluted troposphere in ppb (µg/m^3)

Data obtained from the World Health Organization are in agreement with Jacobson's report and show that, as expected heavily populated urban areas have very high concentrations of carbon monoxide

Cross[8] reported on data from a literature search on ambient pollutants in urban, rural and military battlefield environments. He found that in urban and rural environments eight pollutants accounted for over 99.9% of all measured pollutants. The most common pollutants found in urban and rural environments were carbon monoxide (CO), particulate matter less than 10 microns in size (PM_{10}), SO_2, toluene, ozone, NO_2, particulate matter less than 2.5 microns in size ($PM_{2.5}$) and formaldehyde. In urban

environments CO was the most prevalent pollutant due to automobile exhaust; in rural environments PM_{10+} was the most prevalent due to road dust and blown dirt. In heavily polluted battlefield environments there were fifteen chemicals accounting for over 99.5% of the pollutants. Carbon monoxide was again the most prevalent, aluminum oxide and other airborne particle were the next highest followed by hydrogen chloride, VOCs, NO_x, NH_3, hydrogen sulfide and hydrogen cyanide. Other chemical warfare agents such as sarin, sulfur mustard and cyanogen chloride may be present, but studies of their concentrations are classified. Moore and coworkers studied the effect of chemical warfare agents and pollutants and found that some cause a depression in fuel cell performance.

Summary of the effect of the contaminants on fuel cell output

Contaminant	Concentration	Percentage of original output during challenge	Percentage of original output during recovery
Carbon monoxide	20 ppm	96%	100%
Nitrogen dioxide	400 ppb	100%	100%
Sulphur dioxide	500 ppb	100%	100%
Benzene	50 ppm	95% (50 mA/cm^2) 93% (100 mA/cm^2) 72% (200 mA/cm^2)	95%
Propane	90 ppm	100%	100%
HCN	1780 ppm	13%	45%
HCN	3560 ppm	9%	35%
CNCl	780 ppm	11%	32%
CNCl	1560 ppm	12%	50%
Sulphur mustard	15 ppm	13%	13%
Sarin	170 ppm	30%	30%
Sarin	340 ppm	23%	23%

Table 7: Effect of Military Pollutants on Fuel Cell Performance

Off road applications will offer unique chemical contamination challenges. Vehicles driving on fields or in forested areas will be subject to a variety of biogenic volatile organic compounds. Forest trees have been shown to emit significant amounts of isoprene and monoterpenes.[9-12] Kristine[13] studied the emissions of VOCs from pasture and found emissions of oxygenated species including methanol, ethanol, propanone, butanone, and ethanal with only a small amount of isoprene and monoterpene. Fluxes as high as 23,000 µg (carbon) m^{-2} h^{-1} were measured, with clover emitting more VOCs than grass. Emission rates after mowing increased dramatically with clover emissions increasing 80 times and grass emissions increasing 180 times. These emissions included the above compounds plus higher levels of (Z)-3-hexenal, (E)-2-hexenal, (Z)-2-hexen-1-ol, (Z)-3-hexen-1-ol, and (Z)-hexenyl acetate.

Concentrations of VOCs from cut grass and clover were measured by de Gouw[14] who found that as the grass dries the VOC emissions increase. The concentrations of methanol and (Z)-3-hexenal rose immediately after cutting both grass and clover. After approximately 200 minutes the VOC emissions started to rise again. Concentrations of (Z)-3-hexenal and acetaldehyde peaked at approximately 1 PPM 400 minutes after cutting grass. Concentration of (Z)-3-hexenal peaked at 0.1 PPM and acetone peaked at 2 PPM 300 minutes after cutting clover.

	Grass		Clover	
Compound	After cutting	Peak at 400 min	After cutting	Peak at 300 min
(Z)-3-hexenal	300	1000	1000	100
(Z)-3-hexenol	200	90	500	10
Hexenyl acetate	9	1	9	<1
Formaldehyde	60	60	20	300
Methanol	300	200	2000	200
Acetaldehyde	200	1000	300	500
Butanone	60	60	200	1000
Acetone			400	2000

Table 8: VOC concentrations (ppb) in air immediately after cutting and after drying

Pesticides are also present in low concentrations during application. Yeary[15] studied the concentrations of various pesticides in the air during application. Pesticide concentrations were measured in the outdoor ambient air and at the applicator breathing zone. In most measurements the concentrations of pesticides were below the detectable limit of 1 μg/m^3. Tables 9 and 10 show the results of their testing.

Pesticide	Number of sample sites	No. Below detectable limit	TWA ppb (μg/m^3)
Acephate	17	16	4.3 (32)
Ammonia	12	12	---
Carbaryl	28	15	1.6 (13)
Dicofel	53	52	0.5 (6)
Diazinon	34	32	0.3 (4)
Malathion	5	5	---
2,4-D	16	11	2.8 (25)
Xylene	30	30	---

Table 9: Outdoor ambient air during pesticide application

Pesticide	Number of sample sites	No. Below detectable limit	TWA μg/m^3
Atrasine	22	16	0.1 (1)
Bensulide	10	10	---
Chlorpyrifos	17	9	0.35 (5)
2,4-D	76	61	0.4 (4)
Dacthal	2	2	---
Diazinon	20	7	1.1 (14)
MCPA	25	25	---
Pendimethalin	8	8	---

Table 10: Applicator breathing zone air monitoring

Conclusion

Air quality is affected by many factors and can vary widely between locations and even from day to day. Particulate levels generally average from 0.01-0.14 mg/m^3 but are frequently higher in off road situations such as dirt roads where the level may be as high as 6000 mg/m^3. In addition, small particles, 0.01-5.0 µm, can have a detrimental effect on fuel cell cathodes. Particles of this size are often secondary particles containing sulfur dioxide and oxides of nitrogen which are detrimental to fuel cell performance. Typical filters for internal combustion engines are not as effective at removing these small particles. HEPA grade filtration is most likely necessary to achieve maximum performance for fuel cells.

Chemical contaminants also vary widely in composition and concentration depending on location and time. The wide range of chemical contaminants should be considered in the fuel cell filtration design. The filter should be able to remove acid gases, base gases and a broad range of volatile organic compounds.

ANALYTICAL METHODS

Donaldson will conduct field testing of air quality, with Toro's assistance, by fitting a Heavy Duty Workman® utility vehicle with air monitoring and sampling devises. Air samples will be taken at a golf course specified by Toro in St. Paul, MN. The goal of the sampling is to determine types and concentrations of contaminants that may be encountered in an off road fuel cell vehicle. This data will be used to test possible contaminants to determine their affect on fuel cell performance and design filter systems. Particulate and chemical contaminant data will be collected. Samples will be collected at various locations around the course and in as many different conditions as possible, i.e. morning, afternoon, during mowing or fertilizing etc. There are numerous methods for measuring contaminant concentrations in air. The USEPA, NIOSH and OSHA all have libraries of methods for general testing and testing for specific chemicals. Methods usually involve using a sample pump to draw air through an adsorbent devise or filter paper, then analyzing the adsorbent. Air samples will be taken at the back of the vehicle (A), in between the box and the cab (B), and on the front of the vehicle (C). Sample location A will allow us to collect contaminant data caused by the vehicle as it disturbs the soil. Sample location B will collect contaminant data near the potential air inlet for the fuel cell. Sample location C will collect contaminant data from the undisturbed environment.

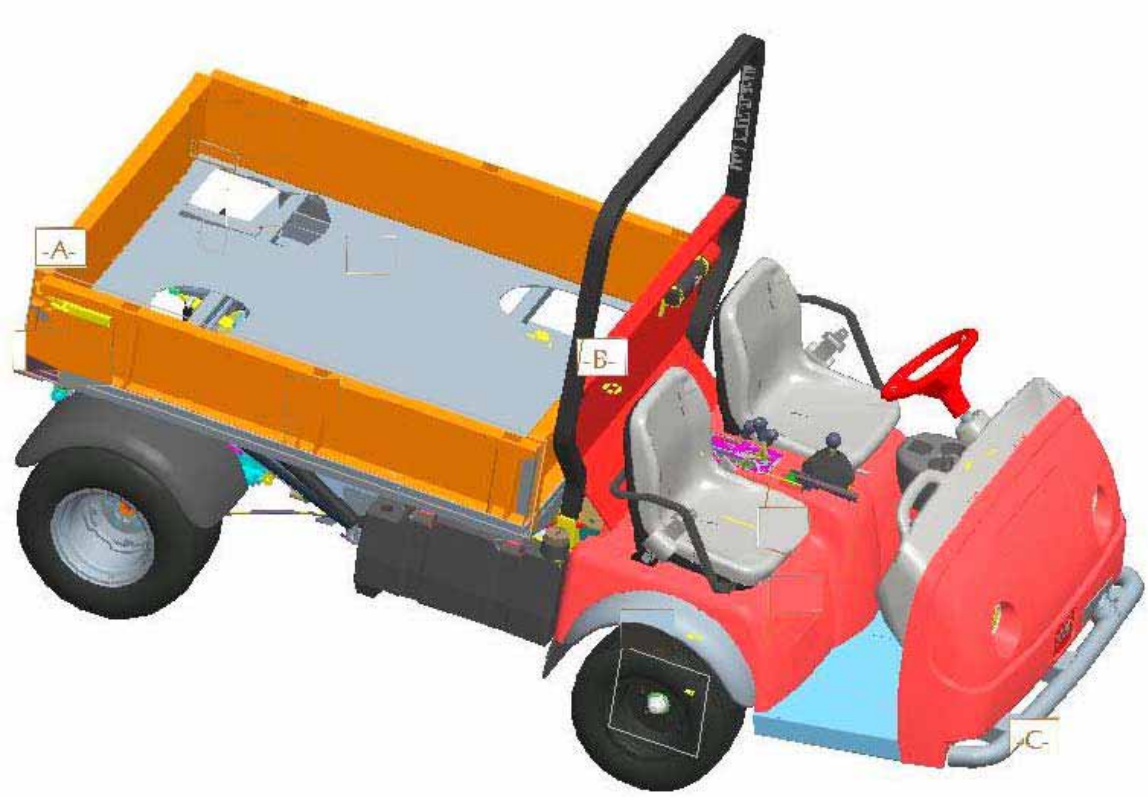

Figure 4: Air sampling locations on Toro Heavy Duty Workman

Particulate Contaminants
Particulate analysis will focus on PM_{10} and will be conducted in accordance with NIOSH method 0600. These particles will adversely affect the performance of fuel cells and are not removed very well by typical IC engine filtration.

Sampling of particulates will use a pump with an impactor used to remove large particles from the air. Particles smaller than 10 microns will be collected on a pre-weighed filter paper to determine the mass of particles in the air. A scanning electron microscope will also be used to try to determine the size distribution and electron dispersion spectroscopy will be used to try to determine the chemical make up of the particles.

Chemical Contaminants
Sampling and measurement will focus on acid gases, specifically sulfur dioxide and oxides of nitrogen, base gases, specifically ammonia, and volatile organic compounds. Sampling and analysis of acid gases will be conducted in accordance with NIOSH methods 6004 for SO_2 and/or NIOSH method 6014 for NO_x. Base gas analysis will be conducted in accordance with NIOSH method 6016 for ammonia. In these analyses, a sample pump will be fitted with adsorbent tubes. The flow rate through each tube is calibrated and the sample time measured and recorded. The adsorbent material in each tube is extracted with de-ionized water. The water sample is then concentrated and analyzed by ion chromatography. Contaminants can then be identified and quantified.

Sampling of VOCs will be conducted in accordance with EPA Compendium Method TO-17, “Determination of Volatile Organic Compounds in Ambient Air Using Active Sampling onto Sorbent Tubes”. In this analysis a pump will again be used to draw air through adsorbent tubes to collect the contaminants for analysis by thermal desorption/gas chromatography/mass spectroscopy. We will use two different adsorbents for VOC sampling. Carbosieve® is used for the collection of light organic compounds typically with boiling points from -60ºC to 80ºC, and Tenax® TA is used for collection of higher molecular weight organics typically with boiling points from 100ºC to 400ºC. Typical flow rates and sampling times will be 0.1-1.0 Liters/minute, and 1-4 hours respectively. Samples will be returned to Donaldson’s Corporate Technology laboratory for analysis.

APPENDIX A: US CONTAMINANT CONCENTRATION FOR SELECTED CONTAMINANT BY COUNTY

These maps illustrate the modeled ambient concentration of air toxics by county in 1996. Map colors indicate ranges of median concentration values, and each county is colored according to its value relative to the rest of the country. The concentration value displayed in maps is the median. Pollutant concentration is expressed in micrograms per cubic meter of air ($\mu g/m^3$).

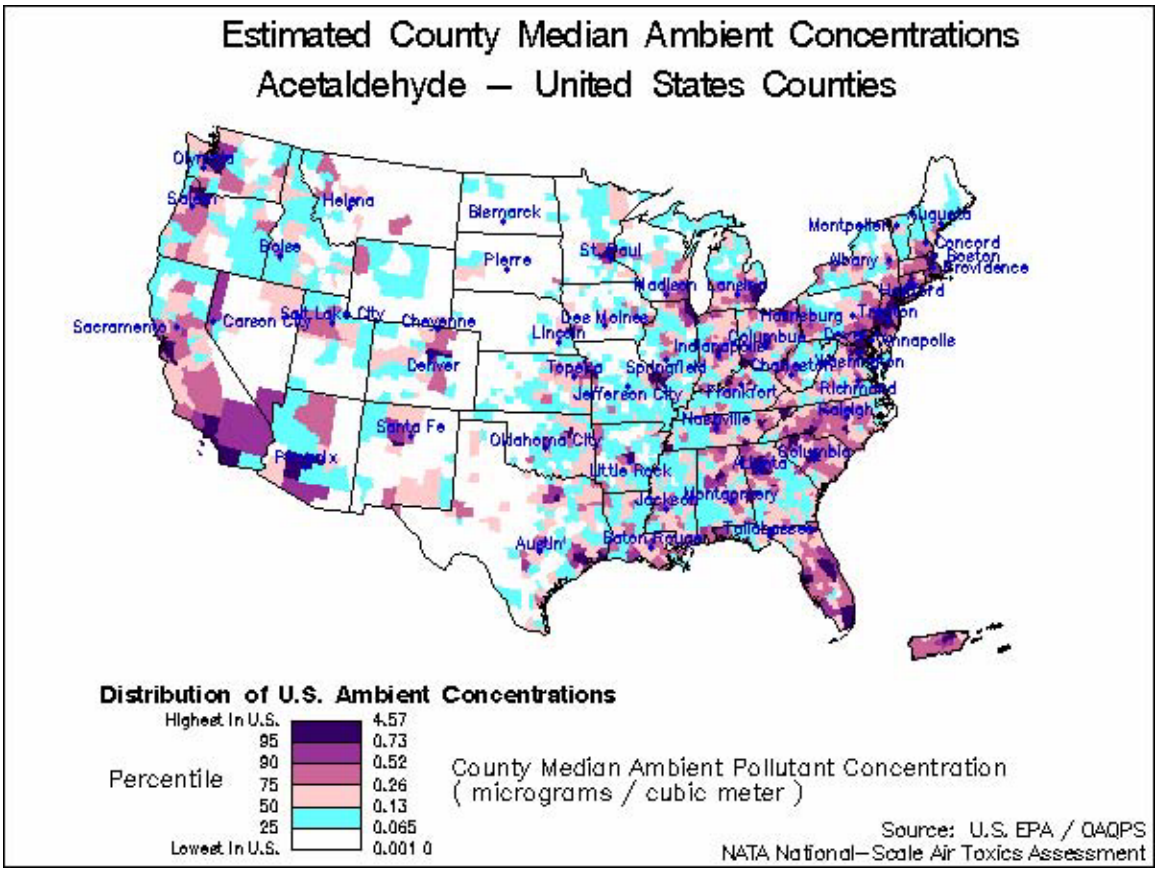

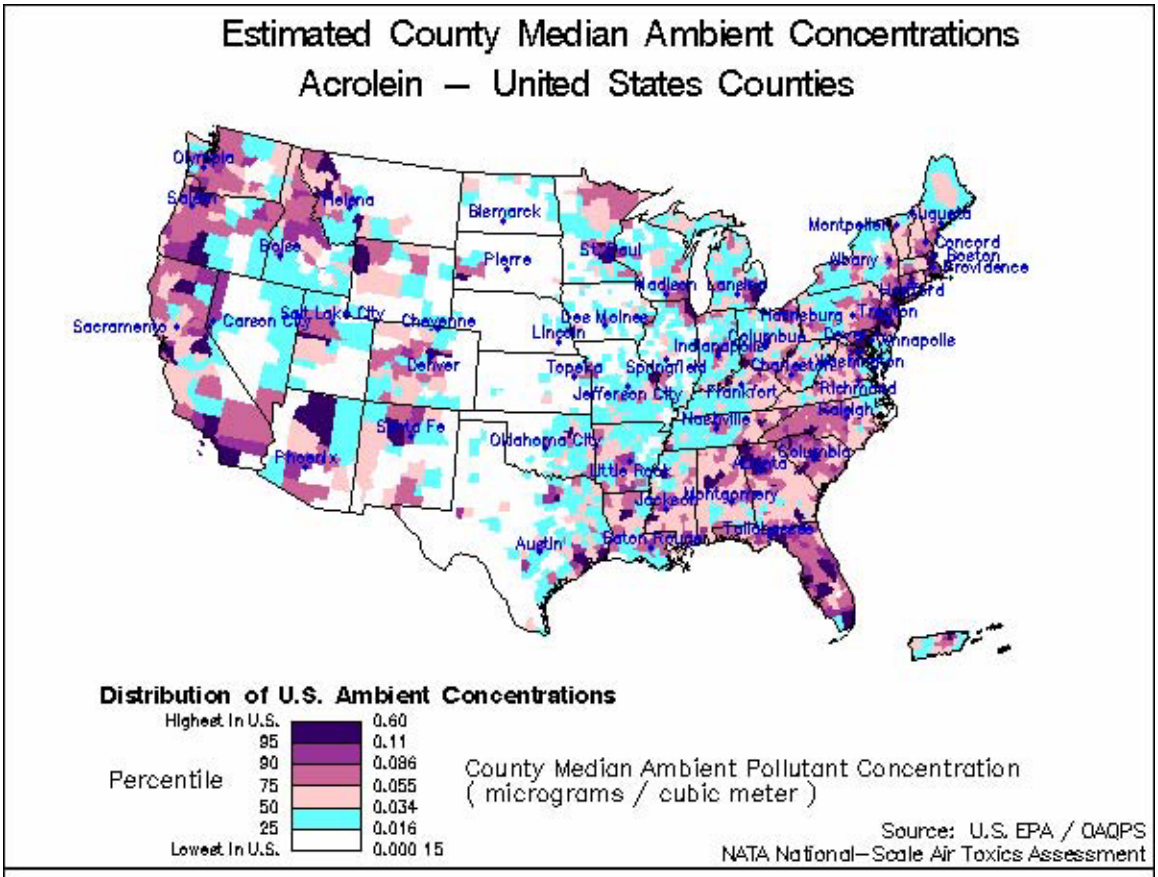
Estimated County Median Ambient Concentrations
Acrolein — United States Counties
Distribution of U.S. Ambient Concentrations
Highest In U.S.
95
90
75
50
25
Lowest In U.S.
Percentile
0.60
0.11
0.086
0.055
0.034
0.016
0.000 15
County Median Ambient Pollutant Concentration
(micrograms / cubic meter)
Source: U.S. EPA / OAQPS
NATA National–Scale Air Toxics Assessment

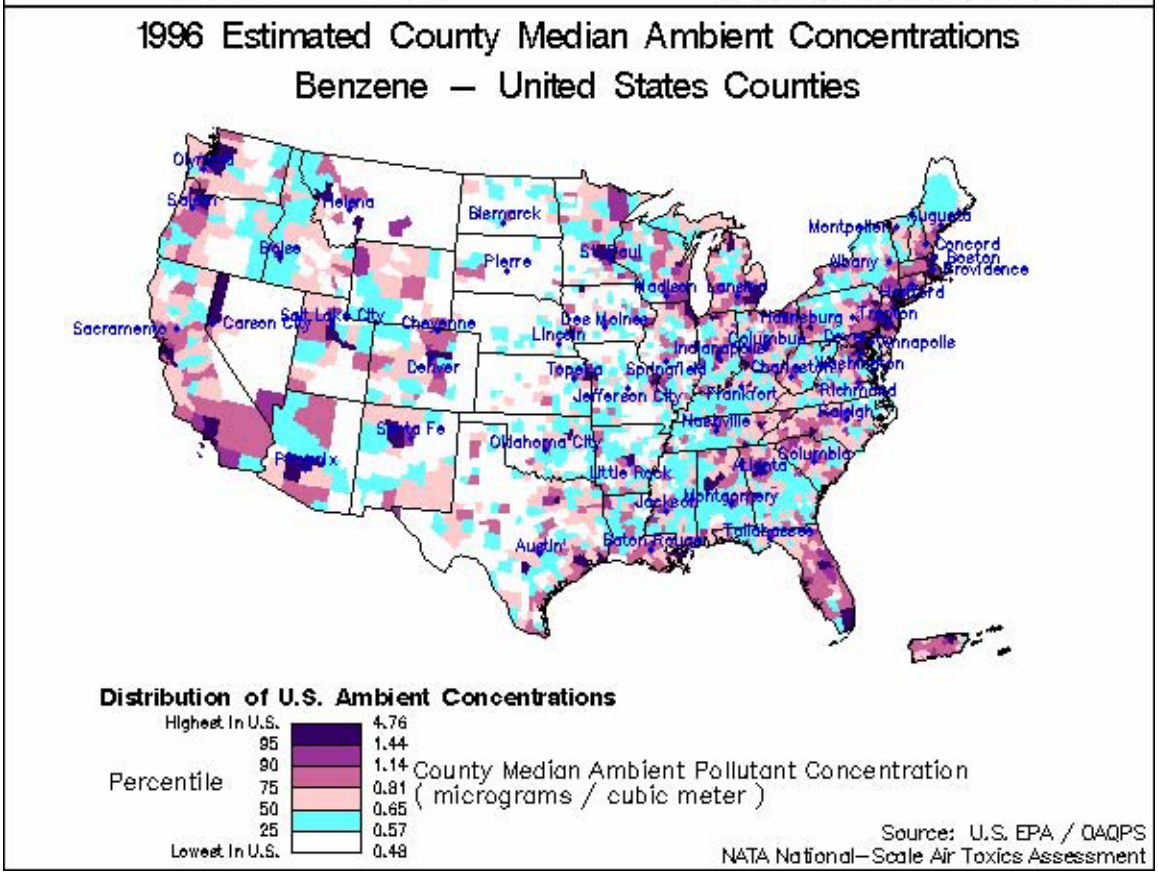
1996 Estimated County Median Ambient Concentrations
Benzene — United States Counties
Distribution of U.S. Ambient Concentrations
Highest In U.S.
95
90
75
50
25
Lowest In U.S.
Percentile
4.76
1.44
1.14
0.81
0.65
0.57
0.48
County Median Ambient Pollutant Concentration
(micrograms / cubic meter)
Source: U.S. EPA / OAQPS
NATA National–Scale Air Toxics Assessment

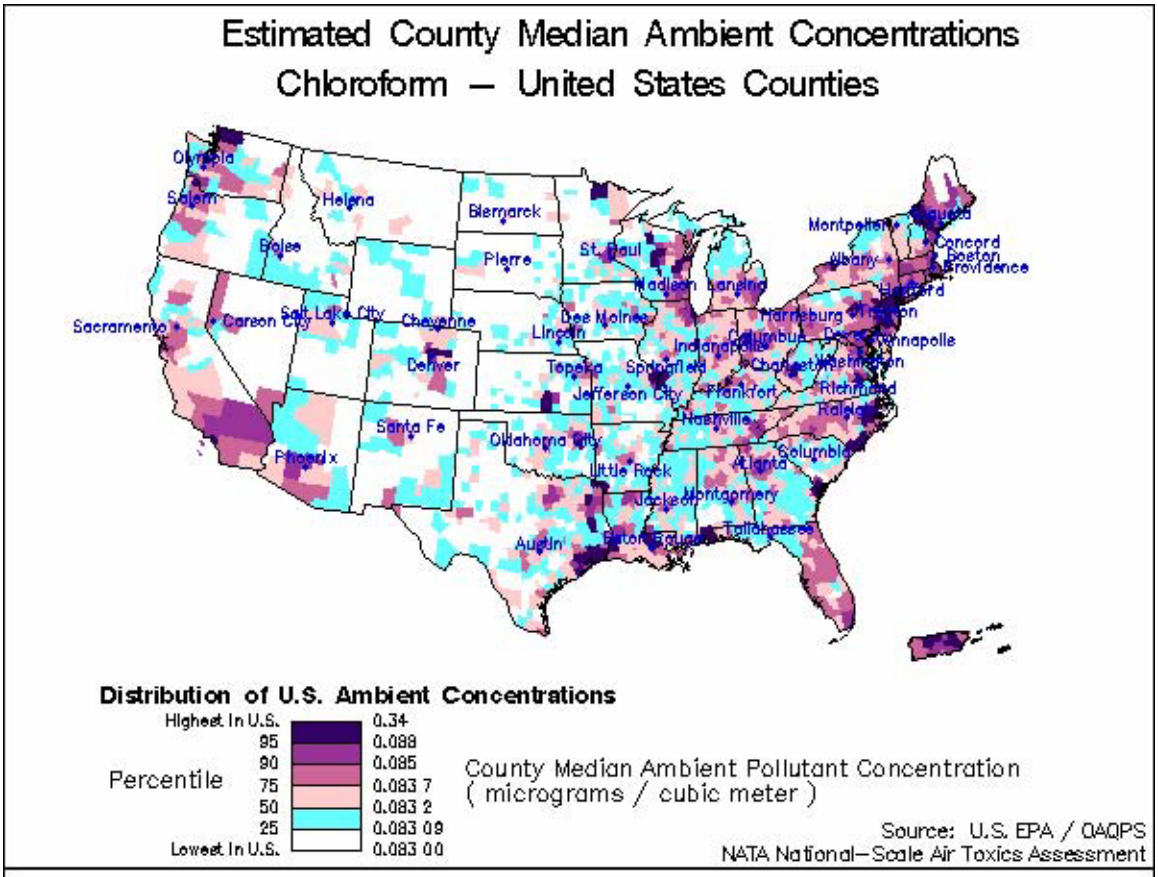
Estimated County Median Ambient Concentrations
Chloroform – United States Counties
Distribution of U.S. Ambient Concentrations
Highest In U.S.
95
90
75
50
25
Lowest In U.S.
Percentile
0.34
0.088
0.085
0.083 7
0.083 2
0.083 09
0.083 00
County Median Ambient Pollutant Concentration
(micrograms / cubic meter)
Source: U.S. EPA / OAQPS
NATA National–Scale Air Toxics Assessment

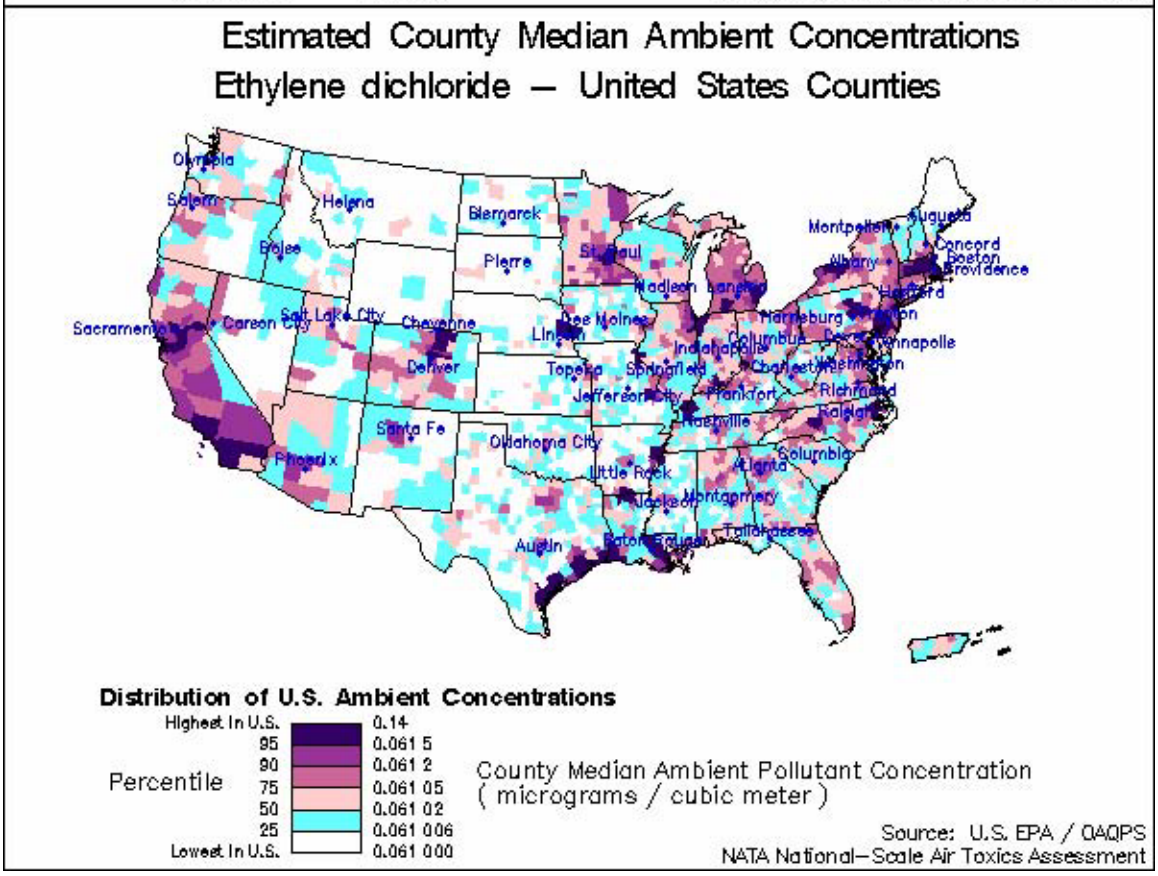
Estimated County Median Ambient Concentrations
Ethylene dichloride – United States Counties
Distribution of U.S. Ambient Concentrations
Highest In U.S.
95
90
75
50
25
Lowest In U.S.
Percentile
0.14
0.061 5
0.061 2
0.061 05
0.061 02
0.061 006
0.061 000
County Median Ambient Pollutant Concentration
(micrograms / cubic meter)
Source: U.S. EPA / OAQPS
NATA National–Scale Air Toxics Assessment

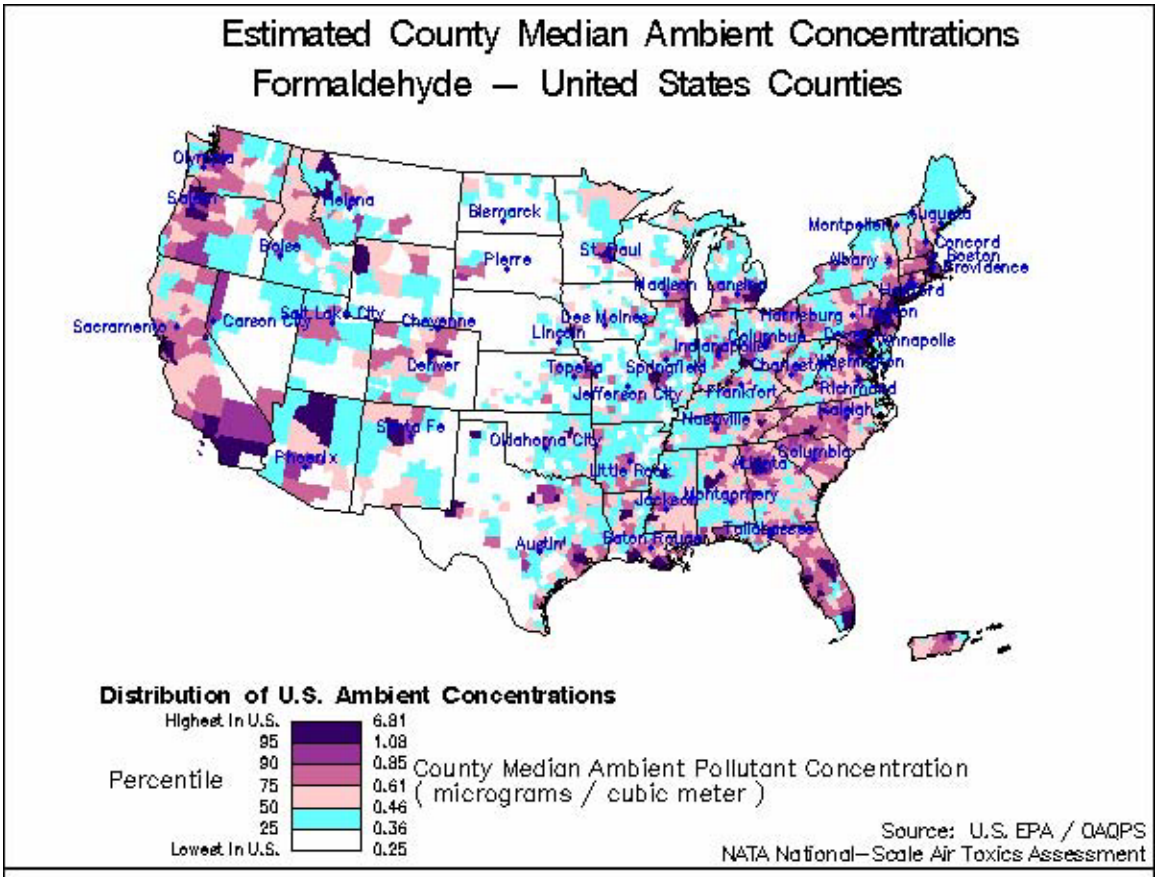
Estimated County Median Ambient Concentrations
Formaldehyde — United States Counties
Distribution of U.S. Ambient Concentrations
Higheet In U.S.
95
90
75
50
25
Loweet In U.S.
Percentile
6.81
1.08
0.85
0.61
0.46
0.36
0.25
County Median Ambient Pollutant Concentration
(micrograms / cubic meter)
Source: U.S. EPA / OAQPS
NATA National–Scale Air Toxics Assessment

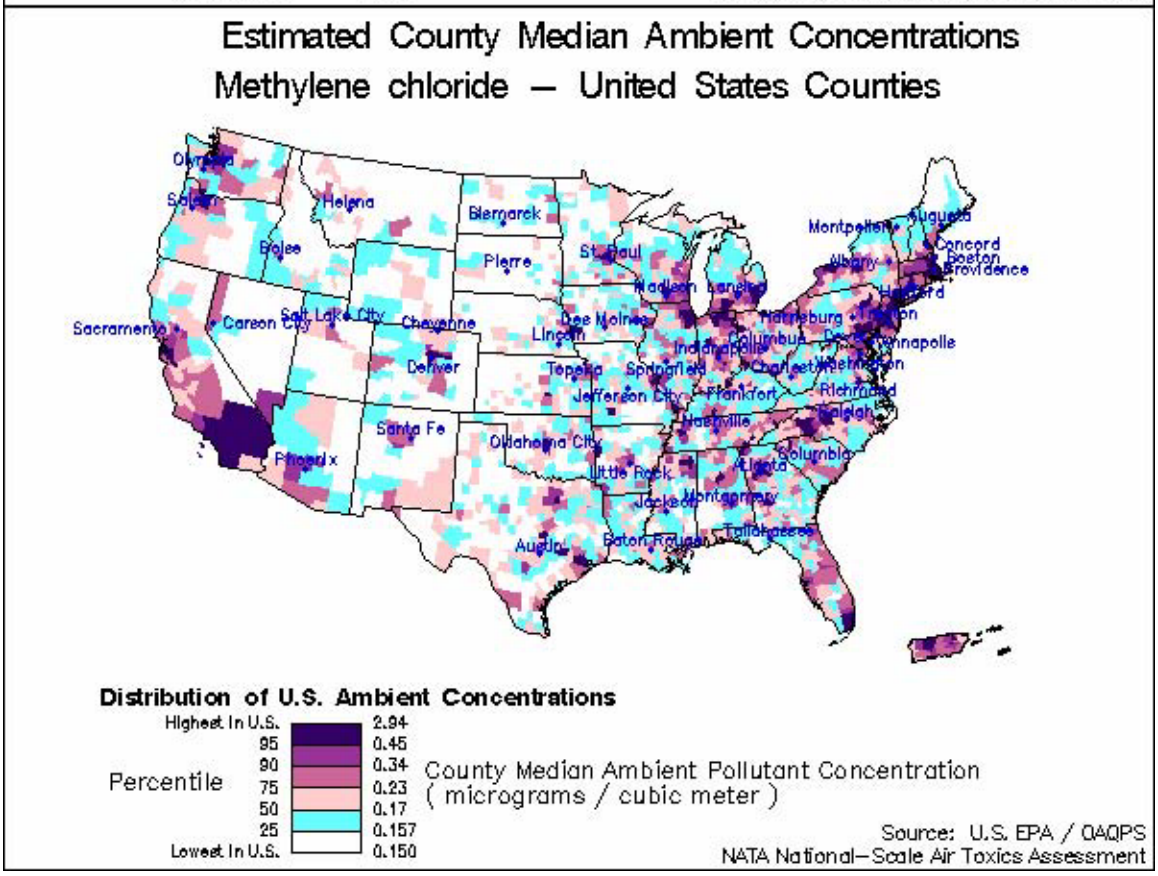
Estimated County Median Ambient Concentrations
Methylene chloride — United States Counties
Distribution of U.S. Ambient Concentrations
Higheet In U.S.
95
90
75
50
25
Loweet In U.S.
Percentile
2.94
0.45
0.34
0.23
0.17
0.157
0.150
County Median Ambient Pollutant Concentration
(micrograms / cubic meter)
Source: U.S. EPA / OAQPS
NATA National–Scale Air Toxics Assessment

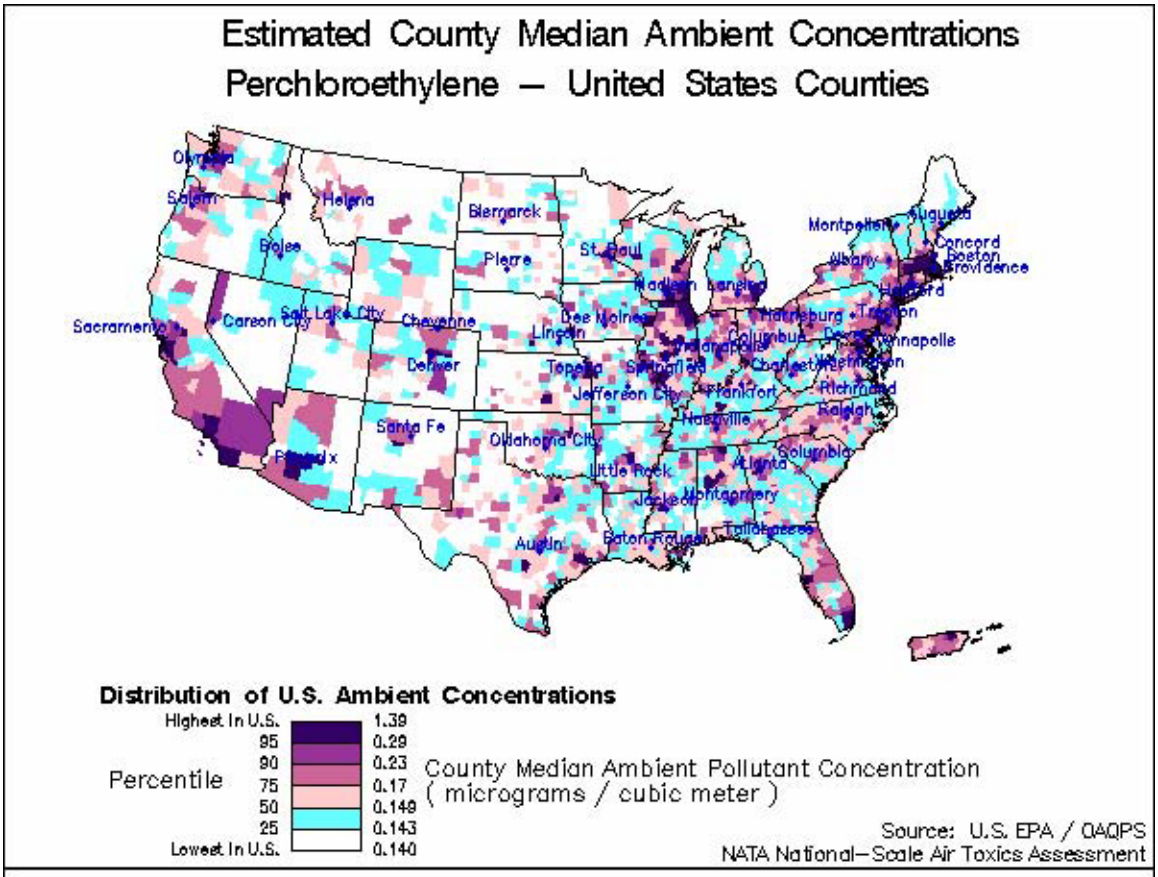
Estimated County Median Ambient Concentrations
Perchloroethylene — United States Counties
Distribution of U.S. Ambient Concentrations
Highest In U.S.
95
90
75
50
25
Lowest In U.S.
Percentile
1.39
0.29
0.23
0.17
0.149
0.143
0.140
County Median Ambient Pollutant Concentration
(micrograms / cubic meter)
Source: U.S. EPA / OAQPS
NATA National–Scale Air Toxics Assessment

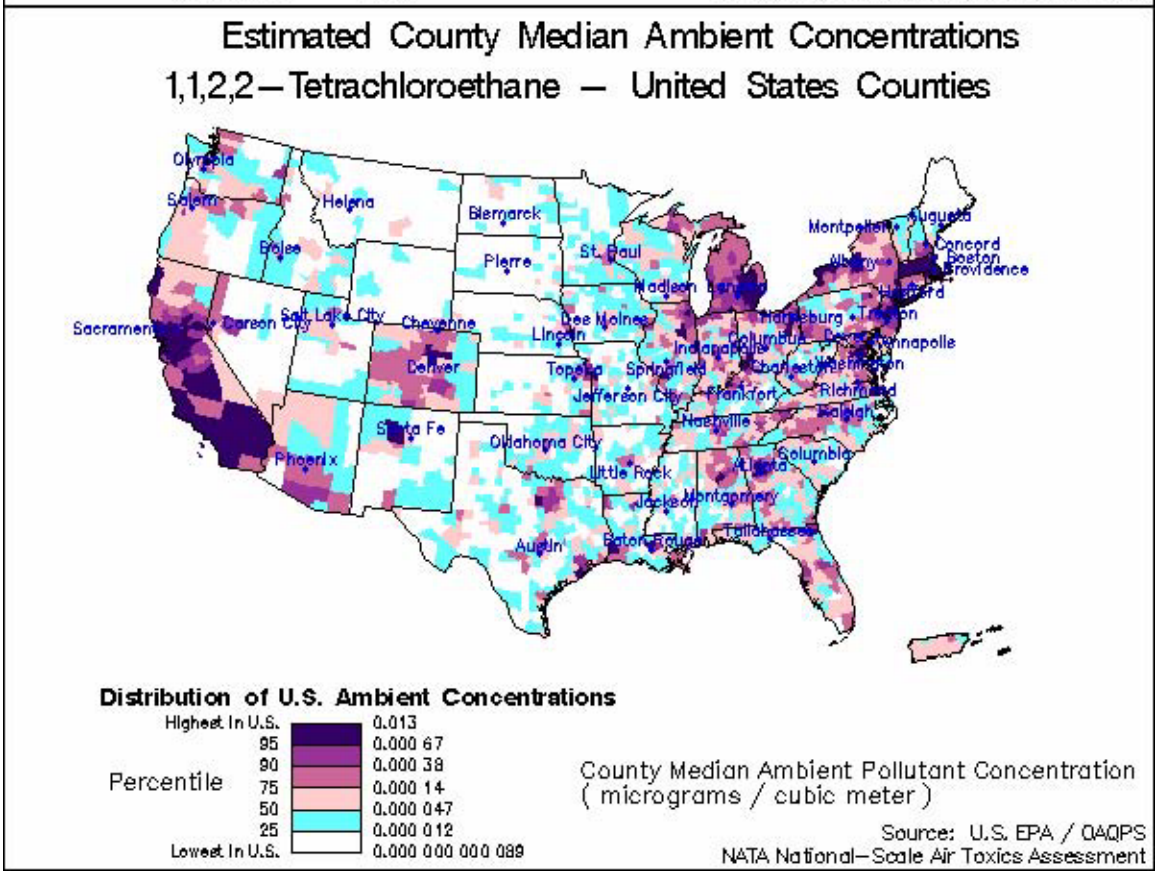
Estimated County Median Ambient Concentrations
1,1,2,2–Tetrachloroethane — United States Counties
Distribution of U.S. Ambient Concentrations
Highest In U.S.
95
90
75
50
25
Lowest In U.S.
Percentile
0.013
0.000 67
0.000 38
0.000 14
0.000 047
0.000 012
0.000 000 000 089
County Median Ambient Pollutant Concentration
(micrograms / cubic meter)
Source: U.S. EPA / OAQPS
NATA National–Scale Air Toxics Assessment

APPENDIX B: DEFINITIONS

Acid gas: Gas that will form acids when mixed with water. Common examples are sulfur dioxide (SO_2) which will form sulfuric acid (H_2SO_4) when dissolved in water, and nitrogen oxide (NO) or nitrogen dioxide (NO_2) which will form nitrous acid (HNO_2) and nitric acid (HNO_3) when dissolved in water.

Anthropogenic: Relating to, or resulting from the influence of human beings on nature.

Base gas: Gas that will form base solutions with water such as ammonia (NH_3) which forms ammonium (NH_4OH) when dissolved in water.

Biogenic Compounds: Compounds produced by the actions of living organisms.

Chromatography: A series of related techniques for the separation of a mixture of compounds by their distribution between two phases. In gas-liquid chromatography the distribution is between a gaseous and a liquid phase. In column chromatography the distribution is between a liquid and a solid phase.

Hydrocarbon: Compounds containing only carbon and hydrogen. Petroleum products are a common example of hydrocarbons.

Ion chromatography: A form of liquid chromatography that uses ion-exchange resins to separate atomic or molecular ions based on their interaction with the resin

Mass spectroscopy: Mass spectrometry is a technique for separating ions by their mass-to-charge (m/z) ratios in order to identify a compound or a molecular structure.

Organic compound: Chemical compounds based on carbon chains or rings and also containing hydrogen, with or without oxygen, nitrogen, and other elements.

Oxides of nitrogen: A mixture of nitrogen oxide (NO) and nitrogen dioxide (NO_2) greenhouse gases produced as by-products in combustion engines and many industrial processes; NO x in the atmosphere are converted to nitric acid (HNO_3) which falls as acid rain.

$PM_{2.5}$: Refers to the concentration of “fine” particles that are less than 2.5μm in diameter.

PM_{10}: Refers to the concentration of “course” particles, less than 10μm in diameter.

Thermal desorption: A method for vaporizing and introducing volatile and semi-volatile compounds present in a sample into an analytical instrument by means of thermal energy.

Troposphere: The portion of the earth's atmosphere from the surface to the tropopause; that is, the lowest 10-20 km of the atmosphere. The troposphere is characterized by decreasing temperature with height, and is the layer of the atmosphere containing most

clouds and other common weather phenomena

Volatile organic compounds (VOCs): Compounds that vaporize (become a gas) at room temperature. Common sources which may emit VOCs include housekeeping and maintenance products, building and furnishing materials, gasoline, kerosene, diesel fuel, industrial solvents, and plants and animals.

REFERENCES

1. Stenersen, E., Canepa, R.; *Reliability and Sound Suppression Improvement of PEM Fuel Cells Through the Development of a New Class of Fail-Safe Contamination Control Systems* Proceedings of Grove Fuel Cell Symposium, 2001
2. US EPA website, *National Air Quality 2001 Status and Trends*
3. Barris, M.A.; *Total Filtration: The Influence of Filter Selection on Engine Wear, Emissions, and Performance* SAE Technical Paper Series 952557,1995
4. Bessee, G. B. and Kohl, K. B.; *Comparison Between Real-Life Dust Samples and Standardized Test Dusts* SAE Technical Paper Series 940322,1994
5. Nelson, G. O.; (1992) *Gas Mixtures: Preparation and Control* Lewis Publishers, Chelsea, MI
6. US EPA website, *Toxic Air Pollutants*
7. Jacobson, M. Z.; *Atmospheric Pollution History, Science, and Regulation* Cambridge University Press, 2002, pg 63
8. Cross, J; *Preventing Degradation in Proton Exchange Membrane Fuel Cells: A Novel, Multicartridge Air Contaminant Control System* Intel International Science and Engineering Fair, 2005
9. Zimmerman,P.R., Chatfield, R.B., Fishman, J., Crutzen, P.J., and Hanst, P.L.; *Estimates on the production of CO and H_2 from the oxidation of hydrocarbon emissions for vegetation* Geophys. Res. Lett., 5, 679-82, 1978
10. Isidorov,V.A., Zenkevich, I.G., Ioffe, B.V.; *Volatile organic compounds in the atmosphere of forests* Atmos. Environ., 19, 1-8, 1985
11. Lamb, B., Westberg, H., Allwine, G., Quarles, T.; *Biogenic hydrocarbon emissions from deciduous and coniferous trees in the United States* J. Geophys. Res., 90, 2380-90, 1985.
12. Khalil, M.A.K., Rasmussen, R.A.; *Forest hydrocarbon emissions: Relationships between fluxes and ambient concentrations* J.Air waste Manage. Assoc., 42, 810-813, 1992
13. Kristine, W., Balbally, I., Ye, Y., Hooper, M.; *Emission of volatile organic compounds (primarily oxygenated species) from pasture* J. Geophysical Research, Vol. 103, No. D9, 10605-19, May 20, 1998
14. de Gouw, J.A., Howard, C.J., Custer, T.G., Fall, R.; *Emissions of volatile organic compounds from cut grass and clover are enhanced during the drying process* Geophys. Res. Lett., Vol 26, No. 7, 811-814, April 1, 1999
15. Yeary, R.A., Leonard, J.A.; *Measurement of pesticides in air during application to lawns , trees and shrubs in urban environments* ACS Symposium Series 522: Pesticides in Urban Environments, Fate and Significance, 275-281, ACS, 1993

TASK 3.C – AIR FILTER TESTING

University of California, Davis
Arjun Tejaswi
Magdalena Brum
Prof. Paul Erickson

INTRODUCTION

Fuel cell systems for back-up power are best suited for use in regions where the grid is unstable. These regions tend to be in the developing world where air quality is often poor to unhealthy. In order for a fuel cell system to operate successfully in these regions, contaminants in the ambient air must be removed or greatly reduced before supplying oxygen to the cathode. As a result, air filters are routinely used to filter the air to remove particulates and contaminants. However, no real data on air filter efficacy and lifetime exists for fuel cell applications. It is the objective of this research to determine efficacy and longevity of air filters with respect to removing NOx and SOx contaminants, two contaminants that are routinely found in high levels in the developing world.

EXPERIMENTAL SET-UP

Schematic

A simple schematic of the experimental apparatus is shown in Figure 1 and a P&ID is provided in Figure 2. The test system can be further separated into the following sub-systems:

- Air delivery (Figure 3): Consists of the air compressor, the air tank, the dryer and the chiller.
- Humidification (Figure 4): Consists of the humidification tank which has an inlet valve for water which is controlled by P&ID through Labview.
- Pollutant injection system (Figure 5): Consists of Mass Flow Controllers (MFCs) which operate in the mSLPM range of interest for NO_2 and SO_2.
- Gas heating (Figure 6). Consists of the heaters and the thermocouples controlled by P&ID through Labview.
- Filter testing (Figure 6): Consists of the assembly that has been built to house the filters in a manner that isolates them from the ambient.
- Gas sampling (Figure 7): Consists of a series of Mass flow controllers (MFCs) which regulate the air flow rates through each of the filters during the test.

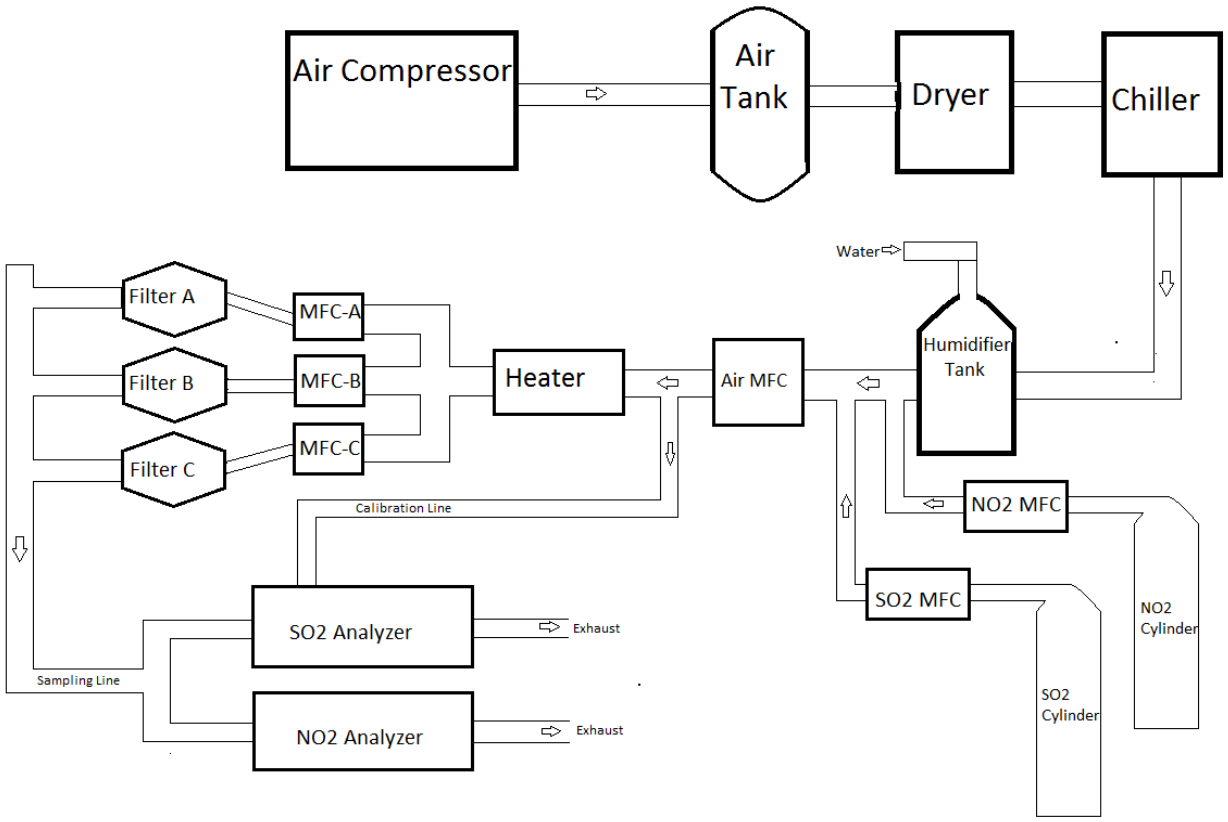

Figure 1: Test set-up schematic

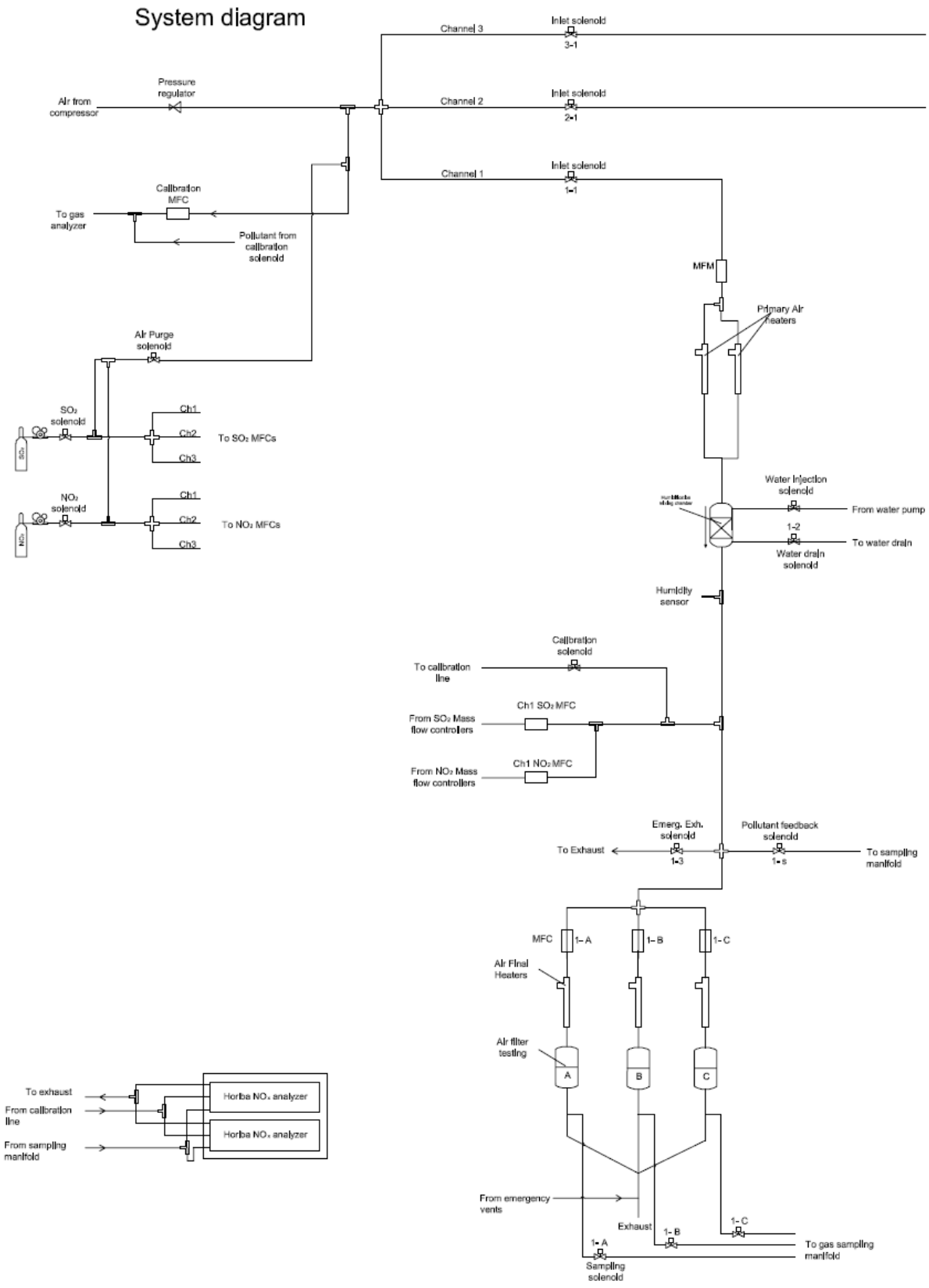
System diagram
Channel 3
Inlet solenoid
3-1
Air from compressor
Pressure regulator
Channel 2
Inlet solenoid
2-1
Channel 1
Inlet solenoid
1-1
Calibration MFC
To gas analyzer
Pollutant from calibration solenoid
MFM
Primary Air Heaters
Air Purge solenoid
SO2 solenoid
Ch1
Ch2
Ch3
To SO2 MFCs
NO2 solenoid
Ch1
Ch2
Ch3
To NO2 MFCs
Water Injection solenoid
From water pump
1-2
To water drain
Water drain solenoid
Humidity sensor
Calibration solenoid
To calibration line
Ch1 SO2 MFC
From SO2 Mass flow controllers
Ch1 NO2 MFC
From NO2 Mass flow controllers
Emerg. Exh. solenoid
To Exhaust
1-3
Pollutant feedback solenoid
1-5
To sampling manifold
MFC
1- A
1- B
1- C
Air Final Heaters
Air filter testing
A
B
C
From emergency vents
Exhaust
1- C
1- B
1- A
Sampling solenoid
To gas sampling manifold
To exhaust
From calibration line
From sampling manifold
Horiba NOx analyzer
Horiba NOx analyzer

Figure 2: P&ID

Figure 3: Air Delivery

Figure 4: Humidification

Figure 5: Pollution gas flow control

Figure 6: Filter housings and heater control

Figure 7: Gas sampling manifold

The air compressor, dryer, and chiller provide cold, dry air for the system to operate (Figure 3). Solenoids at the beginning of each channel allow air to flow for testing. This also allows channels to be shut off individually without interrupting flow to the other channels. Mass flow meters following the solenoids measure inlet air flow and also meters pollutant concentrations.

A first set of heaters brings the air to test temperature for each channel. The humidification system (Figure 4) follows consisting of a chamber to allow mixing of air and water. The system pumps water into the chambers through misting nozzles. Water flow is controlled with variable control valves. Closed loop feedback for humidification control is provided by the humidity sensor downstream.

This temperature and humidity controlled air then passes into the pollutant injection system which meters flow of SO_2 and NO_2 into the air stream. Solenoid valves must open before the pollutant is allowed to flow and are shut off when no pollutant is needed. An air purge solenoid introduces clean air upstream of the pollutant mass flow controllers to clear any trapped pollutant during shutdown (Figure 5).

After the pollutant injection, the flow of each channel is split into three sub-channels and mass flow meters control flow of polluted air to the different filters (Figure 6). A final heating stage heats each sub-channel to offset any heat lost since the initial heaters. Filtered air is sampled and passes through to a common exhaust manifold and expelled from the experimental area.

The sampling system consists of 12 solenoid valves and a manifold (Figure 7) to the gas analyzer. Each channel has an upstream sample and three downstream samples; one for each type of filter. The upstream sample is a short distance downstream of pollution injection and will act as error signal to pollution concentration control as well as

test data for the filters. The downstream samples will read pollution levels after the filter to asses filter performance. The sampling system will open one solenoid while keeping the other 11 closed. The Horiba gas analyzer will draw from the sampling system long enough to clear the tube of previous samples as well as attain a stable reading. This results in long periods between samples of each filter.

The system has emergency release solenoids which vent all gas from each channel during the event of an emergency. These solenoids are normally open and must be energized to close. In the event of a power failure, these solenoids will automatically open causing the entire system to vent.

During the actual test, the test parameters including air flow rate, pollutant flow rates, temperature and humidity are set to the desired values noted in the experimental plan. All of these parameters as well as the solenoid valves are controlled from Labview and are recorded against a date and time stamp. Each test will continue until filter failure. Once a filter fails, the filter will be replaced and the test repeated with a new set of values from the full factorial of the experiment.

Controls

Custom software was written using Labview to control all the test equipment. P&ID loops were written to control the air temperature and air humidity. Code for test data saving is included in the control software. By this means, an excel spreadsheet containing readings for flow rate, temperature and humidity is continuously storing data while the control program is running.

In order to achieve integrated data acquisition, we used a NI systems as detailed in Table 1.

DAC cards	Number of AI	Number of AO	Number of DIO	Counters
NI PXI 6723	0	32	0	0
NI PXIe 6363	32	4	48	4
NI 4353 PXIe	32 (thermocouple)	0	8	0
Total channel count	32/32 thermocouple	36	56	4

Table 1: Table detailing the data cards being used for P&ID control

The acquired data is then processed through Labview to achieve P&ID control. The Labview interface (Figure 8) allows for real time display of the parameter that is being

controlled thereby ensuring that the gains may be manually changed if the control system fails to achieve the desired value.

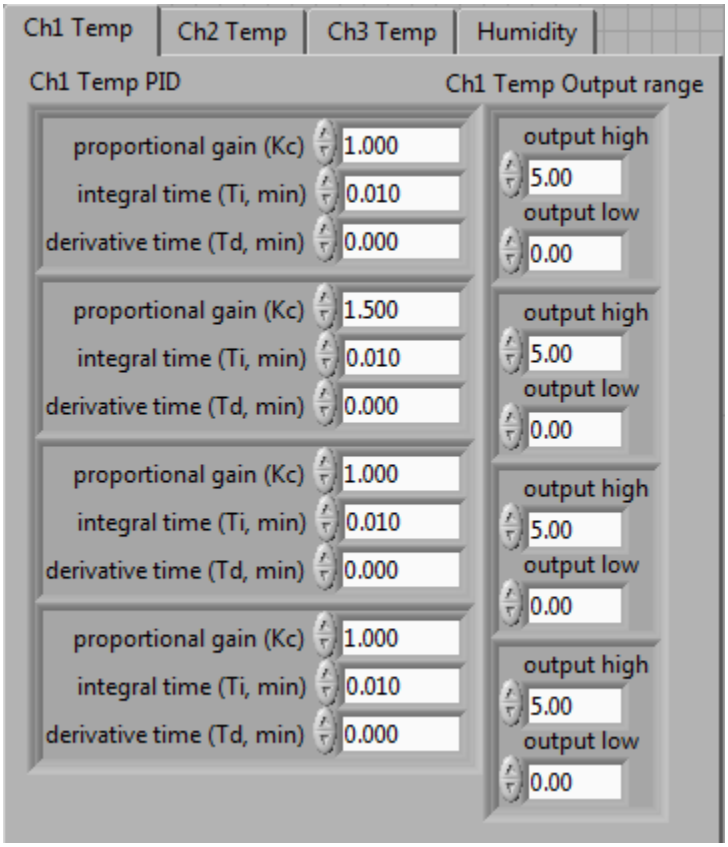

Figure 8: User interface on Labview for P&ID control of temperature and humidity

Due to the fact that there is only one gas analyzer per pollutant and several sampling points in the system, proper multi-point pollutant monitoring can only be achieved by implementing a sampling sequence. For that purpose, separate Labview testing sequence code (Figure 9) was developed in order to get an automated sampling sequence. The code creates a testing sequence in which sampling valves throughout the system are opened one at a time while the rest of the valves are kept closed. The software also allows one to select between manual and automatic valve command and to indicate the sampling time during which the valves remain open until steady readings are achieved in the analyzers. The sampling data containing the status of the valves (open or closed) for each time, is stored on an excel spreadsheet that can be merged with the gas concentration data from the analyzers.

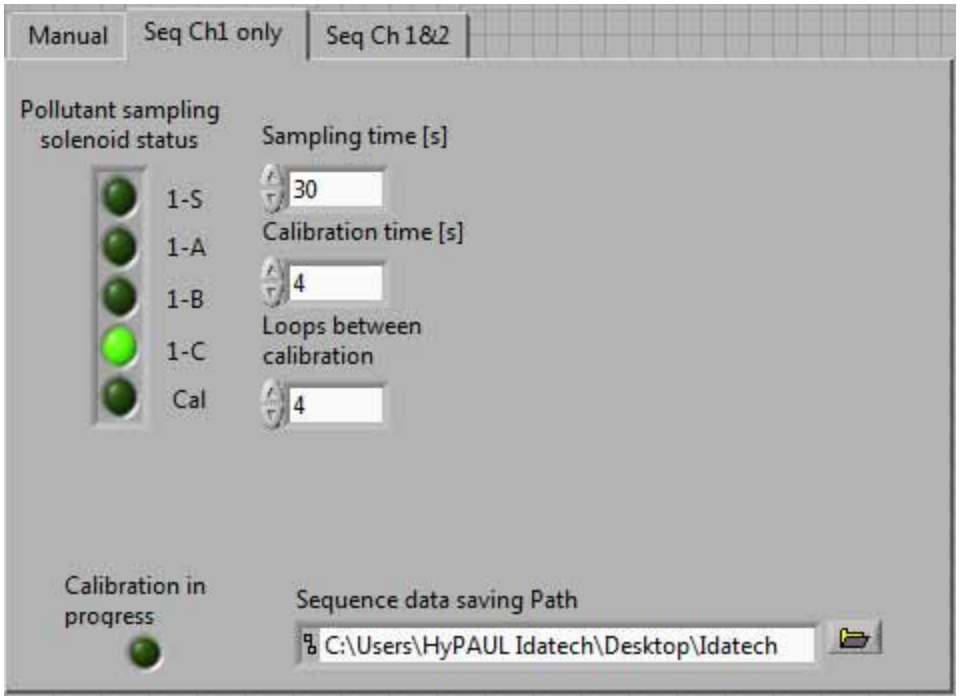

Figure 9: Labview user interface showing the sampling sequence involving the upstream sample and the three filter samples. The sampling time can be set in such a manner that a steady value can be obtained for each sample

Lastly, software to merge the Labview data and the Horiba data into one master data file was created. The testing experiments deal with three different sources of data. The first source is the output from Labview, which generates two separate files, and the other two sources are the Horiba gas analyzers. Since time is the common variable in all the data files, it is possible to merge them into one file. In order to do this, a Windows application was developed, which generates a single output file from the four mentioned inputs. The user interface for the software is shown in Figure 10. The intent is to generate one master data file for each day of testing.

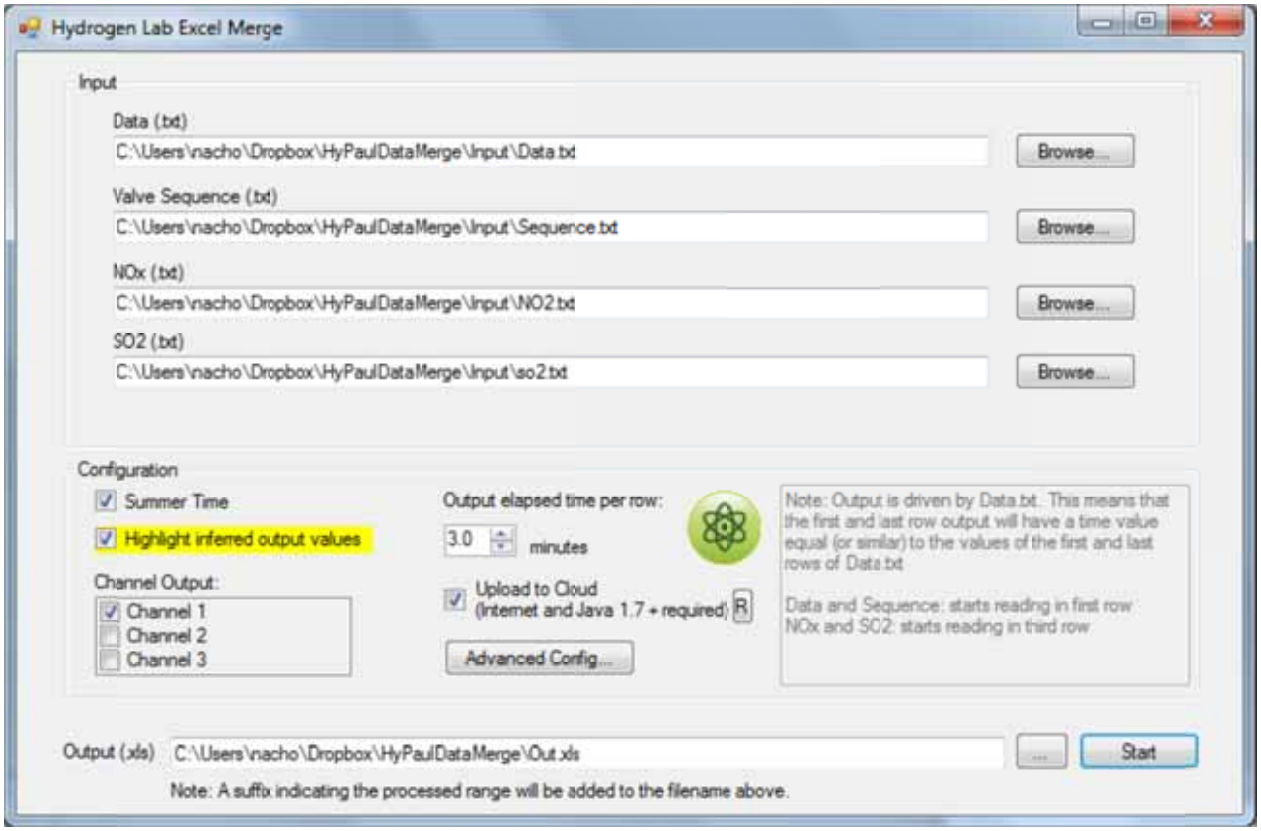

Figure 10: User interface for data merge software

TEST PLAN:

In discussions with air filter companies, the critical factors for determining air filter performance are:

- Contaminant concentration
- Gas flow rate
- Temperature
- Humidity level

With this in mind, we selected the following ranges for the key variables:

- NO_2 – 100 and 170 $\mu g/m^3$
- SO_2 – 25 and 100 $\mu g/m^3$
- Gas flow rate – 100 and 300 slpm
- Temperature – 10°C and 40°C
- Relative humidity – 25% and 70%

Since the interactions between the key variables are not known, we decided to perform a factorial design of experiments, the details of which are provided in Table 2 and Table 3.

Table 2: Full Factorial Experimental Test Plan

Test Number	NO_2 ($\mu g/m^3$)	SO_2 ($\mu g/m^3$)	Flow (slpm)	Temp. (°C)	Relative Humidity
1	100	25	100	10	25%
2	170	25	100	10	25%
3	100	100	100	10	25%
4	170	100	100	10	25%
5	100	25	300	10	25%
6	170	25	300	10	25%
7	100	100	300	10	25%
8	170	100	300	10	25%
9	100	25	100	40	25%
10	170	25	100	40	25%
11	100	100	100	40	25%
12	170	100	100	40	25%
13	100	25	300	40	25%
14	170	25	300	40	25%
15	100	100	300	40	25%
16	170	100	300	40	25%
17	100	25	100	10	70%
18	170	25	100	10	70%
19	100	100	100	10	70%
20	170	100	100	10	70%
21	100	25	300	10	70%
22	170	25	300	10	70%
23	100	100	300	10	70%
24	170	100	300	10	70%
25	100	25	100	40	70%
26	170	25	100	40	70%
27	100	100	100	40	70%
28	170	100	100	40	70%
29	100	25	300	40	70%
30	170	25	300	40	70%
31	100	100	300	40	70%
32	170	100	300	40	70%

Table 3: Gas Flow Rates

			NO2		SO2		Air
Test #	MFC SmLPM NO2 gas	MFC SmLPM SO2 gas	SmLPM NO2	Horiba ppm NO2	SmLPM SO2	Horiba ppm SO2	MFM Slpm Air
1	0.8844142	0.3719336	0.0048643	0.0486	0.0008740	0.0087	99.9943
2	1.5035041	0.3719336	0.0082693	0.0827	0.0008740	0.0087	99.9909
3	0.8844142	1.4877345	0.0048643	0.0486	0.0034962	0.0350	99.9916
4	1.5035041	1.4877345	0.0082693	0.0827	0.0034962	0.0350	99.9882
5	2.6532425	1.1158009	0.0145928	0.0486	0.0026221	0.0087	299.9828
6	4.5105123	1.1158009	0.0248078	0.0827	0.0026221	0.0087	299.9726
7	2.6532425	4.4632035	0.0145928	0.0486	0.0104885	0.0350	299.9749
8	4.5105123	4.4632035	0.0248078	0.0827	0.0104885	0.0350	299.9647
9	0.8844142	0.3719336	0.0048643	0.0486	0.0008740	0.0087	99.9943
10	1.5035041	0.3719336	0.0082693	0.0827	0.0008740	0.0087	99.9909
11	0.8844142	1.4877345	0.0048643	0.0486	0.0034962	0.0350	99.9916
12	1.5035041	1.4877345	0.0082693	0.0827	0.0034962	0.0350	99.9882
13	2.6532425	1.1158009	0.0145928	0.0486	0.0026221	0.0087	299.9828
14	4.5105123	1.1158009	0.0248078	0.0827	0.0026221	0.0087	299.9726
15	2.6532425	4.4632035	0.0145928	0.0486	0.0104885	0.0350	299.9749
16	4.5105123	4.4632035	0.0248078	0.0827	0.0104885	0.0350	299.9647
17	0.8844142	0.3719336	0.0048643	0.0486	0.0008740	0.0087	99.9943
18	1.5035041	0.3719336	0.0082693	0.0827	0.0008740	0.0087	99.9909
19	0.8844142	1.4877345	0.0048643	0.0486	0.0034962	0.0350	99.9916
20	1.5035041	1.4877345	0.0082693	0.0827	0.0034962	0.0350	99.9882
21	2.6532425	1.1158009	0.0145928	0.0486	0.0026221	0.0087	299.9828
22	4.5105123	1.1158009	0.0248078	0.0827	0.0026221	0.0087	299.9726
23	2.6532425	4.4632035	0.0145928	0.0486	0.0104885	0.0350	299.9749
24	4.5105123	4.4632035	0.0248078	0.0827	0.0104885	0.0350	299.9647
25	0.8844142	0.3719336	0.0048643	0.0486	0.0008740	0.0087	99.9943
26	1.5035041	0.3719336	0.0082693	0.0827	0.0008740	0.0087	99.9909
27	0.8844142	1.4877345	0.0048643	0.0486	0.0034962	0.0350	99.9916
28	1.5035041	1.4877345	0.0082693	0.0827	0.0034962	0.0350	99.9882
29	2.6532425	1.1158009	0.0145928	0.0486	0.0026221	0.0087	299.9828
30	4.5105123	1.1158009	0.0248078	0.0827	0.0026221	0.0087	299.9726
31	2.6532425	4.4632035	0.0145928	0.0486	0.0104885	0.0350	299.9749
32	4.5105123	4.4632035	0.0248078	0.0827	0.0104885	0.0350	299.9647

The experimental plan consists of two phases:

Phase I: Initial Shakedown
During the initial shakedown, equipment is tested for functionality and accuracy. During this phase, we:

- Tested control loops on heaters and humidifiers. These tests were conducted with dry runs (no pollutants) to ensure accurate control and stability of environmental systems.
- Checked for leaks and proper pressure drops.
- Calibrated the gas analyzers and pollution injection systems.

After initial shakedown, the first test run may commence along with any additional troubleshooting.

Phase II: Tests
The test plan entails using the above setup to run a range of tests as shown in the full factorial (Tables 2 and 3). The data for the performance of the fuel cell will be measured by the gas analyzers. This data can be plotted against time and the results from the various tests can be combined and assessed based upon a number of parameters. Of particular interest are the lifetime performance curves of the filters. We intend to get two data points under each set of conditions. Due to numerous issues detailed in the "Issues and Recommendations" section, no Phase II test data was collected.

DATA
Equipment Calibration
The calibration of the Horiba gas analyzers involves a procedure which includes first zeroing the device and then calibrating at a determined span value. The Horiba NO analyzer achieved near zero NO readings with ambient air which allowed the zero setting for the analyzer to be set. For effective calibration of the Horibas, the actual reading on the gas analyzers must be in the vicinity of the actual theoretically expected values. This was achieved both for low range and high range calibration (Table 4 and Figure 11).

Air Flow Rate (SLPM)	NO Flow Rate (mSLPM)	Theoretically Expected NO Reading on Gas Analyzer (ppm)	Actual Value on Gas Analyzer (ppm)	Within Satisfactory Calibration Range based on Horiba Manual
2	7.5	0.075	~0.071	Yes
1.2	8	0.133	~0.16	Yes

Table 4: Theoretical and actual values for NO concentrations during gas analyzer calibration.

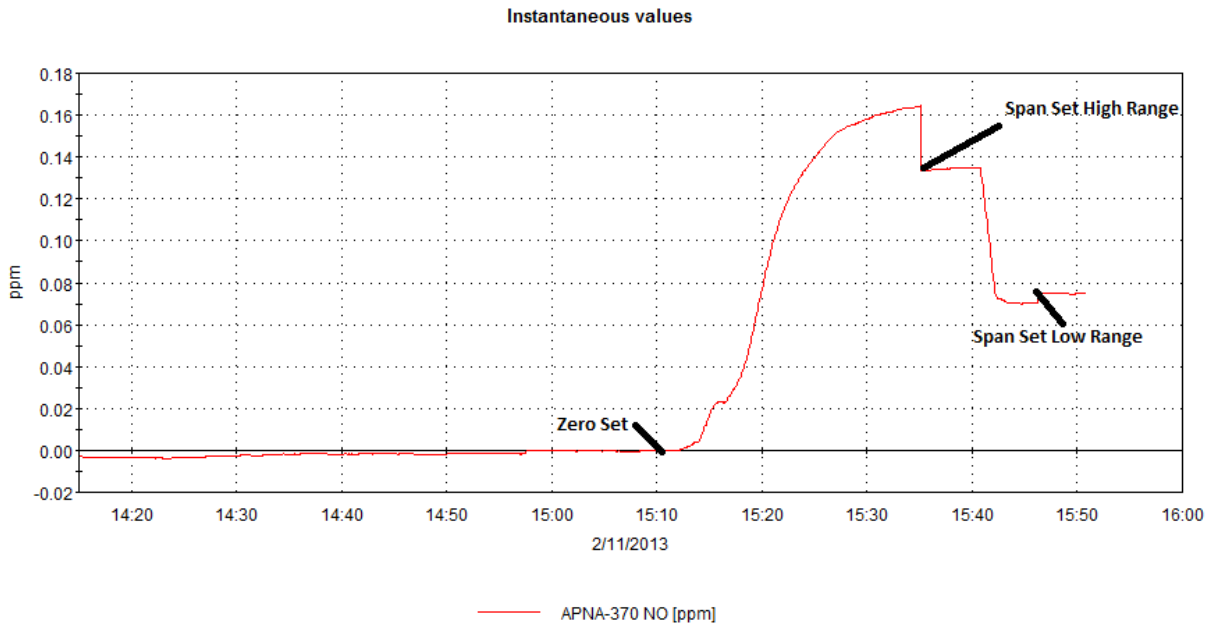

Figure 11: Graph showing stable readings in the vicinity of the expected values. The sudden changes at the span set show the successful calibration to actual values.

A similar calibration was performed on the SO_2 analyzer.

Air Filter Pressure Drop Test

For the initial shakedown, the three channels of the system were operated running dry air (no pollutant content) through it. During this phase, mass flow meters and controllers were calibrated and tested using the LabView interphase. Air heaters were tested using the feedback given by the different thermocouples. Similarly, the humidity equipment was tested for different water flow rates using feedback from the humidity sensors.

As part of the initial shakedown, pressure drop tests were conducted for channel 1. For that purpose, an analog differential pressure gauge was connected at each filter inlet and outlet. Using the LabView interphase, the mass flow controllers of each sub-channel (1-A, 1-B and 1-C) were regulated in order to test different flow rate working values (100 to 300 slpm). For each value of flow rate considered, 3 independent measurements of pressure drop were taken. The three filters and their corresponding pressure drop results are shown in Figures 12 to 15.

Figure 12: Filter A

Figure 13: Filter B

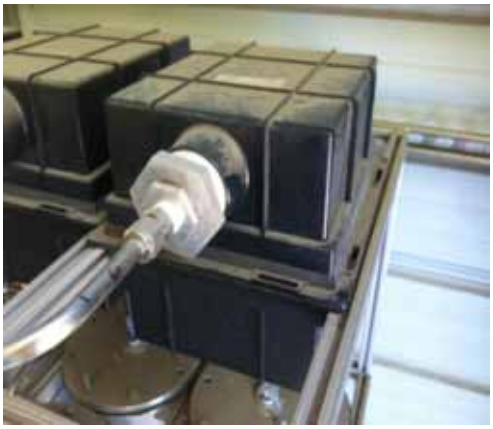

Figure 14: Filter C

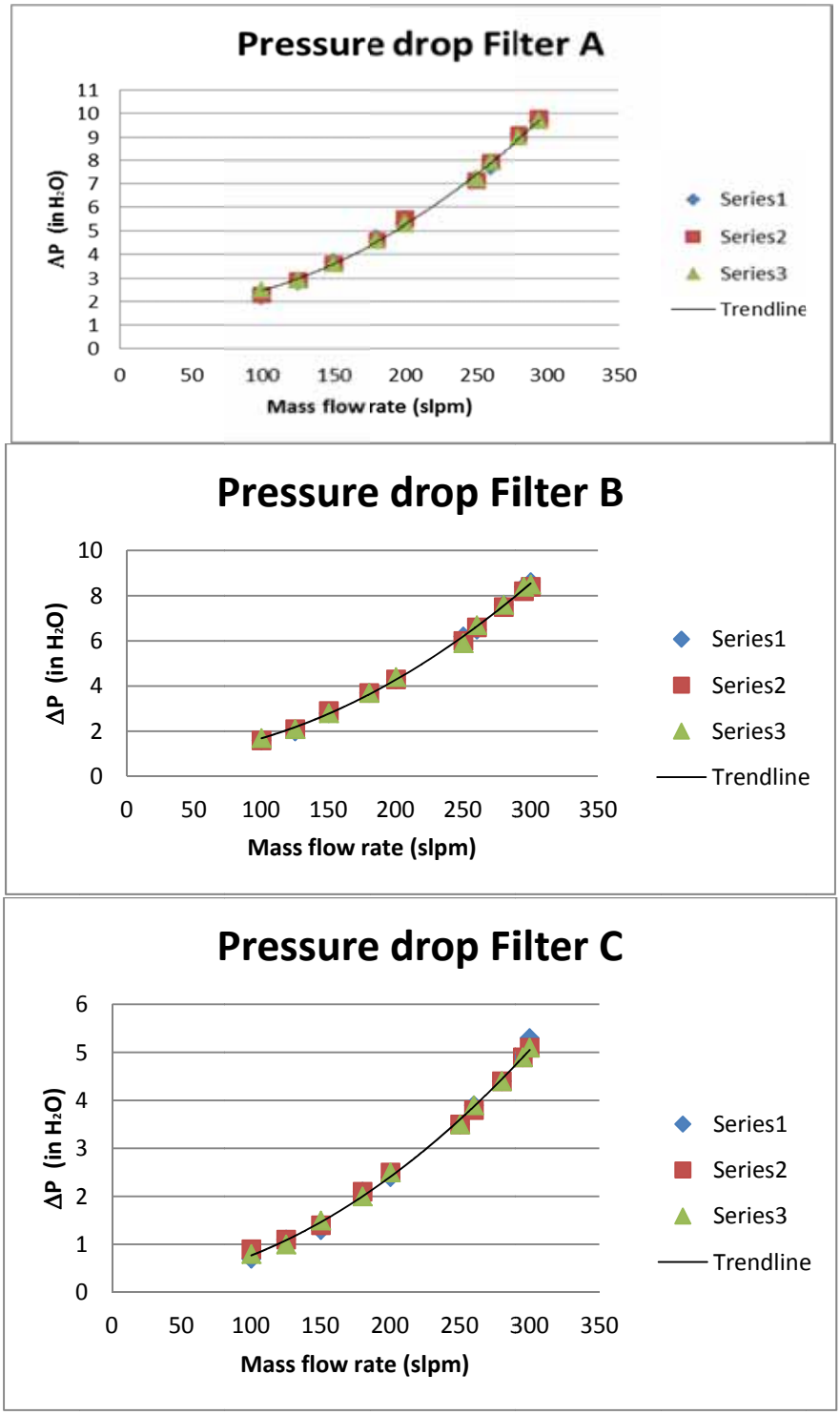

Figure 15: Pressure drop test results

The above results show values of pressure drop between 0.7 and 9.7 in H_2O, with filter A having the highest pressure drop and filter C the lowest. As expected, pressure drop increases with increasing values of flow rate. For all three filters, the measured filter pressure drop is well within the fuel cell system requirements.

ISSUES AND RECCOMENDATIONS

Several major setbacks were encountered in the collection of data which are still ongoing. Many of these issues stem from a design which would operate continuously with dangerous gases. The safety requirements of the university necessitated that the entire system be housed externally and this remote operation requirement for safety created further difficulty with system operation and integration. The problems encountered are inherent in trying to design a fully automatic full scale test for multiple filters. The major issues and recommendations are listed below.

1. The original design was intended for operation in a fume hood with poisonous gases being held external to the personnel area. A safety review required that the system be housed in a remote external area that further necessitated construction of a dedicated facility (outdoor cover). The delay and construction costs of building this cover became a major obstacle to the completion of the project. The original budget planned for an 18 month project. While personnel were overseeing construction of the cover, the budget for personnel was quickly consumed during the delay. The construction also delayed the project significantly such that continuity of personnel was not maintained.
2. Continuity of personnel became a major issue for this project as volunteer researchers were relied upon as the personnel budget was spent in the first 18 months of the project. Generally, these researchers were looking for a project that could be completed quickly and thus recruitment of qualified personnel became a major issue. These researchers were required to learn a complicated system and code before progressing with data collection and analysis. Trouble shooting became major obstacles for those researchers as the original design changed and previous personnel associated with the design were unavailable for discussion. This was a failure of communication that is inherent in a university system.
3. Continuous operation was in the original design but this required complex safety controls and notifications. Integration of this remote continuous day and night operation required more time than it was designed to save. Although we are continuing the operation of this current system at our own expense, we suggest that the operation of the filters be run as a cumulative test in a daily discrete manner rather than a continuous test.
4. The humidifier tanks are designed to inject a water spray into the test air in order to bring the air to the desired relative humidity for a given test. In the original design, a water pump was used to pump water from the faucet into the electronic valve at the top of the humidifier tank. This electronic valve was designed to allow the right amount of water into the tank as per the test requirement. A feedback control loop used the data from a relative humidity sensor to control the opening of the valve. The water pump from the faucet was deemed necessary to provide water to the valve at its operating pressure. This water pump, however, proved to be too big for the purposes of the test and ruptured the water pipe because the electronic valve was not sufficiently open causing a pressure buildup in the pipe itself. This rupture caused some damage to electronic equipment in and around the humidifier tanks. Following this episode, we recently managed to successfully run the humidity control system using water directly from the faucet flowing into the electronic valve. As such, one key recommendation would be to do away with a pump in any future test.

5. We find that the chiller that we are using in our test is not delivering sufficiently cold air to run tests at temperatures as low as 10°C. We, therefore, recommend that any similar test in the future use a much more effective chiller than the one used in our test.
6. It has been reported that the pipe heater used in our test once turned red and ran a temperature in excess of 1000°C while being controlled using the feedback P&ID loop. We recommend finding a way of programming a safety limit into the heater control system.
7. Calibration of the gas analyzers at our operating range proved to be a major problem with no ready solution. The ranges of concentration of the SO_2 and NO_2 gases are near the limits of physical detection. As such, we recommend that the gas analyzers be thoroughly tested before designing the experimental matrix. The experimental matrix may then be designed in such a manner that we may be certain that the gas analyzers would be effective under the test parameters.
8. Integration of the analyzers for remote and continuous operation proved to be problematic. Dependence on solenoids for switching the flow to and from the analyzers to measure inputs and outputs from the various systems also created numerous problems with calibration. Since inputs and outputs need to be monitored, it is suggested that two sets of analyzers be purchased.
9. The air compressor originally procured proved insufficient for the purposes of our test. We, therefore, procured an additional compressor to allow greater capacity. The original budget did not include compressors for air delivery as building air was expected to be used. The removal of the system to a remote location required the compressors be purchased and a complex air delivery system to be installed and used.

TASK 4: DESIGN, ASSEMBLE, AND TEST TWO TORO WORKMAN™ MID DUTY UTILITY VEHICLE WITH AN IDATECH FCS 3000 LIQUID FUELED FUEL CELL SYSTEM

Richard Lawrence
Mike Hicks
IdaTech

TEST VEHICLE 1 (TV-1)

During the suspension of this program, Toro® determined that the IdaTech FCS 3000 fuel cell system (developed during the suspension under a separate contract to the US Navy as a subcontractor to Hoku;Program ID 06UJ9A00008B) matched the operational requirements of the Workman® Model e2065. As a result, a Toro® Workman® Model e2065 light-duty maintenance truck was received (Figure 1) and retrofitted to house an IdaTech FCS 3000 fuel cell system (Figure 2). The model e2065 unit was designated test vehicle-one (TV-1).

Figure 1: Toro's Workman™ Model e2065

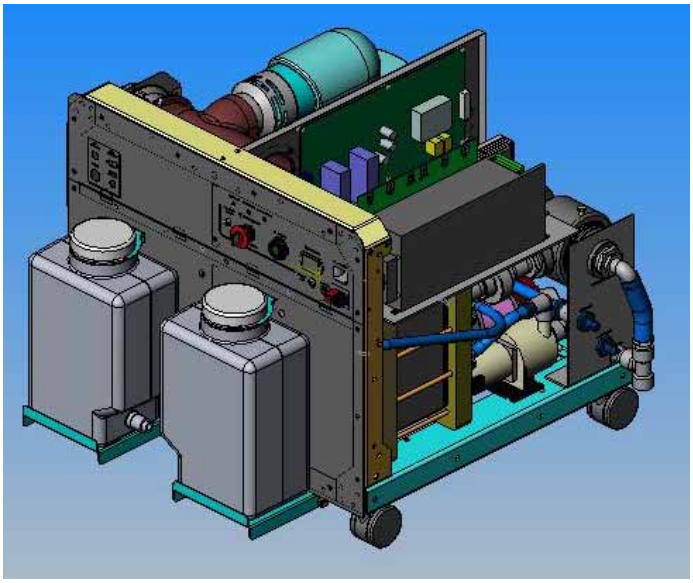

Figure 2: IdaTech's FCS 3000 Liquid Fuelled System

Three FC3000 fuel cell systems were assembled and all three passed operational testing. One fuel cell system, while sitting next to the vehicle, was used to charge the batteries. After successfully demonstrating that the fuel cell system could charge the batteries, the fuel cell system was reconfigured and installed into the vehicle (Figure 3).

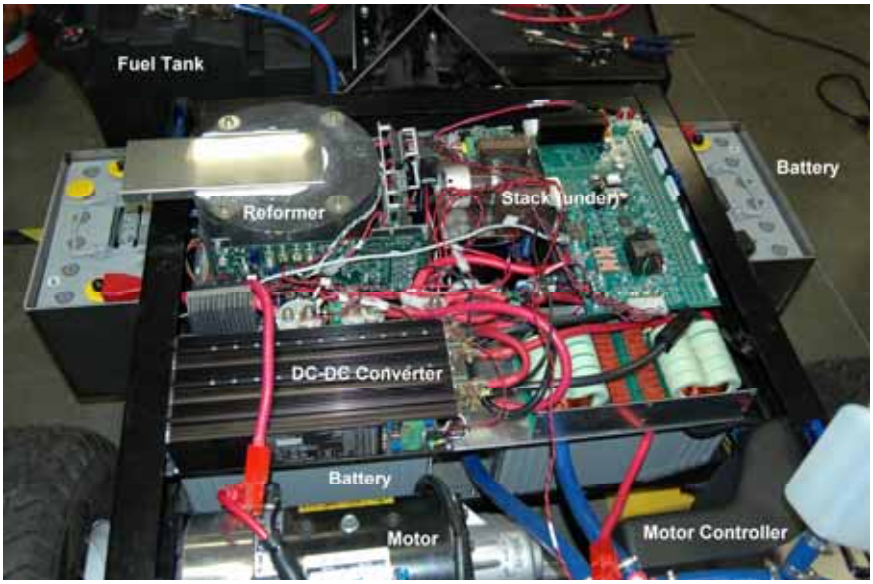

Figure 3: Original configuration of FCS3000 in TV-1

TV-1 was deployed at River's Edge Golf course in Bend, OR (Figure 4) during the summer of 2008. Figure 5 is a graph of the system parameters while the vehicle was driven on the golf course. The control method is for the fuel cell to maintain a battery voltage of 56 Vdc. which means that the fuel cell ramps up and down with battery voltage. In this case, the battery voltage was low at start-up so the fuel cell ramped up and charged the batteries to 56 Vdc. Afterwards, the fuel cell system ramped up and down with power usage and at the end of the run the batteries were at 56 Vdc

Figure 4: TV-1 at River's Edge Golf Course

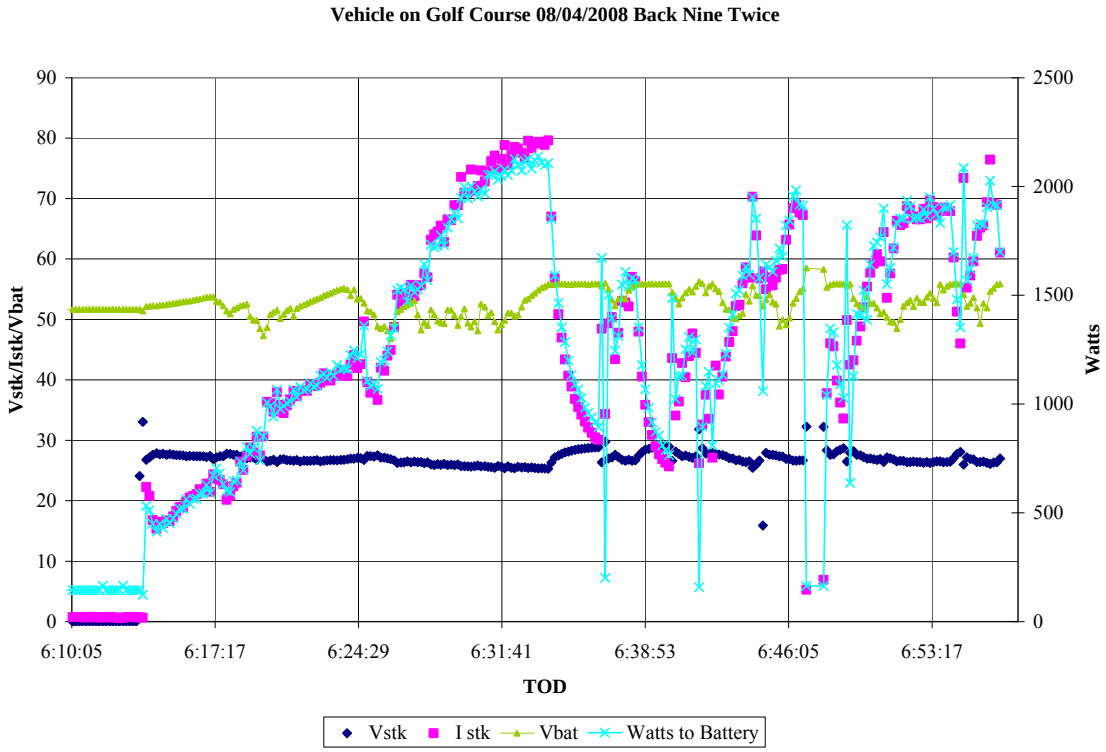

Figure 5: System Parameters of TV-1 while operating at River's Edge Golf Course

The unit did experience several shutdowns during the course of its summer operation, the details of which can be found in Table 1. During the winter an upgrade was performed on the fuel cell system. The upgrade consisted of new H2 recirculation pump mounting, improved cabin fan, new current sensor, improved fuel line routing, new

Table 1: TV-1 Daily Record on Golf Course, Summer 2008

DATE		START	END	BARS	FUEL	MAINTENANCE
14-Jul	Monday, July 14, 2008	3.7	5.1	2	FULL	RETURNED TO SHOP FC NOT ON BATTERY LOW
15-Jul	Tuesday, July 15, 2008	5.1	5.4		FULL	RETUENED TO RIVER'S EDGE
21-Jul	Monday, July 21, 2008	5.4	6.4			STARTED
23-Jul	Wednesday, July 23, 2008	6.4	6.7		7/8	FC COOLANT SW
24-Jul	Thursday, July 24, 2008	6.7	8.7	3		REPLACED REFORMER FUEL PUMP
25-Jul	Friday, July 25, 2008	8.7	8.9	7	1/4	CHECKED FC 2X LOW H2 PSIG AND RAFF. FILLED TANK
25-Jul	Friday, July 25, 2008					HIGH CAB TEMP AND VAPORIER ERROR
28-Jul	Monday, July 28, 2008	8.9	11	6	5/8	RETURN TO SHOP. WILL NOT START EMERGENCY SWITCH OPERATOR ERROR
29-Jul	Tuesday, July 29, 2008	11.1	12	10	5/8	RAN 3 HOURS AT SHOP NO PROBLEM FULL TANK/FULL CHARGE
29-Jul				5		THEY RAN TRUCK
30-Jul	Wednesday, July 30, 2008	12.4	13		1	ON COURSE 1-9 5:30- 7:21
		5:30	12	5	1	
		6:35		8	S/D	RESTARTED
		6:44			S/D	RESTARTED
		7:05			S/D	RESTARTED
		7:20	13	8		OK
		7:21		8	S/D	LEFT COURSE
						MOST OF THE TIME KEY ON. LOTS OF STOPS.
						IN 3 HOURS ACCUMULATED 4 HRS KEY ON
30-Jul	Wednesday, July 30, 2008					
1-Aug	Friday, August 01, 2008	5:30	8:25	6	S/U	
		12.8	15			
	BACK NINE	5:30				SAL IS DRIVER
		6:06			S/D	SUPPLY UNDER VOLTAGE DURING ACCELERATION

DATE		START	END	BARS	FUEL	MAINTENANCE
		6:30				FC ONLINE
		6:39				LONG RUN 12-13
		6:46		5	1/2	
		6:48		6		
		6:52			S/D	LOW CELL VOLTAGE
		6:53			S/U	
		7:01			S/D	MANUAL WILL NOT RAMP UP
		7:03			S/U	RAMPS UP
		7:12				BOUNCING, DOWN HILL RUN
		7:17	15	7		
		7:23		9		
		7:32			S/D	LOW CELL VOLTAGE WHILE ON RUN 17T-17G
		7:32			S/D	
		7:39		9		BATTERY 52.7 V
		7:50	15	10		
		8:25			S/D	MANUAL-WILL NOT RAMP DOWN COULD BE OK.
2-Aug	Saturday, August 02, 2008	10:05	17			STUCK ON COURSE BATTERY DEAD. FC WILL NOT S/U SUSPECT LOW VOLTAGE ATTACHED CHARGER
3-Aug	Sunday, August 03, 2008	6:10				FULLY CHARGED
4-Aug	Monday, August 04, 2008	5:20	17	10	S/U	START SYSTEM
		6:14				FUEL CELL ONLINE
		7:25	18	10	3/4	DROVE BACK NINE TWICE
5-Aug	Tuesday, August 05, 2008	17.5	19	10	5/8	BED FULL OF SAND TOD ONBOARD S/D LOW CELL VOLTAGE 18TH FAIRWAY SECOND RUN
6-Aug	Wednesday, August 06, 2008	19:12	20	6	7/16	FC FAULT 3X
7-Aug	Thursday, August 07, 2008	4:30				FILL FUEL TANK
8-Aug	Friday, August 08, 2008	5:30				S/U

DATE		START	END	BARS	FUEL	MAINTENANCE
		6:17				FC ONLINE
		6:19				FAULT
		7:00			S/U	
		7:10			S/D	LOW CELL VOLTAGE CELL-1
9-Aug	Saturday, August 09, 2008					WASH VEHICLE
10-Aug	Sunday, August 10, 2008					CHARGE VEHICLE GRID
11-Aug	Monday, August 11, 2008	6:10			S/U	
				10	7/8	PUMP CYCLE UP AND DOWN
		6:29			S/D	CATALYST HEAT TIME OUT
		6:31				AUTO RESTART PUMP UO/DOWN THEN STEADY
		6:55			S/D	LOW CELL VOLTAGE CELL-1
		9:56				VEHICLE IN SHOP
13-Aug	Wednesday, August 13, 2008	4:46				S/U IN SHOP
		5:20				FC ONLINE
		5:44				MOVE TO RIVER'S EDGE
		5:50				ON 10th TEE
		20.3	21	10	F	
		6:20				BACK NINE COMPLETED
		6:24				1 HOLE REGEN MOTOR CONTROLLER S/D
		6:51				COMPLETE FRONT NINE
		21.3	22	10	3/4	1.8 kW
		6:59			5 GAL	LEFT RUNNING
		8:00			S/U	FUEL CELL OFF. MAINTENCE CREW USING VEHICLE
14-Aug	Thursday, August 14, 2008	5:10		5	S/U	342.859 HR
		5:52				FC ON LINE

DATE		START	END	BARS	FUEL	MAINTENANCE
		6:15		7	S/D	LCV CELL-1
		6:38			S/D	LCV CELL-1 BATTERY DROP
		6:39			S/U	344.855 HR
		6:43				11 TH G TO 12TH F
		7:02			S/D	LCV CELL-1
		7:03			S/U	
		7:10				POWER DROP RAPIDLY
		7:12			S/D	MANUAL
		7:12				EMO
		7:20				WILL NOT RESTART INSTANT S/D
		7:58			S/U	STARTS
		8:08				POWER OFF NO FAULT BOTH ON LINE ZAHN?
		8:11			S/D	VERY HOT DAY
		8:17			S/U	BED OPEN WILL NOT RAMP
		8:24	24	7		
		8:27			S/D	MANUAL
		9:04			S/U	FC ONLINE RAMPS UP
		11:13		10		SYSTEM OFF
16-Aug	Saturday, August 16, 2008			2		PLACED ON CHARGER
17-Aug	Sunday, August 17, 2008			10		REMOVE CHARGER
18-Aug	Monday, August 18, 2008	5:10		10	1/2	NOISE TEST RAIN THUMDER LIGHTING
				dB	80	MOWER
					48	AMBIENT
				20'	68	CART
					45	AMBIENT
				3'	46	START UP

DATE		START	END	BARS	FUEL	MAINTENANCE
				3'	57	ONLINE
						COMPUTER DOESN'T STORE DATA CLOSED
		6:05			S/D	ON COURSE HEAVY RAIN RETURN S/D UNKNOWN
19-Aug	Tuesday, August 19, 2008	5:25			S/U	
		5:51				SHUT COMPUTER
		5:54				OPEN COMPUTER AND ITS ON
		6:06				FC ONLINE THEN S/D
		6:07				WILL NOT RESTART, REMOVE COMPUTER
		6:13			S/U	MOVE TO YARD S/U
		6:15			S/D	UNKNOWN CAUSE
25-Aug	Monday, August 25, 2008					NEW CATHODE AIR FILTER
						NEW SHORTER CORRAGATED HOSE BURNER BLOWER
						NEW H2 THREE WAY VALVE FOR ANOTHER SYSTEM
						BURNER HEATER WIRE REROUTE
						REROUTE METHANOL FEED LINE
						BOLT DOWN REFORMER - ONE LEG
						FIX CAPACITOR THAT BROKE OFF FROM REFORMER BOARD
						S/U SYSTEM TRY NEW GUI FROM TOD NEEDS WORK
29-Aug	Friday, August 29, 2008					SYSTEM OPERATING FULLY CHARGE BATTERIES
2-Sep	Tuesday, September 02, 2008	7:39	29	10	FULL	MEET WITH DIR. MARKETING. VEHICLE RUNNING
		9:40				S/D, S/U TAKE VEHICLE TO SHOP
		14:40	31	1	3/4	FC OFF, S/U WILL NOT RAMP
		14:56				MANUAL S/D AND S/U FC RAMPS 5 BAR S/D MANUAL NOISE SOUNDS LIKE COOLANT PUMP
3-Sep	Wednesday, September 03, 2008	5:20				S/U

DATE		START	END	BARS	FUEL	MAINTENANCE
		6:08				FC ONLINE 500W AND RAMPING LEAVE VEHICLE FOR CREW W/ COMPUTER CONNECTED
		9:03				FC ONLINE TRY NEW GUI DOESN'T WORK
		9:17				FC S/D LOW H2 PRESSURE
		15:30		10		S/U 2 MINUTES 10 BARS
4-Sep	Thursday, September 04, 2008	10:40			1/2	FC ONLINE PORTABLE CAN'T LOG ON
				8		ADD 1 GAL FUEL. CREW LIKES VEHICLE BECAUSE IT IS QUIET
		10:45	32.0		3/4	CREW TAKING OUT ON COURSE AFTERNOON
5-Sep	Friday, September 05, 2008	6:30	35	10	3/8	S/U
		14:19	36	5	1/2	ADDED FUEL BURNER FLAME OUT SUCK UP FUEL
						S/U GUI STILL NOT WORKING
						REFORMER EXHAUST MELTED BED PLASTIC
				6		FUEL CELL ON RUN 1/2 HOUR
6-Sep	Saturday, September 06, 2008	5:25		6		S/U VEHICLE TO COURSE
7-Sep	Sunday, September 07, 2008	12:45	39	5	1/2	S/U INSTANT RED LIGHT
8-Sep	Monday, September 08, 2008	5:20				S/U
		6:10				F/C FAULT LOW H2 PRESSURE/LOW CELL
		6:13				S/U
		6:15				FC ON LINE AND RAMPING LEFT RUNNING
		9:06		9	5/8	SYSTEM OFF
		9:09				S/U NEW GUI SAVES DATA ADDED FUEL
		9:21				S/D LOW H2 PRESSURE PRV?
9-Sep	Tuesday, September 09, 2008		40	1		PLACED ON CHARGER
		16:00	41	3		FUEL ADDED 1.1 GAL ADDED COOLANT 1"
				5		S/U FC ONLINE THEN FAULTS ON CHARGER O/N
10-Sep	Wednesday, September 10, 2008	6:30	41	10		S/U DRIVE - BLOWER AND RECIRC NOT ON S/D

DATE		START	END	BARS	FUEL	MAINTENANCE
		12:00	41	9		S/U OK
		16:00	42	6	3/4	S/U INTERMINT H2 RECIRC. THEN S/D PUT ON CHARGER
11-Sep	Thursday, September 11, 2008	15:30	43	4	3/4	SYSTEM S/D
						FOUND BROKEN WIRE RELAY SWITCH TO FC POWER
						FOUND INTERMITENT CONNECTOR TO ATLAS BOARD
						REPAIRED AND TRIED THREE TIME TO START S/D LOW CELL VOLTAGE RAMPS TO 50 AMPS? PREF FALLS WITH Pfeed
15-Sep	Monday, September 15, 2008					RETURN TORO TO IDATECH. CHECK REFORMER pREF PRV OK. SUSPECT ZAHN RAMPING TOO QUICK AND TOO HIGH 50 AMPS AT STACK. MAYBE FUEL PUMP, BUT H2 PRESSURE STAYS UP WHILE CELLS FALL
17-Sep	Wednesday, September 17, 2008					FOUND WIRE WE REPAIRED IN FIELD FOR BLOWER WAS REVERSED, CONNECTOR #11 TO BLOWER RELAY. CHARGED BATTERY.
18-Sep	Thursday, September 18, 2008		43	10	FULL	

firmware, onboard data acquisition, dash meter to monitor battery charging current. The new firmware increased the allowable fuel cell ramp rate and improved the maximum net output from 2.2kW to 2.8kW peak. In addition, the new layout design is easier to manufacture and maintain as the new design can be removed as one unit with minor disconnects. The new layout is shown in Figure 6.

Figure 6: Second generation integration of FCS3000 in TV-1

In all, the fuel cell system in TV-1 obtained the following statistics while operating on a rough and highly terrain, during high ambient temperatures and being exposed to several types of particulants – dirt, dust, grass clippings, fertilizer and sand.

- Total run time of 318 hrs
- Consumed 474 liters of HydroPlus^{TM} fuel
- Produced 357 kW-hrs
- Experienced 172 thermal cycles
- kW-hrs/L = 0.753

TEST VEHICLE 2 (TV-2)

IdaTech installed a fuel cell and reformer into a second prototype, a Toro Workman MDE battery-electric utility vehicle. The MDE is a newer version of the Workman e2065 used in TV-1. The new vehicle design incorporates front wheel shocks and an accessible area under the front hood. The batteries were placed two in front and two in the rear compartment which eliminated the “saddle bag” batteries external to the rear compartment in the first vehicle. A photo of TV-2 in front of the High Desert Museum is shown in Figure 7. The FCS design is the same as the upgraded version in TV-1 (Figure 6).

Figure 7: TV-2 at the High Desert Museum

TV-2 was deployed at the High Desert Museum during the summer of 2009. A typical drive cycle is shown in Figure 8 and the summer 2009 operational history is shown in Table 2.

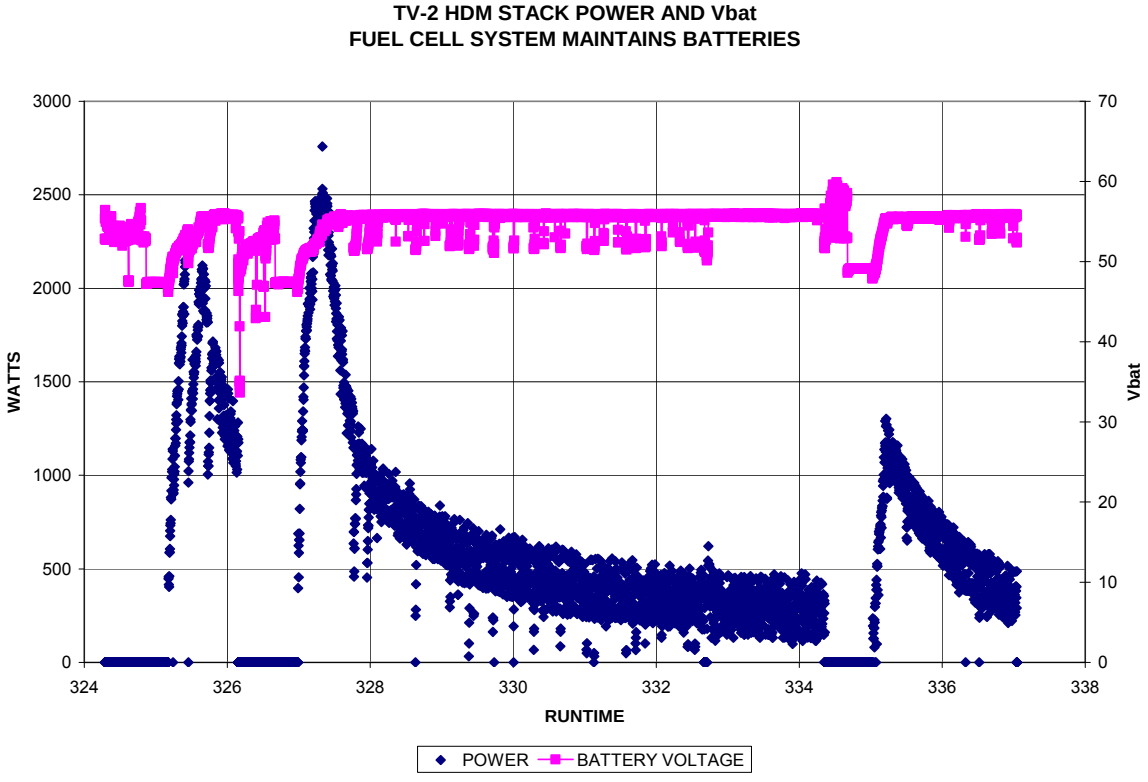

Figure 8: Power output and battery voltage of TV-2 at the High Desert Museum

Table 2: TV-2 Daily Record at the High Desert Museum, Summer 2009

DATE		TOD	HRS	BARS	FUEL	MAINTENANCE
2-Jun	Tuesday, June 02, 2009	6:30	2.1	10	3/4	S/U IN SHOP OK
		7:30				FIRST DAY High Desert Museum (HDM) Difficult to get FC to kick on.
		11:30				Call from Jeff S/Ds
		12:04	2.8	10	1/2	Arrive FC ON fully charged. Why? 1/2 tank. Drive get S/D
3-Jun	Wednesday, June 03, 2009	14:30	4.1	8	1/2	ADD FUEL 3/4 Comments: love vehicle, front battery needs brace fore aft. Accelerator pedal to sensitive. Shocks bottom out they will adjust.
5-Jun	Friday, June 05, 2009	14:30	4.6	9	5/8	ADDED FUEL 7/8 FOR WEEKEND
9-Jun	Tuesday, June 09, 2009	14:16	8.8	9	1/4	ADDED FUEL 7/8 Add 1 pt coolant
						DCDC Converter loose
15-Jun	Monday, June 15, 2009	14:22	11.8	6	3/8	HAD BEEN RUNING. S/U. ADDED FUEL 7/8. BLOWER NOISE, BUT IT GOES AWAY. 1.8kW LEFT ONLINE
19-Jun	Friday, June 19, 2009	14:30	13.6	6	3/8	BED MELTED LOSE VENT REPLACE.ADDED FUEL 7/8
24-Jun	Wednesday, June 24, 2009	14:30	14.6	10	7/8	NEW EXHAUST VENT NEW DCDC CONVERTER SHEET METAL, SEPARATE METER WIRING, FIX STEAM T/C. DELIVERED VEHICLE
25-Jun	Thursday, June 25, 2009	7:30	14.6	10	7/8	PHOTOS OF VEHICLE IN FRONT OF MUSEUM
26-Jun	Friday, June 26, 2009	10:40	15.1	8	7/8	PHOTOS OF VEHICLE SYSTEM
30-Jun	Tuesday, June 30, 2009	10:10	19.4	1.5	7/8	BASICALLY DEAD, ADDED FUEL S/U
30-Jun	Tuesday, June 30, 2009	15:10	19.5	5	7/8	1.4 Kew
2-Jul	Thursday, July 02, 2009	14:51	21	10	1/4	FUEL ADDED TO 7/8, BATTERY WEDGE FELL OUT
7-Jul	Tuesday, July 07, 2009	15:36	25.7	5	5/6	FUEL ADDED TO 7/8
15-Jul	Wednesday, July 15, 2009	14:20	32.5	5	0	FUEL ADDED TO 7/8

DATE		TOD	HRS	BARS	FUEL	MAINTENANCE
21-Jul	Tuesday, July 21, 2009	8:45	33.3	5	1/2	AT RIVERS EDGE WITH UC DAVIS FOR S&V
21-Jul	Tuesday, July 21, 2009	10:37	33.3	10	1/2	AT RIVERS EDGE BACK 9- 2 FRONT 9- 1
22-Jul	Wednesday, July 22, 2009	5:30	33.3	10	1/2	AT RIVERS EDGE FRONT 9
23-Jul	Thursday, July 23, 2009	5:30	33.3	10	1/2	AT RIVERS EDGE FRONT 9-3 BACK 9-2
27-Jul	Monday, July 27, 2009	7:30	36	10	F	DELIVER HDM
29-Jul	Wednesday, July 29, 2009	13:30	37.1	4	5/8	S/D LOOSE VOLTAGE TAPS
31-Jul	Friday, July 31, 2009	14:30	38.3	7	1/4	FILL TANK GET DATA CARD
4-Aug	Tuesday, August 04, 2009	14:20	40	0	1/4	CHARGER ON S/U BURNER FLAME OUT
5-Aug	Wednesday, August 05, 2009					REMOVE TV-2 AND DELIVER TV-1
17-Aug	TROUBLESHOOT TV-2 TO NO AVAIL. REPLACE REFORMER W/ REFORMER FROM TV-1 THEN REPLACE REFORMER BOARD					
19-Aug	Wednesday, August 19, 2009	7:20	40.1	10	3/4	DELIVER TO HDM
21-Aug	Friday, August 21, 2009	13:47	40.8	9	1/2	GOT DATA CARDS, FILLED TANK 7/8
25-Aug	Tuesday, August 25, 2009	7:37	43.6	7	1/2	FIX DAMAGED RADIATOR, GOT DATA CARDS, FILLED TANK 7/8
1-Sep	Tuesday, September 01, 2009	7:37	46.5	3	5/8	FILLED TANK 7/8. Don: SYSTEM DOESN'T CHARGE WHEN DRIVEN S/D
3-Sep	Thursday, September 03, 2009	15:00	47.4	10	5/16	FILLED TANK 7/8
8-Sep	Tuesday, September 08, 2009	14:34	48.7	10	1/4	FILLED TANK 7/8. S/D DRIVING
11-Sep	Friday, September 11, 2009	14:34	50	8	5/8	FILLED TANK 7/8.
15-Sep	Tuesday, September 15, 2009	15:03	52.1	8	1/4	FILLED TANK 7/8.
21-Sep	Monday, September 21, 2009	9:02	54.4	7	1/4	FILLED TANK 7/8.
25-Sep	Friday, September 25, 2009	9:02	57.2	7	1/4	FILLED TANK 7/8.
	REMOVED FROM THE HDM					

Abbreviations: S/U – Start Up; S/D – Shut Down; HDM – High Desert Museum;
BARS: vehicle battery charge level on scale 0 to 10; TOD – Time Of Day; TV – Test Vehicle

Unlike the golf course, the High Desert Museum is a rough but flat terrain and extremely dusty and dirty. In only 57 hours of operation, the amount of dust and dirt build-up on the fuel cell system was significant. Compare the amount of dust in Figure 8 to the as build in Figure 6. However, even with the amount of dust and dirt build-up, the system still operated without issues. In all, the fuel cell system in TV-2 obtained the following statistics at the High Desert Museum:

- Total run time of 368 hrs
- Consumed 315 liters of HydroPlus^{TM} fuel
- Produced 149 kW-hrs
- Experienced 63 thermal cycles
- kW-hrs/L = 0.473

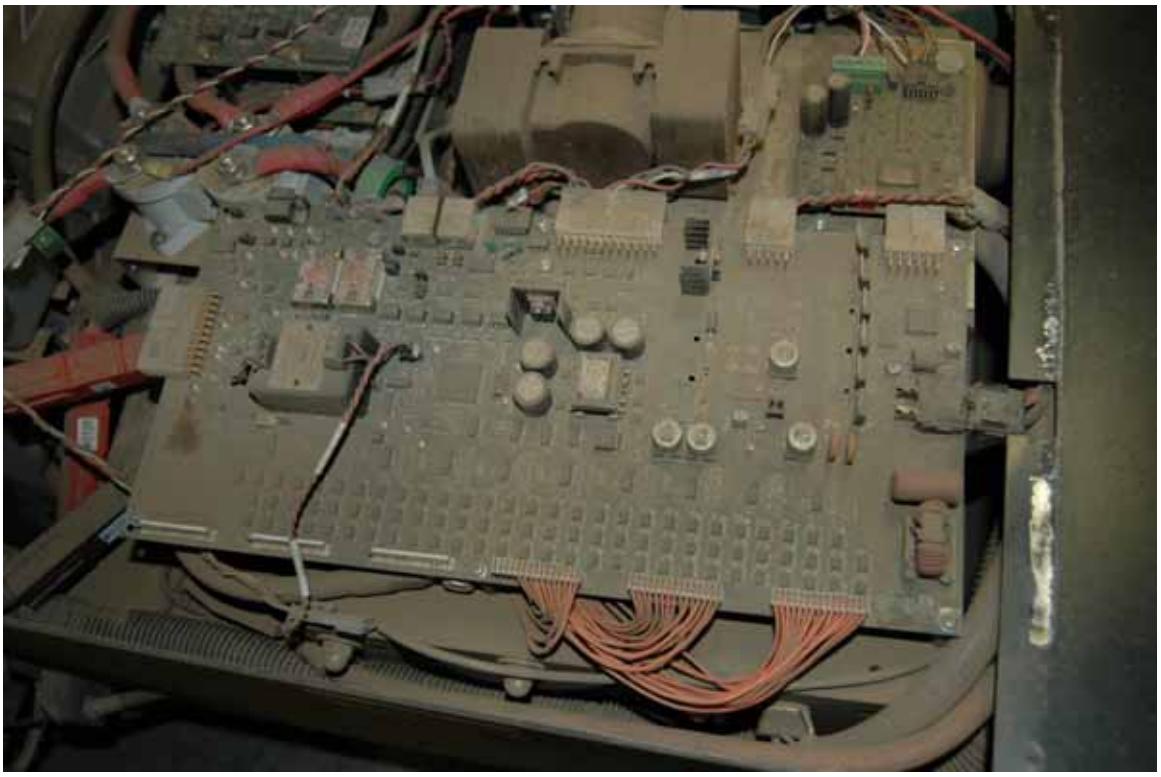

Figure 8: TV-2 Prototype Fuel Cell Powered Vehicle at the High Desert Museum after 57.2 hours Exposure

A picture of TV-2 next to other vehicles at the High Desert Museums is shown in Figure 9. As you can see, TV-2 is approximately the same size as the other vehicles employed by the High Desert Museum.

Figure-9: TV-2 Fuel Cell Powered Vehicle at the High Desert Museum and their other vehicles

LESSONS LEARNED AND CORRECTIVE ACTIONS

There were two main learning's from the field trials: (1) need to restrain all wiring otherwise the vibrations from the off-road conditions will damage the wiring and connections and (2) off-road conditions are significantly more dirty and dusty the on-road conditions so sensitive equipment must be protected. A summary of the lessond learned is shown in Table 3.

Table 3: Issue and Corrective Actions

Issue	Corrective Action
System overheat on hot days	Added additional cooling fans
Thermocouple shorted	Added restraint
Wires fell of coolant switch	Added restraint
Fuel pump slowed down from dirt build-up	Sealed pump gearbox opening
Fuel line dry	Remove tank dip tube and place tanck connection on bottom
Inverter not ramping	Installed new inverter and firmware
Troubleshooting faults takes too much time	Added onboard data acquisition
Too many circuit boards increase likelihood of wiring breakage	Consolidation of circuit board recommended